

Application of Computational Intelligence in Measuring the Elasticity between Software Complexity and Deliverability

Siddharth Lavania¹

Research Scholar, PhD Programme
University of Petroleum & Energy Studies,
Dehradun, India
siddharth.lavania@gmail.com

Dr. Neelu J. Ahuja³

Associate Professor, Department Of Computer Science
University of Petroleum & Energy Studies,
Dehradun, India
neelu@ddn.upes.ac.in

Dr. Manuj Darbari²

Professor, Department of Computer Science
Babu Banarsi Das University
Lucknow, India
manujuma@gmail.com

Dr. I. A. Siddiqui⁴

Senior Project Manager, Celerity Networks Pvt. Ltd.
Noida, Uttar Pradesh
Imran.siddiqui@velocis.in

Abstract— The paper highlights various issues of complexity and deliverability and its impact on software popularity. The use of Expert Intelligence system helps us in identifying the dominant and non-dominant impediments of software. FRBS is being developed to quantify the trade-off between complexity and deliverability issues of a software system.

Keywords— Deliverability, Complexity, Expert System

I. INTRODUCTION

There are various models and schemes developed for checking the quality of the software product. The main concentration of the team is on basic software quality improvement in terms of Flow of Data, Mean time between failure and Mean time to repair, but there exists a huge gap in terms of usability of the software. Usability of the software refers to the ease of use in driving the desired result. ISO/DIS defines usability as “The extent to which a product can be used by specified user to achieve specified goals with effectiveness, efficiency and satisfaction in a specified context of use”. The relation between complexity and usability has an inverse relationship (figure 1). As Complexity rises the usability aspect of deliverable in terms of “Ease of Use” goes down.

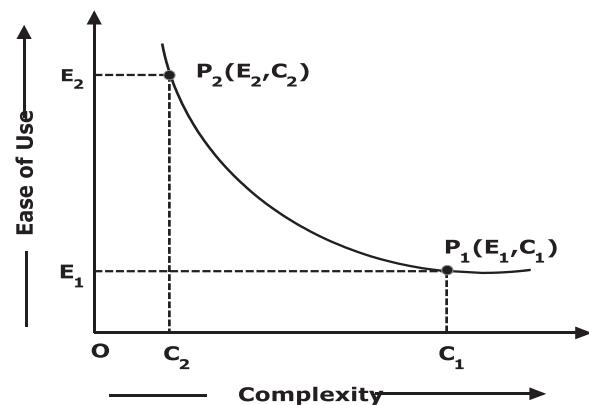


Figure 1: Plot between Complexity and Ease of Use

As functionality of the software increases the deliverability value to the client also increases but at the same time, complexity also increases. There are chances that the user may not use some of the required functionality. In order to proceed with the problem, authors have used the concept of Expert System in calculating the elasticity between the two variables complexity and usability

II. COMPLEXITY ISSUES IN SOFTWARE

Complexity issue related to “Ease of Use” in the line with the end user. A high skilled user may find some task very easy than low skilled (related to computer related knowledge) user. Complexity of the system varies from mere installation of the software to complexity verifying online in real time mode. It provides a relative comparison between the levels of difficulty in software products. For example in Indian scenario, there are number of consumers who have high end

systems but lacks of usage of all the software systems. We classify the complexity aspect of software based on the user's psychographic profiles. It is divided into three parts Personal, Social and Technological. The Personal factors identifies the traits of user depending upon his/her knowledge skills, user is able to perceive things and develops adaptability accordingly. When design a software module for user interface personal traits are given very high priority. Social factor deals with peer environment and their skill set. A user may be able to learn much from peers and even the competitive psychology helps the user to learn about the difficult tasks. Technological support which the software provides like intelligence in Microsoft package and Offline/Online help.

There are various factors on which the software is dependent:

1. Paradigm Shift: It refers to phase shift in terms of technology and software.

2. Non Modal Help: It provides help to the user which is deliberate in nature. User has to attempt it in order to proceed further.

3. Validation Check Help: It refers to the support relating to validation help which is provided by a pop-up support/balloon support.

4. Verification Help: It refers to the system output being generated because of some event initiated by the user.

5. Likability Index: It is the drop-down menu functionalities and sub-functionalities. The more difficult it is to reach to the specific menu the higher is the complexity.

III. USABILITY ISSUES

The branch of computer science dealing with the usability issues is known as User-Controlled-Design. It covers all the aspects of Human Computer Interaction. In this paper we will be focusing on only software aspects. If we say that particular software is very popular, we mean the user is able to drive its full utility value. For example MS-Word by Microsoft provides a much user friendly interface than any other word processing software. In order to push the product in market, software firms are focusing on usability aspect of the software which covers the basic aspects like early focus on user, integrated design, early and continual testing and iterative design.

IV. RULE BASED EXPERT SYSTEM

Rule Based Expert System works on simple logic of "IF THEN" construction. The general notation of this is "IF A THEN B" where "A" and "B" are the propositions of linguistic variables. A is defined as Premises and B is the Consequences of the rule. A general framework of Expert System consists of Knowledge Accumulator Fuzzy Inference System and External Variables (Fine Tuning Variables).

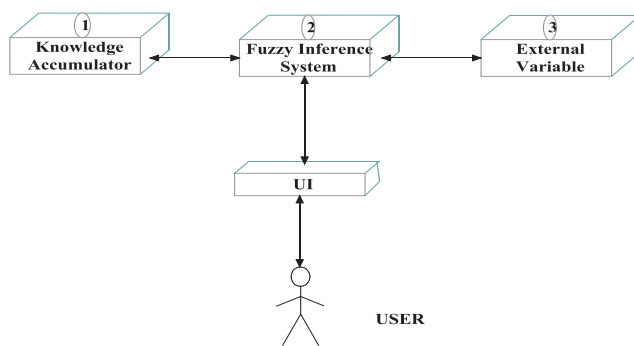


Figure 2: 3-Block Architecture of Expert System

Knowledge Accumulator gathers knowledge of multiple human experts. This knowledge is fed into the Fuzzy Inference System (FIS) supported by any real time variable. The output is either generated by Sugeno or Mamdani FIS which is converted to the user interface for results and analysis.

IV. LITERATURE SURVEY

Complexity issues relating to the usability engineering is very well discussed by Rick Sobiesiak and A Tim O'Keefe[1]. They have highlighted the quantitative approach to software usability engineering. We have used some of the impediments. The paper by Y. Dia and A Keller [6] also discusses some issues on "Quantifying the complexity of IT Service and Management Processes" highlighting some issues relating to the complexity of services quantification and its impact on user psychology. Another paper by Y. Dia and R. Sobiesiak [2] highlights the correlation between complexity and software usability. On the usability side, the white paper by Microsoft deals with the usability engineering aspect of software design. J. Nielsen and R. L. Mack [7] highlights a framework for checking the usability component of any software. Another paper "Application of evolutionary algorithm to manage the trade-off between software complexity and deliverability" by S. Lavania and Manuj Darbari [4] focuses on various factors on which usability of software is dependent. Besides that we have formulated an idea from the book by Neilson Jacob [8] on "Usability Engineering". Lastly, the concept given by L. Zadeh [10] on FRBS helps us in deriving the trade-off relationship between complexity and usability.

V. DEVELOPMENT OF FRBS TO APPROXIMATE THE TRADE-OFF BETWEEN COMPLEXITY AND DELIVERABILITY

The development of FRBS starts with Fuzzy Inference System (FIS). The input to FIS may be fuzzy or crisp but the output from FIS is always a fuzzy set as discussed in 3-Block Diagrams of expert systems. The basic step in FIS is to

convert the crisp set into fuzzy input. This input is fed to the Rule Base which consists of Knowledge Extractor to generate the complex output set. Later on it is defuzzified to produce the crisp output of a particular event. Since, we have to calculate the trade-off value for a software module. We start with the basic building block of categorizing the clusters of software module. The space partitioned is derived from the data partitioning and a rule is associated with each group formed for Complexity and Usability. A simple clustering is achieved by using Fuzzy Decision Tree. From this tree we will be forming the Rule base (Figure 3).

We have three basic categories of rules:

Rule I: If Complexity is Moderate, Usability is also Moderate, Software is Popular.

Rule II: If Complexity is Very High, Usability is Poor, Software is Not Popular.

Rule III: If Complexity is Low, Usability is High, Software is very Popular.

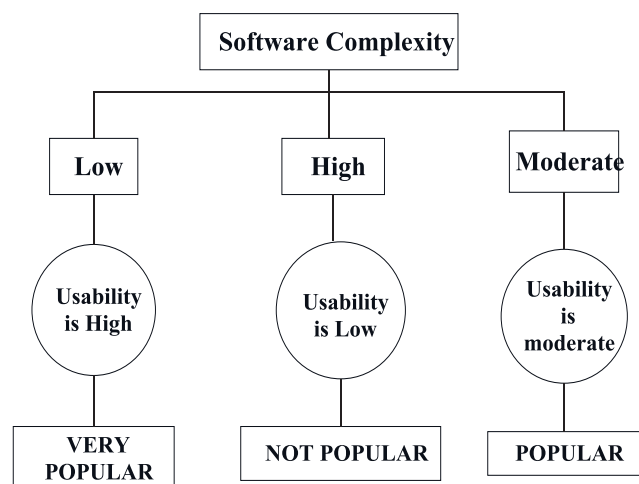


Figure 3: Tree hierarchy of Rule-Base

We extend the basic the above Rule Base of Tree Hierarchy into Fuzzy Inference System in our work

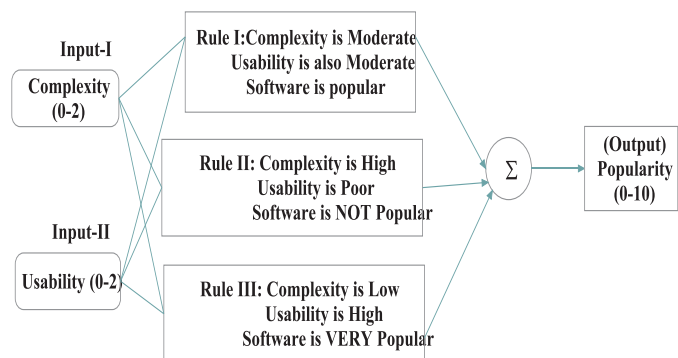


Figure 4: Fuzzy Inference System

The above figure 4 illustrates the rule description of Software Complexity and Usability using Mamdani FIS. Based on the linguistic set, the output is classified into three broad categories: High, Low and Moderate ranging from 0, 1 and 2.

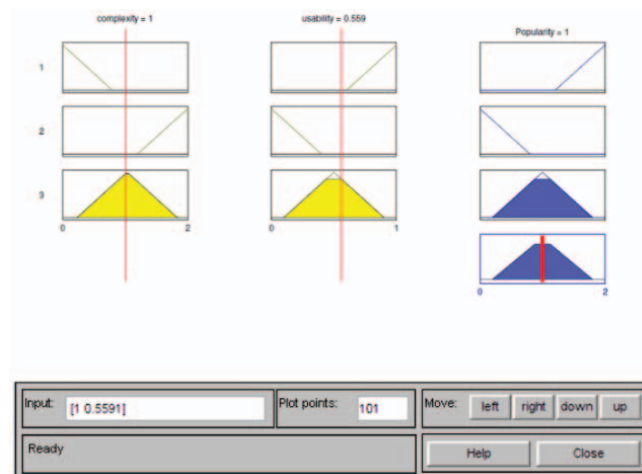


Figure 5: Snapshot of deriving a Trade-Off Value of Complexity and Deliverability

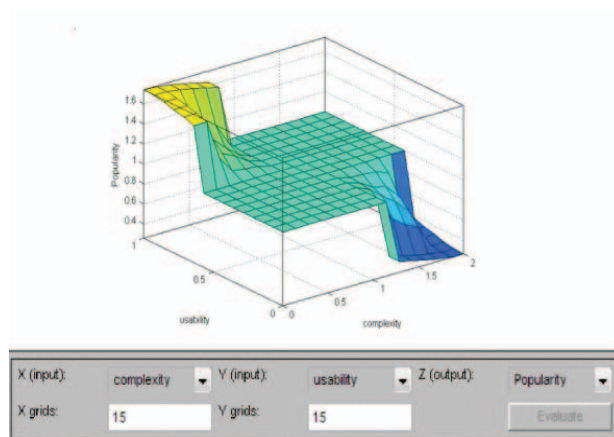


Figure 6: Surface plot of Software Complexity and Usability

The surface plot for the above rule base shows the movement of the spike when Software Complexity is low and Usability is high on the VERY popular side of the 3-D graph.

VI. CONCLUSION

The paper discusses the set of value parameters which are required to maintain the relationship with the Popularity aspect of the software. If the software is less complex then it indicates lesser number of deliverable features to the client. If the software complexity is increased in order to provide high deliverable value, usability drops significantly. Development of Fuzzy Inference System using Expert Knowledge Base

provides a strong decisions making foundation measure the Trade-off between Complexity and Deliverability focusing on Modular Integration and User Interfaces.

ACKNOWLEDGMENT

The author is thankful to **Mr. Mahesh Goel**, the **Managing Director** and **Dr. Devendra Agarwal**, **Director of Goel Group of Institutions, Lucknow** for their kind support and encouragement in promoting research activities in the Campus.

REFERENCES

- [1] Rick Sobiesiak and A Tim O'Keefe, "Complexity analysis: a quantitative approach to usability engineering", Proceedings of the 2011 Conference of the Center for Advanced Studies on Collaborative Research Toronto, Ontario, Canada
- [2] Y. Dia and R. Sobiesiak "Quantifying Software Usability through Complexity Analysis", IBM Design: Papers and Presentations, 2010
- [3] Gould, John D, Stephen J. Bioes and Clayton Lewis, "Making Usable, Useful, Productivity: Enhancing Computer Applications." Communications of the ACM, 1991.
- [4] Siddharth Lavania, Manuj Darbari, Neelu Jyoti Ahuja, Praveen Kumar Shukla, "Application of Evolutionary Algorithm in Managing the Trade-Off between Complexity of Software and Its Deliverables" International Review on Computers and Software , Vol. 7 n. 6, pp. 2899-2903, 2012.

Research Reports:

- [5] Usability in Software Design, "A Report by Microsoft Corporation", 2000
- [6] Y. Dia and A Keller, "Quantifying the Complexity of I.T. Service Management Processes", IBM Research Report, 2006

Books:

- [7] J. Nielsen and R. L. Mack, "Usability Inspection Methods", John Wiley & Sons Inc 1994, ISBN: 0-471-14965-9
- [8] Neilson Jacob, "Usability Engineering", Boston AP Professional, 1994, ISBN: 0-12-518400-X
- [9] D. Dumas, Joseph S., and Janice C. Redish. "A practical guide to Usability Testing", London : Intellect Books, 1999. ISBN: 1841500208.
- [10] L. Zadeh, "Fuzzy Sets, Fuzzy Logic, and Fuzzy Systems", Selected Papers by Lotfi A Zadeh edited by: George J Klir (SUNY, Binghamton) edited by: Bo Yuan (SUNY, Binghamton). ISBN: 978-981-02-2421-9.

Chapter 3

Applications of Genetic Algorithms in Chemical Engineering II: Case Studies

Santosh K. Gupta and Manojkumar Ramteke

3.1 Introduction

Chemical engineering systems are often associated with complex phenomena. The general formulation [described in Part I (Chap. 2)] of a model can be represented as $\mathbf{z} = \mathbf{f}_{\text{model}}(\mathbf{d}, \mathbf{x}, \mathbf{p})$ in which \mathbf{z} is the state of the system for the specific values of the decision variables, \mathbf{x} , specified variables, \mathbf{d} , and parameters, \mathbf{p} . The state of the system is represented through a set of output variables, $\mathbf{y}(\mathbf{x}, \mathbf{p})$. These complex systems, often modeled using a large number of coupled differential and algebraic equations, need to be optimized using multiple objectives. Genetic algorithm (GA) clearly outperforms conventional algorithms for handling multiple objective, non-linear formulations in a derivative-free environment. However, the very stochastic nature that provides a derivative-free operation leads to a requirement of a large computational time. Thus, the application of genetic algorithm (GA) [16, 17, 19, 28, 34] to these complex chemical systems is seldom straightforward. Very often, optimization using GA requires a large computational effort because of the time it takes for solving the model equations. Thus, one needs to use faster and more efficient algorithms in order to obtain reasonably good optimal solutions.

Several interesting and faster variants of GA have been developed over the last four decades to improve the applicability and the convergence speed. A few notable examples are SGA, VEGA, HPGA, NPGA, NSGA, NSGA-II, SPEA, PESA, NSGA-II-JG, Altruistic-NSGA-II, and Real-coded NSGA-II. These are described in

S.K. Gupta (✉)

Department of Chemical Engineering, University of Petroleum and Energy Studies (UPES),
Bidholi, via Prem Nagar, Dehradun, Uttarakhand 248007, India
e-mail: skgupta@iitk.ac.in

M. Ramteke

Department of Chemical Engineering, Indian Institute of Technology Delhi, Hauz Khas,
New Delhi 110016, India
e-mail: mcramteke@chemical.iitd.ac.in; ramtekemanoj@gmail.com

detail in Chap. 2. The application of these to real-life chemical engineering systems such as the optimization of polymerization reactors, catalytic reactors, separation equipment, planning and scheduling, combinatorial optimization, and data-driven applications are described in this chapter.

3.2 Optimization of Polymerization Reactors

In recent years, multi-objective genetic algorithm has been used to optimize several interesting and complex systems in the field of polymer science and engineering [1, 5, 39, 45, 68]. These include the optimization of (existing) industrial reactors as well as optimization of these reactors at the design stage (where more decision variables are available), online optimizing control studies, etc. An example of the MOO of an industrial semi-batch nylon 6 reactor is first discussed in detail. This is followed by a short discussion of several other systems, e.g., poly methyl methacrylate (PMMA), poly ethylene terephthalate (PET), polystyrene (PS), and low-density polyethylene (LDPE).

The MOO of the hydrolytic step growth polymerization of nylon 6 in an industrial semi-batch reactor [48] is one of the early applications of multi-objective GA in polymerization reaction engineering. Fiber-grade nylon 6 is commercially produced using this reactor. The reaction scheme comprises of five reactions given in Table 3.1 [75]. The polymerization is carried out in a semi-batch reactor (see Fig. 3.1; [57]) at a temperature of about 250 °C. Vaporization of the volatile components in the liquid phase, namely, the monomer, ϵ -caprolactam, and the condensation by-product water, takes place as the temperature of the liquid reaction mass increases from the feed temperature of about 90–250 °C. This leads to a gradual build-up of the pressure, $p(t)$, in the vapor space above (since the exit control valve at the exit is closed initially). All the reactions are reversible. Clearly, a relatively high concentration of W is required at the beginning so as to drive the first reaction (ring opening) forward. However, lower amounts of W are needed later so that the second reaction, poly-condensation, is driven in the forward direction to produce longer molecules of the polymer. This is achieved in the industrial reactor by adding higher amounts of water at the beginning, and then having its concentration in the liquid phase (where the reactions take place) decrease with time by vaporization (opening the control valve at a prescribed rate). In other words, the concentration, $[W](t)$, of water (or equivalent) in the liquid phase is a decision variable, a *function* of time.

A mathematical model of this industrial reactor was first developed by Gupta et al. [29] and improved by Wajge et al. [75]. The model comprises 15 ordinary differential equations of the initial value type (ODE-IVP) describing the state of the system. Kinetic and thermodynamic data is compiled from the literature (some are tuned) and empirical correlations are used for heat and mass transfer phenomena. Complete details of the model are available in Wajge et al. [75]. The model has been tested against data in the plant.

This model has been used by Mitra et al. [48] for two-objective optimization using NSGA. The objectives were minimization of the reaction (or the batch) time, t_f ,

Table 3.1 Reaction scheme [75] of nylon 6 polymerization

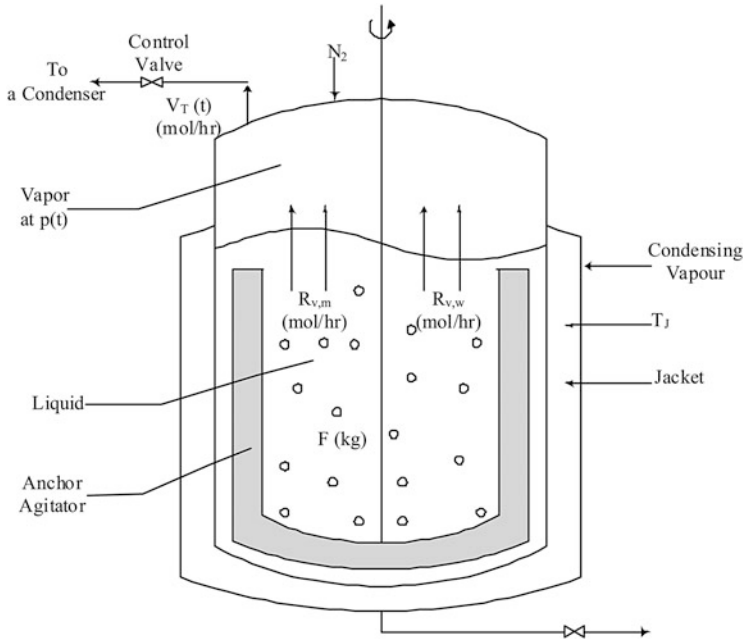
 Ring opening: $C_1 + W \rightleftharpoons S_1$

 Polycondensation: $S_n + S_m \rightleftharpoons S_{n+m} + W$

 Polyaddition: $S_n + C_1 \rightleftharpoons S_{n+1}$

 Ring opening of cyclic dimer: $C_2 + W \rightleftharpoons S_2$

 Polyaddition of cyclic dimer: $S_n + C_2 \rightleftharpoons S_{n+2}$

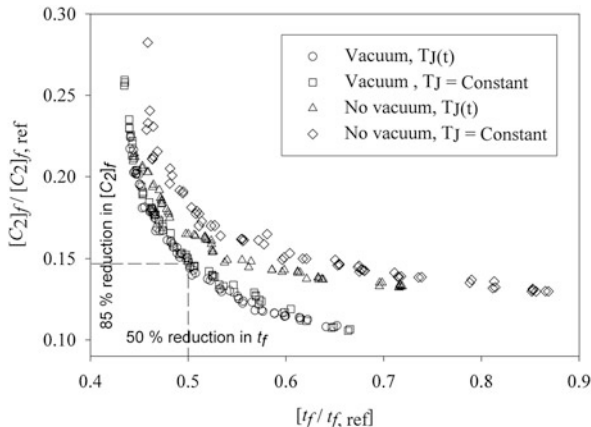
 $C_1 = \varepsilon$ -Caprolactam, $W =$ Water, $C_2 =$ Cyclic dimer, $S_n =$ Polymer chain with chain length, n
**Fig. 3.1** Nylon 6 polymerization in an industrial semibatch reactor (adapted from Ramteke and Gupta [57])

since this increases the annual production of the polymer, and minimization of the undesired side-product concentration of the cyclic dimer, $[C_2]$. The presence of cyclic compounds (of which C_2 is a representative) in the product leads to processing problems as well as gives an unacceptable finished fabric. The following two-objective optimization problem was solved (with penalty functions used for the constraints):

$$\min I_1[p(t), T_j] = t_f + w_1 \times \left[1 - \frac{x_m(t_f)}{x_{m,\text{ref}}}\right]^2 + w_2 \times \left[1 - \frac{\mu_n(t_f)}{\mu_{n,\text{ref}}}\right]^2 \quad (3.1)$$

$$\min I_2[p(t), T_j] = [C_2]_f + w_1 \times \left[1 - \frac{x_m(t_f)}{x_{m,\text{ref}}}\right]^2 + w_2 \times \left[1 - \frac{\mu_n(t_f)}{\mu_{n,\text{ref}}}\right]^2 \quad (3.2)$$

Fig. 3.2 MOO results (adapted from Ramteke and Gupta [57]) of an industrial nylon 6 semibatch reactor in nondimensional form for four different cases (with and without vacuum and with or without a history of the jacket fluid temperature). $[W]_0 = 3.45$ weight percent



$$w_1 = \text{large positive number for } x_m(t_f) < x_{m,ref}, \text{ otherwise } = 0 \quad (3.3)$$

$$w_2 = \text{large positive number for } \mu_n(t_f) \neq \mu_{n,ref} \pm \delta\mu_{n,ref}, \text{ otherwise } = 0 \quad (3.4)$$

End-point (at t_f) constraints were imposed on the monomer conversion, $x_m[x_m(t_f) \geq x_{m,ref}]$, in the product stream as well as on the number average chain length, $\mu_n[\mu_n(t_f) = \mu_{n,ref}]$, of the product. The decision variables used were the pressure *history* (a function of time, t), $p(t)$, of the vapor in the semi-batch reactor and the jacket fluid temperature, T_j (a constant). This was probably the first *trajectory* optimization problem solved using multi-objective GA. Both the minimization functions were converted to equivalent maximization functions using $\max F = [1/(1 + \min I)]$ since the MO-GA code used required all the objectives to be maximized. Pareto optimal solutions were obtained for a specified value of the feed water concentration, $[W]_0$. These studies were further extended recently [57] by incorporating vacuum operation (as done in another industrial reactor) and the use of amino caproic acid, S_1 , in the feed (S_1 was obtained from the depolymerization of scrap nylon 6). NSGA-II-aJG was used for solving four MOO problems: with and without a vacuum pump and with or without T_j being a function of time. Figure 3.2 shows the Pareto sets (in dimensionless form) for four different cases for $[W]_0 = 3.45$ weight percent.

One of the early applications of GA for chain-growth (free radical addition) polymerization was the SOO of a PMMA batch reactor [13]. As for nylon 6, a trustworthy model developed earlier [22, 67, 70] was used for optimization using SGA. The model comprises a reaction scheme, mass and energy balance equations using kinetic information, and several empirical equations for the heat and mass transfer rates. Details of these are available in Chakravarthy et al. [13]. The decision variable used is the temperature *history*, $T(t)$, while the objective function selected was the minimization of the reaction time, t_f . End-point constraints included the attainment of design values of the final monomer conversion, $x_{m,f} \equiv x_m(t_f) = x_{m,d}$, and of the number average chain length, $\mu_{n,f} \equiv \mu_n(t_f) = \mu_{n,d}$. Although,

the SGA algorithm served well for this SOO problem, it hardly touched upon the power of GA that lies in its ability to solve MOO problems effectively. Also, multiple objectives were actually present in this system. For example, the properties of the polymer are known to be dependent on the average molecular weight as well as on the breadth of the molecular weight distribution, as reflected through the polydispersity index, Q . The narrower the distribution, the better is the quality of the polymer. This leads to an MOO problem solved by Garg and Gupta [24]:

$$\min I_1[T_f] = t_f + w_1 \times \left[1 - \frac{x_m(t_f)}{x_{m,d}} \right]^2 + w_2 \times \left[1 - \frac{\mu_n(t_f)}{\mu_{n,d}} \right]^2 \quad (3.5)$$

$$\min I_2[T_f] = Q_f + w_1 \times \left[1 - \frac{x_m(t_f)}{x_{m,d}} \right]^2 + w_2 \times \left[1 - \frac{\mu_n(t_f)}{\mu_{n,d}} \right]^2 \quad (3.6)$$

$$w_1 = \text{large positive number for } x_m(t_f) < x_{m,d}, \text{ otherwise } = 0 \quad (3.7)$$

$$w_2 = \text{large positive number for } \mu_n(t_f) < \mu_{n,d}, \text{ otherwise } = 0 \quad (3.8)$$

End-point constraints were used on $\mu_{n,f}$ and $x_{m,f}$, as for the nylon 6 problem. Also, the minimization functions are converted to maximizations as described above. Interestingly, a *unique* optimal solution (instead of Pareto set) is obtained for this problem, a conclusion that was not apparent at the outset.

Similar to industrial batch reactors, GA is also applied effectively to optimize several other polymerizations. One application is the MOO of the continuous casting of PMMA films in a furnace. Methyl methacrylate (MMA), the monomer, is first pre-polymerized in a plug flow tubular reactor (PFTR) at a constant temperature, T_{PFR} , till a desired value of the monomer conversion, $x_{m,\text{PFR}}$, is attained. A concentration, $c_{I,0}$, of the initiator is used in the feed. Thereafter, the reaction mass passes in the form of a thin film of thickness, t_{film} , through a furnace that has an axial program of the temperature, $T_w(z)$. This study [79, 80] comprises two objectives: maximization of the cross section-average value of the monomer conversion at the end of the furnace, $x_{m,\text{av},f}$, and minimization of the length, z_f , of the furnace. Additionally, the cross section-average value, $\mu_{n,\text{av},f}$, of the number average chain length is constrained to be equal to a desired value, $\mu_{n,d}$, of commercial importance. Also, the temperature at *any* point in the film is constrained to lie below an upper safe value, to prevent degradation/discoloration of the polymer film (referred to as a local constraint). Optimal values of several decision variables, T_{PFR} , $c_{I,0}$, $x_{m,\text{PFR}}$, t_{film} , and the history, $T_w(z)$, are obtained. The constraints were taken care of by using the bracketed penalties described above. This formulation is solved using NSGA to obtain the Pareto optimal solutions [79, 80].

Recently, Agrawal et al. [3, 4] carried out the optimization of an industrial LDPE tubular reactor under steady state conditions, using multiple objective functions, both at the operation stage as well as at the design stage. Grade (of polymer)-change policies were also studied using the dynamic model for polymerization. NSGA-II and its JG adaptations were used. Usually, low-density polyethylene

is produced by the high pressure polymerization of ethylene in the presence of chemical initiators (e.g., peroxides, oxygen, azo compounds), in long tubular reactors. Very severe processing conditions are used, such as pressures from 150–300 MPa and temperatures from 325–625 K. Very flexible and branched polymer molecules are obtained. The typical conversion of ethylene per pass is reported to be 30–35 % and the unreacted ethylene is separated and recycled. Very severe operating conditions deteriorate the quality of the polymer due to the formation of undesired side products (short chain branching, unsaturated groups, etc.). The problem formulation comprises the minimization of these side products and the simultaneous maximization of the monomer conversion (for a given feed flow rate). The desired properties of the LDPE produced, e.g., the number-average molecular weight, are constrained to lie at desired values. Several MOO problems are formulated and solved to obtain the Pareto optimal solutions [3,4].

Polyethylene terephthalate (PET, the most common polyester) is an important commodity polymer. Bhaskar et al. [5–7] optimized the industrial production of PET in a third-stage, wiped-film finishing reactor using terephthalic acid (TPA) as one of the two monomers. The problem formulation comprises of two objective functions, namely, the minimization of the concentrations of the acid end groups (which lead to breakage of filaments during the high-humidity spinning operation) and of the vinyl end-groups (which lead to a coloration of the fiber) in the product. In order to maintain the strength of the fiber, the degree of polymerization of the product is restricted to a desired value [$\mu_{n,f} = \mu_{n,d} (= 82)$] using an equality constraint. Also, inequality constraints are imposed on the acid end-group concentration in the product and the concentration of the diethylene glycol end-group. The former is restricted below a specific value (one constraint is used) whereas the latter is maintained within some range (two constraints are used). These constraints are imposed to maintain the quality of the finished product in terms of the crystallinity and dyeability of the fiber. The three inequality constraints are taken care of by using penalty functions. Temperature was used as one of the decision variables. The MOO using NSGA was found to give a just a *single* optimal solution in each run. However, different solutions were obtained for multiple applications of the algorithm using different values of the random seed number [see Table 2.1 in Part I (Chap. 2)]. These solutions are found to be superior to current operating conditions in the industrial reactor, albeit by only a few percent. The non-dominated collection of all such solutions constituted a Pareto optimal front. This illustrates the inability of NSGA to converge to the Pareto set. This MOO problem is, thus, an unusual one and can be used as a test problem for developing improved optimization algorithms.

Apart from these, several interesting applications of GA to polymer reaction engineering [8,18,69] and polymer designing [72] have been reported. Silva and Biscaia [69] optimized the batch free radical polymerization of styrene. They maximized the monomer conversion rate and minimized the concentration of the initiator residue in the product. Deb et al. [18] optimized the initial stages of the epoxy polymerization process using NSGA-II. The objectives used in this study were the maximization of the number average molecular weight, minimization of the polydispersity index (which, strictly speaking, does not mean much physically), and minimization of

the reaction time. Pareto optimal results were obtained. These showed 300% improvement in the productivity over the benchmark values. Bhat et al. [8] reported the multi-objective optimization of the continuous tower process for styrene polymerization. The two objectives used were the maximization of the final monomer conversion and the minimization of the polydispersity index of the product. All these MOO studies show considerable improvement in the productivity as well as the quality of the product. This also gives the design engineer several choices of selecting the operating conditions. Unfortunately, sometimes the best operating conditions are not the most robust operating points. This is important in real-life situations where unavoidable fluctuations always exist in the process variables. Ramteke and Gupta [60] investigated such fluctuations in the process variables and obtained robust Pareto solutions for the industrial polymerization of nylon 6.

Application of GA to *experimental* online optimizing control of polymerization reactors is a challenging problem. It comprises two parts: re-tuning of the model parameters using measured variables (to negate the effects of model inaccuracies) and computation of *re-optimized* decision variables (to negate the effect of disturbances like heater failure, etc.). Usually, a single objective function such as the batch time is minimized while meeting the requirements on quality, e.g., $x_{m,f} = x_{m,d}$ and $\mu_{n,f} = \mu_{n,d}$. An optimal history of the decision variable [usually, the temperature, $T_{\text{opt}}(t)$] so computed, offline, is implemented on the reaction mass using controllers (using a slave computer with Labview). In between, a simulated disturbance, for example, switching off the electrical heater for a short period, is implemented on the reactor. During this time (as the temperature decreases with time), the two levels of the computer (the master and slave) retunes the model parameters using experimental data collected till then and compute the *re-optimized* temperature history, $T_{\text{re-op}}(t)$. This is implemented as soon as the electrical power comes back (the disturbance passes by). One of the first studies along this direction was that of online optimizing control of MMA polymerization in a specially made viscometer-cum-reactor assembly [44] using a “guided” version of SGA [so as to speed up the computation of $T_{\text{re-op}}(t)$ in about 6 real minutes]. The use of the JG operator in NSGA-II is particularly useful in the cases of online optimizing control due to its faster convergence compared to the usual NSGA-II. This was further illustrated by Bhat et al. [9] on a 1 L Labview-interfaced stainless steel batch reactor using NSGA-II-aJG. In this study, the power input to the stirrer-motor and the temperature history were used as a soft sensor to estimate, experimentally, the average molecular weight and the monomer conversion in the reaction mass at any time, thus identifying the *state* of the system (continuously). Sangwai et al. [66] extended the online optimizing control studies on PMMA polymerization in a viscometer-cum-reactor assembly for the more complex case of non-isothermal conditions using NSGA-II-aJG. In addition to the JG operation, the adaptation of the biogenetic law of embryology [59] was found to be quite effective in handling the complex problems of online optimizing control. In this adaptation, the offline results were used as a seed population, akin to the embryo, while solving actual online optimizing control problems. This reduces the computational efforts considerably. This is illustrated in Ramteke and Gupta [59] for the nylon 6 system.

3.3 Optimization of Catalytic Reactors

Catalytic reactors are an integral part of the chemical industry. These are commonly encountered in several petrochemical units and are associated with a turnover of billions of dollars. Multiple objectives are present quite naturally in these systems. Thus, MOO of these operations has been studied extensively [5, 45, 68]. A few interesting cases are discussed here, e.g., production of phthalic anhydride (PA) and maleic anhydride (MA), steam reforming, fluidized-bed catalytic cracking (FCC) of heavier components of crude oil like gas oil, to value-added lighter products, like gasoline or naphtha, etc.

Phthalic anhydride is a common raw material for polyester production. Commercially, it is produced using the gas phase catalytic oxidation of *o*-xylene in multi-tubular reactors. A single reactor tube involves several zones of catalysts with alternate regions in between either being hollow or having an inert packing. This is shown in Fig. 3.3a. The reaction scheme is shown in Fig. 3.3b. The reactions are highly exothermic and the hollow regions or inert packings in between the catalyst zones help keep the temperature of the gas within limits. The gaseous reaction mixture coming out of the reactor is processed in “switch” condensers operating alternately to separate the PA. At any time, the PA is condensed (and solidified) on the metal surface of *one* of the condensers, while in the other, the solidified PA is melted and the condenser made ready for use in the next cycle. The treated gas from the condensers is then scrubbed with water, or incinerated catalytically or thermally. This system has been modeled and multi-objectively optimized by Bhat and Gupta [10]. The mass and energy balance equations for this reactor are available in Bhat and Gupta [10]. The gas phase is described by ODE-IVPs while the nonlinear algebraic equations describe the *impervious* catalyst particles. The industrial reactor to be optimized comprises of nine catalyst zones with eight intermediate inert cooling zones. The state of the system is defined using 20 decision variables: the lengths, $L_1 - L_8$, of each of the eight catalyst beds (the length of the ninth catalyst bed is calculated by using of the total specified reactor length), lengths, $S_1 - S_8$, of the eight intermediate inert beds, concentration, c_{in} , of *o*-xylene (OX) in the feed per m^3 air at NTP, the temperature, $T_{F,in}$, of the feed, the mass flow rate, \dot{m} , of the co-currently flowing coolant, and the feed temperature, $T_{c,in}$, of the coolant. The two objective functions (with penalty functions) to be optimized for this reactor are maximization of the yield, X_{PA} , of PA and minimization of the total length, L_{cat} , of the (actual) catalyst bed [10]:

Objective functions:

$$\max I_1[\mathbf{u}] = X_{PA} + w_1 \times \left[1 - \frac{X_{PA}}{X_{PA,ref}} \right]^2 + w_2 \times \left[1 - \frac{L_{cat}}{L_{cat,ref}} \right]^2 + w_3 \quad (3.9)$$

$$\max I_2[\mathbf{u}] = \frac{1}{1 + L_{cat}} + w_1 \times \left[1 - \frac{X_{PA}}{X_{PA,ref}} \right]^2 + w_2 \times \left[1 - \frac{L_{cat}}{L_{cat,ref}} \right]^2 + w_3 \quad (3.10)$$

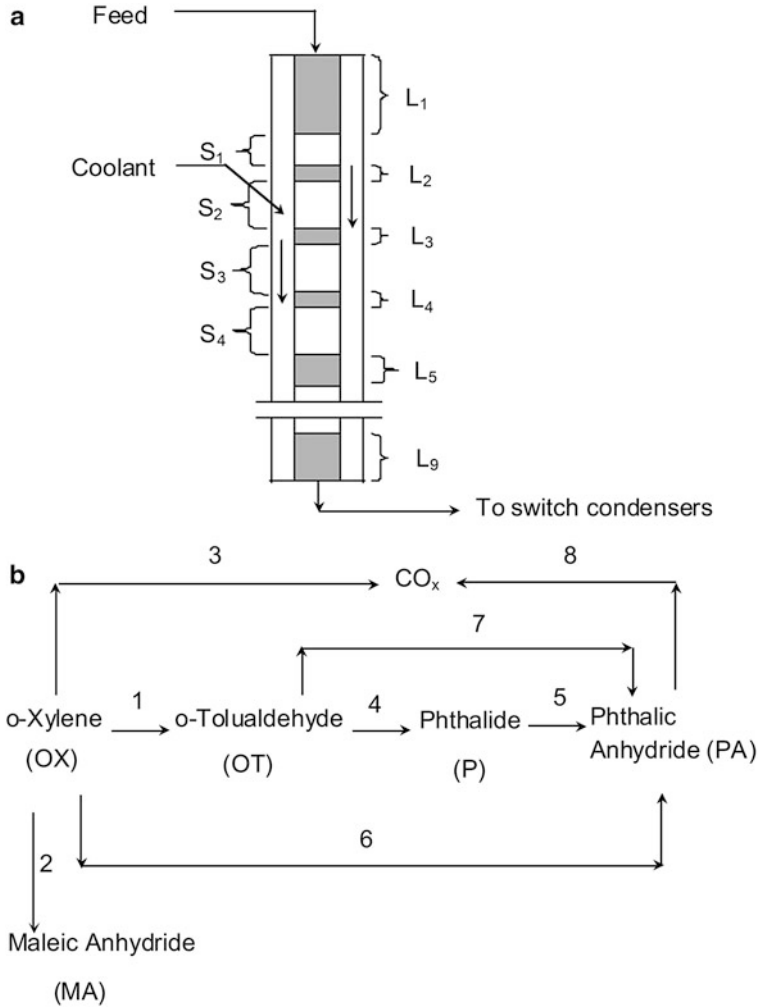


Fig. 3.3 (a) Reactor setup with nine catalyst zones for PA production and (b) the reaction scheme [10]

where, $\mathbf{u} = [c_{in}, T_{F,in}, T_{c,in}, \dot{m}, S_1, S_2, \dots, S_8, L_1, L_2, \dots, L_8]^T$ and $L_{cat} = \sum_{i=1}^9 L_i$ (3.11)

Subject to:

Constraints:

$$T_{max} \leq 510^\circ\text{C} \tag{3.12}$$

$$\text{Total length of the reactor tube, } L_{\text{tube}} = 3.5 \text{ m} \quad (3.13)$$

$$L_9 = 3.50 - \sum_{i=1}^8 L_i - \sum_{i=1}^8 S_i \quad (3.14)$$

$$\text{Model equations (Bhat and Gupta [10])} \quad (3.15)$$

Bounds:

$$65 \leq c_{\text{in}} \leq 85 \text{ g OX}/(\text{m}^3 \text{ air at NTP}) \quad (3.16)$$

$$147^\circ\text{C} \leq T_{F,\text{in}} \leq 287^\circ\text{C} \quad (3.17)$$

$$337^\circ\text{C} \leq T_{c,\text{in}} \leq 447^\circ\text{C} \quad (3.18)$$

$$0.001 \leq \dot{m} \leq 0.005 \text{ (kg coolant)/s} \quad (3.19)$$

$$0.2 \leq S_i \leq 0.45 \text{ m, } i = 1, 2, \dots, 7 \quad (3.20)$$

$$0.1 \leq S_8 \leq 0.45 \text{ m,} \quad (3.21)$$

$$0.05 \leq L_1 \leq 0.9 \text{ m,} \quad (3.22)$$

$$0.01 \leq L_i \leq 0.2 \text{ m, } i = 2, 3, \dots, 8 \quad (3.23)$$

The values of $X_{\text{PA,ref}} = 1.2$ and $L_{\text{cat,ref}} = 3.6$ m are used as reference values in the penalty functions (somewhat arbitrarily). The values of $L_1 - L_8$ and $S_1 - S_8$ are selected optimally by the optimization algorithm. L_9 is then *computed* using Eq. (3.14). The weighting functions in the penalties used for constraint-violations are selected as:

$$\text{if } X_{\text{PA}} \leq 1.1, w_1 = -500; \text{ else } w_1 = 0 \quad (3.24)$$

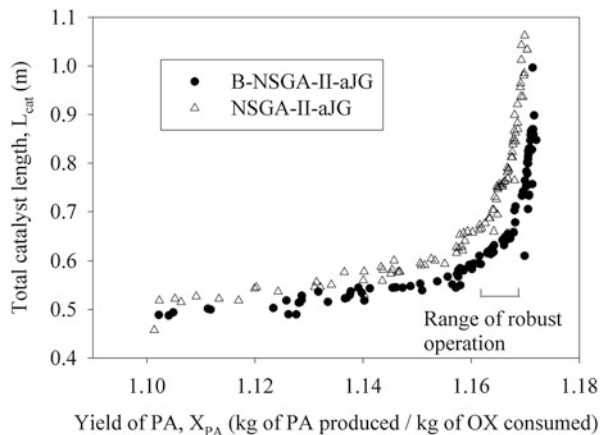
$$\text{if } L_9 \leq 0 \text{ m, } w_2 = -3000; \text{ else } w_2 = 0 \quad (3.25)$$

$$\text{if } T_{\text{max}} \leq 510^\circ\text{C in bed } i, i = 1, 2, \dots, 9; w_3 = 0; \text{ else } = -3000 + 250(i - 1) \quad (3.26)$$

$$\text{if } L_i \geq 0.01 \text{ m, } i = 1, 2, \dots, 9; w_3 = 0; \text{ else } w_3 = -300 \quad (3.27)$$

The system parameters are given as: diameter of each reactor tube = 25 mm, mass flux, $G = 19,455 \text{ kg m}^{-2}\text{h}^{-1}$, and diameter of the $\text{V}_2\text{O}_5 - \text{TiO}_2$ catalyst particles = 3 mm. This optimization problem has been solved by Bhat and Gupta [10] using a slightly adapted version of NSGA-II-aJG. Also, the same problem has

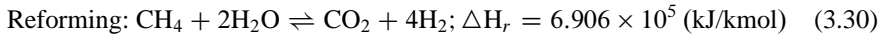
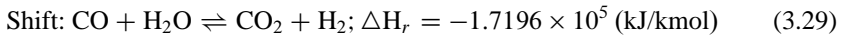
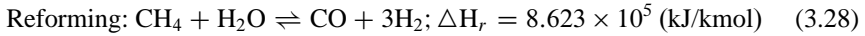
Fig. 3.4 Pareto-optimal front for the two-objective optimization problem (Eqs. 3.9–3.27) of PA production in a nine-bed tubular catalytic reactor (25 generations) (adapted from Ramteke and Gupta [59])



been used as a test problem for the Alt-NSGA-II-aJG [58]. The results obtained by the latter algorithm were better than those from NSGA-II-aJG. Further, the study was extended by Ramteke and Gupta [59] using the Biogenetic-NSGA-II-aJG adaptation in which the seed solutions from the 7-catalyst bed MOO problem (with 16 decision variables) are used. This gave optimal solutions in around 25 generations (see Fig. 3.4) whereas NSGA-II-aJG (without seeds) took around 71 generations.

Maleic anhydride (MA) is used for the production of unsaturated polyester resins. It is commercially produced using fixed bed catalytic reactors with VPO catalyst and with n-butane as the raw material. An improved model has been developed recently by Chaudhari and Gupta [14]. The model incorporates Langmuir–Hinshelwood kinetics. This model is similar to that of PA reactors and comprises of ODE-IVPs for the gas phase and ODE-BVPs for the porous catalyst phase. The ODE-BVPs of catalyst phase are converted into nonlinear algebraic equations using the orthogonal collocation (OC) technique. The ODE-IVPs are solved using Gear’s algorithm (D02EJF subroutine from NAG library) whereas the nonlinear algebraic equations are solved using the modified Powell’s hybrid method (C05NBF from NAG library). The MO optimization problem comprises of combinations of several objective functions chosen from among maximization of the productivity, minimization of the operating cost, and minimization of the pollution. The MOO problems are solved using NSGA-II-aJG. The problems are also solved using the Alt-NSGA-II-aJG. Interestingly, the latter algorithm was found to be superior to NSGA-II-aJG for this *two*-objective problem but inferior for the *three*-objective problems. Details are available in Chaudhari and Gupta. [14]

Steam reforming is used for the production of synthesis gas and hydrogen from natural gas. A typical steam reforming unit consists of the reforming reactor, a shift converter, and a pressure swing adsorption (PSA) unit. The reaction scheme [51,56] for a feed of methane is given by:



Methane is mixed with steam and recycle hydrogen in the reforming reactor where it is converted to CO and H₂. This processed gas mixture is cooled by exchanging heat with the boiler feed water. The cooled gas is further processed in the two-stage adiabatic shift converter where CO is converted to CO₂ and more H₂ is produced. The exothermic heat of reaction increases the temperature of the gas mixture. The heated gas leaving the shift converter again releases heat to the boiler feed water to produce very high pressure (VHP) steam. This cooled gas mixture is then treated in a pressure swing adsorption (PSA) unit to separate out the hydrogen and the off-gases. These off-gases with additional fuel are burned in the furnace associated with the reforming reactor to supply the required endothermic heats of reaction. This operation has been optimized using multiple objectives by Rajesh et al. [56]. The objectives of the study were the minimization of methane feed rate and maximization of the flow rate of carbon monoxide in the synthesis gas for a fixed rate of production of hydrogen. A Pareto optimal front is obtained. The details of the model and the results can be obtained from Rajesh et al. [56]. This study has been extended for the dynamic operation of steam reformers by Nandasana et al. [51]. The problem comprises of the minimization of the *cumulative* disturbances of H₂ and CO production for a given (simulated) disturbance in the input feed flow rate of methane. The details of the formulation and the results are available in Nandasana et al. [51].

Fluidized-bed catalytic cracking (FCC) is another important conversion operation in most integrated refineries. The FCC unit (FCCU) comprises two important equipment: the riser reactor to catalytically crack heavy crude-fractions like gas oil to gasoline or naphtha, and the regenerator to burn off the deposited coke inside the porous catalyst particles. An industrial FCCU has been modeled and optimized by Kasat et al. [38] using NSGA-II. The model comprises a five-lump kinetic scheme. Several MOO problems were formulated. The objective functions used are maximization of gasoline yield, minimization of air flow rate, and minimization of the percent CO present in the flue gas. The study was further extended using the jumping gene adaptation, NSGA-II-JG. Indeed, this was the first application of this adaptation in chemical engineering. The results obtained using NSGA-II-JG were found to be superior and the new algorithm was faster as compared to the original NSGA-II. The details of the model and results can be obtained from the respective references. The MOO of hydrocracking reactors using NSGA-II was studied by Bhutani et al. [12]. Several such studies have been listed extensively by Masuduzzaman and Rangaiah [45] and Sharma and Rangaiah [68].

3.4 Optimization of Separation Equipment and Network Problems

Separations equipment and networks play an important role in chemical engineering. The overall cost effectiveness of chemical plants depends significantly on the effective application of separations units. This leads to several interesting optimization studies. These include the optimization of scrubbers, cyclones, adsorbers, froth floatation units, etc. Among these, the optimization of froth floatation is described in detail and the MOOs of other units, including heat exchanger networks (HENs), are described briefly.

Froth floatation is used for separating valuable minerals, associated minerals, and gangue from their finely ground ores. The process utilizes differences in the surface properties of the minerals involved. In this process, finely ground ore comprising of a mixture of minerals is suspended in an aerated liquid in which a froth is generated using frothing agents (surfactants). In such conditions, one of the constituents from the mixture, which is more difficult to wet by the liquid, tends to adhere preferentially to the gas bubbles. The gas bubble-particle aggregates having a lower effective density rise to the surface and float leading to a froth rich in a given constituent. The froth is continuously discharged through an overflow weir as a concentrated stream. Efficient separation depends on the percent loading of the solids, type of frothing agent, rate of aeration, the pH of the aerated liquid, etc. A typical flotation cell comprises of a single feed stream and two exit streams, a mineral-rich concentrated stream, and gangue-rich tailings. The performance of the flotation cell is measured using two parameters: recovery, R_c , and grade, G . The former is the ratio of the flow rates of the solid in the concentrated stream to that in the feed stream, whereas the latter is the fraction of the valuable mineral in the concentrated stream. Usually, several flotation cells are used in combination (circuit) to increase the overall separation efficiency. A common strategy to improve the grade is to introduce the feed to a rougher cell and the concentrate stream from it is further refloatated subsequently in more and more cleaner cells, whereas the gangue-rich tailings are refloatated in scavenger cells. Mineral beneficiation is a billion dollar business and is used for the processing of several thousands of tons of ore per year. Clearly, the marginal improvement in the overall efficiency can have significant economic impact. Moreover, minerals are gradually depleting and it is becoming increasingly important to extract lower-quality ores. This gives significant impetus for the optimal design of froth floatation circuits.

Guria et al. [30] modeled and optimized (for SOO and MOO) a general circuit [46] having two flotation units. The schematic of such a simple circuit is shown in Fig. 3.5. A feed of just two species, valuable and gangue, is fed to the circuit. The objective of the study is to maximize the overall recovery (R_c) of the concentrate while maintaining the desired grade (G_d) of the concentrate and having a desired value of the total volume (V_d) of the cells. The decision variables are the two residence times, λ ($\equiv [\lambda_1, \lambda_2]^T$), and the cell-linkage parameters, β ($\equiv [\beta_{10}, \beta_{11}, \beta_{12}, \beta_{20}, \beta_{21}, \beta_{22}]^T$) and δ ($\equiv [\delta_{F1}, \delta_{F2}, \delta_{10}, \delta_{11}, \delta_{12}, \delta_{20}, \delta_{21}, \delta_{22}]^T$). The SOO formulation is given as:

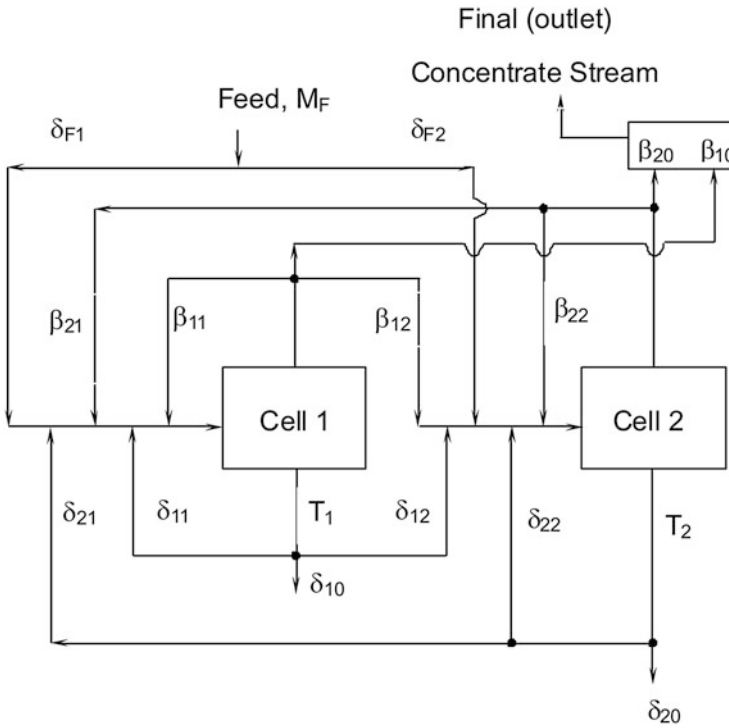


Fig. 3.5 Generalized froth flotation circuit (adapted from Guria et al. [30]) with two cells

Objective function:

$$\max I_1[\lambda, \beta, \delta] = R_c \tag{3.31}$$

Subject to:

Constraints:

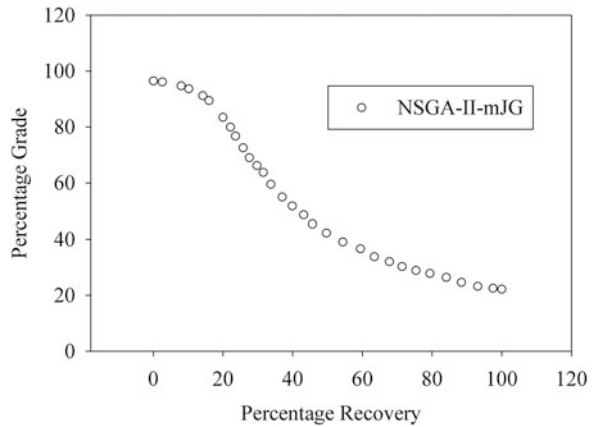
$$G = G_d; V = V_d \tag{3.32}$$

$$\sum_{i=1}^m \delta_{F,i} = 1.0 \tag{3.33}$$

$$\sum_{i=1}^m \delta_{k,i} = 1.0; k = 1, 2, \dots, m \tag{3.34}$$

$$\sum_{i=1}^m \beta_{k,i} = 1.0; k = 1, 2, \dots, m \tag{3.35}$$

Fig. 3.6 Pareto-optimal front (adapted from Guria et al. [30]) for the MOO of a froth flotation circuit



$$\text{Model equations [30]} \quad (3.36)$$

Bounds:

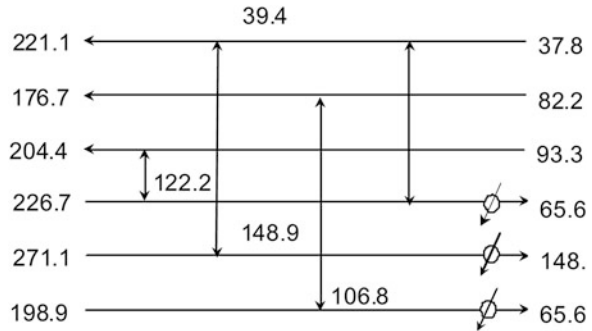
$$0 \leq \beta \leq 1; 0 \leq \delta \leq 1 \quad (3.37)$$

$$\lambda_{i,L} \leq \lambda_i \leq \lambda_{i,U}; i = 1, 2 \quad (3.38)$$

Here, m represents the number of cells ($= 2$). Equations (3.33)–(3.35) ensure the sum of the fractions of the split streams to be equal to 1. The problem comprises of a total of 16 variables and five constraints. The other details can be obtained from Guria et al. [30]. These workers have solved this problem using NSGA-II-mJG. The results obtained were found to be superior to those of Mehrotra and Kapoor [46] using the conventional Luus Jaakola [43] technique (it is clear that the latter algorithm led to local optimal solutions instead of a global optimum). The study was extended for multiple objectives with the maximization of the overall grade (G) being the second objective function. The Pareto optimal front for this MOO study is shown in Fig. 3.6. The study was further extended to the MOO of an industrial fluorspar beneficiation plant [32].

Cyclone separators (or just cyclones) are frequently used for vapor-solid separations in the chemical industry. Most of the early designs were based on practical experience. These crude designs, however, required further refinement. Also, in the competitive industrial environment of today, optimization of these units is desired. One such study was carried out by Ravi et al. [63] to optimize a train of several industrial cyclone units using NSGA. The MOO problem comprises of two objectives, the maximization of the overall collection efficiency and the minimization of the pressure drop. The decision variables used were the number of cyclones and some geometric parameters of the cyclones, e.g., diameter of the cyclones, diameter of the exit pipe, diameter of the base of the cyclone, total height of the cyclone, depth of the exit pipe, height of the cylindrical portion of the cyclone,

Fig. 3.7 A typical simple heat exchanger network (adapted from Agarwal and Gupta [2])



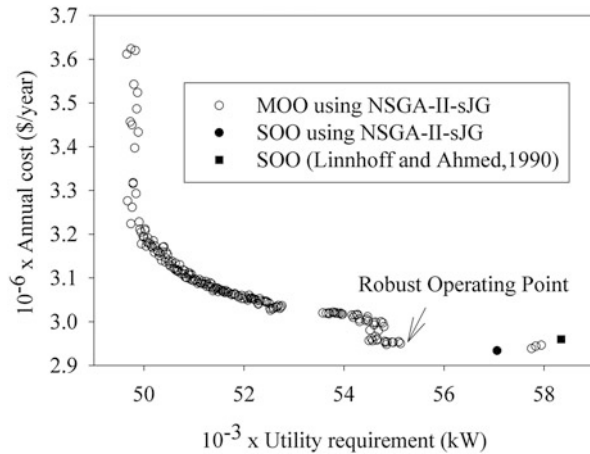
height of the cyclone inlet, width of the cyclone inlet, and inlet vapor velocity. Pareto optimal fronts were obtained using NSGA. The study gave important insights that the diameters of the cyclones and vortex finder, and the number of cyclones used in parallel, are critical parameters in deciding the optimal performance. More recently, the MOO of cyclone separators using GA was investigated by several researchers [55, 65]. Ravi et al. [64] further extended their study for the MOO of venturi scrubbers. These are used for the separation of gaseous pollutants. The objectives used were the maximization of the overall collection efficiency and the minimization of the pressure drop. Pareto optimal fronts for this system were again obtained. Details can be had from the respective references.

The principle of adsorption is used in a variety of processes for separation. Adsorption in a chromatographic process such as a simulated moving bed (SMB) system or the Varicol process is one such interesting operation. These are used in the pharmaceutical sector for the separation of large-scale fractionation of xylene isomers or sugar isomers. One of the earliest MOO studies of this operation was reported by Zang et al. [77, 78] and Subramani et al. [71]. The objectives used were the simultaneous maximization of the productivity and of the purity. Pareto optimal fronts were obtained using NSGA. The results reported by Subramani et al. [71] show significant improvement for both the SMB and Varicol processes. These studies were extended by several other researchers from same group.

GA has also been applied to several other separation processes such as membrane separations [76], desalination [31], and crude distillation [37]. Details may be obtained from the respective references.

Network systems similar to the froth flotation circuits discussed above, are quite commonly encountered in chemical engineering. Important examples are heat exchanger networks (HENs) and networks incorporating several heat exchangers and distillation units. Optimal designing of heat exchanger networks is an important chemical engineering problem. Recently, Agarwal and Gupta [2] optimized heat exchanger networks using NSGA-II-sJG and NSGA-II-saJG. A typical simple heat exchanger network studied by these workers is shown in Fig. 3.7. It comprises of three cold streams (the upper three horizontal lines with the arrows pointed toward the left) and three hot process streams (lower three horizontal lines with arrows pointed to the right). The heat exchange between these streams is shown by vertical

Fig. 3.8 Pareto-optimal front for MOO of heat exchanger network (adapted from Agarwal and Gupta [2])



connecting lines. The objectives of the study are minimization of the annualized cost and minimization of the total hot and cold utility (water and steam) required, the latter fast becoming a scarce natural resource. The decision variables used are the number of intermediate heat exchangers (which decrease the utility requirements but increase the capital cost) and the intermediate temperatures of the streams. An important point in such problems is that since the number of heat exchangers is not a fixed value, the number of decision variables is different for different chromosomes. That is, the length of the chromosome changes dynamically. The sJG and saJG adaptations handle such unequal lengths of chromosomes. One of the formulations solved by Agarwal and Gupta [2] is:

Objective function:

$$\max I_1 = \text{Annual cost} \quad (3.39)$$

$$\min I_2 = \text{Total requirement of the hot + cold utility (kW)} \quad (3.40)$$

Subject to:

Constraints:

$$\text{Model equations (Agarwal and Gupta [2])} \quad (3.41)$$

Complete details of the model can be obtained from Agarwal and Gupta [2]. The MOO results are shown in Fig. 3.8. The results are also compared with SOO results obtained by the *heuristic* approach of Linnhoff and Ahmed [42]. The MOO results give an important insight for selecting the operating point, which in this case is to operate the system at a slightly higher value of the annual cost since it reduces the total utility requirement from about 58,000 kW for the single-objective solution (min cost) to about 54,000 kW (see Fig 3.8). Several studies on separation units have been listed extensively by Masuduzzaman and Rangaiah [45] and Sharma and Rangaiah [68].

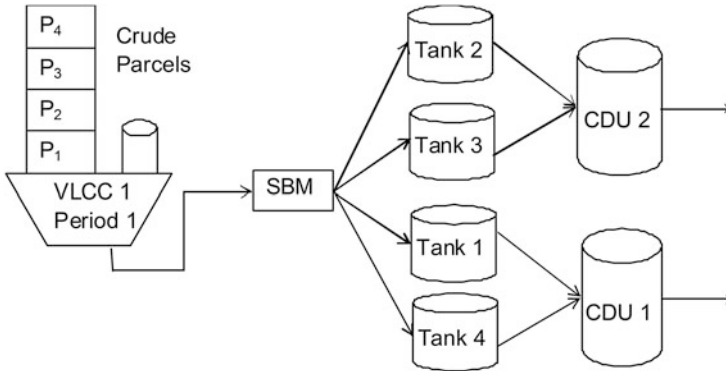


Fig. 3.9 A simple crude oil scheduling problem (adapted from Ramteke and Srinivasan [62])

3.5 Planning and Scheduling Optimization of Chemical Processes

Scheduling and planning problems are conventionally optimized [47] using linear programming (LP) solvers. Recently, however, the use of evolutionary algorithms such as GA has become popular for solving such problems due to the distinct advantages they offer for solving problems involving multiple objectives. Also, several studies have been reported using hybrid LP-GA. The crude oil scheduling optimization of a marine-access refinery is explained in detail.

Crude oil scheduling in marine-access refineries involves the unloading of crude from ships into storage tanks and thereafter charging the crude to distillation units (CDUs). Usually, crudes arrive in very large crude carriers (VLCCs) with compartments for multiple crude parcels, or in smaller, single-parcel ships. VLCCs are docked off-shore at a single buoy mooring (SBM) station whereas small ships can be unloaded directly at on-shore jetties. The operation involves simultaneous unloading of several ships. The continuous fluctuation in oil prices makes the refinery business highly agile in nature. Also, low profit margins put an excessive pressure for optimum planning and scheduling to increasing the throughput, intelligent use of less expensive stocks, reduction in logistics and demurrage (waiting) costs, and better control. Ramteke and Srinivasan [62] have solved several SOO and MOO problems for crude scheduling of large-scale refinery operations using the structure-adapted GA (SAGA).

A simple representation of the crude oil scheduling problem is given in the Fig. 3.9. It comprises of a single VLCC unloading of four different parcels, $P_1 - P_4$, one by one in four tanks, Tanks 1–4. The crude from these tanks is then charged to two CDUs, CDU 1 and CDU 2. The profit margin on processed crude depends on the components present in the crude. Different parcels have different compositions that change continuously while charging and discharging them from the tanks. Also, CDUs have restrictions on the processing compositions. Clearly, the unloading of the crude to the tanks and then charging to the CDUs requires intelligent planning

and scheduling in order to maximize the profit. Ramteke and Srinivasan [62] have solved several SOO and MOO problems. The system is modeled using a discrete-time formulation. In such a formulation, the scheduling horizon is divided into several equal-length time-periods. The flow rates of the various streams remain constant during a time period but change across time periods. The flow rates of the streams for all the time periods represent the decision variables. Also, the flow rates of the streams are constrained based on the flow rates of the streams in the previous and the successive time periods. This leads to a significantly high number of decision variables and constraints. Complete details can be obtained from Ramteke and Srinivasan [62]. The objectives used were the maximization of the profit and the minimization of the fluctuations in the crude charging to the CDUs. The formulation is:

Objective function:

$$\max I_1 = M - L - P \quad (3.42)$$

$$\min I_2 = \sigma^2 - P \quad (3.43)$$

Subject to:

Constraints:

$$\text{Model equations [62]} \quad (3.44)$$

In Eq. (3.42), M is the total margin after processing the crude, L is the total logistics cost, and P is the total penalty for violating the minimum fill required in the tank, exceeding the demand and violating the quality specifications. In Eq. (3.43), σ^2 is the square of differences of the successive inter-period flow rates of the crude. The number of decision variables and constraints associated with this problem is of the order of several thousands. Obviously, solving such a large system of equations using the stochastic procedure of GA is a herculean task. However, the concepts of graphs play an important role in reducing the size of the algorithm to manageable limits of the order of a few hundred variables (still too large compared to usual applications of GA where it is of the order of about a hundred). Here, most of the combinatorial constraints are taken care of by the graph that would otherwise have required tackling using penalty functions. The results obtained using SAGA for SOO formulations are close to those obtained using mixed-integer LP (MILP) solvers, and in some cases are even better. However, the most important observation is in terms of the CPU time that scales linearly with size using SAGA compared to MILP. For a simple problem, MOO results have also been obtained. The optimal results were found to reduce the fluctuations in the CDU flow rates considerably (see Fig. 3.10). Also, the CPU time required for solving these problems is quite low (of the order of hours for several problems) compared to the requirement for LP-GA hybrid procedures for similar formulations [50]. More details of the model and the optimization can be obtained from Ramteke and Srinivasan [62].

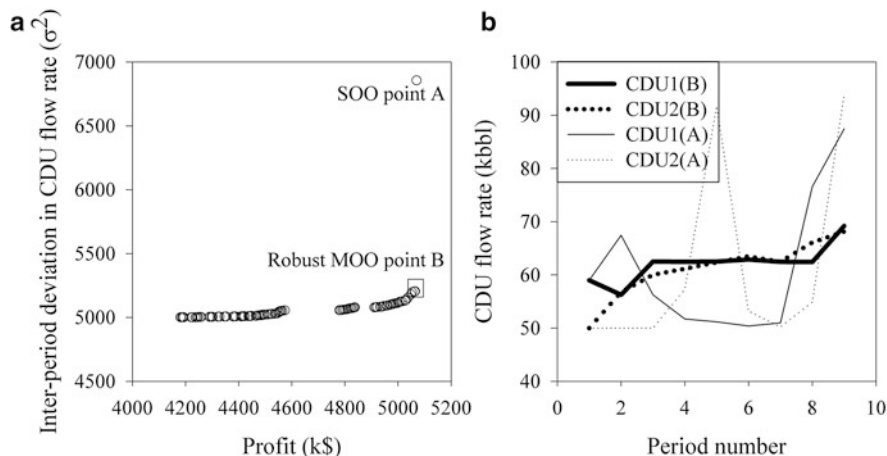


Fig. 3.10 (a) Pareto-optimal front for the MOO of a simple refinery crude oil scheduling problem shown in Fig. 3.9 and (b) the further analysis of a selected point, A (obtained for SOO), and the robust optimal point, B, obtained using MOO (adapted from Ramteke and Srinivasan [62])

In polymerization plants, generally, several grades of product are produced from the same reactor. A common example is the production of different grades of polymer based on their tint. Usually, the polymer produced from the reactor is processed further through different parallel extruders. The sequence of predecessor and successor grades decides the transition times and the amount of off-spec production. Thus, the selection of an optimal sequence of production of multiple grades is an important problem and is commonly referred to as short-term scheduling. Ramteke and Srinivasan [61] have modeled and optimized such short-term scheduling of a multi-product polymer plant using both SOO and MOO. They have used real-coded adapted GA. The formulation utilizes a continuous-time representation. The objectives used were the minimization of make-span and the minimization of lateness. The results obtained were comparable to those from MILP solvers. Process scheduling and planning problems have been extensively studied using GA in the literature. Details can be had from the reviews by He and Hui [33], Oliveira et al. [52], Masuduzzaman and Rangaiah [45], and Sharma and Rangaiah [68].

3.6 Optimization of Combinatorial Problems

Many real-life situations often lead to combinatorial formulations. In these, the input variables are combinatorial sequences. A popular and simple combinatorial optimization problem is the travelling salesman problem (TSP). In this problem, a salesman has to visit each city once from the given set of cities and finally return to the starting city. The objective function is to minimize the total distance travelled.

The decision variable is the sequence of cities which the salesman has to visit. Such situations are commonly encountered in scheduling and planning of chemical plants, protein folding, etc. Straightforward application of GA to such problems is a futile exercise since only a few of the combinatorial sequences generated randomly are feasible [23]. Thus, in most of the cases the procedure of identifying the feasible sequences are incorporated in the initial generation and operating procedures of GA. One such interesting illustration of the application of GA is protein folding, as reported by Unger and Moulton [73] using Dill's HP model [20]. In this, the amino acids are categorized into two types based on the hydrophobic (H) and polar (P) nature of its residues. The formulation [35, 41, 73, 74] is as follows:

Objective function:

$$\min I_1(\sigma) = \left(\sum_{i,j} \Delta r_{i,j} E_{i,j} \right)_{\sigma}; i, j \in [1, n] \quad (3.45)$$

$$\text{where } E_{i,j} = -1 \text{ for each non-bonded H-H contact, otherwise } = 0 \quad (3.46)$$

$$\Delta r_{i,j} = 1 \text{ when } s_i \text{ and } s_j \text{ are adjacent but not connected amino acids,} \\ \text{otherwise } = 0 \quad (3.47)$$

Subject to:

Constraints:

$$\text{Amino acids fill in the lattice of 2D or 3D in non-self-intersecting paths} \quad (3.48)$$

Here, σ is the variable representing the sequence of non-bonded adjacent amino acids, n is the total number of amino acids present in the protein molecule, and $E_{i,j}$ represents the energy of interaction between s_i and s_j adjacent, but not connected, amino acids. For a simple problem of 36 amino acids with a sequence PPPHHPPHPPPPHHHHHHPPHPPHPPHPPHPPHPP, the optimum conformation is obtained by Unger and Moulton [73] for a 2D lattice using SGA with some modified moves. The optimal conformation obtained is found to comprise all the hydrophobic residues embedded inside the surrounding polar residues, which agree well with reality. For a given sequence of amino acids the lowest energy conformation is obtained at an average energy of -14 . The details can be obtained from Unger and Moulton [73]. These studies are further extended in the literature [35, 41, 74] for more complex cases of 3D folding. Although, the global optimum is not guaranteed using GA for such problems owing to its NP (non-deterministically polynomial time) complete nature and the energy functions used are too simplified compared to reality, it still provides very good starting solutions for more rigorous deterministic searching. Similar challenges are commonly seen in various other NP complete problems such as the travelling salesman, graph coloring, knapsack problems, etc. This is also illustrated in the adaptations used for planning and scheduling problems described above. Several recent advances for such problems have been reviewed by Hu et al. [36].

3.7 Application of GA to Data-Driven Problems

Very often, large amounts of data are generated in rigorous experimentation or simulation (molecular dynamics, computational fluid dynamics, finite element methods, etc.) of real-life processes. Optimization of such processes is often associated with the use of data-driven models. These models represent a simplified version of the rigorous model used to generate the data. Thus, these are associated with several challenges in order to represent the system accurately and at the same time keeping the formulation simple. Frequently, concepts from several other artificial intelligence techniques are combined with evolutionary algorithms to handle such systems. Recently, evolutionary neural networks (EvoNN [49, 53, 54]) and bi-objective genetic programming (BioGP [26, 27]) have been applied to handle data-driven problems in materials science for steel making [11, 40]. One such application of real-coded NSGA-II for process monitoring optimization of the Tennessee Eastman challenge process [21] is reported by Ghosh et al. [25].

The Tennessee Eastman challenge process is a popular test process used for analyzing the process monitoring models and comprises of a reactor, a compressor, a condenser, a separator, and a stripper unit. The process involves the reaction of gaseous reactants, A, C, D and E, in the presence of an inert, B, to produce liquid products, G and H, with a by-product, F. Process monitoring involves a total of 52 measured variables comprising 19 composition measurements, 22 process measurements and 11 manipulated variables. These are recorded every 3 min. The data comprises 21 kinds of programmed known faults. The 500 samples from normal operating conditions and 480 samples from normal and each of the 21 fault conditions are present in training and validation datasets, respectively. The problem formulation involves the minimization of missed detection rate (MDR) plus false alarm rate (FAR) and minimization of the number of variables (N) used in the reduced principle component analysis (PCA) model as follows [25]:

Objective function:

$$\min I_1(\sigma) = \text{MDR} + \text{FAR} \quad (3.49)$$

$$\min I_2(\sigma) = N \quad (3.50)$$

Subject to:

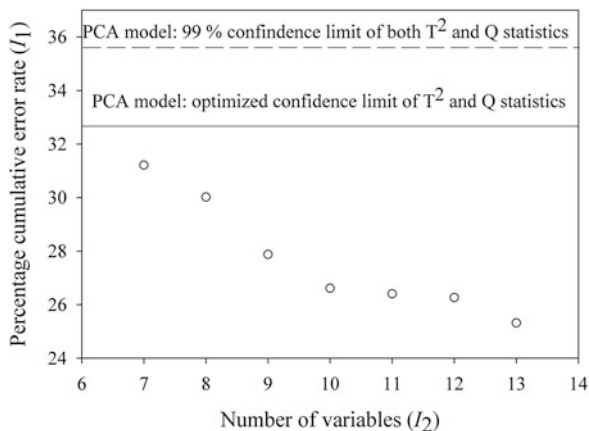
Constraints:

$$\text{Datasets [15, 21, 25]} \quad (3.51)$$

$$\text{Reduced PCA model equations [25]} \quad (3.52)$$

Here, σ represents the reduced set of selected variables from a total of 52. The results obtained using real-coded NSGA-II are plotted in Fig. 3.11, which shows that the performance improves significantly by combining GA and reduced PCA over

Fig. 3.11 Pareto-optimal front for the Tennessee Eastman challenge problem using real-coded NSGA-II (adapted from Ghosh et al. [25])



PCA. The minimization of the number of variables particularly helps in reducing the false alarm rate by 3.6 %, while simultaneously reducing the missed detection rate. Further details can be obtained from the respective references.

3.8 Closure

The last four decades have seen the complete revamping of the area of optimization from derivative-based SOO to computationally intensive stochastic MOO. GA has played a pioneering role in knocking the doors of stochastic optimization, which, earlier, was thought as a distinct dream, at least for real-life chemical engineering applications. The performance of production units, separations units, and even decision-making has improved immensely with the use of GA. Even the most complex model equations of these systems with variables ranging from over several thousand and with multiple objectives are now handled with ease. In the process, many faster and flexible versions of GA have been developed. While computing has become easier, new challenges are continually opening up in interdisciplinary areas such as complex biological systems, energy applications, biomedical applications, etc.

References

1. Aatmeeyata, Gupta, S.K.: Simulation and optimization of an industrial nylon 6 reactor: a review. *Polym. Plast. Technol. Eng.* **37**, 201–239 (1998)
2. Agarwal, A., Gupta, S.K.: Multi-objective optimal design of heat exchanger networks using new adaptations of the elitist non-dominated sorting genetic algorithm, NSGA-II. *Ind. Eng. Chem. Res.* **47**, 3489–3501 (2008b)

3. Agrawal, N., Rangaiah, G.P., Ray, A.K., Gupta, S.K.: Multi-objective optimization of the operation of an industrial low-density polyethylene tubular reactor using genetic algorithm and its jumping gene adaptations. *Ind. Eng. Chem. Res.* **45**, 3182–3199 (2006)
4. Agrawal, N., Rangaiah, G.P., Ray, A.K., Gupta, S.K.: Design stage optimization of an industrial low-density polyethylene tubular reactor for multiple objectives using NSGA-II and its jumping gene adaptations. *Chem. Eng. Sci.* **62**, 2346–2365 (2007)
5. Bhaskar, V., Gupta, S.K., Ray, A.K.: Applications of multiobjective optimization in chemical engineering. *Rev. Chem. Eng.* **16**, 1–54 (2000a)
6. Bhaskar, V., Gupta, S.K., Ray, A.K.: Multiobjective optimization of an industrial wiped film poly (ethylene terephthalate) reactor. *AIChE J.* **46**, 1046–1058 (2000b)
7. Bhaskar, V., Gupta, S.K., Ray, A.K.: Multiobjective optimization of an industrial wiped-film PET reactor: some further insights. *Comput. Chem. Eng.* **25**, 391–407 (2001)
8. Bhat, S.A., Sharma, R., Gupta, S.K.: Simulation and multiobjective optimization of the continuous tower process for styrene polymerization. *J. Appl. Polym. Sci.* **94**, 775–788 (2004)
9. Bhat, S.A., Gupta, S., Saraf, D.N., Gupta, S.K.: On-line optimizing control of bulk free radical polymerization reactors under temporary loss of temperature regulation: an experimental study on a 1-liter batch reactor. *Ind. Eng. Chem. Res.* **45**, 7530–7539 (2006)
10. Bhat, G.R., Gupta, S.K.: MO optimization of phthalic anhydride industrial catalytic reactors using guided GA with the adapted jumping gene operator. *Chem. Eng. Res. Des.* **86**, 959–976 (2008)
11. Bhattacharya, B., Kumar, G.R.D., Agarwal, A., Erkoc, S., Singh, A., Chakraborti, N.: Analyzing Fe - Zn system using molecular dynamics, evolutionary neural nets and multi-objective genetic algorithm. *Comput. Mater. Sci.* **46**, 821–827 (2009)
12. Bhutani, N., Ray, A.K., Rangaiah, G.P.: First-principles, data-based, and hybrid modeling and optimization of an industrial hydrocracking unit. *Ind. Eng. Chem. Res.* **45**, 7807–7816 (2006)
13. Chakravarthy, S.S.S., Saraf, D.N., Gupta, S.K.: Use of genetic algorithms in the optimization of free radical polymerizations exhibiting the Trommsdorff effect. *J. Appl. Polym. Sci.* **63**, 529–548 (1997)
14. Chaudhari, P., Gupta, S.K.: Multi-objective optimization of a fixed bed maleic anhydride reactor using an improved biomimetic adaptation of NSGA-II. *Ind. Eng. Chem. Res.* **51**, 3279–3294 (2012)
15. Chiang, L.H., Russell, E.L., Braatz, R.D.: *Fault Detection and Diagnosis in Industrial Systems*. Springer, London (2001)
16. Coello Coello, C.A., Veldhuizen, D.A.V., Lamont, G.B.: *Evolutionary Algorithms for Solving Multi-objective Problems*, 2nd edn. Springer, New York (2007)
17. Deb, K.: *Multi-objective Optimization using Evolutionary Algorithms*. Wiley, Chichester (2001)
18. Deb, K., Mitra, K., Dewri, R., Majumdar, S.: Towards a better understanding of the epoxy-polymerization process using multiobjective evolutionary computation. *Chem. Eng. Sci.* **59**, 4261–4277 (2004)
19. Deb, K.: *Optimization for Engineering Design: Algorithms and Examples*, 2nd edn. Prentice Hall of India, New Delhi (2004)
20. Dill, K.A.: Theory for the folding and stability of globular proteins. *Biochemistry* **24**, 1501–1509 (1985)
21. Downs, J.J., Vogel, E.F.: A plant-wide industrial control problem. *Comput. Chem. Eng.* **17**, 245–255 (1993)
22. Dua, V., Saraf, D.N., Gupta, S.K.: Free radical polymerizations associated with the Trommsdorff effect under semibatch reactor conditions - III: experimental responses to step changes in initiator concentration. *J. Appl. Polym. Sci.* **59**, 749–758 (1996)
23. Forrest, S.: Genetic algorithms: principles of natural selection applied to computation. *Science* **261**, 872–878 (1993)
24. Garg, S., Gupta, S.K.: Multiobjective optimization of a free radical bulk polymerization reactor using genetic algorithm. *Macromol. Theory Simul.* **8**, 46–53 (1999)

25. Ghosh, K., Ramteke, M., Srinivasan, R.: Optimal variable selection for effective statistical process monitoring. *Comput. Chem. Eng.* **60**, 260–276 (2014)
26. Giri, B.K., Hakenen, J., Miettinen, K., Chakraborti, N.: Genetic programming through bi-objective genetic algorithms with study of a simulated moving bed process involving multiple objectives. *Appl. Soft Comput.* **13**, 2613–2623 (2013a)
27. Giri, B.K., Pettersson, F., Saxen, H., Chakraborti, N. Genetic programming evolved through bi-objective genetic algorithms for an iron blast furnace. *Mat. Manuf. Process* **28**, 776–782 (2013b)
28. Goldberg, D.E.: *Genetic Algorithms in Search, Optimization and Machine Learning*. Addison-Wesley, Reading (1989)
29. Gupta, A., Gupta, S.K., Gandhi, K.S., Mehta, M.H., Padh, M.R., Soni, A.V., Ankleshwaria, B.V.: Modeling of hydrolytic polymerization in a semibatch nylon 6 reactor. *Chem. Eng. Commun.* **113**, 63–89 (1992)
30. Guria, C., Verma, M., Mehrotra, S.P., Gupta, S.K.: Multi-objective optimal synthesis and design of froth flotation circuits for mineral processing using the jumping gene adaptation of genetic algorithm. *Ind. Eng. Chem. Res.* **44**, 2621–2633 (2005a)
31. Guria, C., Bhattacharya, P.K., Gupta, S.K.: Multi-objective optimization of reverse osmosis desalination units using different adaptations of non-dominated sorting genetic algorithm (NSGA). *Comput. Chem. Eng.* **29**, 1977–1995 (2005b)
32. Guria, C., Verma, M., Mehrotra, S.P., Gupta, S.K.: Optimal synthesis of an industrial fluorspar beneficiation plant using a jumping gene adaptation of genetic algorithm. *Miner. Metall. Process.* **26**, 187–202 (2009)
33. He, Y., Hui, C. W.: A rule based genetic algorithm for the scheduling of single-stage multi-product batch plants with parallel units. *Comput. Chem. Eng.* **32**, 3067–3083 (2008)
34. Holland, J. H.: *Adaptation in Natural and Artificial Systems*. University of Michigan Press, Ann Arbor (1975)
35. Hoque, M.T., Chetty, M., Dooley, L.S.: A guided genetic algorithm for protein folding prediction using 3D hydrophobic-hydrophilic model. In: *IEEE Congress on Evolutionary Computation*, Vancouver (2006)
36. Hu, X. B., Leeson, M. S., Hines, E. L., Wang, M., Paolo, E. D.: A review on ripple-spreading genetic algorithm for combinatorial optimization problems. In: Sun, F., Wang, Y., Lu, J., Zhang, B., Kinsner, W., Zadeh, L. A. (eds.) *Proc IEEE International Conference on Cognitive Informatics (ICCI' 10)*, IEEE (2010)
37. Inamdar, S.V., Gupta, S.K., Saraf, D.N.: Multiobjective optimization of an industrial crude distillation unit using the elitist non-dominated sorting genetic algorithm. *Chem. Eng. Res. Des.* **82** (A), 611–623 (2004)
38. Kasat, R.B., Kunzru, D., Saraf, D.N., Gupta, S.K.: Multiobjective optimization of industrial FCC units using elitist non-dominated sorting genetic algorithm. *Ind. Eng. Chem. Res.* **41**, 4765–4776 (2002)
39. Kasat, R.B., Ray, A.K., Gupta, S.K.: Applications of genetic algorithm in polymer science and engineering. *Mater. Manuf. Process.* **18**, 523–532 (2003)
40. Kumar, A., Chakrabarti, D., Chakraborti, N.: Data-driven Pareto optimization for microalloyed steels using genetic algorithm. *Steel Res. Int.* **83**, 169–174 (2012)
41. Lin, C.J., Su, S.C.: Protein 3D HP model folding simulation using a hybrid of genetic algorithm and particle swarm optimization. *Int. J. Fuzzy Syst.* **13**, 140–147 (2011)
42. Linnhoff, B., Ahmed, S.: Cost optimum heat exchanger networks - 1: minimum energy and capital using simple models for capital cost. *Comput. Chem. Eng.* **14**, 729–750 (1990)
43. Luus, R., Jaakola, T.H.I.: Optimization by direct search and systematic reduction of the size of search region. *AIChE J.* **19**, 760–766 (1973)
44. Mankar, R.B., Saraf, D.N., Gupta, S.K.: On-line optimizing control of bulk polymerization of methyl methacrylate: some experimental results for heater failure. *J. Appl. Polym. Sci.* **85**, 2350–2360 (2002)

45. Masuduzzaman, Rangaiah, G. P.: Multi-objective optimization applications in chemical engineering. In: Rangaiah GP (ed.) *Multi-objective Optimization: Techniques and Applications in Chemical Engineering*, World Scientific, Singapore (2009)
46. Mehrotra, S.P., Kapoor, P.C.: Optimal-suboptimal synthesis and design of flotation circuits. *Sep. Sci.* **9**, 167–184 (1974)
47. Mendez, C.A., Cerda, J., Grossmann, I.E., Harjunkoski, I., Fahl, M.: State of art review of optimization methods for short-term scheduling of batch processes. *Comput. Chem. Eng.* **30**, 913–946 (2006)
48. Mitra, K., Deb, K., Gupta, S.K.: Multiobjective dynamic optimization of an industrial nylon 6 semibatch reactor using genetic algorithm. *J. Appl. Polym. Sci.* **69**, 69–87 (1998)
49. Mondal, D.N., Sarangi, K., Pettersson, F., Sen, P.K., Saxen, H., Chakraborti, N.: Cu - Zn separation by supported liquid membrane analyzed through multi-objective genetic algorithms. *Hydrometallurgy* **107**, 112–123 (2011)
50. Naraharisetti, P.K., Karimi, I.A., Srinivasan, R.: Supply chain redesign - multimodal optimization using a hybrid evolutionary algorithm. *Ind. Eng. Chem. Res.* **48**, 11094–11107 (2009)
51. Nandasana, A.D., Ray, A.K., Gupta, S.K.: Dynamic model of an industrial steam reformer and its use for multiobjective optimization. *Ind. Eng. Chem. Res.* **42**, 4028–4042 (2003)
52. Oliveira, F., Hamacher, S., Almeida, M.R.: Process industry scheduling optimization using genetic algorithm and mathematical programming. *J. Intell. Manuf.* **22**, 801–813 (2011)
53. Pettersson, F., Chakraborti, N., Saxen, H.: A genetic algorithms based multiobjective neural net applied to noisy blast furnace data. *Appl. Soft Comput.* **7**, 387–397 (2007)
54. Pettersson, F., Biswas, A., Sen, P.K., Saxen, H., Chakraborti, N.: Analyzing leaching data for low-grade manganese ore using neural nets and multiobjective genetic algorithm. *Mat. Manuf. Process* **24**, 320–330 (2009)
55. Pishbin, S.I., Moghiman, M.: Optimization of cyclone separators using genetic algorithm. *Int. Rev. Chem. Eng.* **2**, 683–691 (2010)
56. Rajesh, J. K., Gupta, S.K., Rangaiah, G.P., Ray, A.K.: Multiobjective optimization of steam reformer performance using genetic algorithm. *Ind. Eng. Chem. Res.* **39**, 706–717 (2000)
57. Ramteke, M., Gupta, S.K.: Multi-objective optimization of an industrial nylon-6 semi batch reactor using the a-jumping gene adaptations of genetic algorithm and simulated annealing. *Polym. Eng. Sci.* **48**, 2198–2215 (2008)
58. Ramteke, M., Gupta, S.K. Biomimicking altruistic behavior of honey bees in multi-objective genetic algorithm. *Ind. Eng. Chem. Res.* **48**, 9671–9685 (2009a)
59. Ramteke, M., Gupta, S.K.: Biomimetic adaptation of the evolutionary algorithm, NSGA-II-aJG, using the biogenetic law of embryology for intelligent optimization. *Ind. Eng. Chem. Res.* **48**, 8054–8067 (2009b)
60. Ramteke, M., Gupta, S.K.: Bio-mimetic adaptations of GA and SA for the robust MO optimization of an industrial nylon-6 reactor. *Mater. Manuf. Process.* **24**, 38–46 (2009c)
61. Ramteke, M., Srinivasan, R.: Novel genetic algorithm for short-term scheduling of sequence dependent changeovers in multiproduct polymer plants. *Comput. Chem. Eng.* **35**, 2945–2959 (2011)
62. Ramteke, M., Srinivasan, R.: Large-scale refinery crude oil scheduling by integrating graph representation and genetic algorithm. *Ind. Eng. Chem. Res.* **51**, 5256–5272 (2012)
63. Ravi, G., Gupta, S.K., Ray, M.B.: Multiobjective optimization of cyclone separators. *Ind. Eng. Chem. Res.* **39**, 4272–4286 (2000)
64. Ravi, G., Gupta, S.K., Viswanathan, S., Ray, M.B.: Optimization of venturi scrubbers using genetic algorithm. *Ind. Eng. Chem. Res.* **41**, 2988–3002 (2002)
65. Safikhani, H., Hajiloo, A., Ranjbar, M.A.: Modeling and multiobjective optimization of cyclone separators using CFD and genetic algorithms. *Comput. Chem. Eng.* **35**, 1064–1071 (2011)
66. Sangwai, J.S., Saraf, D.N., Gupta, S.K.: On-line optimizing control of free radical bulk polymerization of methyl methacrylate (MMA) in a rheometer-reactor assembly. *Chem. Eng. Sci.* **62**, 2790–2802 (2007)

67. Seth, V., Gupta, S.K.: Free radical polymerizations associated with the Trommsdorff effect under semibatch reactor conditions: an improved model. *J. Polym. Eng.* **15**, 283–326 (1995)
68. Sharma, S., Rangaiah, G.P.: Multi-objective optimization applications in chemical engineering. In: Rangaiah, G.P., Petriciolet, A.B. (eds.) *Multi-objective Optimization in Chemical Engineering: Developments and Applications*, 1st edn. Wiley, Oxford (2013)
69. Silva, C.M., Biscaia, E.C.: Genetic algorithm development for multi-objective optimization of batch free-radical polymerization reactors. *Comput. Chem. Eng.* **27**, 1329–1344 (2003)
70. Srinivas, T., Sivakumar, S., Gupta, S.K., Saraf, D.N.: Free radical polymerizations associated with the Trommsdorff effect under semibatch reactor conditions - II: experimental responses to step changes in temperature. *Polym. Eng. Sci.* **36**, 311–321 (1996)
71. Subramani, H.J., Hidajat, K., Ray, A.K.: Optimization of simulated moving bed and varicol processes for glucose-fructose separation. *Chem. Eng. Res. Des.* **81**(A), 549–567 (2003)
72. Sundaram, A., Venkatasubramanian, V.: Parametric sensitivity and search-space characterization studies of genetic algorithm for computer-aided polymer design. *J. Chem. Inf. Comput. Sci.* **38**, 1177–1191 (1998)
73. Unger, R., Moul, J.: Genetic algorithm for protein folding simulations. *J. Mol. Bio.* **231**, 75–81 (1993a)
74. Unger, R., Moul, J.: Genetic algorithm for 3D protein folding simulations. In: *5th International Conference on Genetic Algorithm*, pp. 581–588 (1993b)
75. Wajge, R.M., Rao, S. S., Gupta, S. K.: Simulation of an industrial semibatch nylon 6 reactor: optimal parameter estimation. *Polymer* **35**, 3722–3734 (1994)
76. Yuen, C.C., Aatmeeyata, Gupta, S.K., Ray, A.K.: Multiobjective optimization of membrane separation modules using genetic algorithm. *J. Membr. Sci.* **176**, 177–196 (2000)
77. Zhang, Z., Hidajat, K., Ray, A.K.: Multiobjective optimization of simulated countercurrent moving bed chromatographic reactor (SCMCR) for MTBE synthesis. *Ind. Eng. Chem. Res.* **41**, 3213–3232 (2002a)
78. Zhang, Z., Hidajat, K., Morbidelli, M., Ray, A.K.: Multiojective optimization of SMB and varicol process for chiral separation. *AIChE J.* **48**, 2800–2816 (2002b)
79. Zhou, F.B., Gupta, S.K., Ray, A.K.: Multiobjective optimization of the continuous casting process for poly (methyl methacrylate) using adapted GA. *J. Appl. Polym. Sci.* **78**, 1439–1458 (2000)
80. Zhou, F.B., Gupta, S.K., Ray, A.K.: Modeling of the sheet-molding process for poly (methyl methacrylate). *J. Appl. Polym. Sci.* **81**, 1951–1971 (2001)

ARM based Real time video Streaming using XBee for Perimeter Control in Defense Application

Abdul Wahid Ansari
Graduate Student, Dept of Electronics Engineering
UPES
India
Awahidansari.re@gmail.com
Sushabhan Choudhury
Head,
schoudhury@ddn.upes.ac.in

Mannika Garg
Graduate Student,
mannika91.garg@gmail.com

Rajesh Singh
Assistant Professor,
rsingh@ddn.upes.ac.in

Abstract—The use of video streaming for communication is becoming very popular among social and industrial applications such as video calling Skype, ‘we chat’, security system, surveillance system etc. This paper presents the analysis & prototype design of system for wireless video streaming in ISM band which make the system very low power and of much lower cost for perimeter control. Conventional rate policing such as generic cell rate algorithm is inadequate to sufficiently regulate transmission of data sources over Zigbee limited by bandwidth. Hence, it is very difficult to transmit JPEG pictures over Zigbee channel. A segment entitled traffic is introduced to prevent excessive overflow of JPEG pictures data over the Zigbee channel. We are proposing a system which will capture pictures through Vision Sensor (Serial JPEG camera – RS232) and transmit through XBee, 2.4GHz(ISM) as RF Transceiver and can be deployed in any highly sensitive defense area for perimeter control.

Keywords— *Vision Sensor, Microcontroller, Video Streaming, JPEG, Wireless protocol (Zigbee), perimeter control*

I. Introduction

Wireless sensor networks (WSNs) have received lots of attention in recent years. WSN have been applied to multiple fields such as video surveillance, home automation, and health care [13]. Video streaming in wireless networks could be a promising and difficult application. The reduced quantity of obtainable information measure, similarly because the low-computational power offered for exploit and process video frames on little devices, imposes the transmission of low resolution video frames at a coffee frame rate. In such a situation the number of knowledge carried by each video frame must be preserved as much as possible in order to avoid possible artifacts in the reconstructed dynamics of the scene [14]. The system is based on ARM microcontroller (LPC2138) from Phillips. Images are captured from an onboard camera connected to an embedded single board computer [12]. The captured pictures are read by the Microcontroller which is capable of transmitting it to receiver with the help of a suitable transceiver device like XBee. The system comprises of the video monitoring system [1, 2]. Conventional rate policing such as generic cell rate algorithm is inadequate to sufficiently

regulate transmission of data sources over bandwidth limited Zigbee [9]. Therefore, it is impossible to transmit JPEG pictures over Zigbee channel. Segmentations introduced to prevent excessive overflow and Control bandwidth [4, 5] of JPEG pictures data over the Zigbee channel. In this system we have used Camera (Serial JPEG camera – RS232) for capturing pictures and it transmit multiple pictures in one second to receiver in such a way that it look like a video. The image sensor node senses and transmits the variations in the local environment to the central computing unit placed within the range. The receiver receives the pictures and displays continuously on MATLAB GUI on PC through USB to serial cable which look like a motion picture or video.

II. BLOCK DIAGRAM

A Controller receives image information from vision sensor. This information is transmitted to the coordinator and the transceiver. Now, the nodes Transceiver send a signal to the coordinator Transceiver to share the information in the wireless network. We take into a account a network of one slave nodes using ZigBee module and one master node (sink). Slave node can send the non heritable information to the master node. The master node is interfaced with computer with the assistance of USB to serial cable. The result can be logged of with the help of GUI on PC. The program of each node is written on embedded C through coder and debugger Keil. Figure. 2.1 And Figure. 2.2 shown below show the block diagram for the proposed model.

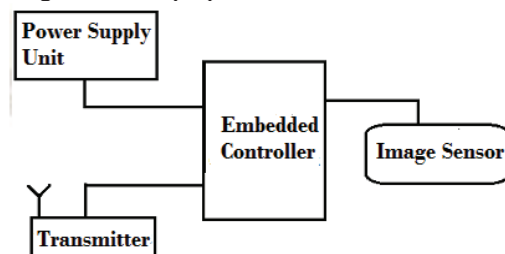


Figure 2.1: Block diagram for video Monitoring System

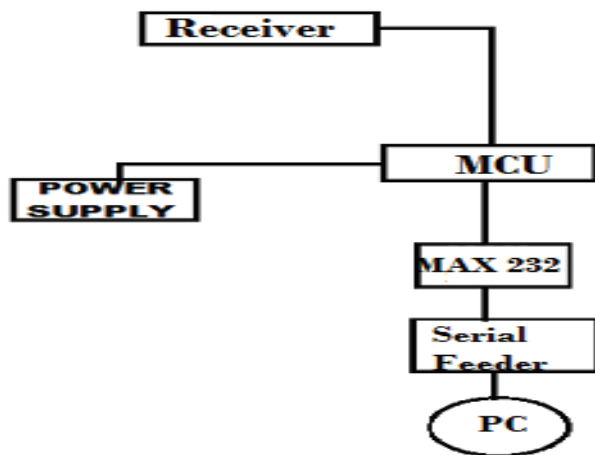


Figure 2.2: Block diagram for display unit

III. REAL TIME DEVELOPMENT

The monitoring unit captures the image from main unit. This data is fed to microcontroller. Microcontroller fetches the data and transmits it over the network. The following is the list for the components used in the proposed model:

- LPC2138 (ARM7TDMI-S)
- Vision Sensor
- MAX232
- Power supply units
- Zigbee module
- GUI Display

A. ARM (LPC2138)

It is a Controller from Phillips which is powered by the ARM core. It is a 16/32-bit, low powered with 512 kilobytes in-system self-programmable flash. This core is capable of running with a 60MHz crystal. The microcontroller features programmable serial two USART and master/slave SPI serial interface. It has Fast GPIO lines and 64 pin QDIP.

B. Vision Sensor

Video streaming in wireless networks is also a promising and tough application. The reduced amount of procurable system of measurement, equally as a result of the low-computational



Figure 3.2.1: vision sensor

power out there for effort and method video frames on little devices, imposes the transmission of low resolution video frames at associate degree occasional frame rate [10]. The 0.3M pixel Serial JPEG Camera [3] module incorporates a small size, low power consumption, and stable operation. Rate for transferring JPEG footage is 115200bps [4, 5] [6, 7]. The camera uses the advanced Omni Vision color detector JPEG codec for varied resolutions. The use of the Omni Vision CMOS VGA color detector makes this associate degree occasional powered consumption unit.

C. MAX232

This is level converter IC from MAXIM which is used to make logic compatibility between TTL and RS232 logic. The IC converts the 5V logic into a 8V negative logic. This converter is located between the microcontroller and the Zigbee module, the microcontroller uses TTL logic whereas the Zigbee module uses RS logic. The main purpose of this converter is to convert the TTL logic to RS logic.

D. POWER SUPPLY UNIT

This unit is basically designed to power up the node 1 and node 2. This provides 5 V, 500mA output to drive the nodes. Here, the AC voltage at 220V is stepped down to 20V using a 220/20V steps down transformer. This AC voltage at 20V is fed to rectifier that converts it to DC voltage and is then filtered using 40 Farad shunt capacitor. The filtered DC voltage is then regulated using a 7805 regulator, and is then supplied to the the microcontroller work at 5V, 500 mA.

E. Zigbee MODULE

This is radio frequency transceiver module, which may facilitate the OEM designers to style their remote applications within the fastest manner. ZigBee sensor network for collecting location information as well as an 802.11 network for streaming video contents [11]. The circuit is meant with SMD elements and therefore the module size is little enough to be able to be fitted in nearly any application. These modules square measure supported IC CC2500 by chipcom. It works at frequency of 2.4GHz, bandwidth of 250 kbps at LAN 802.15.4

protocol. The device works in half duplex mode. Zigbee modules are low power consuming devices, i.e. they can even work on battery power for long durations. These modules are one time expenditure devices; they do not require constant maintenance. These devices have no moving parts and are rugged in construction hence can tolerate rough usage. The node shown in Figure 3.4.3. Is the simulation model of transceiver node of hardware unit, in which USART1 is work as receiver and USART0 work as transmitter.



Figure 3.4.1: Zigbee View

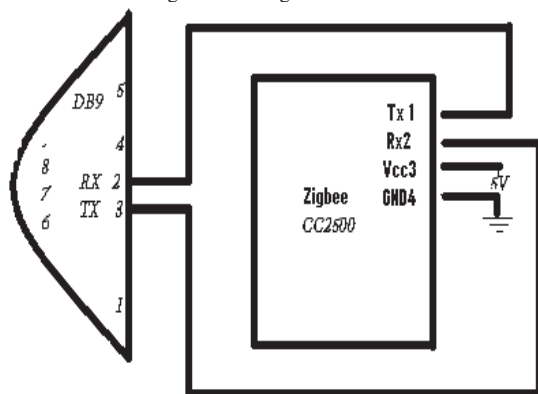


Figure 3.4.2: ZigBee Interfacing with DB9

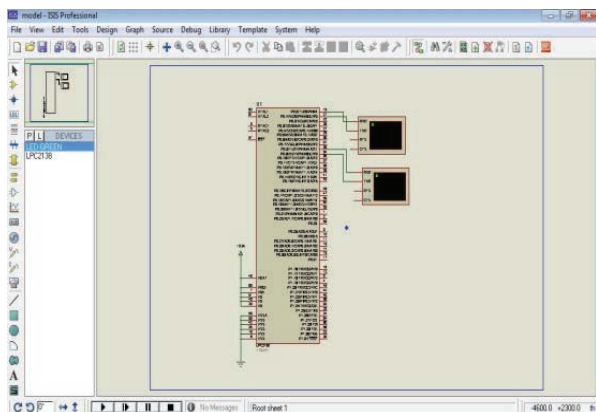


Figure 3.4.3: -Simulation Model of Node

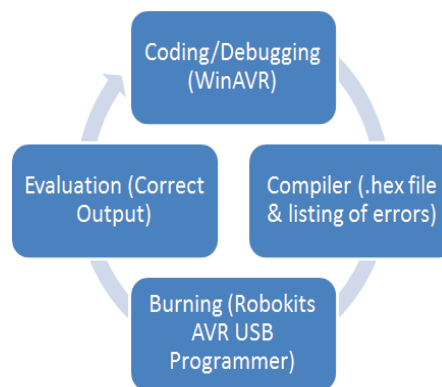


Figure 4 Steps for software development

IV. SOFTWARE DEVELOPMENT

The firmware for the model is developed using C programming language. The binary code is generated with the help of Win ARM compiler based on GCC port by GNU. The IDE used is keil uV4. Microcontroller has been programmed to test the hardware as well to achieve the goal of WSN application, which involved the following steps

A. CODING / DEBUGGING

Coding / debugging in a high-level language (such as C, or Java) or assembler. A compiler for a high level language helps to reduce production time. To program the microcontrollers the Win ARM was used. Programming was done strictly within the C language. The ASCII text file has been commented to facilitate any occasional future improvement and maintenance.

I. Algorithm for slave node

1. Initialize Controller port as Output with respect to USART Communication.
2. Receive data from Image sensor.
3. Delay up to completion of data reception.
4. Transmit Sensor data through WSN Protocol.
5. Delay up to transmission Completion.
6. Go to step 3 (Infinite looping).
7. If Any Error, Terminate Program.

II. Algorithm for Master node

1. Create Graphical User Interfacing Window.
2. Open Serial Port to Communicate.
3. Receive data via Serial port from WSN Protocol.
4. Delay up to receive data Completion.
5. Convert data in to Matrix.
6. Convert data in to Gray Scale Image.
7. Display Image in GUI
8. Image matching with data base for authentication
9. Go to Step 3.
10. If any Error, Terminate Program.

B. COMPILING&BURNING

The compilation of the C program converts it into machine language file (.hex). This is the sole language the microcontroller can perceive; as a result of it contains the first program code regenerate into a positional notation format. Machine language (hex) file of compile program burned into the microcontroller's program memory is achieved with a dedicated programmer.

C. EVALUATION

The system performed all the required tasks and behaved as expected and hence the software development phase is completed. The whole procedure was repeated several times to arrive at the final result.

V. SETUP OF SYSTEM

The slave node shown in Figure 5.1 consists of the transmitting end of the Picture capturing Unit hardware which contains JPEG Camera, a power supply unit, the ARM controller, and the XBEE Unit as the main components.

The master node shown in Figure 5.2 consists of receiving end of hardware which contains the power supply unit, ARM Controller and the XBEE module as its main components.

The graphical user interface is shown in Figure 5.3. The image of the intruder is connected in real time through serial communication to receiver unit. In this Figure the output image of an intruder (sample) which is captured by a slave node placed near the boundary wall of the compound of

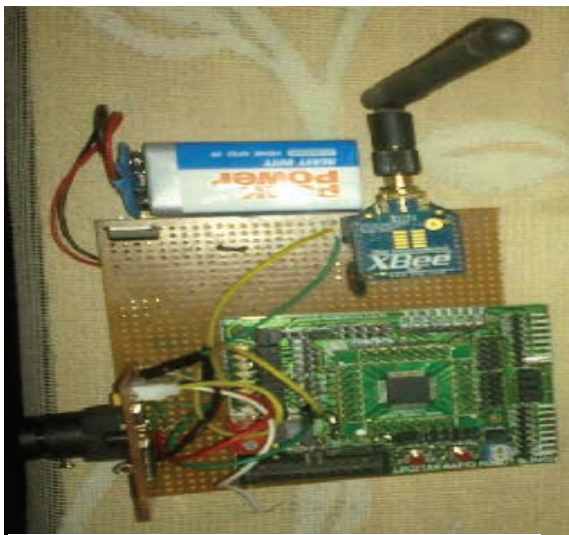


Figure 5.1: Slave Node



Figure 5.2: - Master Node

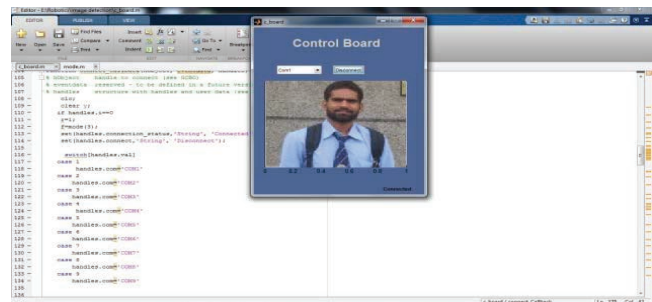


Figure 5.3: Mat lab GUI for Image Display

VI. RESULTS AND DISCUSSION

The proposed algorithm was applied on developed hardware. The algorithm was implemented successfully to stream video data wirelessly that is received at end point for monitoring. This system takes one image of 160X128 pixel sizes, which can send 85 images data respectively in one second as per bandwidth of XBee. This system can be applied to monitor and control the video and data on any mobile platform. Since it is impossible to transmit MPEG video through Zigbee because of its limited bandwidth, this paper has devised a method to transmit the JPEG image via Zigbee. JPEG which is sufficient for any security and surveillance purposes for perimeter control, The individual nodes were deployed on the periphery of the boundary wall of the campus. If any intruder is detected by any node, then the image of the intruder will be sent wirelessly to the control room of the security. In the control room the image of the intruder will be reconstructed by using MATLAB algorithm and then verified by matching the image with the image of the authenticated person.

VII. CONCLUSION AND FUTURE SCOPE

Conventional bandwidth problem can be removed or overcome by using such algorithm, currently we are working with low quality images, in future we will try to improve the quality of image.

ACKNOWLEDGEMENT

The authors are thankful to the administration of the UPES, Dehradun for their support in implementation of the work.

REFERENCES

- [1] Thomas Schierl, Thomas Wiegand and Markus Kampmann "3GPP Compliant Adaptive Wireless Video Streaming Using H.264/AVC" , ISSN – 0-7803-9134-9, IEEE-2005.
- [2] EhsanHaghani, Nirwan Ansari, Shyam Parekh and Doru Colin "Traffic-Aware Video Streaming in Broadband Wireless Networks", ISSN - 978-1-4244-6398-5, IEEE-2010.
- [3] "Serial JPEG Camera - RS232" by Sunrom Technologies, <http://www.sunrom.com/99>
- [4] Minghua Chen and AvideshZakhor," Rate Control for Streaming Video over Wireless", ISSN - 0-7803-8356-7, IEEE INFOCOM 2004.
- [5] S. Biaz, N. H. Vaidya, "Distinguishing congestion losses from wireless transmission losses: a negative result", Computer Communications and Networks, 1998.
- [6]S. Biaz, N. H. Vaidya, "Discriminating congestion loss from wireless losses using inter-arrival times at the receiver", Proc. of IEEE Symposium on Application-specific System and Software Engr. and Techn., pp. 10-17, Richardson, TX, Mar 1999
- [7] N. Samaraweera, "Non-congestion packet loss detection for TCP error recovery using wireless links", in IEE Proceedings of Communications,146(4), pp. 222C230, Aug 1999.
- [8] Y. Tobe, Y. Tamura, A. Molano, S. Ghosh, and H. Tokuda, "Achieving moderate fairness for UDP flows by pathstatus classification," inProc.25th Annual IEEE Conf. on Local Computer Networks (LCN 2000), pp. 252C61, Tampa, FL, Nov 2000
- [9] Kazemian, H.B., "An intelligent video streaming technique in zigbeewireless" FUZZY-IEEE 2009.PP NO. 121 – 126.
- [10] Petracca, M. ; Ghibaudi, M. ; Salvadori, C. ; Pagano, P. ;Munaretto, D. "Performance evaluation of FEC techniques based on BCH codes in video streaming over wireless sensor networks", ISCC-2011 ,Page(s): 43 – 48.
- [11] Mei-Hsuan Lu ; Tsuhan Chen , " CMUseum: A Location-aware Wireless Video Streaming System" ,ICME-2006, Page(s): 2129 – 2132.
- [12] Paolini, C. ; Natarajan, S., Adaptive ajax-based streaming video for the irobot create platform for use in buildings with infrastructure mode 802.11 networks, WAC-2010, Page(s): 1-6.
- [13] Chia-Wen Lu ; Quincy Wu, "Performance study on SNMP and SIP over SCTP in wireless sensor networks"Advanced Communication Technology (ICACT), 2012 14th International Conference on, Page(s): 844 - 847 .
- [14] Petracca, M. ; Ghibaudi, M. ; Salvadori, C. ; Pagano, P. ; Munaretto, D., "Performance evaluation of FEC techniques based on BCH codes in video streaming over wireless sensor networks" IEEE Symposium on Computers and Communications (ISCC) -2011 , Page(s):43–48

Communication Systems Design of Cooperative Safety Systems in Broadband Public Safety Communications Network*

S B Aanandh
Honeywell Life Safety,
Honeywell Technology Solutions
Bangalore
s.b.aanandh@gmail.com

Chinmaya Kar
HONEYWELL / SAFCO,
SABIC
Al Jubail, KSA
chinmaya.kar@gmail.com

Nihal Siddiqui
Department of Safety Engineering
University of Petroleum & Energy Studies
Dehradun
nsiddiqui57@gmail.com

Abstract - The Communication needs for public safety networks and the Process Management are compared and the concept of Safety Grid is deduced. The elemental & cognitive functional safety in a System of Systems View is related to Safety Grid. Safety management of chemical storage tank is used to analyse influences of Theory of constraints, Cognitive Safety and Functional Safety. Safety information model is derived as a function of People, Process and Things. People in the context are either Informed (Aware), Associated or Acknowledge (Act). Process is segregated as Rules, Verify, Measure or Simulate. The system structure is modelled with respect to People, Process and Things as related in Internet of Everything with a Thing Architectural Model defined by an OR3C communication interface using CoAP transport model.

Index Terms – Safety Grid, Functional Safety, LTE, IoE, CoAP.

I. INTRODUCTION

Safety Management can be defined as a businesslike approach to safety. It is a systematic, explicit and comprehensive process for managing safety risks. As with all management systems, a safety management system provides for goal setting, planning, and measuring performance. A safety management system is woven into the fabric of an organization. Globally governments have begun to adopt a national broadband plan and also provide a dedicated spectrum for Public Safety utilizing the Evolved Packet Core Long term Evolution cellular technology. Safety Management deals with both the prevention of accidents and as well as managing emergencies. The suitability of the LTE networks and the architectures for emergency response has been detailed out by the Dept. of Homeland Security [1]. The systems thinking paradigm creates a human centered approach in the systems design and the overall system safety is then a function of interactions, interfaces and risk reduction by proactive monitoring and probabilistic failure models. This work is part of an ongoing research on Safety Communication Systems Design using Public Safety Broadband LTE Networks. The research was scheduled as 4 chapters

- a) Review of functional Safety Models for Safety Management Systems.
- b) Functional & Cognitive Safety Aspects for Disaster Preparedness & Management.
- c) Safety Information Modeling in the IoE context
- d) Safety System Design – Architecture, Models & Communications.

In this forum, we present the results of our work so far in the chapters A, B & C, and put forward the work in progress in chapter D.

II. SAFETY MANAGEMENT SYSTEM : STUDY & RESEARCH HYPOTHESIS

Enterprise Process Safety Management Systems and Public Safety Management systems were compared and this took us to a level of understanding on the subject of modelling the public safety systems and its communication back-bone.

The enterprises have developed their internal safety management processes to build and operate their processes they face challenges like a) compliance, b) presumptions, c) Tacking & measurements, d) Business impact, e) systematic fault avoidance that impacts overall safety performance. In Hydrocarbon Processing journal, Turk & Mishra [2], explain the role of Process Safety Management beyond functional safety principles by identifying the Key Performance Indicators (KPI). They list down nine steps for effective industrial management that goes beyond functional safety in an organization as way to monitor and control the risk and safety in the industry.

In one form the overall safety integrity is a function of the above challenges, it is a complex manifestation of the above factors as described by Turk & Mishra. In another form the challenge of Compliance Adherence remains a major threat with its associated situational manifestations as per the ASM^(R) Consortium. SMS for Public Safety, Handbook for ESI and GSI companies New Zealand, has outlined what the Electricity and the Gas Distribution companies should adhere for creating public safety and how should they be complying with the jurisdictions and standard bodies. They also explain the implementation model in one of the distribution companies and its details are shared in the hand book [3]. The California department of public safety had given in its view the next generation public safety system shall be a system of systems and this helps the scalability and reliability of the overall system [4].

In the Public Safety Communication Model Fig. 1, the foundation principles are based on the elemental and cognitive functional safety models as the next generation public safety is a socio-technical system as discussed about the different models of functional safety. The accident models lay emphasis on the cognitive aspects

and the functional resonance model [5] and the STAMP model [6] lay focus on the theory of constraints for the accident occurrence. The safety management information model layer represents the HSEQ(Health , Safety, Environment & Quality) models similar to that described in the industrial world. As the next generation public safety communications is conceived in the flat-IP networks, it is important to have communication layers of protection as in any cyber security means. The emergency response service oriented applications form the last layer of protection to combat the disasters and this layer assists in disaster preparedness. The two other layers conceived are the distributed sensor management and the demand response layers which act as information providers and consumers on the safety loop.

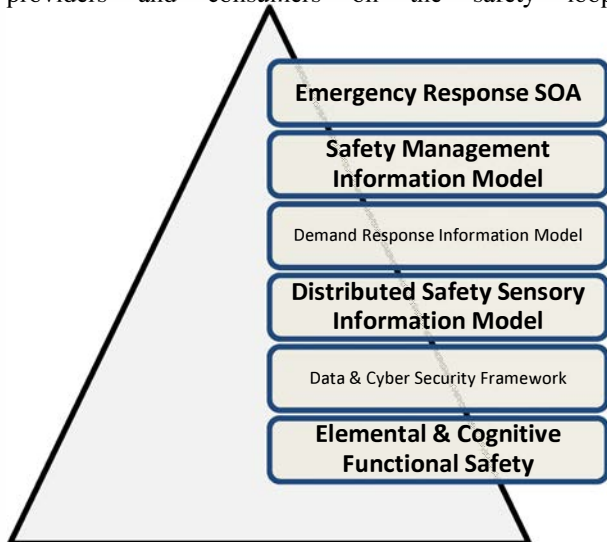


Fig. 1. Safety Grid [7]

III. FUNCTIONAL & COGNITIVE SAFETY ASPECTS : ANALYSIS

Table 1. Relation of Safety Grid & Integrated Safety Systems

Safety Grid	Integrated Safety System
Elemental Functional Safety	Asset Management & Detection
	Emergency Shutdown Systems
Data & Cyber Security Framework	Physical Protection
	Secure Process Control
Distributed Safety Sensory Model	Effective Operating Environment
Demand Response Information Model	
Safety Management Information Model	
Emergency Service SoA	Emergency Response
	Boundary Management
	Abnormal Situation Management

The Safety-Grid was compared against the Integrated Safety system [5] shown in Table 1. The emergent needs of integrated safety systems are strongly grounded on Functional Safety, effective operating environments and emergency response as a layer of protection. In Emergency Management, cognitive aspects of Alarm Visualization and Perception take higher root as defined in Abnormal Situation Management.

There has been an insufficiency in effective and regular auditing by authorized third parties as cited by Mannan [6] . Compliance to Guidelines and Constraints are surrounded by Cognitive Capabilities of the users and are situational as well as are bound by the organizational commitments. A series of accidents were reviewed and they signify the lapses in compliance adherence and inadequacy of audits to prevent failures and accidents specifically in chemical storage tanks. Mannan puts that audit functions from bodies like OSHA are also at lapses, it is impossible to have government bodies alone to sufficiently monitor compliance [6]. Auditing Bodies and Supplementary Auditing Systems (Manned and Unmanned Sensors) have to be placed to enforce compliance and reduce such accidents. With this ground, total of 118 requirements in tank construction and operations were categorized with respect to a) *Theory of Constraints*, b) *Functional Safety* and c) *Cognitive safety*. They were further annotated with respect to 1) *Diagnostic Sensing*, 2) *Automated Sensing*, 3) *Manual Verification* & 4) *Periodic Inspection* and the summary is shown in Table 2.

Table 2. Summary of Safety Classification & Sensing

Safety Requirement Category	Measurement Method					Total
	Diagnostic Sensing	Automated Sensing	Manual Verification	Periodic Inspection	Not Applicable	
Cognitive Requirements	6	7	22	7	8	50
Theory of Constraints	10	7	14	5	1	37
Functional Safety	12	2	14	2	1	31
Total	28	16	50	14	10	118

In Table 2 diagnostic sensing and manual verification display a significant share and thus human cognizance plays an important role. Hence wilful or inadvertent errors in operations as well compliance management have to be minimized. Thus the communication design requirement involves the human communication in the loop. On the other hand the emergency response handling is characterized by Boyd's tactical OODA

(Observe, Orient, Decide, Act) framework [7]. OODA needs & Situational Awareness needs during a disaster of a storage tank fire or explosion was determined as in Table 3. The Enumeration codes or the Standard Objects defined by the Emergency Management [10] domain do not provide a situational awareness or a Common Operating Picture view to the different subscriber community i.e. Law Enforcement, EMS, Fire Department. This observation is also corroborated with the findings and recommendations from APCO international on the High Priority Information Sharing Needs for Emergency Communications and First Responders [8], which observes twelve critical needs, out of which NIEM emergency communications domain, Situational awareness via CAD and Public Safety LTE API are cited as critical.

Table 3. OODA Information Sharing needs

Description	First Responder	
	Fire	EMS
Records Management		
Availability of Onsite Plans, Jurisdiction, Compliance Adherence Information – OBSERVE	X	
1) <u>Tank Size</u>		N
2) <u>Stored Chemical Identifier</u>		
3) <u>Tank NDT – Proof Testing Information</u>		A
4) <u>Mandatory regulatory Health Check Records</u>		N
Rapid Assessment		
Situational Assessment, typically available from the first crew to investigate damages, typically the First Responder – Initiator - ORIENT	X	
1) Identification of Gas Leak or Chemical Spill		N
2) Estimated number of People / Life under threat		A
3) Best Muster Zone		X
Hazard Assessment		
Typical Assessment of Hazard and potential cause. – ORIENT – OBSERVE	X	
1) Identifying Safe resorts and Musters		X
2) PPE Identification and call for specialists		X
3) Identifying known and unknown chemicals.		
		A
Resource Management		
Deployment Planning of Trained Resources, PPE, Hospital Management – DECIDE	X	
	A	
	X	
	X	
Tasking		
Execution Strategy and real-time availability of information - ACT	X	
	X	
	X	
	A	
Legend	EMS – Emergency Services	Medical
X – Need is there	LE – Law Enforcement	
A – Information Source	ECC – Emergency Communications Center	
N – Information Not Needed		
Common Operating Picture		

IV. INFORMATION, MODEL , ARCHITECTURE

Disaster preparedness and control requires information that is regularly sampled and informs about compliance adherence. For the study purpose, the scope was restricted to Fire & Gas Hazard Management. The overall Disaster Management takes into account both the conditions, i.e. the mitigation planning and the disaster containment after an incident as occurred i.e. Disaster prevention and Disaster containment. The Safety Information Model for the former provides the view about the compliance on constraints of a systems boundary and a safety practitioner could verify or correlate the details for measuring the practice-compliance integrity. The Disaster Containment module post incident is used to aggregate the safety information and present a situational awareness view for the containment personnel’s including the incident commanders.

The goals with observables categorize into three types of categories, i.e. the Key Performance Indicators, Asset Design & Construction, and the last on the periodic compliance and categorized across the People, Process & Things. The “things” are either **Smart Tags** or **Smart Sensors**. The connectivity process is described as **Rules** – If this then that, **Verify** – manual verification procedures, **measure** – a method or system to measure, and **simulate** – conditions are artificially injected and simulated. The people in the entire chain are either **associated** or **informed** or people **acknowledge** the measurements or process and are consciously aware.

The normal OODA framework, does not seek to obtain evidences as it is tied to the strict decision-action chain. This enhancement of adding the Evidencing module to the classical OODA helps in incident control and post incident analysis.

Constrained Applications Protocol was chosen as the communication protocol for its suitability over LTE networks [11]. There are open challenges with respect to M2M connectivity and data communication with respect to bandwidth. Some of the developments in CoAP over control plane could address these challenges [12]. At this point in this research the application of CoAP is considered to satisfy the use cases identified earlier. The system structure is further modelled with a **Thing Architectural Model** defined by an **OR3C communication interface**. The thing model is based on the IEC 61499 function block model. The safety management service orientation is realized using the CoAP service orientation with CoAP URIs. The OR3C interfaces are being defined as extensions to the options field in the CoAP protocol.

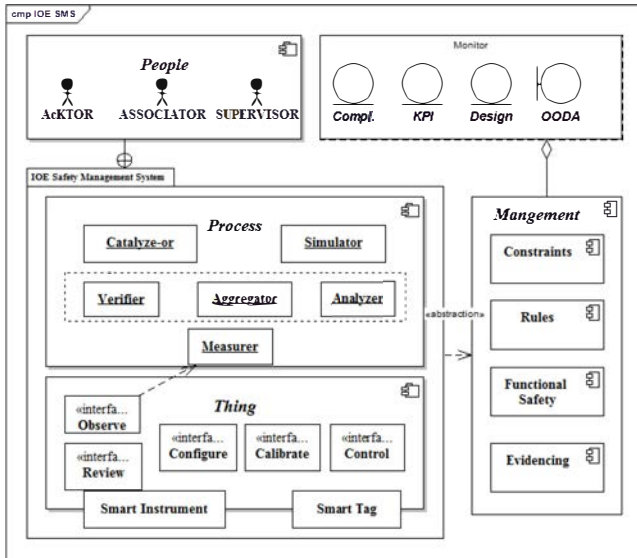


Fig. 2. IOE Safety Management System Model

V. CONCLUSION & FUTURE WORK

The research so far has established the systemic needs for the Safety management systems and the communication backbone requirements. CoAP was thoughtfully selected to provide the Emergency response SOA. A thing architectural model is elucidated with CoAP. In future the use cases identified in the analysis and information against People, Process and Things shall be mapped to the OR3C interfaces and service options for the Evidencing OODA framework shall be added to the CoAP service layer. Subsequently M2M communications with CoAP over control plane shall be analysed and recommendations submitted.

VI. REFERENCES

- [1] Dept. of Homeland Security, "Public Safety Architecture Framework Volume I, II, III," Department of Homeland Security, 2006.
- [2] M. Turk, "Process Safety Management : Going Beyond Functional Safety," *Hydrocarbon Processing*, 01 03 2013.
- [3] Gas Association of New Zealand, SMS for Public Safety – Handbook for ESI & GSI Companies, New Zealand: Electricity Engineers Association , New Zealand, July 2011.
- [4] "Capsnet Strategic Plan," California Technology Agency, 03 03 2011. [Online]. Available: http://www.caloes.ca.gov/PSC/Documents/PDF/CAPSNET_Strategic_Plan_03-03-2011.pdf. [Accessed 10 10 2012].
- [5] E. Hollnagel, FRAM – The Functional Resonance Analysis Method., London: Ashgate, 2012.
- [6] N. Leveson, Engineering a Safer World, Massachusetts : MIT Press, 2011.
- [7] C. K. N. S. S B Aanandh, "Review of Functional Safety for Public Safety Systems," *Journal of System Safety*, no. August, 2014.
- [8] Honeywell Process Solutions, "Integrated Fire and Gas Solution - Improves Plant Safety and Business Performance," Honeywell Process Solutions, 2011.
- [9] D. S. Mannan, "Environment and Public Works," Mary Kay O'Connor Process Safety Center Texas A&M Engineering Experiment Station, 27 June 2013. [Online]. Available: http://www.epw.senate.gov/public/index.cfm?FuseAction=Files.View&FileStore_id=12b33b05-57d8-474a-a5d2-ded91814b20c. [Accessed 29 June 2013].
- [10] J. Boyd, "Organic design for command and control," *A discourse on winning and losing*, 1987.
- [11] NIEM, "NIEM Emergency Management," [Online]. Available: www.niem.gov.
- [12] APCO International, "Unified CAD Project," 2013. [Online]. Available: https://www.apcointl.org/component/docman/doc_download/375-high-priority-info-sharing-needs-for-emergency-comm-and-first-responders-final-pdf.html?Itemid=725.
- [13] J. Swetina, G. Lu, P. Jacobs, F. Ennesser and J. Song, "Toward a standardized common M2M service layer platform: Introduction to oneM2M," *Wireless Communications, IEEE*, vol. 21, no. 3, pp. 20-26, 2014.
- [14] M. Becker, K. Kuladimithi and T. Ptsch, *Transport of CoAP over SMS and GPRS*, 2011.
- [15] Visiting Committee on Advanced Technology, National Institute of Standards and Technology, "Desirable Properties of a Nationwide Public Safety Communication System," NIST, 2012.

Data Encryption and Decryption Algorithms using Key Rotations for Data Security in Cloud System

Prakash G L
Research Scholar, Department of
Computer Science and Engineering,
University of Petroleum and Energy
Studies, Dehradun,

Dr. Manish Prateek,
Associate Dean, Center for
Information Technology,
University of Petroleum and
Energy, Dehradun

Dr. Inder Singh
Assistant Professor, Center for
Information Technology,
University of Petroleum and
Energy, Dehradun

Abstract— Outsourcing the data in cloud computing is exponentially generating to scale up the hardware and software resources. How to protect the outsourced sensitive data as a service is becomes a major data security challenge in cloud computing. To address these data security challenges, we propose an efficient data encryption to encrypt sensitive data before sending to the cloud server. This exploits the block level data encryption using 256 bit symmetric key with rotation. In addition, data users can reconstruct the requested data from cloud server using shared secret key. We analyze the privacy protection of outsourced data using experiment is carried out on the repository of text files with variable size. The security and performance analysis shows that the proposed method is highly efficient than existing methods performance.

Keywords- Data Block, Security, Outsource, Encryption, Decryption, Key Rotation.

I. INTRODUCTION

Cloud computing provides on-demand resource access from a shared pool of computing resources such as; hardware and software for efficient manage. By outsourcing the user data to the public cloud environment, this decreases the control of data for data owner. To maintain the control of data in rest or data in motion within networks, offers more advantages for data security.

Protecting data in the cloud, authentication and integrity, access control, encryption, integrity checking and data masking are some of the data protection techniques. Cryptography is the one of the efficient method for data security in cloud computing. This includes the design and implementation of an efficient encryption and decryption algorithms. In symmetric cryptography, before outsourcing data to cloud server is encrypted into cypher text using secret key and later user decrypted using same shared secret key.

Encryption is the one of the way to protect data at rest in cloud server. There are four ways to encrypt the data at rest, such as; full disk level, directory level, file level and application level.

The most critical part for implementation of any of these methods is key management for data encryption and decryption. The common way to protect data in motion is to utilize encryption with authentication, which safely pass data to or from the cloud server [1].

From the perspective of protecting data privacy, the data owners rely on TTP for the storage security of their data. Moreover, there are legal regulations, such as the U S Health Insurance Portability and Accountability Act (HIPAA) [2], further demanding the outsourced data not to be leaked to external parties. Exploiting data encryption before outsourcing is one way to the privacy preserving public auditing scheme.

In cloud computing, data owners become increasingly outsource their sensitive data in encrypted form from local system to public cloud for more flexibility and economic savings [3]. To protect data in transit to and from the cloud as well as data stored in the cloud, efficient data encryption and decryption algorithms are used for security. The block diagram of symmetric key encryption and decryption data storage as shown in the Figure 1. It involves the use of single secrete key for both encryption and decryption. Data owner split the file into smaller blocks and encrypts all the blocks using symmetric secrete key before sending in to the cloud service provider. Then the cloud service provider stores all the encrypted blocks of source file in cloud server[4].

When the authorized user request a file from the cloud server, cloud service provider gets the encrypted file blocks from the cloud server and send to the user. After receiving all the requested blocks from the cloud server, user decrypt all the encrypted blocks using same secrete key before accessing it.

The rest of the paper is organized as follows; The existing cloud data security methods and its performance are presented in the Section II. Section III and IV, introduces the system model and mathematical model for the proposed system respectively. The detailed data encryption, decryption and access algorithms are presented in the section V and section VI, gives the result and performance analysis. Finally, the overall proposed method and future enhancement concludes in section VII.

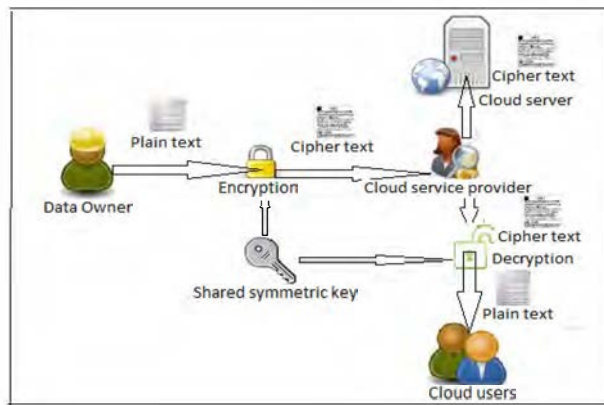


Figure 1: Block Diagram of Data Encryption and Decryption in Cloud System.

1. RELATED WORK

Jing-Jang Hwang et al. [5], has proposed a business model for cloud computing for data security using data encryption and decryption algorithms. In this method cloud service provider has responsible for data storage and data encryption/decryption tasks, which takes more computational overhead for process of data in cloud server. The main disadvantage of this method is, there is no control of data for data owner i. e, data owner has completely trusted with cloud service provider and he has more computational overhead.

Junzuo et al. [6], proposed an Attribute Based Encryption (ABE) and verifiable data decryption method to provide data security in cloud based system. They have been designed the data decryption algorithm based on the user requested attributes of the outsourced encrypted data. One of the main efficiency drawbacks of this method is, cloud service provider has more computational and storage overhead for verification of user attributes with the outsourced encrypted data. While introducing third party auditor we can reduces the storage, computation, and communication overheads of the cloud server, which improves the efficiency of the cloud data storage.

Fatemi Moghaddam et al. in [7], discussed the performance of six different symmetric key RSA data encryption algorithms in cloud computing environment. They have proposed two separate cloud servers; one for data server and other for key cloud server and the data encryption and decryption process at the client side. The main drawback of this method is to maintaining two separate servers for data security in cloud, which creates a more storage and computation overheads.

3. PROBLEM FORMULATION

3.1 Block Status Table(BST)

The Block Status Table(BST) is a small data structure used to access the outsourced encrypted file from the cloud service

provider. It consists of two column such as SN_j and BN_j , where SN_j is the sequence number of physical storage of data block j in the file and BN_j is the data block number. Initially the data owner stores table entries as $SN_j = BN_j = j$. For insertion of data blocks, the BST is implemented using linked list.

3.2. System Model

The cloud data storage system model for secure data access sequences are explained in the Figure 2. The following sequence numbers are represented for data storage and access operations in cloud server.

1. The data owner splits the source file in to blocks of 128 characters and encrypt all the blocks using efficient encryption algorithm and prepare the Block Status Table(BST) for encrypted blocks, then send the encrypted file, key, BST to the Trusted Third Party(TTP) auditor.
2. The TTP calculate the combined hash values for BST(TH) and encrypted file (FH), then send only encrypted file and BST to the cloud server for storage.
3. The authorized user sends the data access request to both TTP and cloud server.
4. TTP verifies the authorized user, if the user is verified then, it send the authorization signal to the cloud server.
5. TTP send the hash values of BST (TH) and encrypted file (FH) to the requested user.
6. Cloud server send the BST and encrypted file to the user.
7. User calculate the hash values of BST and encrypted file received from the cloud server then verifies with hash values received from the TTP. If both values are verified then user gets a data decryption key and decrypt the data blocks.

3.3. Objectives

Data security for outsourcing and accessing data from cloud server, our proposed security model achieves the following objectives.

- i. Lightweight overhead: design a lightweight computation, storage and communication overhead for verification of authorized cloud users and access the cloud date.
- ii. Block level data operation: design an efficient block level encrypted data operations
- iii. Confidentiality and integrity: design an efficient data encryption before outsourcing to cloud server and

decryption algorithms at user side.

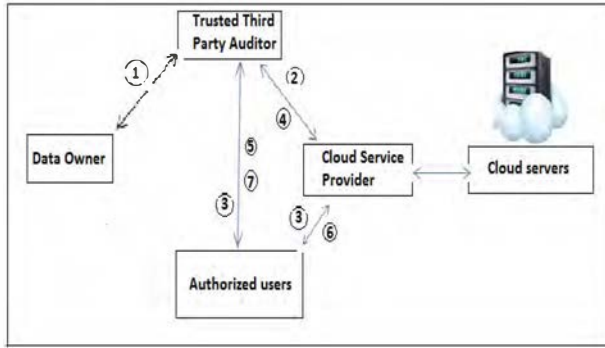


Figure 2: Block Diagram of Encrypted Data Storage

4. MATHEMATICAL MODEL

4.1. Notations

The various symbols used in this paper for the encryption and decryption algorithms is listed in the following Table 1.

Table 1: Notations

Symbol	Meaning
τ_b	File Chunk Size /Block size of block b
χ	Encryption Key
F	Data Owners file targeted for Encryption
b	File chunk/block.
E_m	Encoding Map for every Character
b_c	Binary Equivalent of Chanater c
\overline{CA}	Circular Vector of Characters.
C_{ch}	Cipher Text for character for ch.
φ_F	Size of a file F

4.2. Definitions

File Chunk Size: The security is provided at the block level. The file is divided into blocks and confidentiality is ensured on every block and finally on file. The block size is fixed for experimental purpose.

Data Owner File: The file or the content that data owner is looking for confidentiality. File is a set of blocks and file size depends on the block size and defined as below in equation.

$$F = \{b_1, b_2, b_3, \dots, b_m\} \dots (1)$$

Similarly every block and an Encryption key is a set of characters as defined below,

$$b = \{c_1, c_2, c_3, \dots, |b|\} \dots (2) \text{ and}$$

$$\chi = \{k_1, k_2, k_3, \dots, |\chi|\} \dots (3)$$

The file size is defined as the summation of its component block size.

$$\Phi_F = \sum_{i=0}^{|F|} |\tau_{b_i}| \dots (4)$$

Encoding Map(Em): The encoding Map/Encoding table is a map between a character to every other random character in ASCII range. The ASCII value of a character is splitted into digits and the characters from every digit position is summed

up in ASCII range to find new character as follows, Let rc be a random character for c and ac is a set of digits forming a ASCII value of Character c ,

$$\overline{ac} = \{d_i | \forall d_i \in Z^+, 0 \leq i \leq |\overline{ac}|\} \dots (5)$$

The random character ASCII value is defined as ,

$$ar_c = \sum_{i=0}^{|\overline{ac}|} b_i \% 256 \dots (6)$$

Circular Array(CA): The circular array is used in both encryption and decryption process. The circular array is used for shift operations on both character and on a key character.

The binary equivalent of a character is stored on array and hence the values are either 0 or 1. The circular array has the value obtained as a result from signed right shift operation. The shift operation is performed to disguise the information by changing its bits position and defined as below in equation,

$$CA = \{v_i | 0 \leq i \leq |CA|, v_i \in \{0, 1\}\} \dots (7)$$

Key Chooser(KC): The key chooser is a vital component which defines the criteria for selecting key character for disguising the block character of a file. The key character is selected in such a way that, if 1st chunk character is selected for encryption then first character of key is considered for encryption, if a selected block character comes outside the range of key size, modulus of block character position to key size is performed to fetch a key. Two Key characters are selected for every block character if i th character of a block i.e. c_i is chosen for encryption then its corresponding key character at position i is selected as below,

$$\chi_i = \chi_{i \% |\chi|} \dots (8)$$

Similarly second key character χ_j is selected from the third position away from χ_i

$$\chi_j = \chi_{i+2 \% |\chi|} \dots (9)$$

CA Inverter (CAI): The CA Inverter inverts/complements the circular array for high degree of security. The criteria on which the complements happens based on the resultant number obtained after processing the adjacent key characters. The ASCII values of adjacent key characters are added, if the resultant is even then CA is inverted. Let CA be the circular array having binary equivalent of block character c_i and let χ_i be the chosen key character, then Inverted CA is defined as below

$$ICA = -CA, \text{ iff } \chi_i + \chi_{i-1} \% 2 = 0 \dots (10)$$

CA Shifter (CAS): The CA shifter shifts/rotates the circular array. The stepper movement for circular array is based on the summation of two key characters. If the summation is a factor of 5 then circular array is moved by 2 else it is moved by the remainder obtained from the division of summation by 5 as below,

$$SCA = CA \ggg (2 | (\chi_i + \chi_j) \% 5) \dots (11)$$

Where χ_i, χ_j are the chosen key characters, SCA is the shifted Circular for i th block character c_i and CA is a Circular Array storing binary value of c_i .

Encryption Engine/Cipher Engine: Encryption Engine is a black box which takes block character to produce cipher character. The Encryption Engine is composed of above three components (Key Chooser, CA Inverter and CA Shifter) in that order as below, Let c_i be the i th block character and CE be the cipher engine

$$CE = KC \cup CAI \cup CAS \dots (12)$$

Decryption Engine/Decipher Engine(DE): The Decryption Engine is composed of same components as Encryption Engine but these components are applied in reverse order as below in equation .

$$DE = CAS \cup CAI \cup KC \dots (13)$$

Table 2: Data Encryption Algorithm

<p>Encryption key size : 256 bits , 16 characters in java. as one character = 16 bits. The input file/string will be split into data chunks, each chunk sizing 16 characters equal to key size for encryption. Chunk Size = 256 bits , 16 characters in java.</p> <p>Preparations</p> <ol style="list-style-type: none"> 1. Split the data into chunks 2. Fill in the key into a doubly linked list (for rotation) , each character in a node so totally 16 nodes in the linked list . 3. Create a map with the possible characters as key and values as different character . (simple encoding) <p>Algorithm steps :</p> <ol style="list-style-type: none"> 1. select the unprocessed chunks in order. 2. select the key for the selected chunk , key would be head to 16 characters length in the doubly linked list (counting through doubly linked list) refer step 4 for better understanding on this . 3. Iterate over the characters in the chunk and select one for encoding Look up the map and get the mapped value for the selected character in the chunk and consider it a current character. Add the iterate indexed character from key and 16th character from doubly linked list .. for example if selected character is 15 the last character would be 14th (as we are counting through the doubly linked list key) if the addition value is even : current character = Complement the bits of the character Add the first and 3rd character of the selected key find the Mod 10 of addition value if mod 10 is 0 right shift character = 2 else right shift character = mod 10 value right shift the bits of the current character current character is the encoded character 4. change the head pointer of doubly linked list (this is done to have different key for next chunk encryption), dynamically we are doing it for better security. For example if the key is "abcdefghijklmnop " for first chunk data , " bcdefghijklmnop" would be the key for second chunk this keeps changing 5. Continue steps 1 through 4 until all the chunks are processed.

5. ALGORITHMS

The data owner encrypts the file before sending it to the Cloud Service Provider(CSP)[9],[10]. The encryption algorithm has several steps and composed of key Chooser, Circular Array Inverter and Circular Array shifter. The encryption algorithm is designed, the information at highest factor by applying

series of rotations on every block character and the key is rotated for every character. From this it is ensured that same key is not used for encrypting every character and hence this algorithm is called as key motor encryption algorithm.

The file is divided into blocks and confidentiality is emphasized on every character level of a block. The binary equivalent of block character is stored in circular array and

number of moves the circular array is rotated is decided by the CA Shifter. Where every rotation divides the data by 2 and this will optimize the data to its least value and hence the privacy of data is ensured. Since stepper movement of CA is different for different character it's hard/impossible to determine the actual value of CA as explained in Table 2.

The key portion of algorithm is the CA inverter and CA shifter which is performed on every block character and finally on entire block. If File has N blocks and if every block has n characters then CAI and CAS is performed by $N*n$ operations. And therefore this algorithm has complexity of $O(N * n)$.

When the user wants to access data from cloud server, the user authorization and data verification procedure is explained in Table 3. The decryption process happens exactly opposite to encryption which finds a block character from cipher text as per equation (13). The Decryption process, suggests that CA shifter is performed first then Key chooser component is used to select two keys and they are added before inverting CA. Since CA already contains complemented value and complement of CA now yields original encoded value. The Encoding Map (Em) is searched to get its original character. The Algorithm has same complexity as Encryption.

Table 3: Data Access Procedure

Algorithm Data Access Procedure	
1.	An authorized user sends a request to both the CSP and TTP auditor.
2.	CSP sends the encrypted file and BST to the requested user.
3.	TTP sends the FHhttp, THhttp and key to the user.
4.	user computes the THuser using THcsp and FHuser using data blocks and compared with THhttp and FHhttp respectively for integrity check.
5.	Then the user verifies the file by comparing FHuser and FHhttp
6.	If both BST and file computed hash values are matches, then user decrypt the file using shared secret key

6. EXPERIMENTAL RESULTS

6.1. Performance Analysis

The experiment is carried out on the repository of text files with varying size. For testing purpose the text file is composed of alphanumeric characters. The Encoding Map is restricted to have mapping values for lower case alphabets and numerical values. The key used for experimental purpose is "doitdueletschee" which is of 256 bits in size. The key size is fixed for experimental purpose. The file is divided into blocks of 256 characters *i.e.* 4096 bits in size. The algorithms are implemented in JAVA. The eclipse IDE and Linux OS forms the complete execution environment.

The vital or key operations in both processes are CA shifter and CA inverter. The time for encryption/decryption is directly depends on these two operations. The number of movements of CA and its inversion process decides the accuracy of encryption/decryption. Along with CA shifter the key is also rotated for every block character. This ensures that same key is not used for multiple characters. The analysis is performed on different files and number of movements used for shifting CA and key remains same.

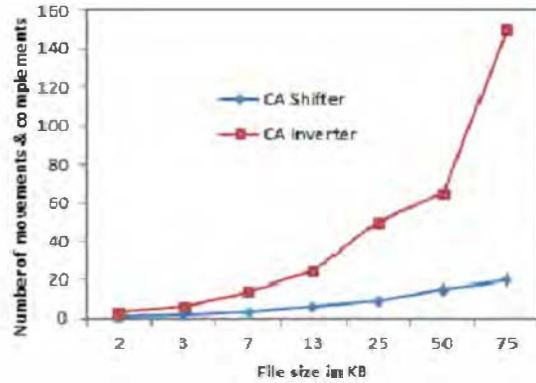


Figure 3: CA Shifter and CA Inverter comparison

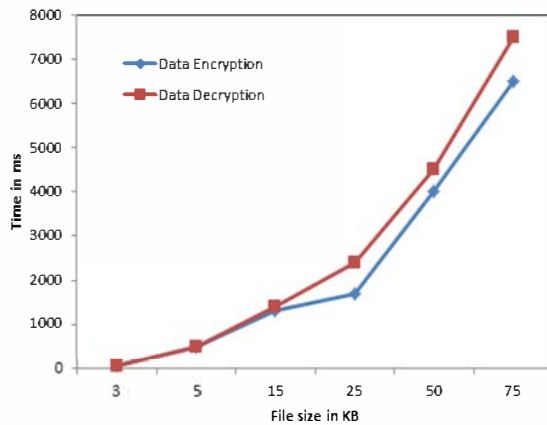


Figure 4: Data Encryption and Decryption time comparison.

From Figure 3, for the file with size 313 characters the number of movements performed was 646, similarly for file with size 3139 it is 6479 movements which is almost double the file size. In other words every movement considers 0.5 character *i.e.* half the character which is 8 bits. This infers that shift operation is performed on every byte and hence the data is disguised at fine level(byte level).

The other parameter for analysis is the CA inverter operation. As shown in Figure 3, 118 times the complement is performed for the file size of 313 characters similarly for the files size of 3139 characters the number of complements performed was

1178 which is approximately 3 characters. This implies that complement operation is performed for every 3 characters and hence the data is disguised at coarse level(bytes level). As CA shift is performed for every character compared to complement operation it has more impact on the encryption/decryption process and therefore it can be concluded that encryption is happening at finer level *i.e.* byte level.

In figure 4, the execution time is plotted on the graph. With increase in file size the number of movements and complements are high and hence the execution time is directly proportional to file size. It is observed that decryption is taking more time than encryption process.

6.2. Advantages

To retain control over data in cloud environment, the encryption and strong key management is more important to the organization to meet the security challenges. The benefits of the encryption in cloud environment are;

- Encryption ensuring the privacy of the organization data, while encrypted data is in the transmission, in use and at storage location.
- Encryption Helps Achieve Secure Multi-Tenancy in the Cloud Encrypting data in the cloud and holding encryption key data owner can avoid the cloud service provider to access the data.
- Encryption Provides Safe Harbor from Breach Notification, If a data breach occurs and personally identifiable information is lost, the breached party must notify all individuals who are impacted.
- Encryption Provides Confidence of data backups are safe in cloud environment from the breached party.
- Encryption can expand revenue potential to customers with sensitive or regulated data by maintaining the key by cloud data owner and gives cloud service providers a competitive edge.

7. CONCLUSION AND FUTURE ENHANCEMENT

In this paper, we have proposed an efficient data encryption and data decryption algorithm to protect the outsourced sensitive data in cloud computing environment. With data encryption, data owner can utilize the benefits of file splitting to reduce storage and computational overheads. On the other hand, to reduce the burden of data owner, trusted third party is introduced for verification of authorized users to access the data from cloud server. We demonstrate the performance of encryption and decryption algorithms in terms of data privacy, computational efficiency and effectiveness of the cloud storage system. On top of this architecture, we can also demonstrate for dynamic block level operations on encrypted data blocks for insertion, deletion and update, which we consider is our improvement future work.

REFERENCES

- [1]. J R Winkler, Securing the Cloud: Cloud Computing Security Techniques and Tactics, *Elsevier Inc., USA*, 2011.
- [2]. <http://aspe.hhs.gov/admsimp/pl104191.htm>, *104th United States Congress, Health Insurance Portability and Accountability Act of 1996*.
- [3]. Tim Mather, Subra Kumaraswamy, and Shahed Latif, Cloud Security and Privacy, *Published by O Reilly Media, Inc.*, 2009.
- [4]. <http://security.setecs.com>, Security Architecture for Cloud Computing Environments, *White paper*, 2011.
- [5]. Jing-Jang Hwang, Taoyuan, Taiwan, Yi-Chang Hsu, Chien-Hsing Wu, A Business Model for Cloud Computing Based on a Separate Encryption and Decryption Service, in *International Conference on Information Science and Applications (ICISA)*, pages 1-7, 2011.
- [6]. Junzuo Lai, Deng R H, Chaowen Guan, Jian Weng, Attribute-Based Encryption With Verifiable Outsourced Decryption, in *IEEE Transactions on Information Forensics and Security*, vol. 8(8), pages 1343-1354, 2013.
- [7]. Fatemi Moghaddam F, Karimi O, Alrashdan M T, A Comparative Study of Applying Real-Time Encryption in Cloud Computing Environments, in *IEEE 2nd International Conference on Cloud Networking*, pages 185-189, 2013.
- [8]. Lan Zhou, Varadharajan V, Hitchens M, Integrating Trust with Cryptographic Role-Based Access Control for Secure Cloud Data Storage Trust, in *12th IEEE International Conference on Security and Privacy in Computing and Communications (Trust Com)*, pages 560-569, 2013.
- [9]. Qin Liu, Tan CC, Jie Wu, Guojun Wang, Reliable Re-Encryption in Unreliable Clouds, in *IEEE International Conference on Global Telecommunications (GLOBECOM)*, pages 1-5, 2011.
- [10]. Miwen, Rongxinglu, Kuanzhang, Jing Shenglei, Xiaohuiliang and Xueminshen, PaRQ: A Privacy-Preserving Range Query Scheme Over Encrypted Metering Data for Smart Grid, in *IEEE International Journal of Computer Networks*, pages 178-191, 2013.

Dependence of low energy incomplete fusion on projectile's α -Q-value

Abhishek Yadav^{1,a}, Pushpendra P Singh^{2,b}, P Kumar³, Mohd Shuaib³, Vijay R Sharma³, Indu Bala¹, D P Singh⁴, Sunita Gupta⁵, U Gupta³, M K Sharma⁶, R Kumar¹, S Muralithar¹, R P Singh¹, B P Singh³, and R Prasad³

¹NP-Group, Inter-University Accelerator Centre, Aruna Asaf Ali Marg, New Delhi-110 067, Delhi, India

²Department of Physics, Indian Institute of Technology Ropar, Roopnagar-140 001, Punjab, India

³Department of Physics, Aligarh Muslim University, Aligarh-202 002, Uttar Pradesh, India

⁴Department of Physics, University of Petroleum and Energy Studies, Dehradun-248 007, Uttarakhand, India

⁵Department of Physics, Agra College, Agra-282 001, Uttar Pradesh, India

⁶Department of Physics, S. V. College, Aligarh-202 001, Uttar Pradesh, India

Abstract. An attempt has been made to understand the effect of entrance-channel parameters on low-energy incomplete fusion and a strong projectile dependence in terms of projectile's α -Q-value has been observed. In the present work, the excitation functions of ^{16}O , $^{13,12}\text{C}+$ ^{159}Tb systems have been measured and compared with PACE4 predictions to study the involvement of different reaction processes. The strength of incomplete fusion reactions for all the studied systems have been extracted and compared to find out the systematics.

1 Introduction

During the last couple of decades, with the observation of incomplete fusion (ICF) reactions at low energies ≈ 4 -7 MeV/nucleon [1], considerable efforts are being employed to look for the systematics of ICF reactions at these energies, where complete fusion (CF) is supposed to be the sole contributor to the total fusion cross-section [2, 3]. The ICF reactions comes into picture with the first experimental observation of "fast α -particles" at energies ≈ 10.5 MeV/nucleon [4] and soon after it variety of experimental & theoretical studies have been devoted to understand the ICF-reactions [1–3, 5, 6]. Some of these studies are summarized in a review article by Gerschel [7], where the localization of the entrance channel angular momentum window with target deformation has been studied. In general, the CF and ICF-reactions are categorized on the basis of driving angular momenta (ℓ -values) [8]. For central and/or near-central interactions, ℓ -values are ranging from 0 to ℓ_{crit} , the CF is expected to be the dominant process, where a composite nucleus is formed with the intimate contact of transient amalgamation of the projectile and target nuclei. Such a composite nucleus may either last for a long time to become a compound nucleus, or disrupted into two fragments known as fission fragments after a short life-time as equilibrium is not entirely achieved, particularly in the shape of the system. However, for ICF-reactions there is no definitive amalgamation between the projectile and target nuclei and these processes favour at peripheral collisions or at sufficiently higher energies for which the ℓ -values will be higher than ℓ_{crit} , and

the fusion of entire projectile is hindered and gives way to the ICF. Thus the composite system formed have less mass/charge and excitation energy (due to partial fusion of projectile), but have high angular-momenta (imparted due to non-central/peripheral interactions) as compared to the CN formed via CF [9, 10]. The important characteristics of the ICF-reactions are; (i) enhancement in the fusion cross-section for α -emitting channels [1], (ii) fractional linear momentum transfer [11], (iii) entirely distinct spin distribution patterns for CF and ICF-residues [9], etc. The additional break-up degrees of freedom make the fusion process more complicated and the possible reaction processes may be; i) the non-capture break-up, when none of the breakup fragments is captured, ii) ICF, when one of the breakup fragments is captured, iii) sequential complete fusion (SCF), the successive capture of all fragments by the target nucleus. Experimentally, it is not possible to disentangle the cross-sections for direct (σ_{DCF}) and sequential (σ_{SCF}) complete fusion, because both channels lead to the same final reaction residues. Hence, the CF cross-section (σ_{CF}) is taken as the sum of σ_{DCF} and σ_{SCF} , whereas the sum of σ_{CF} and incomplete fusion cross-section (σ_{ICF}) may be referred to as the total fusion cross-section ($\sigma_{TF} = \sigma_{CF} + \sigma_{ICF}$) [6].

Further, it may be pointed out that the existing models/theories fairly explain ICF data obtained at energies $E \geq 10.5$ MeV/nucleon or so, but there is no theoretical model available to predict ICF at lower energies [1–3]. Apart from this, several contradicting dependences of the fraction of incomplete fusion (F_{ICF}), which is a measure of relative strength of ICF to the total fusion, have been discussed in recent reports [6, 12–16]. In refs. [12, 13] it has been reported that the F_{ICF} is independent of the tar-

^ae-mail: abhishekyadav117@gmail.com

^be-mail: pushpendrapsingh@gmail.com

get charge (Z_T). However, Gomes *et al.* [6] found a trend of systematic behavior for the F_{ICF} as a function of the Z_T . Morgenstern *et al.* [16] correlated the ICF fraction with entrance channel mass asymmetry (μ_A). Recently, Singh *et al.* [1] has modified the Morgenstern's mass-asymmetry systematics by introducing the importance of projectile structure through the ProMass-systematics. Apart from this, one of our recent works [14] reported the dependence of F_{ICF} on the target mass or $Z_P \cdot Z_T$ of interacting partners for a wide range of projectile-target combinations.

Due to unavailability of reliable theoretical model and the presence of contradicting dependences of low-energy ICF reactions on entrance-channel parameters, the study of these reactions is still an active area of investigation. In recent years, the study of ICF at near barrier energies gained interest to correlate the onset of ICF with entrance channel parameters and to look for the general systematics. As such, we have undertaken a programme to measure the excitation functions for different projectile-target combinations at low energies. In order to explore the low-energy incomplete fusion and to find a consistent general systematics for low energy ICF reactions, the measurements of excitation function for $^{16}\text{O}, ^{13,12}\text{C} + ^{159}\text{Tb}$ systems at energies $\approx 4\text{-}7\text{MeV/nucleon}$ have been performed and compared. The present paper is organized as follows; section-2 deals with the experimental details and methodology, section-3 with analysis and interpretation of results, however, comment on the projectile effect on ICF-reactions are given in section-4.

2 Experimental methodology

In order to ascertain some of above aspects, experiments have been performed by our group at the Inter-University Accelerator Centre (IUAC), New Delhi to measure “the excitation functions” of radio-nuclides populated during the interaction of $^{16}\text{O}, ^{13,12}\text{C} + ^{159}\text{Tb}$ systems at energies $\approx 4\text{-}7\text{MeV/nucleon}$. Here, brief experimental details are given for the ready reference; however, the details are given in refs [1, 14, 15]. In these experiments the activation technique followed by off-line γ -ray spectroscopy has been used. Natural ^{159}Tb targets ($t_m \approx 1.2\text{-}2.5\text{mg/cm}^2$) and Al-catcher foils ($t_m \approx 1.5\text{-}2.8\text{ mg/cm}^2$) were prepared by rolling technique. Each target was backed by an Al foil of appropriate thickness (hereafter called the target-catcher foil assembly) to stop heavy recoiling products produced in the reactions. To cover a wide energy range in the limited beam time, a stacked-foil energy degradation procedure was used. The irradiation of the samples have been carried out in the General Purpose Scattering Chamber having an in-vacuum transfer facility, which has been used to minimize the lapse time between the stop of the irradiation and beginning of the counting of the activity induced in the target-catcher assembly. Considering the half-lives of interest, the irradiations have been carried out for $\approx 8\text{-}10\text{ h}$ duration for each stack. A Faraday cup has been installed behind the target-catcher foil assembly to measure the beam current. Constant beam current has been maintained during all irradiations. The activities in-

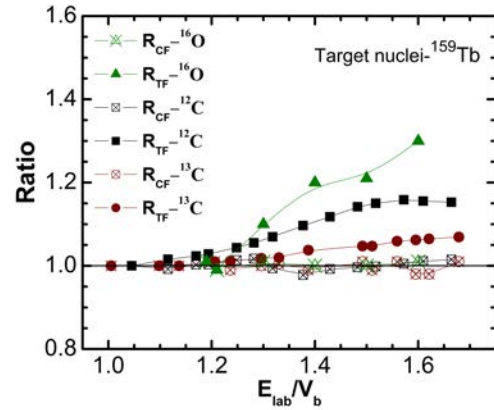


Figure 1. The comparison of experimentally measured and theoretically calculated cross-sections for $^{16}\text{O}, ^{13,12}\text{C} + ^{159}\text{Tb}$ systems have been shown in the form of ratios $R_{CF} = \Sigma \sigma_{CF}^{expt} / \Sigma \sigma_{CF}^{pace4}$ and $R_{TF} = \Sigma \sigma_{TF}^{expt} / \Sigma \sigma_{TF}^{pace4}$ (for details see the text).

duced in the target-catcher foil assemblies were recorded by counting each target along with the catcher foil, using a pre-calibrated high resolution HPGe γ -ray detector coupled to a CAMAC based data acquisition system CANDLER [17]. The efficiency calibration of the detector in the specified geometry was carried out using a standard ^{152}Eu source of known strength at various source (target-catcher foil assembly)-detector separations to wash out the solid angle effect. The energy resolution of the detector has been estimated $\approx 2.5\text{ keV}$ for 1408 keV γ -line of ^{152}Eu source. A 50 Hz pulser was used to determine the dead time of the detector. The source-detector separation has been adjusted to keep the dead-time below 10% during the counting so as to minimize the pile up effects. The characteristic γ -lines have been used to identify reaction products. Further, the decay curves of the identified reaction products have also been analyzed to confirm the identification. Nuclear data on radio-nuclides, such as the corresponding γ -ray abundances and half-lives were taken from ref [18]. The production cross sections of the reaction products have been determined using the standard formulation [1]. It may be pointed out that the errors in the measured production cross sections may arise due to (i) the non-uniformity of target/catcher foils, (ii) fluctuations in the beam current, (iii) the uncertainty in geometry dependent efficiency of HPGe detector, and (iv) due to the dead time of the spectrometer. Detailed discussion on the error analysis is given elsewhere [5, 6]. The overall errors including statistical errors are estimated to be $\leq 15\%$, excluding the uncertainty in branching ratio, decay constant, etc.

3 Results & their interpretation

To understand the formation mechanism of reaction products during the interaction, the experimentally measured excitation functions of $^{16}\text{O}, ^{13,12}\text{C} + ^{159}\text{Tb}$ systems at energies $\approx 4\text{-}7\text{MeV/nucleon}$ have been analyzed within the framework of statistical model code PACE4 [19, 20], which is based on the equilibrated compound nucleus (CN)-decay of Hauser-Feshbach theory. It may, however, be

pointed out that the ICF and pre-equilibrium-emission (PEE) couldn't be taken into consideration during the calculations through this code. In this code, level density parameter 'a' ($=A/K$; A is mass number of CN and K is free parameter) is an important input parameter which affects the CF cross-sections and may be varied to match the experimentally measured cross-sections. The experimentally measured EFs of all $xn+pxn$ -channels populated in interactions of projectile and target have been found to be reproduced by calculations done with a suitable set of parameters. In the present work, at studied energy range and for these systems, the level density parameter "a=A/8" has been found to reproduce the data satisfactorily. The comparison of experimentally measured EFs and the theoretically measured cross-sections are shown in Fig.1. In this figure, the ratio of experimentally measured CF cross-sections, deduced from summing the cross-section of all $xn+pxn$ -channels, to that of theoretically calculated using PACE4 and defined as $R_{CF} = \Sigma\sigma_{CF}^{expt} / \Sigma\sigma_{CF}^{pace4}$, are shown in Fig.1 by hollow symbols. It can be inferred from this figure that the ratio R_{CF} is nearly equal to 1.0, indicating the production of $xn+pxn$ -channels via CF processes only. However, the ratio of measured total fusion cross-section (sum of all measured $xn+pxn+\alpha xn$ channels) to that of theoretically calculated using PACE4, $R_{TF} = \Sigma\sigma_{TF}^{expt} / \Sigma\sigma_{TF}^{pace4}$, has been found to be above the unity line, which increases as the energy increases. This clearly indicates that the cross-sections of α -emitting channels are found to be substantially higher than the PACE4 calculations done employing the same set of input parameters as used for CF-channels. It has already been mentioned that PACE4 do not take ICF, PEE into account and hence, this enhancement clearly reflects the importance of ICF processes at relatively higher energies. Almost similar behavior has been obtained for all the studied systems i.e., $^{16}\text{O}, ^{13,12}\text{C}+^{159}\text{Tb}$. The enhancement in R_{TF} above the unity line for these systems shows that apart from CF, the ICF processes also contribute to the TF cross-section.

These observations show that the α -emitting channels can be populated via two ways; (i) CF of the projectile with the target nucleus ^{159}Tb leading to the formation and decay of CN via light nuclear particles and/or one or two α clusters together with the neutrons and/or protons and (ii) ICF of the projectile with the target nucleus ^{159}Tb i.e., the projectile may break up into its constituent α clusters. One of the fragments fuses with the target nucleus to form a reduced CN, and the remnant behaves as a spectator.

3.1 Incomplete fusion fraction

It is established from the analysis of EFs measurements that ICF-reactions contribute significantly to the production cross-section of α -emitting channels at studied energies in case of all studied projectile-target system. Further, a close examination of Fig.1 reveals that the enhancement over the unity line for R_{TF} increases with energy for all the systems and is different in amount for different projectile, which reflects the sensitivity of ICF on the projectile energy as well as on the projectile type. For a better insight

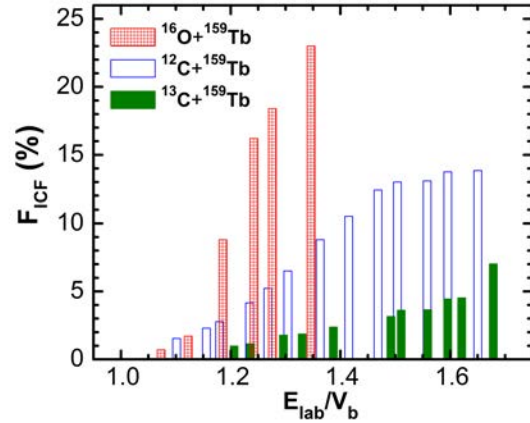


Figure 2. The comparison of F_{ICF} for $^{16}\text{O}, ^{13,12}\text{C}$ projectiles with ^{159}Tb target nuclei.

into the onset and influence of ICF processes in terms of various entrance channel parameters, the percentage fraction of ICF (F_{ICF}) has been deduced from the analysis of data for the presently studied systems. The fraction of incomplete fusion is defined as $F_{ICF} = (\Sigma\sigma_{ICF}^{expt} / \Sigma\sigma_{TF}^{expt}) \times 100$, where $\Sigma\sigma_{ICF}^{expt} = \Sigma\sigma_{TF}^{expt} - \Sigma\sigma_{CF}^{pace4}$. In order to investigate the projectile structure effects, the F_{ICF} values for all these systems are plotted in Fig. 2 and are referred to as the ICF strength function.

4 Projectile structure effect on ICF: the α -Q-value systematics

In order to understand the projectile structure effect on ICF the incomplete fusion fraction have been deduced and plotted in Fig.2 for all studied systems as a function of normalized beam energy, to wash out the effect of different Coulomb-barriers, for comparison. It can clearly be pointed out from this figure that the values of F_{ICF} for ^{16}O are large than the $^{12,13}\text{C}$ projectiles and the F_{ICF} values for ^{12}C is larger than the ^{13}C as projectile at the entire energy range. This indicates a effect of the projectile structure on ICF reaction dynamics.

Further from Fig.2, other than the amplitude of incomplete fusion fraction, it can also be noticed that the onset of ICF are also differ for different type of projectile. In case of ^{12}C , the onset of ICF seems to start from a relatively lower energy (i.e., $1.1V_b$) than for ^{13}C induced reactions. Further, in case of ^{16}O the onset of ICF is lowerer than the ^{12}C as projectile. This strikingly different feature of ICF fractions for $^{16}\text{O}, ^{13}\text{C}$ and ^{12}C induced reactions point mainly towards the projectile structure effect. However, the binding energies of $^{16}\text{O}, ^{12,13}\text{C}$ are 7.98, 7.68 and 7.47 MeV, respectively. Hence, the features revealed in Fig.2 could not be understandable as ^{16}O projectile (with more binding energy) having more incomplete fusion fraction. It may, further, be pointed out that ^{16}O & ^{12}C are well-known α -cluster nuclei with alpha-Q-value ' Q_α ' ≈ -7.16 & -7.37 MeV, respectively. However, ^{13}C has a more negative Q_α value (≈ -10.64 MeV) than ^{16}O and/or ^{12}C . This Q_α value for ^{13}C translates into the smaller breakup prob-

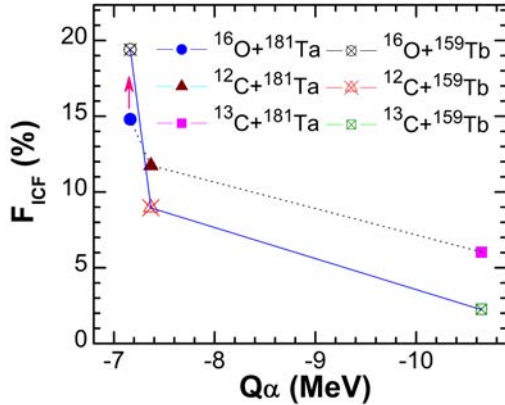


Figure 3. The comparison of F_{ICF} values for six different projectile-target combination at a constant relative velocity $v_{rel}=0.053$.

ability into constituent α clusters, resulting in a smaller ICF fraction than for $^{16}\text{O}/^{12}\text{C}$ induced reactions. In order to validate the above observed α - Q -value systematics, the probability of ICF ($\%F_{ICF}$) has been deduced for ^{12}C , ^{13}C , and ^{16}O induced reactions on another target ^{181}Ta [11, 21] at a constant relative velocity $v_{rel} = 0.053$, and are plotted with Q_α values in Fig. 3. The probability of ICF is found to decrease for more negative Q_α -value of the projectiles. For example, the value of F_{ICF} deduced for the ^{16}O ($Q_\alpha \approx -7.16$ MeV) + ^{159}Tb system is $\approx 19\%$ and is only $\approx 3\%$ for the ^{13}C ($Q_\alpha \approx -10.64$ MeV) + ^{159}Tb system. The same systematics has been observed for the ^{181}Ta target as well. Hence, the comparison of these systems reveals that the Q_α value is an important entrance channel parameter which dictates the probability of ICF reactions at low energies ≈ 4 -7 MeV/nucleon. Further, from this figure it may also be pointed out that the F_{ICF} values support the Morgenstern's mass-asymmetry systematics [16], for a particular projectile, along with ProMass systematics given by Singh et al. [1].

5 Summary

In the present work the excitation functions have been measured for ^{16}O , $^{13,12}\text{C}$ + ^{159}Tb systems and the probability of low energy ICF have, also, been deduced. The comparison of F_{ICF} for six target-projectile combinations strongly follow the α - Q -value systematics for strongly bound projectiles. The fraction of ICF has been found to decrease for projectiles having large negative Q_α -values. If confirmed for other projectile-target combinations, this may provide an important input to achieve a general systematics for the complex ICF dynamics at low incident energies. More inclusive experiments with different

projectile-target combinations are planned to cover this aspect thoroughly.

Acknowledgements

The authors thank to the Director, IUAC, New Delhi, India, for providing all the necessary facilities to carry out this work. The authors thank to the Pelletron technical staff for providing excellent beams. BPS, RP and DPS thank to DST and UGC for providing financial support. A.Y. thanks the DST for providing support through Young Scientist Scheme (Project No. SB/FTP/PS-194/2013) under start-up research grant.

References

- [1] Pushpendra P. Singh *et al.*, Phys. Rev. C **77**, 014607 (2008); Euro. Phys. J. A **34**, 29-39 (2007).
- [2] M. Dasgupta *et al.*, Nucl. Phys. A **787**, 144-149 (2007); Phys. Rev. C **70**, 024606 (2004); *ibid* **66**, 041602(R) (2002).
- [3] L. F. Canto *et al.*, Phys. Rev. C **58**, 1107 (1998).
- [4] H. C. Britt *et al.*, Phys. Rev. **124**, 877 (1961).
- [5] A. Diaz-Torres and I. J. Thompson, Phys. Rev. C **65**, 024606 (2002); Phys. Rev. Lett. **98**, 152701 (2007).
- [6] P. R. S. Gomes *et al.*, Phys. Rev. C **73**, 064606 (2006); Phys. Lett. B **601**, 20 (2004).
- [7] C. Gerschel, Nucl. Phys. A **387**, 297 (1982).
- [8] K. Siwek-Wilczynska *et al.*, Phys. Rev. Lett. **42**, 1599 (1979).
- [9] Pushpendra P. Singh *et al.*, Phys. Lett. B **671**, 20-24 (2009).
- [10] T. Inamura *et al.*, Phys. Lett. B **68**, 51 (1977); Phys. Lett. B **84**, 71 (1982); Phys. Rev. C **32**, 1539 (1985).
- [11] D. P. Singh *et al.*, Phys. Rev. C **89**, 024612 (2014); *ibid* **81**, 054607 (2010); *ibid* **80**, 014601 (2009).
- [12] L. R. Gasques *et al.*, Phys. Rev. C **79**, 034605 (2009).
- [13] R. Rafiei *et al.*, Phys. Rev. C **81**, 024601 (2010).
- [14] Abhishek Yadav *et al.*, Phys. Rev. C **85**, 034614 (2012); *ibid* **85**, 064617 (2012); *ibid* **86**, 014603 (2012).
- [15] V R Sharma *et al.*, Phys. Rev. C **89**, 024608 (2014).
- [16] H. M. Morgenstern *et al.*, Phys. Rev. Lett. **52**, 1104 (1984); Z. Phys. A **313**, 39 (1983).
- [17] CANDLE-Collection and Analysis of Nuclear Data using Linux nEtnetwork, B. P. Ajith Kumar et al. DAE SNP, 2001, Kolkotta.
- [18] E. Browne and R. B. Firestone, Table of Radioactive Isotopes (Wiley, New York, 1986).
- [19] A. Gavron, Phys. Rev. C **21**, 230 (1980).
- [20] O. B. Tarasov and D. Bazin, Nucl. Instrum. Methods Phys. Res., Sect. B **204**, 174 (2003).
- [21] K. Sudarsan Babu *et al.*, J. Phys. G **29**, 1011 (2003).

Design of Double sided Metamaterial Antenna for Mobile Handset Applications

N. Prasanthi Kumari,
Mem IEEE., Asst Prof (SG) Dept., of ECE ,
U P E S.,
 Dehradun , India.
 prasanti@ddn.upes.ac.in

Praful Ranjan,
³Asst. Prof.,
 THDC Inst., of Hydropower Engg and Tech,
 Tehri, India.

Dr. Ravi Gowri,
S.M.,IEEE., Director.,
GEHU.,
 Dehradun, India.

Dr. Piyush Kuchhal,
 HOD., *Department of Physics ,*
U P E S,
 Dehradun, India.

Abstract—Composite Right Left Hand (CRLH) based Printed and dual band antenna which is suitable to mobile handset is proposed and investigated in this paper. The proposed antenna exhibits Composite right left handed nature with help of transmission lines on the printed circuit board (PCB) substrate which has epsilon value for RT Duriod 5880 LZ (epsilon is 2.2). Designed antenna is structure based on composite right/left handed (CRLH) metamaterial transmission lines. To facilitate broader frequency resonance, the antenna consists of two discrete unit cells. Through these two SRR like unit cells, this antenna can have a broad bandwidth which is from 1700 MHz to 1850 MHz, and higher efficiencies of each frequency range are observed. With the introduction of slot in the radiating patch, which could offer better reception signal and radiation characteristics. Return loss, radiated power, radiation patterns, and current distribution are provided in this paper. Proposed antenna occupies is $40 \times 14 \text{ mm}^2$ out of the total PCB size of $40 \times 60 \text{ mm}^2$ with 0.762 mm thickness. This antenna covers a variety of commercial frequency bands which fall on DCS, USPCS and part of WIBRO. In this work, an electrically small tunable antenna structure is designed, simulated, which achieves good tunability and size reduction compared with a conventional (Double Negative antennas).

Keywords—Metamaterials, CRLH Transmission line, split ring resonators, slot.

I. INTRODUCTION

Growing demand for personal mobile systems is the origin for requirement for those mobile handsets with better signal reception in various voice and data communication service bands. These mobile handsets are required to operate at different more frequency bands. In addition, to the demand of compact, slim, and multi-function handsets put stricter requirements on the antenna design. Physical size *the* antenna is the greatest limitation for the mobile antenna set. The antenna proposed is printed circuit board and planar type. In order to accomplish the limiting antenna design parameters circumstance, a lot of antenna design guides have been introduced, for example, helical antenna, planar inverted F antenna (PIFA), and chip antenna. To realize proposed one,

two methods are proposed in this paper. Very first method is to make the antenna the planar PCB embedded type.

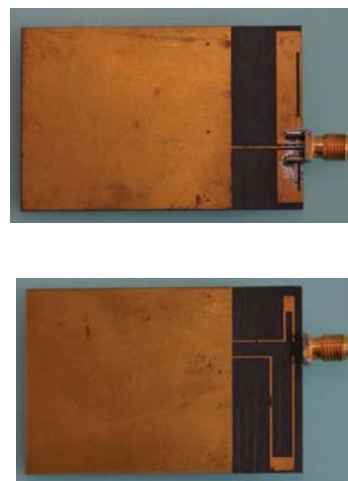


Fig. 1. Front and rear views of the fabricated Antenna

The proposed antenna is based on transmission lines on the PCB for reducing antenna volume such as height. So, designing thin and slim handsets is possible without restricting antenna height. Weight has also been reduced as size is reduced. When the antenna is fabricated on PCB, the cost for manufacturing mobile handset also reduces. This is very critical point, for the mobile phone manufacturers. Proposed antenna is based on composite right/left handed (CRLH) metamaterial transmission lines for size reduction [1]. This kind of metamaterial structure has been explored over the past years [2-6]. According to these papers, metamaterial is a novel structure which has unique electromagnetic properties such as supporting infinite wavelength wave at a specific non-zero frequency. From the L-C equivalent network of SRR, with resonant frequency f_0 , and r_0 is the radius of the SRR, C and L are the capacitance and inductance of unit length, respectively [2]. When the area covered by square and circle are equal, the

characteristics also similar for square and circular SRRs. Since SRR is also an electrically tunable structure, the desired resonance frequency could be varied as with dimensions, which makes a SRR structure a very promising design for an electrically small antenna with better directivity[3]. In this paper, the antenna is proposed as an internal antenna for mobile handsets. A slot in the radiating patch on either side of feeding line, also gives additive effect of improved impedance matching. The slots caused to improve the bandwidth control for the antenna.

II. PROPOSED GEOMETRY

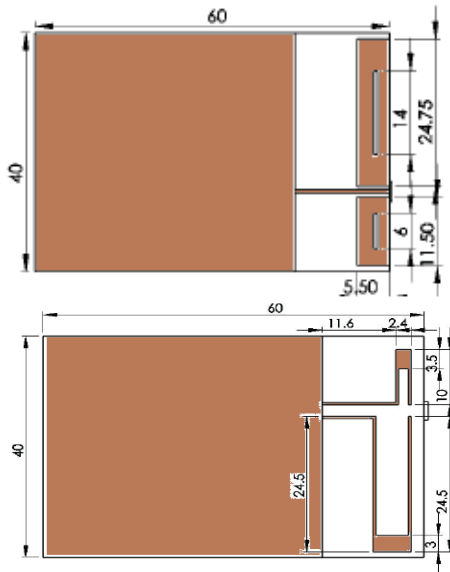


Fig. 2. Front and rear views of the Proposed Antenna

The snapshot of fabricated antenna on both sides is shown in the Fig 1. The geometry of the proposed metamaterial antenna is depicted in the fig 2. The overall dimension of the proposed structure with a printed type on a substrate of RT Duroid 5880LZ ($\epsilon_r=2.2$) is $40 \times 60 \times 0.762$ mm³, which is small enough to be built in mobile devices such as a mobile phone, and the space for antenna is 40×15 mm², which is PCB embedded type. Fig. 3 presents the antenna parts on either side of printed circuit board. Ground (GND) of front and rear side is connected through vias. Component TL in Fig. 3 is feeding line and P1 and P2 are radiating patches which are connected to split rings of different sizes (part R1 and R2) through vias (part via). Feeding line (part TL) and radiating patches (part P1 and P2) are located at front side of PCB. Split ring resonators (part R1 and R2) are located at rear side. These radiating patches are excited by feeding line through a small gap in between. The current patches passes through vias to excite split rings. The split rings are of S-shaped.

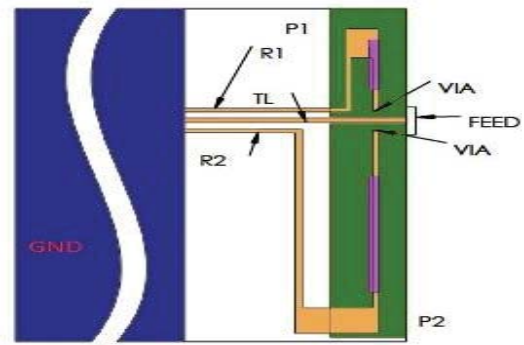


Fig.3. Overview of antenna

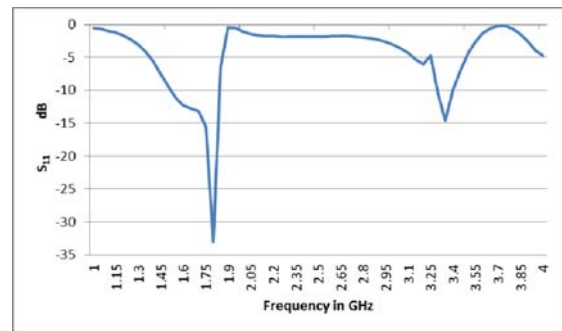


Fig 4 Reflection Coefficient (S_{11})

Finally, lines are connected with rear side GND. Part FEED is feeding point, which is edge feeding [8]. The proposed antenna has a two different unit cells. One is composed of part P1 and R1 with via, and the other is composed of part P2 and R2 with via. Those two unit sections appear to have a same kind of structure, but not symmetric. These cells share the feeding line (part TL). The size of each part is shown in Fig. 3. The width of via lines (Part D and F) is 0.5 mm. The width of feeding line (TL) is also 0.5 mm. And the gap between each unit cell and feeding line is 0.2 mm which is the distance between radiating patches (P1 and P2) and feeding line (TL). The diameter of vias is 0.5 mm. This novel antenna is based on CRLH metamaterial structure mentioned in [4]. This CRLH transmission line structure consists of series inductance, series capacitance, shunt inductance, and shunt capacitance. The characteristics of these inductances and capacitances are best illustrated [5].

III. ANALYSIS

The measurement of reflection coefficient for prototype antenna is presented in Fig. 4. The operating frequency of the antenna is calculated from the -10 dB bandwidth. The Response depicts that the antenna covers four bands which are DCS, PCS, WCDMA and a part of WIBRO. Especially, the resonant frequency of 1.8GHz has a best impedance matching value. Measured radiation patterns comprising of azimuth and elevation are presented at each frequency in Fig.5. These

patterns are measured over 1400 MHz to 1850 MHz. These patterns depict the figure eight pattern and as the frequency moves away from resonant frequency the shape gets deviated. Fig. 6 shows total radiation power for the frequency range from 1400 MHz to 1900 MHz. Efficiency of each commercial band is over 60% as shown in Table I. At 1800 MHz, its efficiency is almost 90%. Fig 7. Shows current distributions at various parts of the antenna. Through these current distributions, operating mechanism at the resonant frequency can be verified. At different frequencies different parts of the antenna resonant for better reception and transmission. The verification of current distribution, which is simulated using ANSOFT HFSS [7], can be useful method for antenna tuning. Proposed antenna is printed on the PCB, tuning the resonant frequency is convenient by the means of variation of transmission lines' dimensions ultimately changing the impedance of antenna. First, the length and width of transmission lines affect both the inductance and capacitance of the antenna. The length of transmission line is proportional to inductance. Similarly the width transmission line is more, inductance is low. Secondly, the gap between transmission lines affects the capacitance of the antenna. If the closer the transmission lines are closer, the capacitance is high. Moreover, how much area transmission lines are overlapped can also decide the capacitance value. The resonant frequency of the structure can be varied to the desired frequency through the modification of capacitive and inductive equivalent values of transmission line. Lastly the size of slot present in the radiating patch also affects the impedance matching. In this work miniaturization without the loss of frequency resonance is obtained [9].

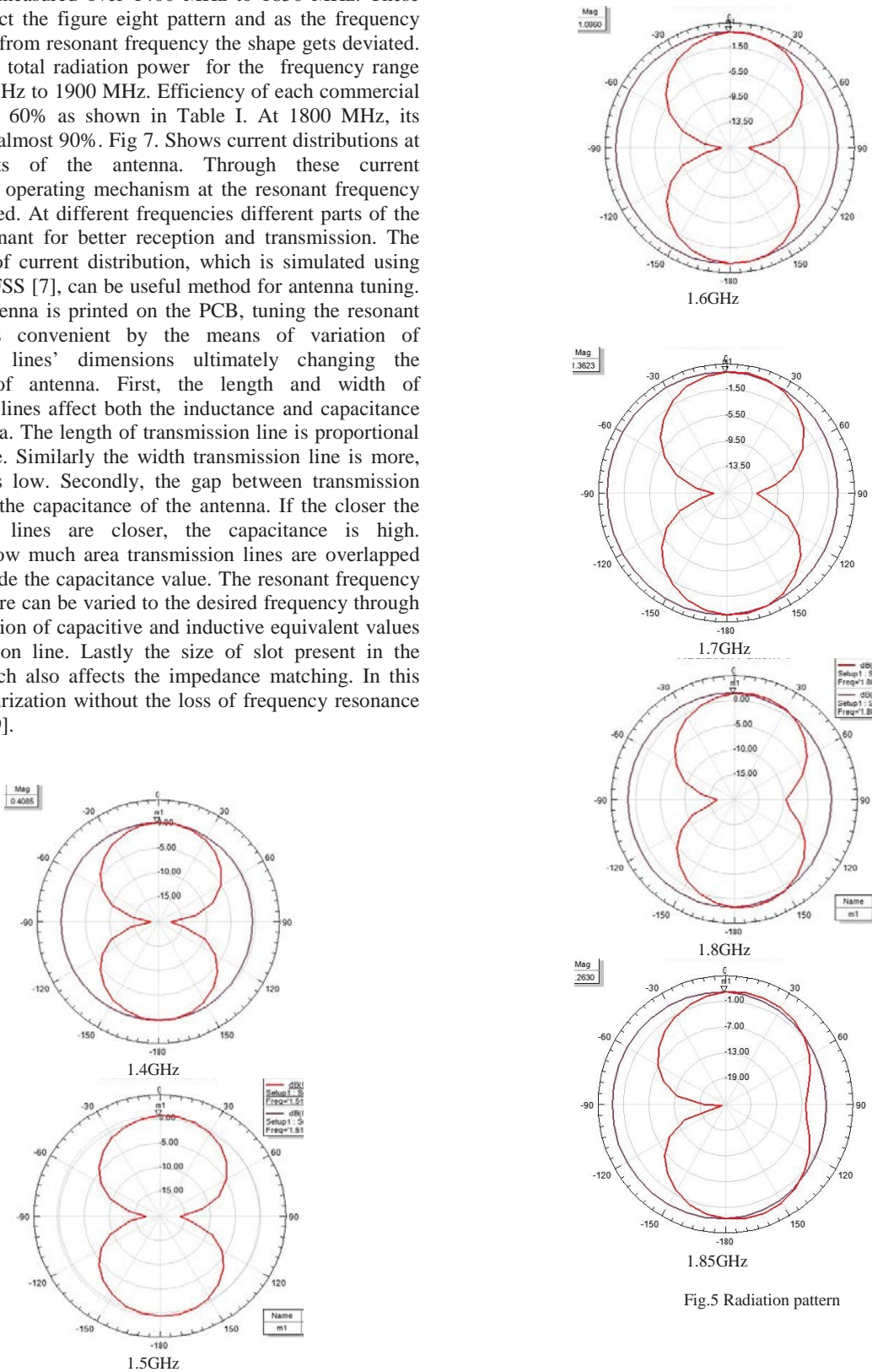


Fig.5 Radiation pattern

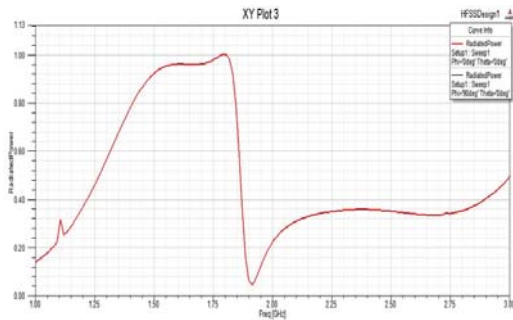


Fig.6 Radiated power

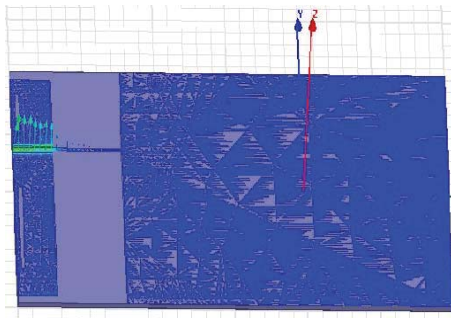


Fig.7 Current distribution

CONCLUSION

The presented wideband PCS antenna, basically designed with idea of metamaterial structure. Concept of Metamaterial structures is revolutionary miniaturization method for RF devices. Improvement of antenna performance such as bandwidth and efficiency, is achieved by two different SRR like unit cells. By introducing slot in the radiating patches the power of radiation is increased due to the slot antenna effect in overall structure. Variation of sizes of split rings and patches gives the required resonant frequency. Through this sample

design, broad bandwidth and high radiation efficiency are proven in this work. It is very useful to apply light weight RF devices like a small and slim mobile handset for different commercial bands since the proposed antenna is implemented on PCB.

REFERENCES

- [1] C. J. Lee, K. M. K. H. Leong, and T. Itoh, "Composite right/left-handed transmission line based compact resonant antennas for RF module integration," *IEEE Transaction on Antennas and Propagation*, col. 54, issue 8, pp. 2283-2291, Aug. 2006.
- [2] R. Marques's et al., "Role of bianisotropy in negative permeability and lefthanded metamaterials," *Phys.Rev.B.*, vol. 65, no. 14, pp. 144440.1-144440.6, April 2002.
- [3] A. Lai, T. Itoh, and C. Caloz, "Composite right/left-handed transmission line meta-materials" , *Microwave Magazine*, IEEE, Volume 5, Issue 3, pp. 34 – 50, Sept. 2004
- [4] G. V. Eleftheriades, A. Grbic, and M. Antoniades, "Negative refractive index transmission line metamaterials and enabling electromagnetic applications," *IEEE Antenna and Propagation Society International Symposium*, vol. 2, pp. 1399-1402, June 2004.
- [5] A. Gummalla, M. Achour, G. Poilasne, and V. Pathak, "Compact Dual-Band Planar Metamaterial Antenna Arrays For Wireless LAN", *Antennas and Propagation Society International Symposium 2008*, IEEE, 7-11 July
- [6] A. Gummalla, C. J. Lee, and M. Achour, "Compact Metamaterial Quad-Band Antenna for Mobile Application", *Antennas and Propagation Society International Symposium 2008*, IEEE, 7-11 July
- [7] Ansoft HFSS 2007 Ver. 11.0
- [8] David M Pozar .,"Five novel feeding techniques for microstrip antennas ".,*IEEE Antenna & Propagation Society International Symposium Digest paper AP23-1*Jun 1987.
- [9] J.L. Volakis et al., "Miniaturization methods for narrowband and ultra-wideband antennas," *Proc. of the 2005 IEEE International Workshop on Antenna Technology*, March 2005.

Detecting Community Structure based on Traffic at Node in Networks

V. K. Sihag
Sardar Patel University of Police, India
vikaskumarsihag@gmail.com

Abhineet Anand
UPES, Dehradun
abhineet.mnnit@gmail.com

Ravi Tomar
UPES, Dehradun
rtomar@ddn.upes.ac.in

Jagdish Chandra
UPES, Dehradun
jcpatni@ddn.upes.ac.in

Rajeev Tiwari
UPES, Dehradun
rajeev.tiwari@ddn.upes.ac.in

Ankur Dumka
UPES, Dehradun
adumka@ddn.upes.ac.in

A. S. Poonia
College of Engineering & Technology, Bikaner
pooniaji@gmail.com

I. ABSTRACT

In the study of networks, such as complex network, social network or biological network; number of different characteristics of many nodes are found common. These characteristics includes small-world property, clustering and community structure, among others. In the context of networks, community structure refers to occurrence of groups of nodes in a network that are more densely connected internally, then with the rest of network. This heterogeneity of connection suggests that network has certain natural division within it. Being able to identify their sub-structure within the network can provide inside into how network function and topology affects each others.

Index terms - Activity Recognition, Social Networks, Acyclic Directed Graphs, Bayesian Networks, Online Commercial Intention, Customer Service, Digital Forensics, Live data acquisition.

II. INTRODUCTION

A. Community Structure

The modern science of networks has brought significant advances to our understanding of complex systems. One of the most relevant features of graphs representing real systems is community structure i. e. the organization of vertices in clusters, with many edges joining vertices of the same cluster and comparatively few edges joining vertices of different clusters. Such clusters, or communities, can be considered as fairly independent compartments of a graph, playing a similar role.

Communities can have concrete applications. Creating communities of web clients who have similar interests and are geographically near to each other may improve the performance of services provided on World Wide Web, in that each community of clients could be served by dedicated mirror server. Identifying clusters of customer with similar interest in the network of purchase relationships between customers and products of online

retailers enable one to set up efficient recommendation systems.

The problem of detecting Community Structure, at first sight stresses on grouping nodes in a network into sets called Community. A good community, comprises of more edges among nodes within the community than edges linking nodes of the cluster with the rest of the community. The ability to find and analyze such clusters can be of great significance in understanding and visualizing network structures. Community detection in networks has attracted a lot of attention in past years. Various methods have been developed to detect community structure. This dissertation concerns about networks with traffic generation capabilities for example communication networks. Suppose there are number of nodes interconnected with each other, trying to communicate, it is required to find the best suitable path for a node to communicate with its counterpart located either within or outside its community. Identification of structural clusters is possible only for sparse graphs i.e. number of edges n is of the order of number of nodes n of the graph.

Social communities exist since long time and the grouping pattern of humans has been studied for long time on different platform. Stuart Rice collected the data of political blocs, on the basis of their legislative behavior and arrange data manually to understand political behavior, in his book named The American Political Science Review in 1927 [23]. George C. Homans 6th president of united states, classified variables (for Concepts) that need to be taken into account when studying a set of phenomena. Then, he arranged there data in the form of matrix for understanding underlying structure. They explain their concept in his book named The Human Group in 1950 [3]. Social Communities has been present everywhere, arranging the animals for different purpose or in social organization in human society: group of hunter, royal families, towns, political and business structure, countries, and even virtual communities like different social networking websites [3]. Sociologist Mark Granovetter

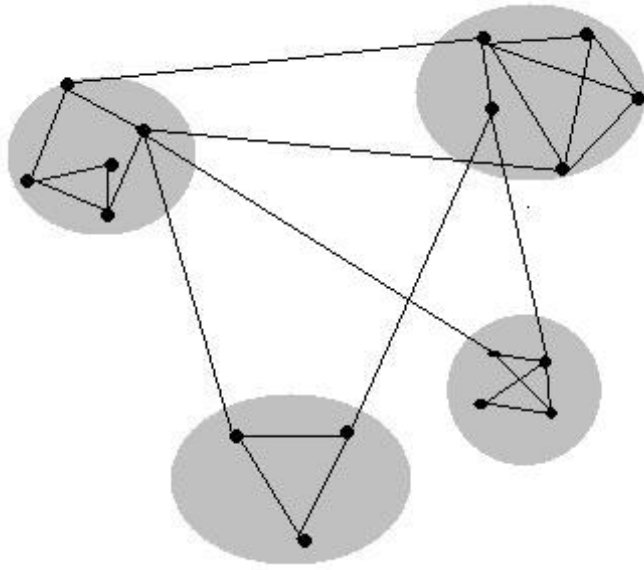


Fig. 1. Small Network Containing 4 Community Structure

wrote in 1973 [3], "Large scale statistical, as well as qualitative, studies offer a good deal of insight into such macro phenomena as social mobility, community organization, and political structure. But how interaction in small groups aggregates to form large-scale patterns eludes us in most cases." Very soon it was found that a very powerful mathematical and large data scalable tool is required and that was a challenging problem. It was very much solved by Michelle Girvan and Mark Newman by graph-partitioning problem solution [1][4][5], which brings the attention of scientist from statistical physics and mathematical communities.

In the study of networks, such as computer and information networks, social networks or biological networks, a number of different characteristics have been found to occur commonly, including the small-world property, heavy-tailed degree distributions, and clustering, among others. Another common characteristic is community structure.

The study of community structure is also required in computer science and graph theory to solve problems like intercommunicating computer processors, where the processors may not required communicating with all others. It can be illustrated with the help of graph, where vertex represented as processors and edges represented as communication. In it, the community structure can be used to find the solution which will minimize the inter-processor communication. Many algorithm have been suggested to solve the problem, few of them are discussed in next chapter.

B. Motivation

Community structures are quite common in real networks. Networks often include community groups

based on common locations, interests, occupations, etc. Metabolic networks have communities based on functional groupings [16]. Citation networks form communities by research topic. Being able to identify these substructures within a network can provide insight into how network function and topology affect each other [1].

C. Problem Statement

The concept of betweenness, which is a variable expressing the frequency of participation of edge to a process, has been used by different scientists for detecting community structure. These approaches calculate the betweenness measure for all the edges, which makes them more complex. So, there is need of more efficient algorithm whose complexity is lesser than the available algorithms.

D. Contribution

Finding communities within an arbitrary network can be a difficult task. The number of communities within the network is typically unknown and the communities are often of unequal size and/or density. Despite these difficulties[3], however, several methods for community finding have been developed and employed with varying levels of success.

Here, a new algorithm for creating community structure is proposed whose complexity betters the existing algorithm, in case when the graph is having more leaf nodes. The main idea of the algorithm is that it reduces the leaf nodes from the graph and then calculates the edge betweenness based on node traffic.

E. Outline

Next section discusses various algorithms which have been used to detect the community structure using different approaches; section IV describes the proposed. Section V checks the quality of proposed work. It shows the resultant clusters after the clustering of network. The approach is applied on the artificially generated network and real world problem of Zackarys Karate club. At last we conclude our work with future directions.

III. DIFFERENT ALGORITHM FOR DETECTING COMMUNITY STRUCTURE

Recently, complex networks have attracted considerable attention in many fields for representation of a variety of complex systems, such as biological and social systems, the Internet, the World Wide Web, and so on. Community structure is an important property of complex networks, which is the tendency for nodes to divide into groups, with dense connections within groups and only sparse connections between them.

The study of community structure in networks has a long history. It is closely related to the ideas of graph partitioning in graph theory and computer science, and hierarchical clustering in sociology [3]. Before presenting our own findings, it is worth reviewing some of this

preceding work, to understand its achievements and where it falls short.

These techniques are aimed at discovering natural divisions of networks into groups, based on various metrics of similarity or strength of connection between vertices. They fall into two broad classes, agglomerative and divisive [17], depending on whether they focus on the addition or removal of edges to or from the network.

In agglomerative method, the edge are added to initially empty network if the similar characteristics are found. The process starts from the single vertex ends with complete graph, which is presented by with help of dendrogram (hierarchical tree). By bisecting that dendrogram, different communities are discovered. The classic example of Agglomerative clustering is species taxonomy. Agglomerative hierarchical clustering starts with every single gene or sample in a single cluster. Then, in each successive iteration, it agglomerates or merges the closest pair of clusters by satisfying some similarity criteria, until all of the data is in one cluster.

While in the divisive approach, it starts with the complete graph and ends with the particular community. For that it try to find out least similar connected pair of vertex and remove that edge from the graph.

A community is a densely connected subset of nodes that is only sparsely linked to the remaining network. A community is a subset of nodes on the network. Suppose the network is represented as graph $G = (V, E)$ with V vertices to say places and E edges to say roads that exist between two places. Detecting community structure is dividing G into K disjoint partitions.

A large number of methods have been developed to detect community structure in networks in the past years. Some of them are as follows:

A. Minimum-Cut Method

The minimum cut method follows a divisive approach, in which the network is divided into predefined parts in approximately same size of network, chosen such that the number of edges between group is minimized [15]. The algorithm works well in the case for which it was intended for example, in load balancing for parallel computing in order to minimize communication between processor nodes. The method works well in many of the applications for which it was originally intended but is less than ideal for finding community structure in general networks since it will find communities regardless of whether they are implicit in the structure, and it will find only a fixed number of them.

B. Hierarchical Clustering

The starting point of any hierarchical clustering method is the definition of a similarity measure between vertices. After a measure is chosen, one computes the similarity for each pair of vertices, no matter if they are connected or not. Hierarchical clustering techniques aim

at identifying groups of vertices with high similarity, and can be classified in two categories:

- Agglomerative algorithms, in which clusters are iteratively merged if their similarity is sufficiently high;
- Divisive algorithms, in which clusters are iteratively split by removing edges connecting vertices with low similarity.

It first computes the intensity of link between each pair nodes based on different methods, such as edge betweenness [1], edge clustering coefficient, dissimilarity index, information centrality, similarity based on random walks, clustering centrality, and so on. Then, by repeatedly incorporating the two nodes with the highest intensity of link (agglomerative method), or repeatedly removing the edge with the lowest intensity (divisive methods), the partition results of the networks are obtained [17].

Hierarchical clustering has the advantage that it does not require a preliminary knowledge on the number and size of the clusters. However, it does not provide a way to discriminate between the many partitions obtained by the procedure, and to choose that or those that better represent the community structure of the graph. The results of the method depend on the specific similarity measure adopted. The procedure also yields a hierarchical structure by construction, which is rather artificial in most cases, since the graph at hand may not have a hierarchical structure at all. Moreover, vertices of a community may not be correctly classified, and in many cases some vertices are missed even if they have a central role in their clusters [5]. Another problem is that vertices with just one neighbor are often classified as separated clusters, which in most cases does not make sense. Finally, a major weakness of agglomerative hierarchical clustering is that it does not scale well.

C. Kernighan and Lin's Algorithm

Brian Kernighan and Shen Lin in 1970, showed that the node in different board can be linked to each other using least number of connections. The Kernighan - Lin algorithm [18], which uses a greedy algorithm to optimize the value of the edges with in community minus those between community, and the spectral bisection algorithm [18], which is based on the eigenvectors of the Laplacian matrix of graph, are two classical algorithms related to the ideas of graph partitioning in graph theory and computer science. They can find the community structure efficiently in the networks in the case that the number of communities in the networks is given before.

D. Girvan and Newman's Algorithm

Girvan and Newman focused on the concept of betweenness[1], which is a variable expressing the frequency of the participation of edges to a process. They considered three alternative definitions: geodesic

edge betweenness, random-walk edge betweenness and current-flow edge betweenness.

Geodesic - Edge Betweenness is the number of shortest paths between all vertex pairs that run along the edge. It is an extension to edges of the popular concept of site betweenness, introduced by Freeman in 1977 [16] and expresses the importance of edges in processes like information spreading, where information usually flows through shortest paths.

Random - Walk Betweenness - betweenness of an edge is given by the frequency of the passages across the edge of a random walker running on the graph.

Current- Flow Betweenness is defined by considering the graph a resistor network, with edges having unit resistance.

In 2002, Girvan and Newman proposed a divisive method that based on the concept of edge betweenness to identify the community structure of the network [1][4][5]. Although this method has been successfully applied to a variety of networks, the complexity of it is not ideal, running in $O(m^2n)$ time on an arbitrary network with m edges and n nodes, or $O(n^3)$ time on a sparse network (a network with mn , which covers most real-world networks of interest).

It identifies edges in a network that lies between communities and then removes them, leaving behind just the communities themselves. It has been used in many real life examples.

E. Modularity Optimization

One of the most widely used methods for community detection is modularity maximization [8]. Modularity is a benefit function that measures the quality of a particular division of a network into communities. The modularity maximization method detects communities by searching over possible divisions of a network for one or more that have particularly high modularity. Since exhaustive search over all possible divisions is usually intractable, practical algorithms are based on approximate optimization methods such as greedy algorithms, simulated annealing, or spectral optimization, with different approaches offering different balances between speed and accuracy [19]. The usefulness of modularity optimization is however questionable: on the one hand, it has been shown that modularity optimization often fails to detect clusters smaller than some scale, depending on the size of the network.

F. Issues

All the algorithms discussed here, do have their own advantages or usability in a particular situation. They have restrictions also. Edge betweenness measure, which measures the intensity of edge in the network, is taken as main issue in the proposed algorithm. For finding better community structure, complexity of algorithm has to be reduced. Finding betweenness measure for edges between the node having one adjacency node and other

nodes, is making no change in making of communities. So, the proposed method removes the calculation process for those edges.

IV. PROPOSED APPROACH AND IMPLEMENTATION

A complex network can be represented in terms of nodes and edges indicating connections between nodes. In Internet, for example, the nodes represent routers and the edges the physical connections between them. In the same way, in transport networks, the nodes can represent the cities and the edges the highways that connect them. These edges can have weights, which can represent the flux of car in a highway or a frequency of interactions between two words in a language network.

In the study of complex networks, a network is said to have community structure if the nodes of the network can be easily grouped into sets of nodes such that each set of nodes is densely connected internally. This implies that the network divides naturally into groups of nodes with dense connections internally and sparser connections between groups.

A graph G can be defined as a pair (V,E) , where V is a set of vertices, and E is a set of edges between the vertices $E \subseteq \{(u,v)|u,v \in V\}$. If the graph is undirected, the adjacency relation defined by the edges is symmetric, or $E \subseteq \{(u,v)|u,v \in V\}$ (sets of vertices rather than ordered pairs). If the graph does not allow self-loops, adjacency is irreflexive. An example graph is shown in Fig 2.

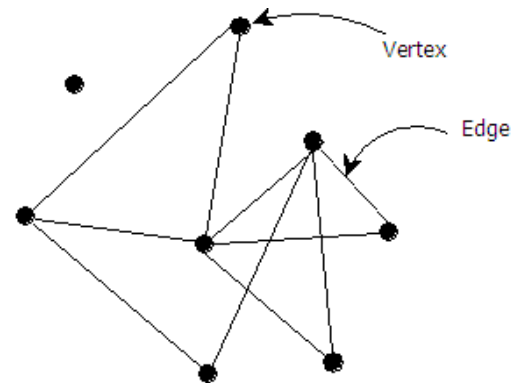


Fig. 2. A Sample Graph with Eight Vertices and Ten Edges

Each graph $G=\{V, D\}$ can be conveniently represented in the form of an $N \times N$ adjacency matrix A where if $A_{ij} \neq 0$ then i points to j . The main motive of algorithm is just check the presence or absence of a connection between two entities therefore, it have an unweighted graph, with $A_{ij} \in 0, 1$. It follows the convention that $A_{ii} = 0$. In the more general case of a weighted network, A_{ij} takes values that reflect the strength with which i is connected to j .

Community detection in large networks is potentially very useful. Nodes belonging to a tight-knit community are more than likely to have other proper ties in common.

A. Proposed Approach for Detecting Community Structure

Here, a new method for creating community structure is proposed, which works more efficiently in cases when the graph has more leaf nodes. Leaf nodes are those nodes which are having only one adjacent node connected to it. It is assumed each node is generating equal amount of traffic, so the traffic of each node is assigned value 1 at the start of calculation. The nodes, which are having only one adjacent node, add their value to its adjacent node, which is having multiple adjacent nodes and delete them from the graph. Betweenness measure of the existing edges is calculated, which considers the traffic of the node and betweenness of the recently traveled edges. This is divided by number of path towards the source. The calculated betweenness is assigned to the edges. Now, the edge which is having highest betweenness is detected and deleted from the network. This process is repeated until all the edges of the graph have been traveled. That means no edge in the graph has been left for the calculation.

B. Implementation

Edge betweenness of an edge is the number of shortest paths between pairs of nodes that run along it. If there is more than one shortest path between a pair of nodes, each node is assigned equal traffic such that the total traffic of all of the nodes is equal to unity. If a network contains communities or groups that are only loosely connected by a few intergroup edges, then all shortest paths between different communities must go along one of these few edges. Thus, the edges connecting communities will have high edge betweenness. By removing these edges, the groups are separated from one another and so the underlying community structure of the network is revealed.

The betweenness measure of edge is assigned by using the formula discussed in the algorithm. Consider

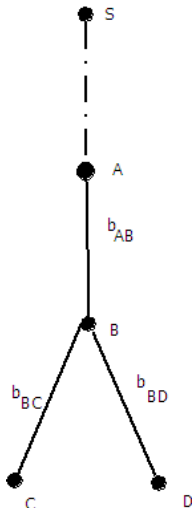


Fig. 3. Betweenness Measure

figure 3 on which we are performing our algorithm by considering S as source. Following steps are carried out to get the communities:

- **Step 1:** Assign traffic, t to all nodes.
- **Step 2:** If the node has only one adjacent node connected to it, add the traffic of that node to the adjacent node.
- **Step 3:** Delete nodes which are having only one adjacent node.
- **Step 4:** Calculate the Betweenness measure of each edge, b_e using

$$b_{near} = \frac{t_{itself} + \sum b_{far}}{\delta_{itself}} \quad (1)$$

- **Step 5:** Assign betweenness measure calculated to the edge.
- **Step 6:** Deduct the edge having highest betweenness.
- **Step 7:** Go to step 1 until all the edges of the graph has been traveled. That means no edge in graph has been left.

Now, repeat this process for all source vertices and summing the resulting scores on the edges gives us the total betweenness.

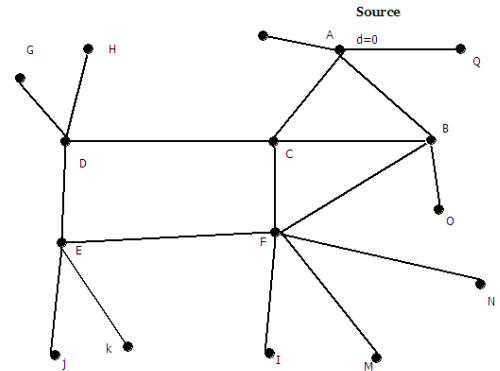


Fig. 4. Artificially Generated Random Graph. Having 16 Node and 18 Edges.

So, in context of the graph shown above betweenness may be calculated as,

$$b_{AB} = \frac{t_B + b_{BC} + b_{BD}}{1} \quad (2)$$

In the traditional definition of vertex betweenness [16][20], multiple shortest paths between a pair of vertices are given equal weights summing to 1. For example, if there are two shortest paths, each will be given weight . Same definition for our edge betweenness has been adopted, although with betweenness, traffic of the node is also used. Initially, traffic of each node is given 1 including leaf node. According to algorithm, all the leaf nodes is removed and assign the traffic of leaf node to

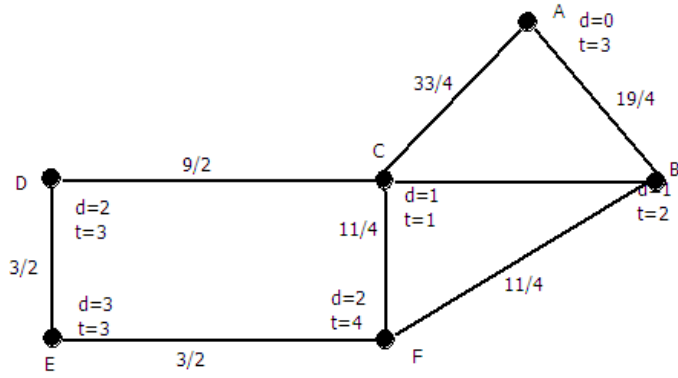


Fig. 5. After Removal of Leaf Nodes and with Betweenness Measure of all Edges.

the non leaf nodes by summing the traffic of leaf node to the non leaf node. As shown in the figure 4 node A is assigned traffic $t_A = 2$ and so on, at node B, $t_B = 3$, at Node C, $t_C = 2$, at node D, $t_D = 4$, at node E, $t_E = 3$ and at node F, $t_F = 4$.

Betweenness can be calculated by following formula,

$$b_B = \frac{t_B + \sum \text{betweenness}_{in}}{\text{Outdegree}_{in}} \quad (3)$$

As in case of node x, we can calculate the Score as,

$$b_B = \frac{t_B + b_{BC} + b_{BD}}{\text{totaloutdegree}_B} \quad (4)$$

Now, to calculate the edge Betweenness from all shortest paths betweenness measure for different edge will come as shown in figure 5. Like betweenness $b_{EF} = b_{ED} = 3/2$. So on, betweenness value of different edges are shown in the figure above. Calculation step is calculated for each edge removed from the network. After removable of each edge are deducting the leaf nodes, which reduces the time complexity for the algorithm in comparison to previous algorithms. The next graph shown in figure 5 is with betweenness measure of all the edges. Network with strong community structure often break apart into separate components quite early in the progress of the algorithm, substantially reducing the amount of the work that needs to be done on the computational complexity of the algorithm. Some networks are directed, i.e. their edges run in one direction only. Like in World Wide Web links in web page point in one direction only. It is imagined a generalization of shortest path betweenness by counting only those paths that travel in the forward direction along with edges. Therefore, our algorithm applied to the undirected version as well as directed version of the networks, and no special algorithm is required for the either case.

C. Quantifying the Strength of Community Structure

The proposed algorithm detects good communities both in artificially generated random network and in real

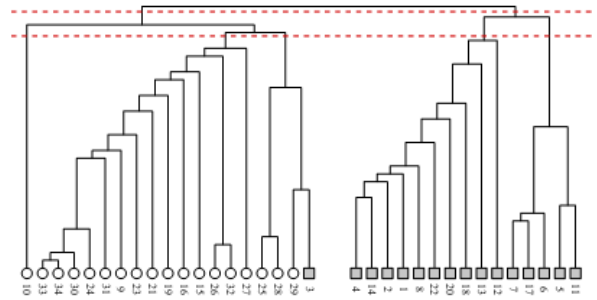


Fig. 6. Dendrogram of Zachary's Karate Club

world examples. However, practically how many communities should be generated using the algorithm is not known ahead of time. So the problem is how to grade the algorithm? Algorithms always produce some division of network into communities, even in completely random networks that have no meaning community structure. So, it is to find some way of getting good structure. Normally, the algorithm output is in form of dendrogram which represents an entire nested hierarchy of possible community division for the network. To find out the best one for a given network, dendrogram is divided to get a sensible division of network.

To define a measure of the quality of a particular division of a network, **modularity** has been used. Modularity is one measure of the structure of networks or graphs. It was designed to measure the strength of division of a network into modules (also called groups, clusters or communities). Networks with high modularity have dense connections between the nodes within modules but sparse connections between nodes in different modules. Modularity is often used in optimisation methods for detecting community structure in networks. However, it has been shown that modularity suffers a resolution limit and, therefore, it is unable to detect small communities.

Consider a particular division of a network into k communities. Let us define $k \times k$ symmetric matrix e whose element e_{ij} is the fraction of all edges in the network that link vertices in community i to the vertices in community j . The modularity is calculated taking all edges into consideration i.e. edges which have been removed by community structure algorithm. The trace of this matrix $\text{Tr } e = \sum_i e_{ii}$ gives the fraction of edges in the network that connect vertices in the same community, and a good division is high value of trace. The trace on it's own is not a good indicator of the quality of division.

So, the sum of row or column $a_i = \sum_j e_{ij}$, which represent the fraction of edges fall between vertices without regard for the communities they belong to, it would have $e_{ij} = a_i a_j$. Thus, modularity measure is

defined by,

$$Q = \sum_i (e_{ij} - a_i^2) = \text{Tr} \mathbf{e} - \|\mathbf{e}^2\| . \quad (5)$$

where, $\|\mathbf{x}\|$ indicates the sum of the elements of the matrix \mathbf{x} . It measures the fraction of edges in the network that connect vertices of the same type (within community edges) minus the expected value of the same quantity in a network with the same community divisions, but random connections between the vertices. If the number of within community edges is no better than random, then $Q=0$. Values approaching $Q=1$, which is maximum, indicate networks with strong community structure.

D. Complexity Evaluation

The proposed algorithm calculates edge betweenness over rounds. In a round, keeping a node as a source node and calculating the edge betweenness of all edges, the complexity depends on the number of edges. Until all the nodes are taken as source nodes, the rounds are incremented. Edge betweenness for an edge is the summation of it over all the rounds.

Thus, for a graph $G=(N,M)$, the computational complexity for calculating edge betweenness of all edges is:

$$O((n-l) * m). \quad (6)$$

where,

n : number of nodes, l : number of leaf nodes, m : number of edges.

V. RESULT

The algorithm used here detects community structure on Artificially Generated Random Network and real world example of Zachary's Karate Club Network [22]. It produces the communities among the network by using the modularity function which is discussed in the chapter 5.

A. Artificially Generated Random Network

Our community structure algorithm does an excellent job of recovering known communities both in artificially generated random network and in real world example. We have applied our algorithm on this artificially generated graph shown in figure 4, which we have discussed in the last chapter with our example. By using the modularity function, it is divided into three different communities as shown in figure 6. It shows the fraction of vertices in a self-generated network sample classify into the three community correctly.

The algorithm takes a text file having the edges between the vertices of the graph in a line, as an input. Then, the algorithm computes input and detects the community structure. It results output in the form of text file containing the modularity and the possible community structure in the graph. It also shows which vertex belongs to which community.

1) *16 Node Network*: This is the example on the basis of which the working of algorithm is shown in the chapter 3. It is a 16 node network which is having 18 edges. The betweenness measure has been calculated for each edge which is between the non-leaf nodes. Then it deletes the edges with highest betweenness measure. Highest possible modularity measure then decides the number of communities in the network.

Figure 7 shows the input file, it contains the node numbers which are having edge between them. The said file is given as input to the algorithm and it generates the output file as shown in figure 8. It contains number of nodes, modularity, number of communities and the nodes with their communities they belong to. While processing the result it also shows the list of edge, which are removed one by one from the graph.

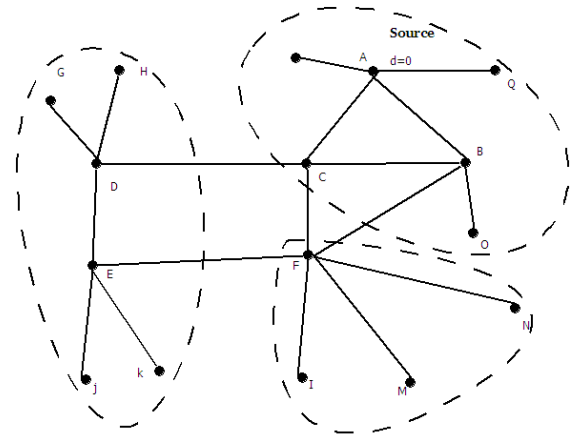


Fig. 7. Artificially Generated Random Network which is having 16 Nodes

2) *13 Node Network*: Here is another example for the finding community structure on the artificially generated random graph. Figure 10 is an artificially generated random network, having 13 nodes and 16 vertices. After applying the algorithm, discussed in the chapter 3, it calculates the between measure for the different edges. Again according to the highest modularity measure number of community structures is decided, which is 3 in this example.

B. Zachary's Karate Club Network

Now, we apply our algorithm to real-world network data. We will apply this on one of the classical studies in the social network analysis. In Early 70s, Wayne Zachary observed social interactions between the members of karate club. Social interaction between the members was shown within the club and outside it through the network of ties. In the mean while some dispute erupts between the administrator and the principal karate teachers, and so the club divided into groups.

Figure 12 shows the consensus network structure of Zachary's club before the split. Feeding this into our

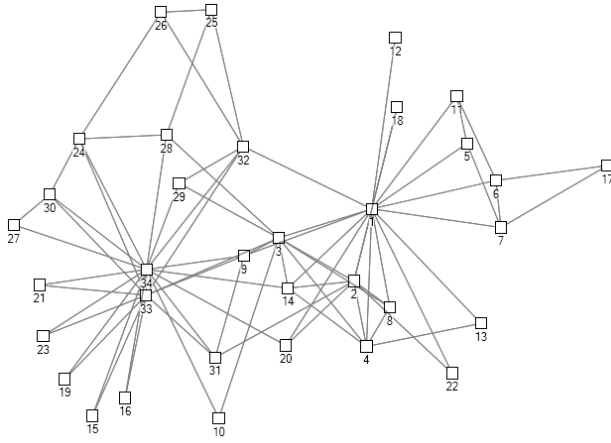


Fig. 8. Zachary's Karate Club Network which is having 34 Nodes representing the Members of Club and Administrator

algorithm, we find the result shown in the figure 13. Dendrogram, which represents the network into the layers architecture that at what level the different members of club are associated with each other. In figure 6 the links between the different members are shown with the help of bar association and the vertical bar shows the different communities of the network. This is also shown with the help of graph in figure 13. It is clearly showing that the network is divided into to four communities in which two community is major, which are associated with node 1, which is representing the administrator and node 33 which is representing the main trainer of the club. The members those are associated with the administrator are represented by circle and members associated with trainer are represented with the help of filled circle. Two other communities are also there which is not closely connected with any of the group of club.

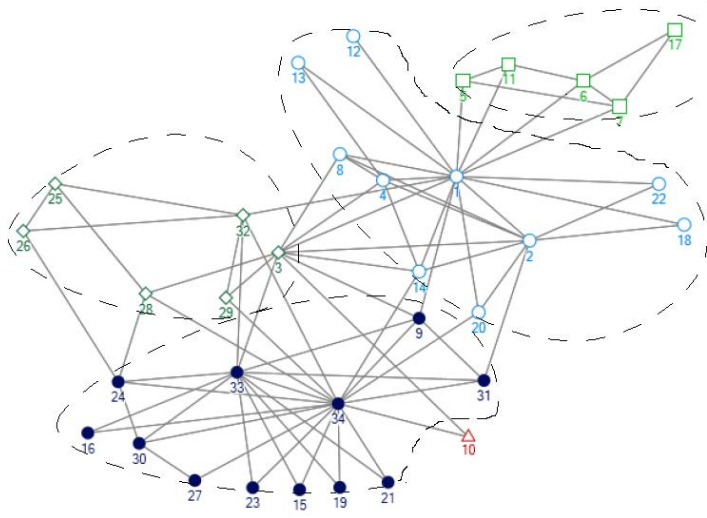


Fig. 9. Zachary's Karate Club after the classification done by our Algorithm

C. Summary

This chapter discuss about the applications and results of approach on different artificially generated random network and real world problem. We have seen with the help of these examples that algorithm works quite well in the different situation. Quantifying the strength of Community Structure gives best level of communities in the given network.

VI. CONCLUSION & FUTURE WORK

The proposed algorithm perform network clustering i.e. the task of extracting the natural community structure from networks of vertices and edges. The approach is simple and intuitive, gives excellent result on the networks, which is having multiple trails, which is termed leaf node in this work, like in the case of Internet traffic, Internet topology or so. The approach discussed, is different form the previous approaches. It doesn't calculate the betweenness measure for the leaf node. It passes the traffic of these nodes to the non- leaf nodes. And so reduces they complexity of the algorithm. This algorithm includes a recalculation step in which betweenness score are reevaluated after the removal of every edge. Then, the quality of the cluster is evaluated with the help of modularity function. The implementation of algorithm has demonstrated the efficacy and utility of our method with a number of examples. It has been shown that it is reliable and sensitively extracts community structure from artificially generated networks with known communities. It has been also applied to real-world networks with known community structure.

The traffic of one node varies from the traffic of other nodes, which plays an important role in the calculation of intensity of the traffic between any two nodes. The proposed work can be extended in future for the calculation of betweenness measure having different intensity of traffic on edges between the nodes.

REFERENCES

- [1] M. Girvan and M. E. J. Newman, "Community structure in social and biological networks", *Proc. Natl. Acad. Sci. USA* 99 (12): 78217826. doi:10.1073/pnas.122653799. PMC 122977. PMID 12060727. (2002).
- [2] S. Fortunato, "Community detection in graphs", *Phys. Rep.* 486 (3-5): 75174. doi: 10.1016/j.physrep.2009.11.002 (2010).
- [3] M. A. Porter, J.-P. Onnela and P. J. Mucha, "Communities in Networks", *Not. Amer. Math. Soc.* 56: 10821097, 11641166.(2009).
- [4] M. E. J. Newman, "Detecting community structure in networks" *Eur. Phys. J. B* 38 (2): 321330. doi:10.1140/epjb/e2004-00124-y. (2004).
- [5] M. E. J. Newman, "Fast algorithm for detecting community structure in networks". *Physical review E* 69 (6): 066133. doi:10.1103/PhysRevE.69.066133. (2004).
- [6] L. Danon, J. Duch, A. Daz-Guilera and A. Arenas, "Comparing community structure identification", *J. Stat. Mech.* 2005 (09): P09008. doi:10.1088/1742-5468/2005/09/P09008. (2005).
- [7] S. Fortunato and M. Barthelemy, "Resolution limit in community detection". *Proceedings of the National Academy of Science of the USA* 104 (1): 3641. doi:10.1073/pnas.0605965104. PMC 1765466. PMID 17190818. (2007).

- [8] B. H. Good, Y.-A. de Montjoye and A. Clauset, "The performance of modularity maximization in practical contexts". *Phys. Rev. E* 81 (4): 046106. doi:10.1103/PhysRevE.81.046106. (2010).
- [9] V.D. Blondel, J.-L. Guillaume, R. Lambiotte and E. Lefebvre, "Fast unfolding of community hierarchies in large networks", *J. Stat. Mech.* 2008 (10): P10008. doi:10.1088/1742-5468/2008/10/P10008, (2008).
- [10] M.G. Everett and S.P. Borgatti, "Analyzing Clique Overlap Connections", *Connections* 21: 49. (1998).
- [11] T.S. Evans, "Clique Graphs and Overlapping Communities", *J. Stat. Mech.*: P12037. arXiv:arXiv:1009.0638. doi:10.1088/1742-5468/2010/12/P12037. 2010).
- [12] G. Palla, I. Derényi, I. Farkas and T. Vicsek, "Uncovering the overlapping community structure of complex networks in nature and society", *Nature* 435 (7043): 814818. doi:10.1038/nature03607. PMID 15944704.(2005).
- [13] Condon, A.; Karp, R. M., "Algorithms for graph partitioning on the planted partition model", *Random Struct. Algor.* 18 (2): 116140 doi:10.1002/1098-2418(200103)18:2;116::AID-RSA1001;3.0.CO;2-2. (2001).
- [14] Lancichinetti, S. Fortunato and F. Radicchi, "Benchmark graphs for testing community detection algorithms", *Phys. Rev. E* 78 (4): 046110. doi:10.1103/PhysRevE.78.046110.(2008).
- [15] Mechthild Stoer and Frank Wagner, *A simple Min-Cut Algorithm*. "Proceedings of the 2nd Annual European symposium on Algorithms". *Lecture Notes in Computer Science, Vol 855,1994.*
- [16] L. C. Freeman, "A set of measure of centrality based on betweenness", *Sociometry* 40 -35(1977).
- [17] Pan, Ying; Li, De-Hua; Liu, Jian-Guo; Liang, Jing-Zhang, "Detecting community structure in complex networks via node similarity", *Physica A, Volume 389, Issue 14, p. 2849-2857. 2010PhyA..389.2849P.*
- [18] B.W. Kernighan, S. Lin, "An efficient heuristic procedure for partitioning graphs", *Bell. Syst. Tech. J.* 49 (1970) 291307.
- [19] L. Danon, J. Duch, A. Daz-Guilera and A. Arenas (2005). "Comparing community structure identification". *J. Stat. Mech.* 2005 (09): P09008.
- [20] F. Radicchi, C. Castellano, F. Cecconi, V. Loreto, D. Parisi, "Defining and identifying communities in networks", *Proc. Natl. Acad. Sci. USA* 101 (2004) 26582663.
- [21] P. Pons, M. Latapy, "Computing communities in large networks using random walks", in: *Proc. of the 20th International Symposium on Computer and Information Sciences, Springer-Verlag, Berlin, 2005, pp. 284293.*
- [22] Zachary W., "An information flow model for conflict and fission in small groups." *Journal of Anthropological Research*, 33, 452-473. (1977).
- [23] Stuart A. Rice "The American Political Science Review" Vol. 21, No. 3 (Aug., 1927), pp. 619-627, American Political Science Association.

Diversification in Engineering Education through Indian Student Forum

An Experimentation Project in India

Rohit Kandakatla

KG Reddy College of Engineering and Technology
Hyderabad, India
rohit.kandakatla@gmail.com

R. Dhinesh Balaji

University of Petroleum and Energy Studies
Dehradun, India
dinesh@worldspeed.org

Abstract—Diversity in education incorporates varying geographic, cultural, intellectual, ethnic, academic and social elements. An education that would cover this diversification will make the world a more vibrant place to live. India is a country known for its diversified culture, languages, ethnic groups and more importantly its education. There are two interesting questions that foster the discussion for an enhanced engineering education in the country. They are: 1.) what would be the potential, if the numerously diversified engineering minds around the nation are brought together? And 2.) How can this be driven in the right direction? A group of engineering students across the nation are working to find the answers to these questions. This paper discusses the efforts and outcomes of these students' initiatives in creating diversity programs and their motto to unify the student's minds.

SPEED (Student Platform for Engineering Education Development) is an international non-profit student organization that works towards enhancing engineering education. **SPEED-India** is a country chapter that has conducted five regional workshops and one national conference (Indian Student Forum) between June 2013 and January 2014. These sessions have brought together engineering students from across the country and the world to discuss and develop action plans that would result in an enhanced engineering education. Through these working sessions, more than 3000 Indian engineering students were brought together and exposed to the discussions of engineering education. They were later made to contribute to the dialogues and as well as in developing concrete action plans. The action plans were diversified from addressing the infrastructure for engineering education to technology uses in learning to community, project and entrepreneurship based learning methodologies. The paper discusses the creation and outcomes of these action plans in detail.

Keywords—Engineering Education, Action Plans, Diversity, **SPEED**, **ISF**.

I. INTRODUCTION

The concerns surrounding diversifying the engineering workforce have traditionally been linked to research with underrepresented groups. However, as the goal of the field of engineering is to produce a "global engineer," issues of diversity emerge not only among the human capital of engineers but the contributions that can be made by a diverse

education curriculum in engineering education [1]. Diversification provides engineering students the opportunity to capitalize their coursework in fields such as entrepreneurship and sociology so that engineering designs can expand beyond the traditional one-dimensional technical issues into a world that is more inclusive of other disciplines.

Another different context in the nature of diversity is Cultural Diversity. Culture can be related to various intrinsic qualities and extrinsic expressions such as thought processes, habits, manners, emotions, communication skills etc. Today's world is connected by knowledge and is based on global economy. It is essential that a while graduation, an engineering student obtain not only necessary education, but also cultural awareness so that he/she will be efficient in dealing with the challenges due to existing cultural diversity in the world.

India is a highly diverse society in terms of caste, religion, region, place of residence such as rural and urban areas, languages etc. Currently Indian population comprises of 8 major religions and 22 official languages. This implies the need of cultural awareness not only across different countries, but also across different regions in India

According to a study done by Rugarcia, Felder, seven features that pose challenges to future engineers are proliferating information, multidisciplinary technological development, globalized markets, endangered environment, emerging social responsibility, participatory corporate structures and rapid changes [3]. Cultural diversity plays a major role in many of the above features. This shows a great need for the engineering curriculum to account for all these and possibly more features to provide vision, knowledge and skills to the graduates for successfully contributing to the world.

II. STUDENT PLATFORM FOR ENGINEERING EDUCATION DEVELOPMENT

SPEED is a global, non-profit student organization that functions as an interdisciplinary network of engineering students who aspire to stimulate change and impact the development of engineering education (EE) and its effect on society, industry, the environment and local communities. In collaboration with academia, industry and government **SPEED** is committed to improving EE by channeling the student voice and perspective. Through local and global initiatives **SPEED**

empowers students and encourages the development of professional, ethical and social responsibility. Furthermore, through insight into policy, academia/industry relations and organizational structure SPEED serves to continue the professional education of its members and participants of its forums [3].

In June 2013, SPEED collaborated with Indo-US Collaboration for Engineering Education (IUCCEE). IUCCEE works to improve the quality and global relevance of engineering education and research in India with focus on faculty development, student development, curriculum development, as well as improved teaching technologies and research [4]. Both the organizations joined hands to improve the EE scenario in India for the benefit of the student fraternity.

III. INDIAN STUDENT FORUM

A. Introduction

Indian Student Forum (ISF) is a platform where all the enthusiastic Indian engineering students with an interest in enhancing the engineering education gathers together to establish a dialogue on EE through a series of discussions.

The overall plan for the ISF was two-fold: to positively impact Indian student participants current position as budding global engineers eager to affect change within EE and local communities; and to show the professional stakeholders that students are a much larger piece of this puzzle than they are currently given credit for and are entitled to a voice within the engineering education dialogue.

B. Global Student Forum

The Indian Student Forum is a concept derived from the Global Student Forum (GSF). GSF is a global conference organized by the SPEED which draws academics representatives from government bodies, industry, non-profit organizations and an increasing number of students from around the world to discuss issues pertinent to engineering education. During the forum students are a part of an international experience, submerged in the atmosphere of cross-cultural communication and creative thinking. Participants take part in workshops aimed at providing them with tools to find innovative solutions with a global perspective and apply them in their local communities. They get a chance to learn about already existing student projects, get involved and/or start their own regional and global initiatives with the aim of maximizing the student voice within the engineering education community [5].

ISF was planned and structured on similar lines of GSF. ISF was conducted just before the 1st International Conference on Transformation in Engineering Education (ICTIEE) [6] so that student could meet global academicians and industry representatives during the conference.

C. Planning

SPEED leaders in India recruited EE students who displayed good leadership skills during the five regional workshops which were conducted in collaboration with IUCCEE

between June 2014 and August 2014 [7]. The ISF working committee was divided into different roles to improve the efficiency and also speed up the process. The committee was divided into Sponsorship, Relations, Activities, IG Panel, Accommodation, Logistics, Educational Content, Scheduling and Registration groups. Each group was assigned with specific roles which were assigned in virtual meetings conducted once every 2 weeks. Every working committee member was accountable for their respective responsibilities and was required to report the status of work prior to every meeting. This protocol boosted the performance of the team which ensured effective planning for the forum.

The registration for ISF was done online through the SPEED website. Interested students were asked to fill a registration form with details of their previous experiences with the field of EE, Action Plans developed during the regional workshops and their resume. Participants were also allowed to select appropriate track whose topic were aligned to that the tracks.

After receiving the registration form, all submissions were subjected to review by the registration process. Students with prior knowledge on engineering education and action plans aligned to the theme of the forum were accepted. Students were sent a mail after submitting their registration form informing them that their submission was received, second mail was sent informing their acceptance following up with another mail providing them with finance details. All accepted students were sent a welcome package before the start of ISF which consisted of the details such as mode of transport to reach the ISF venue, emergency contact numbers, weather conditions, accommodation details, ISF schedule and dress code. This helped the participants prepare better before arriving for ISF.

D. Execution

ISF was portrayed as a stage 2 for development of action plans prepared during the regional workshops. After the completion of the regional workshops, participants started implementing the action plans in their local regions. During the course of implementation, the participants encountered certain obstacles. Some of the common ones include shortage of financial resources, lack of depth in action plan, inaccurate time frame calculation. Participants from the regional workshops were expected to attend ISF, analyze the challenges faced during implementation and work on enhancing their action plan based on the analysis.

The theme for ISF was "Creativity and Innovation in Indian Engineering Education" which was aligned with the theme of the regional workshops conducted. 50 action plans were developed during the 5 regional workshops conducted. All the 50 action plans were scrutinized and 3 tracks were identified for ISF, 1. Design/Animation/Modelling/Simulation based Learning, 2. Community and Interdisciplinary based learning, 3. Project based learning. Participants were streamlined into different tracks based on their preferences given during registration and also the theme of their action plan.

During the course of ISF, participants brainstormed in groups about the implementation of their action plan and the challenges faced. Each group comprised of students from different parts of the country, which provided each group varied discussions. This helped the participants gauge the drawbacks of each action plan on a national level which eventually provided them better scope of improvement. Each track was facilitated by international SPEED leaders and Industry experts from National Instruments, Quanser, Cypress Semiconductors and Skyfii Labs who mentored the students and guided them to build their action plans using the SMART objectives which points out the importance of an action plan to be smart, measurable, achievable, realistic and time bound [8]. The industry experts enlightened the participants with various ways to approach industries for financial assistance.

Based on the feedback received, participants from all tracks were given time to explore and perform further study to revise their action plan in line with the knowledge obtained. Participants were allowed to use the library and various labs present in the host college to pursue further study. After gathering the required information, participants incorporated the changes into their action plan. Presentations were given to other participants in their respective tracks about the improved version of the action plan followed by feedback from fellow participants and facilitators.

Sustainability refers to the continuation of a project's goals, principles, and efforts to achieve desired outcomes [9]. One important aspect of every action plan is to ensure its sustainability for a long lasting impact. A workshop was conducted on sustainability to provide an insight to participants on its importance and need in every action plan. In order to improve the knowledge transfer, participants were provided with a case study of ISF. The study described the idea, planning, execution and expected outcomes of ISF. Using this information as reference, participants were encouraged to develop strategies to ensure the sustainability of ISF to make sure the forum is conducted every year and benefit the student fraternity. Very good responses were received from this workshop, which helped the participants oversee the possible future obstacles. This guided the participants to make additional changes to their action plan to make it more sustainable and long lasting.

In addition to stage 2 development of action plan, additional sessions were conducted for the overall development of the participants. Cultural evening was organized with a motive of cultural exchange among participants. Participants were dressed in their traditional cultural attire and shared their local food with the participants and also performed their cultural dances. The event helped students from various cultural backgrounds know about the others and also established cross cultural bonds. Participants were taken to visit different industries related to their course of study which helped them attain a real life perception of various manufacturing processes.

All the participants presented their action plans on the last day of ISF. Academicians, deans, industry representatives who arrived to attend the conference were invited to judge the action plans. The judgment was based on the creativity and

originality, sustainability, thoroughness, feasibility, social impact of the action plan and presentation skills of the presenter. The judges gave participants constructive feedback and suggestions. Some of the judges also offered to provide financial resources to few action plans.

After the completion of the presentations, networking and poster session was conducted. Interested students were informed to prepare posters on various projects being implemented in their colleges prior to ISF. Delegated attending the international conference were invited for the networking session. Participants used this as a platform to showcase their poster to fellow participants and the delegates. This interaction helped them network with delegates from across the world which benefited them in establishing a global professional network.

E. Intergenerational Panel

SPEED was nominated to organize an intergenerational (IG) panel during the third day of the main conference. Intergenerational Panel serves to increase the dialog between the professional stakeholders from academia and industry and the students they educate and employ. All parties are interested in increasing communication across generations; this session achieves this in a way that further diversified the discussions held throughout the week during ISF and the ICTIEE. The topic of discussion for the panel was the transformation in engineering teaching methodologies. All the people present for the panel were broken down into groups making sure each had equal number of students and academicians. Every person in each group were given time to discuss and give their perspectives on the topic. These discussions will be pared down into concrete suggestions for the future. This required synthesizing information from all session groups and incorporating the different viewpoints of all the various stakeholders. All the information was shared with the groups later who decided to use this information to modify their teaching methodologies to improve the measure of effective knowledge transfer

IV. ACTION PLANS DEVELOPED

There were 13 action plans which were developed at ISF in the three tracks. All the action plans in each track were aligned to their respective theme. The first track (Design/Animation/Modelling/Simulation based Learning) comprised of 3 action plans. All the action plans were developed with a vision to bring about a change in the way engineering education is delivered in their colleges. The first action plan was intended to improve the quality of deliverability of EE by adopting visual, audio and graphical media that will help the students acknowledge the subject and have a better insight about the course. The second action plan aimed to make a cross platform mobile application which will narrow the gap between students of different fields of EE in a college. This application would be a portal to share interdisciplinary project related data, provide details of available research opportunities and solve major issues such as attendance monitoring and updates from college authorities.

The second track (community and interdisciplinary based learning) consisted of 5 action plans. All of them were developed with a motive of inculcating community and interdisciplinary based learning into their curriculum. This first action plan aimed on providing quick solutions to local community problems using available waste resources. Implementing this action plan required creativity and good knowledge in that specific field of engineering. This idea of community based learning was also suggested to the college authorities for inculcating into the curriculum as an elective. This action plan provided the local community immediate solutions to small problems and also helped the students improve their understanding of their course. The 2nd action plan was developed to spread awareness and also change surrounding non-renewable energy consumption to renewable energy. The first phase of action plan is replacing all energy sources to biogas and biomass. Biomass was intended to provide energy for electricity and biomass for household cooking purposes. This idea was shared with people in respective local regions and they students helped interested people switch to renewable energy sources. The 3rd action plan was developed with the same motive but had different action steps. The students planned to contact their college authorities to replace the existing energy sources with solar energy. This action plan was developed by a group of students studying electrical engineering. They also proposed that all the changes will be made by them which would reduce additional external resources. The 4th action plan was developed by a group of environmental engineers. The action plan aimed to spread environmental awareness among local citizens and educate them about the toxic effects of the usage of plastic. They also formulated a campaign to assemble people and collect plastic in the nearby regions every week and dispatch it to the recycling authorities. The 5th action plan was targeted to recognize the need to bridge the gap between students of different domains of engineering and provide them a platform for interdisciplinary research and development. The last action plan desired to provide students an industry innovator platform where students can interact with industry experts and local innovators to gain industry exposure.

The third track (project and entrepreneurship based learning) comprised of 5 action plans. All the action plans were prepared on mission to highlight and implement project and entrepreneurship based learning in their curriculum. The first action plan aimed to take into account the vast number of engineers who wish to enter the field of techno-entrepreneurship and lack of awareness for the same in India. The strategy was to develop a T-cell program inside the college through collaboration with industry experts, government and provide budding entrepreneurs necessary resources to enter the field of entrepreneurship. The 2nd action plan proposed to host a business competition in each region where interested students can share their business ideas. Investors will be invited to the event of that interested ones can invest in the new ventures. The 3rd action plan emphasized to give engineering education a more practical touch rather than the traditional theoretical way by conducting project expo's, technical workshops and seminar by industry representatives and teachers about their

research and development. The 4th action plan was aimed to improve the collaboration between classroom and laboratory. This was expected to be achieved by conducting experiments in sync with the topics taught so that students visualize the phenomenon taught better and also understand the real live examples. The last action plan aimed create a bridge between industry and college to provide students a platform to enhance their technical as well as practical skills to avoid any struggle adjusting to industry needs after graduation.

V. ACTION PLAN IMPLEMENTATION COMPETITION

In order to motivate the participants to implement their respective action plans after the completion of ISF, SPEED announced the ISF implementation competition. All the participants were briefed about the competition before the closing ceremony of ISF. The winners will be decided 6 months from the end of ISF which is the end of July. All the action plans will be judged based on the progress based till the date of judgment and impact made by each action plan. All the judges and industry representatives were contacted again inviting them to be a judge for the ISF implementation competition.

All participants were sent monthly mails to track the progress. As all the progress was being tracked virtually, SPEED with the help of IUCEE planned weekly webinars which were conducted every Saturday at 18:00 Indian Standard Time. Interested participants were invited to present their action plan implementation which boosted them confidence and also helped get constructive feedback from the other webinar attendees [10]. All the participants were provided regular guidance whenever required by the SPEED. All participants were informed to submit a detailed report on the status of their action plan implementation by the end of July. The winner of the implementation competition will be sponsored by SPEED and IUCEE to the 10th GSF which will be held in December at Dubai.

VI. IMPACT CREATED

According to a survey done by Dr. MG Prasad to evaluate the impact on cultural diversity by process of education, students felt a good mixture of cultural backgrounds between fellow student and also the instructor provides them better global exposure [10]. The composition of each track at ISF was ensured to have diversified students from different parts of the country. Every track was facilitated by international SPEED leaders and industry experts from different parts of the globe. This mixture of diverse participants and facilitators helped them expand their professional network, which eventually provided them global exposure. The weekly webinars conducted to track the Action Plans gave participants additional opportunity to keep in touch with their fellow participant through which enormous amount of knowledge was shared. Participants also took regular feedback from the facilitator while implementing their action plan which ensured a sustainable global professional network was built.

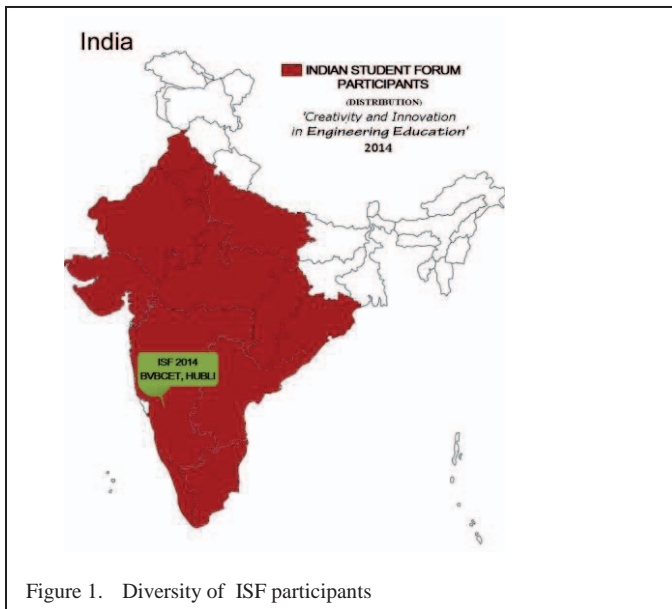


Figure 1. Diversity of ISF participants

While some action plans are still being implemented, there are few participants who have almost finished their implementation. All these action plans have in a way impacted their community and student fraternity. The action plan developed to promote interdisciplinary learning was implemented in RK University and BVB College of Engineering and Technology. They have infused the concept of interdisciplinary learning in their respective curriculum by incorporating multi domain projects which increased the cross domain knowledge transfer when students from different engineering fields work together on a same project. Another action plan was implemented in G Pulla Reddy Engineering College where a participant educated people from the local community to use biogas as a replacement to gasoline which is used to cook food. The participant formed a group and educated them on generating biogas and installed the same in many nearby houses. Participants from CVSR Engineering College have developed an application on android operating system for students in their college. Students can use this to add post and help the needed for any of their projects so other students can join them. The application also helps them monitor their attendance, check the schedule and receive regular updates from the college management. Students from KG Reddy College have got approval from the college to set up an entrepreneurship cell inside the college. They have contacted the ministry of science and technology to provide them necessary funds to establish an entrepreneurship cell. The cell will provide budding entrepreneurs initial investment for setting up their new venture in the initial stage. These action plans implemented have impacted the local communities by diversification in engineering education.

VII. SUCCESS STORIES

ISF implementation competition resulted as success with the action plans being implemented. Here are a few success stories shared in this article. One of the participants B. Mohan

Reddy who successfully implemented his action plan on replacing gas cylinders with biogas for cooking purpose received huge appreciation from the local community and also got featured in the local newspapers. Impressed with his work on community based projects, one of our sponsors Skyfii labs recruited him as a research intern into one of their projects for 6 months. Another participant Vamsi Krishna conducted awareness sessions for school students on the various community problems in the nearby regions and how engineers can work together to solve those problems. This provided the school students an insight about engineering and the role they can play in the community. Impressed by his work, the local government representative has granted him a sponsorship to the 10th GSF which is being held in Dubai during December, 2014.

Two participants from R.K. University and BVB College of Engineering and Technology conducted seminars and workshops on the importance and outcomes of Interdisciplinary learning in their respective universities. They joined hands with interested students from different domains and submitted interdisciplinary project proposals to the research and development cell in their respective colleges. Three projects were accepted and were provided financial resources. One participant from track 3 submitted a proposal and action plan to establish an entrepreneur cell inside his college. The proposal was accepted and forwarded to Indian governments department of science and technology for establishing an incubator center inside the college. These are some of the success stories of ISF in the past 8 months.

VIII. FUTURE SCOPE OF WORK

SPEED plans to continue the same work in collaboration with IUCEE. The 2nd ISF will be conducted from 6th - 6th January 2015 at BMS College of engineering. 7 regional workshops were conducted in different parts of India in September, 2014. All the participants who implement their action plan after these workshops will be invited to participate in the 2nd ISF and work on further development of their action plans.

ACKNOWLEDGMENT

SPEED would like to thank Dr. Krishna Vedula, Executive Director of IUCEE who was solely responsible for collaboration of SPEED and IUCEE and his highest support and guidance in organizing the Indian Student Forum. Sincere gratitude to the officers of IUCEE Mr. Kantha Reddy, Director – Operations of IUCEE, Mr. Ashok Kalbag, Secretary of IUCEE-India and Dr. Ashok Shettar, Principal of B.V.B. College of Engineering for their extreme support and help in conducting the Indian Student Forum successfully. SPEED India is grateful to the global SPEED leaders for their continuous mentorship.

REFERENCES

- [1] Lorraine N. Fleming, Diversity in Engineering Education: An African American Female Professor's Perspective, (2008), Leadership and Management in Engineering
- [2] Rugraciona, Armando, Felder, Richard M, Woods, Donald R, Stice, James E, The Future of Engineering Education I A Vision for a New Century, (2000), chemical Engineering Education.
- [3] D. Delaine et al. (2009) "The Student Platform for Engineering Education Development (SPEED) Empowering the Global Engineer" SEFI Annual Conference, Rotterdam, Netherlands, August 2009. Boyer, E. L. (1996). The scholarship of engagement. *Journal of Public Service and Outreach*, 1 (1).
- [4] <http://iucee.org/iucee/mod/resource/view.php?inpopup=true&id=6330>.
- [5] <http://worldspeed.org/portal/index.php/about-3/information>.
- [6] <http://www.ictiee.org/>
- [7] Rohit Kandakatla, Dhinesh Balaji Radhakrishnan, "Impact of Action Plan workshop in enhancing Indian Engineering Education", 12th LACCEI Latin American and Caribbean Conference for Engineering and Technology, Guayaquil, Ecuador, July, 2014
- [8] http://www.cdc.gov/nccdphp/dch/programs/healthycommunitiesprogram/tools/pdf/action_step_8.pdf
- [9] <http://www.doleta.gov/business/PDF/SustainTips.pdf>
- [10] <http://iuceespeed.wordpress.com/isf-2014-action-plan/>
- [11] Dr. M.G. Prasad, The Role of Cultural Diversity in Enhancing Engineering Education, (2007), Stevens Institute of Technology, New Jersey.

Doorway Monitoring System for Gamma particle detection

A.V.N.R.SAI SHIVA

M.Tech(Robotics Engineering)
University of Petroleum and
Energy studies
Dehradun,India
Saishiva.vn307@gmail.com

B.ANAND

Radiation detectors and
instrumentation division
ECIL
Hyderabad,india
banand@ecil.co.in

ARUN KUMAR YADAV

M.Tech(Robotics Engineering)
University of Petroleum and
Energy studies
Dehradun,India
Aruyad1@gmail.com

Abstract:-The system is developed to detect the radioactive sources like gamma particles. The doorway monitoring system consists two plastic scintillation detectors to detect the gamma source .The system would be designed in such a way that it detects the presence of humans with the help of IR sensor and will count the number of pulses through counters. The detector signal has to be processed for which suitable amplifier module has to be developed .The current status of the system would be transmitted to the remote PC application via Ethernet.The system has audio and visual indications to indicate the status of the system like Ready, Clean and System Fail. The user can set the alarm levels independently for the two detectors, the counting time using the touch display. The system has two modes of operation to meet user requirements. The system continuously acquires the counts and monitors the background radiation.

Keywords:PIC18f46k22,RTC(DS1307),NVRAM,I2C,Int errupts,IR sensor,plastic scintillation detector with PMT tube

1.INTRODUCTION

This SNM baggage system is specifically called special nuclear material baggage system.It is intended that door way monitoring system is by their specifications. Doorway Monitor is a highly reliable system for the radiometric protection of Special Nuclear Material (SNM).It is suitable for indoor installation. The system may be set up in any location where a 230V,AC 50Hz power source is available. Typical locations might be entrances and exits to access areas. It is used mainly for source detection and not normally suitable for contamination monitoring. The radiation sensor used is gamma sensitive Plastic Scintillator coupled with a Photomultiplier Tube (PMT).

The Doorway Monitor uses two plastic scintillator detectors mounted on the two sides (LHS

and RHS) of the portal. The user can set the alarm levels independently for the two detectors, the counting time using the touch display. The system has two modes of operation to meet user requirements. The system continuously acquires the counts and monitors the background radiation. The data is displayed on the front panel touch screen LCD display. The counts are updated for every background counting time. The person's occupancy is detected by IR sensors and the system generates an alarm when the counts exceed the preset alarm values.

The Doorway Monitor automatically detects the presence of the user and stops the automatic background update, and starts the Personnel Monitoring. During the monitoring period or Personnel Monitoring if the user is not passed properly through the system, monitoring starts and stops after 5 sec's automatically. The system will monitor person occupied the system up to his occupancy. During the personnel monitoring cycle the net count rate is collected by subtracting the last background counts with the acquired gross counts.

The collected net count rate is then compared with the preset contamination alarm levels in order to determine if the personnel's are contaminated or not. The Doorway Monitor system then announces the result by audio-visual messages through lamp indication and messages on system display. Once the personnel have passed out of the monitor the switches back to background collection mode. In the background collection mode the counts the background of each detector for pre defined BG Counting time period.

This monitoring system can be either atmel based or micro chip based ,but for our convenient purposes we use micro chip because of in built timers and counters .In this paper ;we will discuss about:

1. How a plastic scintillation detector detects gamma particles and how BF3 detector detects neutrons
2. How detected nuclear signal is converted into electrical signal
3. What is the need of using an inverter and a hv status checker
4. How the conversion of adc (analog to digital) conversion is done
5. How the counter counts the signal
6. How a ir sensor detects a person through that doorway

2. HARDWARE DESCRIPTION

This module works according to the certain modules mentioned above.the description and their specifications are given below:

- Mains : 230 VAC +10%,50/60 Hz
- Controller: PIC 18f46k22 for safe and avoid complexity
- Alarm buzzer : Peizo Buzzer- Lamp indication
- Relay board: ULN 2003
- Ir sensor -2
- Plastic scintillation detector with PMT(photo multiplier tube) – 2
- One front camera and one rear camera
- Gamma amplifier module -2
- Ethernet switch port-1
- LVPS : 12V

If we use 8051 controller, it will not have inbuilt counters .So it is difficult and become more sophisticated for the design of our baggage system

A. Generalised block diagram of the system;

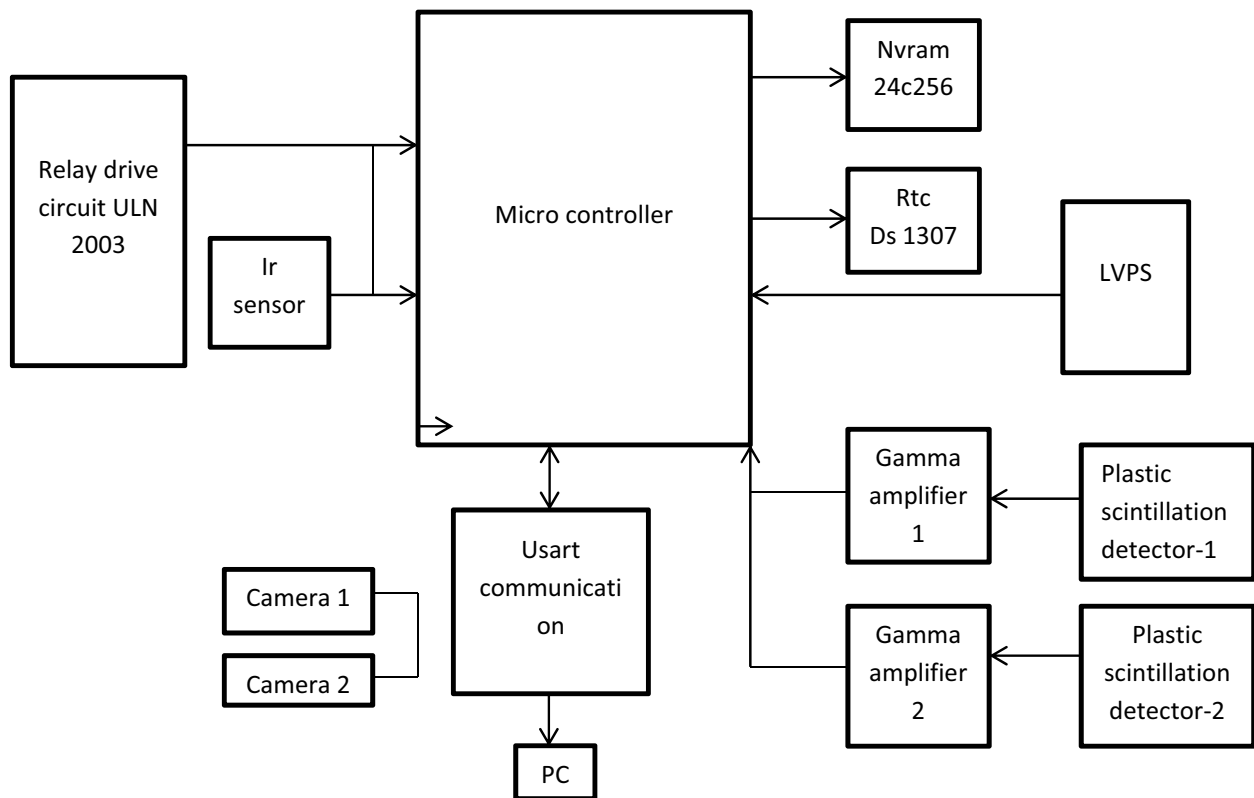


Fig1.Block diagram of doorway monitor system

B. Plastic scintillation detector :

The scintillation process starts with the conversion of high-energy photons into visible light and following steps are:

- 1) A photon incident on the detector creates an energized electron
- 2) As the electron passes through the detector, it loses energy and excites other electrons in the process.
- 3) These electrons go back to their ground state, giving off light .

A popular method for the gamma-rays detection involves plastic scintillators. The general description of a scintillator is a detectors that emits low-energy photons when struck by a high-energy charged particle. When used as a gamma-ray detector, the scintillator does not directly detect the gamma-rays. Instead, the gamma-rays produce charged particles in the scintillator crystals which interact with the crystal and emit photons. These lower energy photons are subsequently collected by photomultiplier tubes (PMTs).

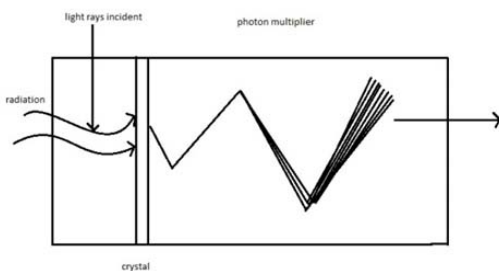


Fig 2. Plastic scintillation detector

C Gamma amplifier module:

The pulse amplifier module takes the output of the detector probe as input and amplifies it and converts it into fixed width TTL pulses. There are two modules for pulse amplification and pulse shaping of pulses coming from two detectors. Each module consists of fast operational amplifier, comparator and a mono-stable multi-vibrator. There are three stage of amplification and pulse shaping is done by AM452-2M .In the first stage of amplification negative tail pulse will be converted into positive tail pulse with less amplitude. In second stage of amplification, positive tail pulse shape without negative base line distortion. In third stage amplification, variable amplified positive pulse. Trim pot RV2 (Disc Adj) is used to make threshold voltage range between to 0 to 5V. IC LM 110 is used as buffer .After amplification the unwanted signal is removed at comparator stage(LM111) by adjusting the threshold of comparator by varying the panel mount pot 'RV4' (Disc Set) from minimum to maximum. Comparator output is square pulses of variable pulse width to convert these pulses into fixed width pulses these pulses are feed to mono stable multivibrator (54LS123) and finally mono stable multivibrator output is TTL pulses with fixed pulse width.

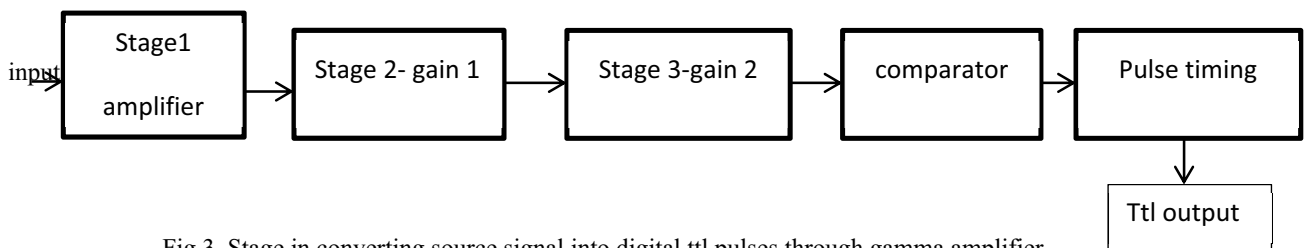


Fig 3. Stage in converting source signal into digital ttl pulses through gamma amplifier

The output of the ttl pulses will be negative trailing pulses .So we will use any inverter circuit in order to change to positive ttl pulses. For eg: LM 324

D *Micro controller:*

In this paper ; we will discuss our paper using PIC 18f45k22 .It is a new family of microcontrollers that take advantage of Microchip’s latest process technology. They contains 5 i/o ports in PIC controller in which some of the pins get multiplexed with some signals.

The hardware included on the board allows for development for different applications.In PIC controller,we use mainly :

1. Timers and counters
2. I2C mode
3. Interrupts
4. ADC

1. *Counters:*

As we use 3 counters to count two gamma pulses and one counter is used as a spare.we use TIMER 0,1,2 modules of PIC controller and we will see how the counter will be configured in the TIMER 0,1,2 modules.

a. *Counter in timer 0 mode:*

Timer0 can operate as either a timer or a counter; the mode is selected with the T0CS bit of the T0CON register. The Counter mode is selected by setting the T0CS bit (= 1). In this mode, Timer0 increments either on every rising or falling edge of pin RA4.The raising edge is determined by the Timer0 Source Edge Select bit, T0SE of the T0CON register; for TOSE = 0 selects the rising edge.

b. *Counter in timer 1 mode :*

In Counter mode, a falling edge must be registered by the counter prior to the first incrementing rising edge after any one or more of the following conditions:

- Timer1/3/5 is disabled (TMRxON = 0) when TxCKI is high then Timer1/3/5 is enabled (TMRxON=1) when TxCKI is low.

2. *I2C mode:*

The Inter-Integrated Circuit Bus is a multi-master and multi slave communication bus. Devices communicate in a master/slave environment where the master devices initiate the communication. A slave device is controlled through addressing.Here we use i2c mode of communication to control and transfer of data from NVRAM and RTC.

a.*software algorithm for i2c mode :*

1.Master mode write operation:

1. Assign the address of the slave under communication and clear i2c which was used previously.
2. Initialize i2c for master using openI2C(x1,x2) and set baud clock
3. Check for bus idle connection in multi master mode and then start ilc using startI2C().
4. Write the address and check if any bus collision and using while loop it until write is successful and similarly for read operation.

3. *Interrupts:*

We use interrupts in detecting the presence of a person using IR sensor.IR sensor detects persons presence and it contains a transmitter and a receiver.Interrupts we use here is high to low interrupts ;because already IR sensor will be high state and when person enter through the doorway it will goes to low state giving an indication of person’s presence.we use INTO and INT1 given to pin 8 and pin 9 of pic controller.

Interrupts have 19 registers for the control of interrupts i.e INTCON(1-3),PIE(1-5),PIR(1-5),IPR(1-5),RCON. interrupt sources have three bits to control their operation. They are:

- Flag bit to indicate an event occurred
 - Enable bit to branch the interrupt vector address after the flag bit is set
 - Priority bit to select high or low priority
- INTCON1- bit 6:PEIE/GIEL: Peripheral Interrupt Enable bit
 When IPEN = 1:
 Enables all low priority interrupts=1
 Disables all low priority interrupts=0
 i.e INTCON=01000000;IPEN=1;

4. ADC module:

We need ADC module in order to display the exact HV status of the system .We will have the HV status from 800V to 1200 V.So,if HV given= 853V;to display the exact HV status ;we convert into 10 bit digital value by proper analog to digital conversion. If 0v and 5v are there;then 0v=0 and 5v=1023;then 1 unit=5/1023 which implies 5/1023 volts means 1 unit. To enable the ADC module, the ADON bit of the ADCON0 register must be set to a '1'. Setting the GO/ DONE bit of the ADCON0 register to a '1' will immediately start the Analog-to-Digital conversion or start an acquisition delay followed by the Analog-to-Digital conversion.

E Relay drive circuit (ULN 2003):

Relay driver circuit is interfaced with micro controller and check the different operational modes of the system like ready,contaminated,clean,system fail and alarms and buzzer are used to denote those modes.the relay circuit used is ULN 2003.

3. OPERATIONAL MODES:

The doorway monitors software consists of six basic operating modes in normal operation.

A. Ready mode:

Normally PMS4021 will be in READY mode. i.e. the system is ready to monitor personnel passing through the system. If nobody occupies it will continuously collect the background and updates the background.

B. Clean mode:

If the net count rates for each detector are below their respective contaminated alarms levels, the user being monitored is considered as "CLEAN".The indication will be in green colour.

C. Contaminated mode:

In any of detector count rate exceeds the alarm level then the system switches to contaminated mode and the indication will be in red colour.

D. DET HV Failure:

If the operating HV voltage of the detector get failed or come down to threshold or alarm level kept for HV Voltage then "HV FAIL" messages are displayed on the system display

E. Background High and low:

when any of the detectors goes into saturation or any high activity source is nearer to the system then the background is more than the alarm, in this case "BACKGROUND HIGH DET1" messages are displayed on the system display and vice versa for back ground low

1.BG High Alarm Level:

BG high alarm level = Last obtained BG Counts + Alarm level

$$= \text{Last obtained BG Counts} + 10 (\sigma)$$

2. BG Low Alarm Level:

BG Low alarm level = Last obtained BG Counts - Alarm level

$$= \text{Last obtained BG Counts} - 10 (\sigma)$$

4.WORKING:

Initially the source is detected by plastic scintillation detector and the negative trail pulse is the output of the detector.Then the detector output is given to gamma amplifier;before gamma amplifier through hv module where high voltage status is maintained between 800V and 1200V.In the gamma amplifier ;amplification and gain setting is done and pulse timing is set and inverted due to of negative pulse from detector. The output of the gamma

amplifier will be digital ttl pulses which are given to counter as input to PIC 18f46k22 controller. We use TQFP (tetra quad flat package) which consists of 44 pins.

The pins of the counters are 23,32 and 13 pins of the micro controller .These ttl pulses are given to these pins.HV status set for the system is

given to adc to maintain exact value of the HV status.the presence of a person is detected by the two IR sensors,one at the entrance and one at exit .The interrupts given for this sensor will have priority high to low.The main operation modes are mentained in the above section 3.1-3.5.those modes are signaled by the relay drive circuit ULN 2003.

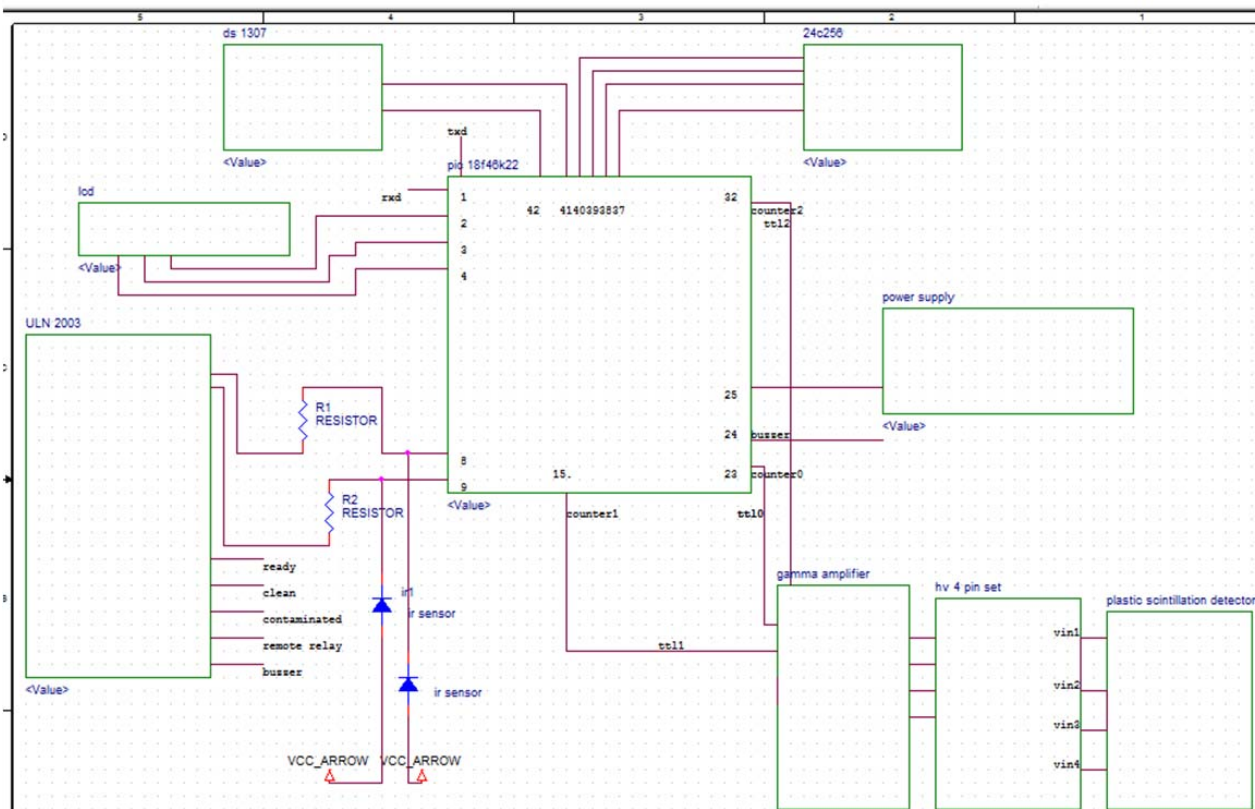


Fig 4.schematics for the design of the system

A.Algorithm of the system:

- Count the pulses
- Check whether bg low<1000 or bg high>5000;then the system is safe and in ready mode
- Interrupt is in high to low ;then it will be in signal counting mode
- In the signal counting;(signal count-bg count) is compared with the alarm level
- (signal count-bg count)>=alarm level;it is in contaminated mode
- (signal count-bg count)< alarm level;then it is clean.

5.CONCLUSIONS AND FUTURE WORK:

This model is designed to detect gamma radiations and monitor the results on lcd .It is used to detect 2 gamma sources using plastic scintillation detector which will result in a negative pulse train.This module can have USART communication using PIC controller as it have EUSART module .It uses Real Time Clock to store the data of source data at a specified time and it will be stored in NVRAM.

This monitoring system can be extended to gamma sources and neutron sources by extending it by placing an external BF3 detector as it is capable of detecting neutrons and then passed through neutron amplifier.The operation of neutron amplifier is same

as that of gamma amplifier which is described above. The future work of this doorway monitoring system can be extended to special nuclear baggage system by placing an X-ray belt to detect both gamma and neutron materials. But in order to detect neutrons also we need to use another counter of PIC controller. But the older version of these systems used Atmel controllers which do not have in-built counter. We have to interface counter peripherals to controller module.

6. REFERENCES:

[1] D. B. Fossan and E. K. Warburton, in Nuclear spectroscopy and reactions (ed. J. Cerny; Academic Press, New York, 1974).

[2] G. Bertollini, M. Cocchi, V. Mahdi and A. Rota, IEEE Trans Nuclear. Sci. NS 13, no. 3 (1966) 119.

[3]. R. E. Bell, in Beta- and gamma-ray spectroscopy (ed. K. Siegbahn; North-Holland Publ. Co. Amsterdam, 1955)

[4]. H. O. Wirth, F. U. Herrman, G. Herrman and W. Kern, Proc. Int. Symp. on Organic crystals (ed. D. Horrocks; Gordon and Breach, New York, 1968).

[5]. 'PIC 18f46k22 operational manual', MICROCHIP

[6]. 'PIC18F4XK22 Development Board User's Guide', MICROCHIP.

[7]. http://csusdspace.calstate.edu/bitstream/handle/10211.9/850/Hardik_final_report.pdf?sequence=2, report on detecting space errors.

[8]. http://prola.aps.org/abstract/PR/v75/i5/p796_1, detection of gamma particles from sodium iodide crystal

[9]. Moghavvemi, Lu Chin Seng 'Pyroelectric infrared sensor for intruder detection', Nov. 2004 Page(s): 656 - 659 Vol. 4.

[10] <http://www.science.gov/topicpages/b/baggage+screening.html>

Efficient Data Security Method to Control Data in Cloud Storage System using Cryptographic Techniques

Prakash G L
Research Scholar, CSE
University of Petroleum and Energy
Studies, Dehradun,

Dr. Manish Prateek,
Center for IT
University of Petroleum and Energy,
Dehradun

Dr. Inder Singh
Center for IT
University of Petroleum and Energy,
Dehradun

Abstract—Cloud computing paradigm enables the users to access the outsourced data from the cloud server without the hardware and software management. For the effective utilization of sensitive data from CSP, the data owner encrypts before outsourcing to the cloud server. To protect data in cloud, data privacy is the challenging task. In order to address this problem, we proposed an efficient data security method using cryptographic techniques. Thus, the proposed method not only encrypts the sensitive data, but also detects the dishonest party to access the data using combined hash functions. We have analyzed the proposed method in terms of storage, communication and computational overheads. The result shows that the proposed security method is more efficient than the existing security system.

Keywords- Hash Function; Data Storage; Data Control; Verification; Encryption; Data Privacy.

I. INTRODUCTION

In cloud computing, data is stored in remote massively scalable data centers where compute resources can be dynamically shared to achieve significant economies of scale. The storage capacity needs to scale with compute resources to effectively manage and gain maximum cloud benefits.

Armbrust et al.[8] explained cloud as the data Center hardware and software that provide services on-demand network access to a shared pool of consumable computing resources. It has the following common characteristics; (i)pay-per-use (ii)elastic capacity (iii)self-service interface and (iv)resources that are abstracted or virtualized.

For organizations into cloud computing, storage management is extremely important. To avoid data loss, the cloud system must provide data protection and resiliency. If loss does occur, the environment must be able to recover the data quickly in order to restore access to the cloud services. The storage management and information protection in cloud environments helps to deliver a workload-optimized approach.

Depending on the type of cloud used, the cloud provider's responsibilities could include providing infrastructure, physical security of the premises, operating system and network security. Sharing of cloud resources such as providing

infrastructure, operating system, application and network security is controlled by the cloud service provider depending on the cloud deployment model.

On the other hand the actively processing cloud data is controlled by cloud users depending on the cloud service model is used in their application. An organization classify the information according to the sensitivity to its loss or disclosure. The level of information sensitivity classification defined by the data owner based on the security control.

The detailed functional components of cloud computing security architecture are explained in the figure 1. Based on three cloud computing service models such as; infrastructure as a service, platform as a service and software as a service, it contains; authorized users, data provider, communication Access Point(CAP), Security Access Point(SAP), Application Access Point(AAP), and Application servers, functional components [1].

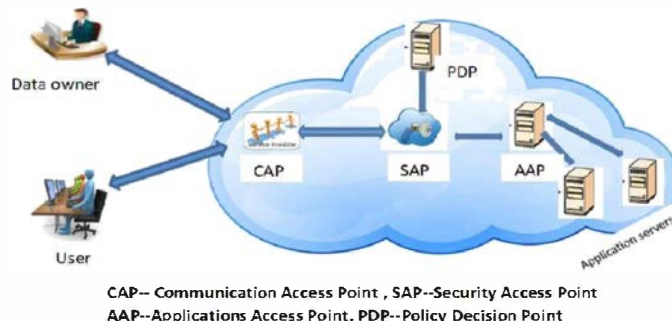


Fig. 1. Functional Components of Cloud Computing Security Architecture

In software as a service model, where software is represented by various application servers of same and/or different types. The main characteristics of cloud computing model is, the data provider and cloud users do not access servers directly. To access the various cloud services based on type of user re-quest and other processing parameters, the Application Access Point Server distribute the service request to the individual application server. The users may access cloud services on demand through internet using communication Access Point.

The SAP server provides the front-end security service before accessing the cloud resources. Once the user has been authenticated, SAP verifies whether the user requests are authorized to access internal cloud resources or not. After authentication, enforcement the final security service is provided by the SAP server.

When a user request some application service via CAP to the cloud, that request will first reach SAP server. The server will forward it to the Policy Decision Point (PDP) Server for the authentication and authorization decision. If both are approved, users application request will be passed to the appropriate application server, where it will be served, and the response will be returned to the user. All described security actions, SAP server, then forwarding it to the PDP server, receiving reply back to the SAP server and, finally access to the application server providing the requested service, are performed instantaneously and transparently to the user [2]-[11]. Therefore, the user is not aware of any of these actions, except if some unauthorized action is attempted.

The rest of the paper is organized as follows. In Section II and III, we have defined the related work and background for the proposed security system respectively. Our proposed system security algorithms and performance analysis are explained in Section IV and V respectively. Finally we conclude in Section VI.

II. RELATED WORK

To ensure the data integrity of a file consisting of a finite ordered set of data blocks in cloud server several solutions are defined by Qian Wang et al, in [3]. The first and straight forward solution to ensure the data integrity is, the data owner pre-compute the MACs for the entire file with a set of secret keys, before our sourcing data to cloud server. During auditing process, for each time the data owner reveals the secret key to the cloud server and ask for new MAC for verification. In this method the number of verification is restricted to the number of secret keys. Once the keys are exhausted, the data owner has to retrieve the entire file from the cloud server to compute the new MACs for the remaining blocks. This method takes the huge number of communication overhead for verification of entire file, which effect the system efficiency.

The another solution to overcome the drawback of previous method, is to generate the signatures for every block instead of MACs to obtain the public audit-ability. This solution can provide probabilistic assurance of data correctness and public audit-ability, which again results in large communication overhead and effect the system efficiency. The above solutions are supports only static data and none of them can deal with the dynamic data updates.

Qian Wang et al, in [4] designed an efficient solution to support the public audit-ability without retrieving the data blocks from server. The design of dynamic data operations is a challenging task for cloud storage system. They proposed a RSA signature authenticator for verification with data dynamic support. To support the efficient handling for multiple auditing task, they extended the technique of bilinear aggregate signature and then they introduced a third party auditor to perform the multiple auditing task simultaneously.

In the recent resource sharing paradigm in distributed system such as cloud computing, the most challenging task.

In data sharing system is defining of access policies and dynamic data updation. In [5], JunbeomHur, explains the cryptographic based solution for data sharing using cipher-text policy attribute-based encryption(CP-ABF) to improve the security of the data. In this method the data owners defines the access policies on the data to be distributed. The major drawback of this method is the unauthorized users can access the key to decrypt the encrypted data.

In cloud computing, both data and applications are controlled by the data owner and cloud service provider. To access the cloud data and applications as a cloud service more securely a data security model has been defined Mohamed, E.M. in [6]. In this security model, it provides a single default gateway as a platform to secure user data across public cloud applications. The default gateway encrypts only sensitive data using encryption algorithm, before sending in to the cloud server. In this method the data is accessed by only authorized users but the cloud service provider can grant the access permission for unauthorized users while cheating to the data owner. Therefore, this method degrades the security as proper key management is not implemented in the system.

To increase the revenue and degree of connectivity from cloud computing model while accessing and updating data from data center to the cloud user, Dubey et al. in [7] developed a system using RSA and MD5 algorithms for avoiding unauthorized users to access data from cloud server. The main drawback of this method is that the cloud service provider has also an equal control of data as the data owner and the computation load for cloud service provider is proportional to the degree of connectivity so that the performance of the system can degrade.

III. MODEL/ARCHITECTURE

A. Background

The block diagram of cloud computing system architecture is defined in the figure 2. It contains there are four functional blocks for data storage and accessing data from data centers in public cloud servers such as, data owner, Cloud Service Provider(CSP), authorized users, and Trusted Third Party [2]. The functions of these functional blocks are as follows;

Data owner: The data owner can be any organization for generating outsourcing data to store in data center of public cloud model for the external use on the demand of the authorized users on the basis of pay per usage.

Cloud Service Provider: Manage the cloud servers and data centers in the public cloud and provide the storage infrastructure to the data owner for storage of outsourced data in data center on the payment based on the requested storage capacity. It coordinates the trusted third party to verify the authorized users and to retrieve the data from cloud server to make them available for authorized user on demand.

Users: the set of authorized users to access the remote data stored in cloud server through trusted third party and

cloud service provider. All the users are the clients of the data owner.

Trusted Third Party: an entity who is trusted by all other entities of the system such as CSP, data owner and users. The functions of TTP is to verify whether the requested user is authorized or not, updating the block status table of file and calculate the hash value for file and block status table [10].

B. Assumptions

The following assumptions are considered to evaluate the data privacy of the proposed system

- 1) The data owner and users have mutual distrust relation with cloud service provider.
- 2) Trusted third party helps to make the indirect mutual trust between authorized user and data owner with cloud service provider.
- 3) Public cloud model is considered for storage of outsourced data in data centers

The data owner has a file (*F*) consisting of *m* blocks of equal size. Since the data is storing on remote data center, for confidentiality all the blocks are encrypted using symmetric data encryption algorithm before sending to the cloud server.

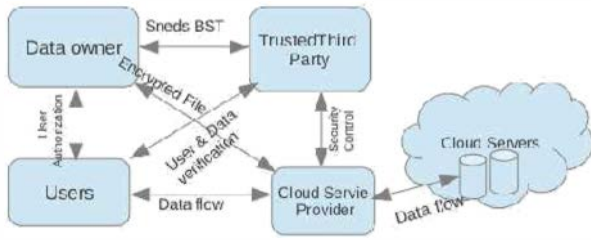


Fig. 2. Block diagram of Cloud Computing System Architecture

C. Objectives

The objectives of our proposed security system are summarized as follows.

- 1) Design an efficient data privacy algorithm using cryptographic techniques.
- 2) Detect the dishonest party using combined hash values verification.
- 3) Reduce the computational overheads of CSP, while introducing TTP.
- 4) Access the out sourced data, even if data owner is in off-line.

IV. PROPOSED SECURITY SYSTEM

1) Block Status Table

The Block Status Table(BST) is a small data structure used to access the outsourced encrypted file from the cloud service provider. It consists of two column such as SN_j and BN_j , where SN_j is the sequence number of physical storage of data

block *j* in the file and BN_j is the data block number. Initially the data owner stores table entries as $SN_j = BN_j = j$. For insertion of data blocks, the BST is implemented using linked list. The structure of BST for insertion of data blocks as shown in the Table 1.

TABLE I. STRUCTURE OF BLOCK STATUS TABLE

Sequence Number	Block Number
1	1
2	2
3	3
4	4

2) Proposed System

The proposed system consists of a four functional role; data owner, user, trusted third party and cloud service provider.

Owner: the data owner generates the initial symmetric key for data encryption and decryption. The key is rotated forward direction to generate the new key for next block data encryption and rotate backward direction for previous block encryption. For a file where b_j is the j^{th} block and *m* is the number of data blocks, initially the owner generate a BST with $SN_j = BN_j = j$ for the input file and character map table explained in the Table 2. To protect the data from the unauthorized users, before *F*, BST, key to the TTP. The BN_j and b_j are concatenated to helps to reconstruct the original file in the correct order while file retrieving.

Trusted Third Party Role: The TTP receives the {*F*, BST, key} from data owner, then it computes the combined hash values for the encrypted file *F* and BST using the following formula.

$$FH_{TTP} = h(b_1[i] \oplus b_2[i] \oplus \dots \oplus b_m[i]) = \oplus \{ h(b_j[i]) \}_{i=1}^m \quad \forall i = 1 \dots n \dots (1)$$

$$TH_{TTP} = h(BN_1[i] \oplus BN_2[i] \oplus \dots \oplus BN_m[i]) = \oplus \{ h(BN_j[i]) \}_{i=1}^m \quad \forall i = 1 \dots n \dots (2)$$

where *m* is the number of data blocks, *n* is the number of bits in each block. The TTP store the computed hash values of file (FH_{tp}) and BST (TH_{tp}) in the local storage, then it sends only {*F* and BST } to the cloud service provider.

User Role: The authorized user sends a request to both the CSP and TTP to access the outsourced file from the cloud server. After receiving {*F*, BST} from the CSP, and { FH_{tp} , TH_{tp} , key} from the TTP, the user verifies the contents of BST_{csp} entries by computing the combined hash values of BST_{csp} using the following equation.

$$TH_{user} = h(BN1[i] \oplus BN2[i] \oplus \dots \oplus BNm[i]), \dots (3)$$

where $i=1, \dots, n$ and $h(\cdot)$ is the hash value i^{th} bit. The user compares the H_{tpp} received from TTP and TH_{user} . If $(TH_{user} \neq TH_{tpp})$, then issue a dishonest party report to the TTP and data owner. In case of $(TH_{user} = TH_{tpp})$ the user verifies the contents of the encrypted file F by calculating the FH_{user} using the following equation and comparing with FH_{tpp} .

$$FH_{user} = h(b1[i] \oplus b2[i] \oplus \dots \oplus bm[i]), \dots \dots \dots (4)$$

If $(FH_{user} \neq FH_{tpp})$, then informs to the TTP to resolve such a conflict. The authorized user decrypt all the encrypted blocks (b_j) using the decryption algorithm explained in the Table 4, and symmetric key, then returns $(BN_j || b_j)$. The BN_j and BST_{csp} are utilized to reconstruct the original source file (F).

TABLE II. ENCODING MAP SETUP

<p>Algorithm Setup(file, key)</p> <p>Input: source file and 256 bits key</p> <p>Output: Number of data blocks (m) and key rotation setup</p> <p>step 1: Divide the source file in to blocks of equal size. Number of blocks (m) = file size/block size</p> <p>step 2: Create circular double linked list of 16 nodes for key rotation and store one character in each node.</p> <p>Step 3: Create a simple data encoding map table for all the characters.</p>
--

TABLE III. DATA ENCRYPTION ALGORITHM

<p>Algorithm Data Encryption(Source file(F), key, Decrypted file)</p> <p>Input: Source file and key</p> <p>Output: Decrypted file</p> <p>step 1: Split the characters of the file/string into chunks 128 characters</p> <p>step 2: Get the binary equivalent of the current Character (process character by character of chunks)</p> <p>step 3: Remove the first character from the binary value and store it into first Character variable and consider the rest of binary value for shift operations.</p> <p>step 4: Store binary value into a circular doubly linked list for bit operations.</p> <p>step 5: Select a key character from i^{th} position, such a way that if 1st chunk character is selected for encryption, then select the first character of the key, so $i = 1$.</p> <p>step 6: if selected chunk character greater size of key(16), get the modulus of chunk character position.</p> <p>step 7: add the stripped off first Character to the resultant binary value of circular array after bit operations.</p> <p>step 8: add the selected i^{th} key character and $(i + 2)^{th}$ key character.</p> <p>step 9: right shift the binary bits in circular array by (added value mod 5), if mod 5 is 0 then do by 2.</p> <p>step 10: add the selected i^{th} key character value and its previous $(i - 1)^{th}$ character value, for instance if 1^{st} key character is selected then the previous character would be the 16^{th} character (key is stored into circular array or double way linked list for this operations)</p> <p>step 11: get the character equivalent of the binary value</p> <p>step 12: Get the mapped value from encoding Map, which is the decrypted value of the character.</p> <p>step 13: Repeat steps 2 through 12 for all the chunks with different Key (by shifting the key character right using Circular double linked list)</p>

TABLE IV. DATA DECRYPTION ALGORITHM

Algorithm Data Decryption(Decrypted file), key, Source file(F)
Input: Encrypted file and KEY for encryption 16 characters
Output: Source file
step 1: Split the characters of the file/string into chunks 128 characters
step 2: Get the binary equivalent of the current Character (process character by character of chunks)
step 3: Remove the first character from the binary value and store it into first Character variable and consider the rest of binary value for shift operations.
step 4: Store binary value into a circular doubly linked list for bit operations.
step 5: select a key character from i^{th} position, such a way that if 1 st chunk character is selected for encryption then select the first character of the key, so $i = 1$. if elected chunk character greater than size of key (16) get the modulus of chunk character position.
step 6: add the stripped off first Character to the resultant binary value of circular list after bit operations.
step 7: add the selected i^{th} key character and $(i + 2)^{th}$ key character.
step 8: right shift the binary bits in circular list by (added value mod 5), if mod 5 is 0 then do by 2.
step 9: add the selected i^{th} key character value and its previous $(i - 1)^{th}$ character value, for instance if 1 st key character is selected then the previous character would be the 16 th character (key is stored into circular array or double way linked list for this operations)
step 10: get the character equivalent of the binary value
step 11: get the mapped value from encoded Map, which is the decrypted value of the character.
step 12: Repeat steps 2 through 11 for all the chunks with different Key (by shifting the key character right using Circular double linked list)

V. PERFORMANCE ANALYSIS

We evaluate the performance of the proposed cloud security method by analyzing the storage, communication and computation overhead in terms of data block storage and processing for the data security requirements using data encryption and decryption algorithm explained in the table 3 and table 4 respectively.

A. Storage Overhead

It is the additional storage space required to store the necessary information for data security, other than the stored file. The data owner stores only the data encryption key and BST in its local storage, where the size of the key is 256 bits. The size of the BST is calculated based on the number of data blocks. The BST contains two columns, both are integer it occupies total 8 bytes of memory space for single data block, therefore the total storage space of BST is $8 \times m$ bytes, where

m is the number of data blocks. While increasing the data block size still we can reduce the BST storage overhead.

The storage overhead for the combined hash values of the file and BST is 64 bytes, each of size 32 bytes. The total storage overhead at TTP is the sum of the storage space required for the key, FH_{tpp} and TH_{tpp} is 96 bytes. The total storage overhead of the proposed security system is the sum of the storage overhead at data owner, TTP and CSP side. The overall storage overhead is calculated using the following equation.

$$\begin{aligned}
 \text{Overhead}_{\text{Storage}} &= \text{overhead}_{(\text{Owner})} + \text{overhead}_{(\text{TTP})} \\
 &\quad + \text{overhead}_{(\text{CSP})} \\
 &= (8 \times m + 32) + 96 + (8 \times m) \\
 &= (16 \times m + 128) \text{ bytes. } \dots (5)
 \end{aligned}$$

B. Communication Overhead

It is the additional information sent other than the outsourced data blocks, to access the data from the CSP. When the user request a file from the CSP, the CSP sends the encrypted file and BST_{csp} to the user and also TTP sends the TH_{tpp} , FH_{tpp} and key to the user. The total communication overhead for the system is the sum of the communication overheads between the owner, user, TTP and CSP. The overall communication overhead is calculated using the following equation.

$$\begin{aligned} Overhead_{commn} &= overhead_{(owner,TTP)} + overhead_{(TTP,CSP)} \\ &+ overhead_{(TTP,CSP)} \end{aligned} \quad (6)$$

C. Computation Overhead

For confidentiality requirement the static data in the cloud storage system has the computational cost for data access from the CSP. The computation cost is the cost of the time required to perform the data encryption, data decryption, BST generation, key generation and verification. Before accessing the data from the CSP, the authorized user verifies BST_{csp} and the data file. the cost required for these verification is $2 * m * h$, where h is the cost of one hash value computation [2]. The total computation overhead for data access is the sum of the cost of the verification, key rotation and data decryption. The total cost required to access the file from CSP is calculated using the following equation.

$$\begin{aligned} Cost_{computation} &= 3 * m * h + keyrotation \\ &+ decryption..(7) \end{aligned}$$

The maximum computation overhead required for detecting the unauthorized user on the TTP side is $2 * m * h$.

VI. CONCLUSIONS AND FUTURE ENHANCEMENT

In this paper, we discuss the problem of data security in cloud storage system. To control the outsourced data and provide the quality of the cloud storage service for the users, we propose an efficient data encryption, data decryption, key rotation and cryptographic hash function techniques. To detect the dishonest party we implemented the verification techniques using hash function at TTP. We have investigated the computation overhead, communication overhead and storage overhead for the outsourced data. The simulation result for accessing the outsourced data from the CSP shows

that the proposed cloud security system is highly secure than the existing security systems. To support, insertion, deletion and updating dynamic operations on encrypted data block, we can further extend this security system.

REFERENCES

- [1] <http://security.setecs.com>, *Security Architecture for Cloud Computing Environments white Paper*, 2011
- [2] Ayad Barsoum and Anwar Hasan, *Enabling Dynamic Data and Indirect Mutual Trust for Cloud Computing Storage Systems*, In IEEE Transactions on Parallel and Distributed Systems, 2012.
- [3] Cong Wang, KuiRen, and Jia Wang, *Secure and Practical Outsourcing of Linear Programming in cloud computing*, In IEEE International Conference on INFOCOM, pages 820-826, 2011.
- [4] Q. Wang, C. Wang, J. Li, K. Ren, and W. Lou, *Enabling Public Verifiability and Data Dynamics for Storage Security in Cloud Computing*, In Proceeding of 14th European Symposium, Research in Computer Security (ESORICS 09), pages 355-370, 2009.
- [5] Junbeom Hur, *Improving Security and Efficiency in Attribute-Based Data Sharing*, In IEEE Transactions on Knowledge and Data Engineering, Volume:25, Issue: 10, pages 2271-2282, Oct. 2013.
- [6] Mohamed E M, Abdelkader H S, El-Etriby S, *Enhanced Data Security Model for Cloud Computing*, Informatics and Systems (INFOS), 8th International Conference on, pages 12-17, May 2012.
- [7] Dubey A K, Dubey A K, Namdev M, Shrivastava S S, *Cloud-user Security based on RSA and MD5 Algorithm for Resource Attestation and Sharing in Java Environment*, Software Engineering (CONSEG), CSI Sixth International Conference on, pages 18, September 2012
- [8] M Armbrust, A Fox, R Griffith, A D Joseph, and R Katz, *Above the Clouds: A Berkeley View of Cloud Computing*, U C Berkeley Reliable Adaptive Distributed Systems Laboratory White Paper, 2009.
- [9] Cong Wang, Ning Cao, Jin Li, KuiRen and W Lou, *Secure Ranked Keyword Search over Encrypted Cloud Data*, In IEEE 30th International Conference on Distributed Computing Systems (ICDCS), pages 253-262, 2010.
- [10] Kuyoro S O, Ibikunle F, Awodele O, *Cloud Computing Security Issues and Challenges*, In International Journal of Computer Networks, vol.3, issue 5, 2011.
- [11] Cong Wang, KuiRen, W Lou, Jin Li, *Toward Publicly Auditable Secure Cloud Data Storage Services*, In IEEE Computer Networks, pages 19-24, 2010.
- [12] Sumita Tyagi and R Singh Yadav, *Cryptography and Network Security*, Educational and Technical Publishers, 2010.

Fuzzy Reliability Analysis of Washing Unit in a Paper Plant Using Soft-Computing Based Hybridized Techniques

Komal and S. P. Sharma

Abstract The present study deals with the fuzzy reliability analysis of washing unit in a paper plant utilizing available uncertain data which reflects their components' failure and repair pattern. Paper computes different reliability parameters of the system in the form of fuzzy membership functions. Two soft-computing based hybridized techniques namely Genetic Algorithms Based Lambda-Tau (GABLT) and Neural Network and Genetic Algorithms Based Lambda-Tau (NGABLT) along with traditional Fuzzy Lambda-Tau (FLT) technique are used to evaluate the fuzzy reliability parameters of the system. In FLT, ordinary fuzzy arithmetic is utilized while in GABLT and NGABLT ordinary arithmetic and nonlinear programming approach are used. The computed results, as obtained by these techniques, are compared. Crisp and defuzzified results are also computed. Based on results some important suggestions are given for future course of action in maintenance planning.

1 Introduction

The important performance measure for repairable system are system reliability and availability. When system reliability is low, efforts are desired to improve it by reducing the failure rate or increasing the repair rate for each subsystem/component. To this effect the knowledge of system (or components) failure/repair

Komal (✉)

Department of Mathematics, University of Petroleum and Energy Studies (UPES),
Dehradun, Uttarakhand 248007, India
e-mail: karyadma.iitr@gmail.com

S. P. Sharma

Department of Mathematics, Indian Institute of Technology Roorkee (IITR),
Roorkee, Uttarakhand 247667, India
e-mail: sspprfma@iitr.ernet.in

behavior is customary in order to plan and adapt suitable maintenance strategies. Reliability analysts analyze the system reliability with the help of various qualitative and quantitative techniques such as reliability block diagram (RBD), fault tree analysis (FTA), event tree analysis (ETA), markov models (MM), Petri-nets (PN), failure mode and effect analysis (FMEA), Bayesian approach etc [1–5]. These techniques generally require knowledge of precise numerical probabilities and functional component dependencies, information which are sometimes relatively difficult to obtain in any large-scale system. In view of these problems, selection of the appropriate method depends upon the complexity of the system and measures used to analyse system reliability. After selecting appropriate method or technique, system behavior is analysed by using collected or available historical data. But, data either collected or historical are often inaccurate, imprecise, vague and collected under different operating and environmental conditions. The causes may be age, adverse operating conditions and the vagaries of manufacturing processes which affect each part/unit of the system differently, and thus the issue is subject to uncertainty [6]. Considering these facts, many researchers pay attention on these issues and analyzed various industrial systems behavior in terms of reliability/availability using traditional markovian approach without quantifying uncertainties involved in the data [7]. Knezevic and Odoom [3] introduced the concept of FLT utilizing quantified data for analyzing the behavior of a general repairable system. In their approach, PN is used to model the system while fuzzy set theory is used to quantify the uncertain, vague and imprecise data. Fuzzy arithmetic is used for computation of different reliability indices of a general repairable system [8]. Rajeev [5] analysed reliability of different subsystems in a paper mill using FLT and FMEA. Komal et al. [1] established a new technique based on nonlinear programming approach and named it as GABLT for evaluating fuzzy reliability indices of repairable industrial systems. All the above discussed approaches are limited only for those systems whose components' functional dependencies are precisely known. So, these approaches cannot be applied to evaluate those systems reliability indices for which components functional dependencies are partially known. To overcome the problem, Sharma et al. [2] extended GABLT technique by coupling it with ANN and named it as NGABLT technique. The major benefit of using ANN is that it can be used effectively in the situations where output pattern is precisely known (supervised) and where output pattern is partially known (unsupervised). Present study is based on the systems whose functional dependencies are precisely known.

The objective of the chapter is to analyze the fuzzy reliability of washing system in a paper plant using available information and uncertain data through two soft-computing based hybridized techniques GABLT and NGABLT along with traditional FLT technique.

2 A Brief Overview of FLT, GABLT and NGABLT Techniques

The basic assumptions used in these techniques are given as:

- component failures and repair rates are statistically independent, constant, very small and obey exponential distribution function;
- the product of the failure rate and repair time is small (less than 0.1);
- after repairs, the repaired component is considered as good as new;
- system structure is precisely known.

2.1 FLT Technique

Fuzzy Lambda-Tau methodology is a traditional method for analyzing system fuzzy reliability [3]. The methodology is based on qualitative modeling using PN and quantitative modeling using Lambda-Tau method (Table 1) of solution with basic events (AND-gates and OR-gates) represented by triangular fuzzy numbers. This approach is limited as the number of components of the system increases or system structure becomes more complex, the computed reliability indices (Table 2) in the form of fuzzy membership function have wide spread due to various fuzzy arithmetic operations used in the computations [8]. It means these indices have high range of uncertainty and cannot give exact idea about the system reliability and consequently its performance. Thus this approach is not suitable for large and complex repairable industrial systems' reliability analysis when data is imprecise and represented by fuzzy numbers.

2.2 GABLT Technique

To analyze the complex industrial system reliability stochastically up to a desired degree of accuracy, GABLT technique has been used in this chapter [1]. GABLT utilizes ordinary arithmetic and mathematical programming approach instead of

Table 1 Basic expressions of lambda-tau methodology

Gate →	λ_{AND}	τ_{AND}	λ_{OR}	τ_{OR}
Expressions	$\prod_{j=1}^n \lambda_j \left[\sum_{i=1}^n \prod_{i \neq j} \tau_j \right]$	$\frac{\prod_{i=1}^n \tau_i}{\sum_{j=1}^n \left[\prod_{i=1}^n \tau_i \right]}$	$\sum_{i=1}^n \lambda_i$	$\frac{\sum_{i=1}^n \lambda_i \tau_i}{\sum_{i=1}^n \lambda_i}$

Table 2 Some reliability indices for repairable system with constant repair rate model

Reliability indices	Expressions
Mean time to failure	$MTTF_s = \frac{1}{\lambda_s}$
Mean time to repair	$MTTR_s = \frac{1}{\mu_s} = \tau_s$
Mean time between failures	$MTBF_s = MTTF_s + MTTR_s$
Expected number of failures	$ENOF_s(0, t) = \frac{\lambda_s \mu_s t}{\lambda_s + \mu_s} + \frac{\lambda_s^2}{(\lambda_s + \mu_s)^2} [1 - e^{-(\lambda_s + \mu_s)t}]$
Availability	$A_s(t) = \frac{\mu_s}{\lambda_s + \mu_s} + \frac{\lambda_s}{\lambda_s + \mu_s} e^{-(\lambda_s + \mu_s)t}$
Reliability	$R_s(t) = e^{-\lambda_s t}$

fuzzy arithmetic. In this technique expression of various reliability indices of the system in terms of system’s components’ failure rate and repair time are evaluated using Tables 1 and 2. Since system have complex structure, so evaluated reliability indices are nonlinear in nature. Also, system’s components’ failure and repair data i.e. input parameters are uncertain due to various practical reasons already discussed and hence represented by triangular fuzzy numbers [8, 9]. To finding system fuzzy reliability indices utilizing quantified failure and repair data in the form of fuzzy numbers, optimization problems (1) at each cut-level α is formulated and given as follows.

Minimize/Maximize:

$$\tilde{F}(\lambda_1, \lambda_2, , \lambda_n, \tau_1, \tau_2, , \tau_m) \text{ or } \tilde{F}(t/\lambda_1, \lambda_2, , \lambda_n, \tau_1, \tau_2, , \tau_m) \tag{1}$$

$$\begin{aligned} \text{Subject to : } & \mu_{\lambda_i}(x) \geq \alpha, \\ & \mu_{\tau_j}(x) \geq \alpha, \\ & 0 \leq \alpha \leq 1, \\ & i = 1, 2, , n; \quad j = 1, 2, , m. \end{aligned}$$

where $\tilde{F}(\lambda_1, \lambda_2, , \lambda_n, \tau_1, \tau_2, , \tau_m)$ and $\tilde{F}(t/\lambda_1, \lambda_2, , \lambda_n, \tau_1, \tau_2, , \tau_m)$ are time independent and dependent fuzzy reliability indices respectively. The obtained minimum and maximum value of F are denoted by F_{min} and F_{max} respectively. The membership function values of \tilde{F} at F_{min} and F_{max} are both α that is,

$$\mu_{\tilde{F}}(F_{min}) = \mu_{\tilde{F}}(F_{max}) = \alpha$$

The obtained optimization problem is non-linear in nature, needs some effective techniques and tools for its solution. Variety of methods and algorithms have been developed for solving nonlinear optimization problems and have been applied in various types of real life problems [10, 11]. Genetic algorithm (GA) is one of the most popular evolutionary algorithm. GA has been applied effectively to many different types of reliability optimization problems [1, 11]. GA is capable to solve nonlinear optimization problems without checking the convexity and differentiability of

objective functions [11, 12]. Owing to these advantages, GA is used to solve the nonlinear optimization problem (1) for each cut-level α . After solving nonlinear optimization problems (1), we have fuzzy reliability indices with reduced range of uncertainty at each cut-level α .

2.3 NGABLT Technique

In NGABLT technique, first the failure rate (λ) and repair time (τ) of each component of the system is extracted from various sources like available historical records, logbooks, system analysts, etc. and integrated with expertise. Finally, extracted data are imprecise and vague in nature due to the previously stated reasons. To handle these uncertainties, fuzzy triangular numbers instead of crisp numbers are used to incorporate the uncertainties in the analysis [1–3, 5]. In the next step, reliability indices expressions are obtained with the help of fault tree model of the system and expressions given in Tables 1 and 2. For complex repairable industrial systems, these expressions are of non-linear in nature. So to simplify the calculation process, each reliability index expression is to be approximated by using ANN [13]. We are using a three layer ANN, different types of transfer functions attached with input, hidden and output layers will be used according to the nature of reliability indices.

For all the reliability indices, the transfer function used in the hidden layer is the tan-sigmoidal function. Since the reliability and availability values are in between 0 and 1, we choose the transfer function for the output layer to be the log-sigmoidal function. For other reliability indices (failure rate, repair time, MTBF and ENOF), the transfer function of the output layer is the linear function [4, 14]. Training algorithm is used to minimize the output error by adjusting network weights and biases. The standard backpropagation algorithm (gradient descent algorithm) is used. The input signals are sent forward and then the errors are propagated backward. The algorithm provides supervised learning with examples of input-output pairs to train the network and begins with random weights and biases, adjusted to minimize the errors. Once the training is complete, we have the approximated system reliability indices expressions in the form of matrix of weights attached with input, hidden and output layers of ANN [14].

After approximation of these reliability indices, fuzzified data (λ'^s and τ'^s) at cut level α are used as input variables in the approximated reliability indices for estimating these reliability indices at the same cut level α . The aim is that the computed reliability indices in the form of fuzzy membership functions should have optimized spread i.e. small range of prediction at each cut level α . In this search process, a nonlinear optimization problem is formulated. To find the lower and upper boundary values of any fuzzy reliability index at cut level α in the process of membership function construction, we need to solve the nonlinear optimization problems (1). Since the problem is nonlinear in nature and the

function is approximated by ANN, so conventional methods are inadequate to solve these nonlinear optimization problems. To solve the nonlinear optimization problems (1), GA is used. After solving nonlinear optimization problem (1) for each cut-level α by using GA, we have fuzzy reliability indices.

In the present analysis binary coded GA is used. To solve the nonlinear optimization problems, system's components' failure rate (λ_i^s) and repair time (τ_i^s) are encoded in strings of desired bit length l , that finally constitute a chromosome. The objective function for maximization problem (1) while the reciprocal of the objective function for minimization problem (1) are taken as the fitness function. Roulette wheel selection criterion is employed to choose better fitted chromosomes. One-point crossover and random point mutation are used in the present analysis. To stop the optimization process maximum number of generations and change in population fitness value are used. MATLAB 7.1 has been used for coding purpose.

3 Washing System Description

Here in a paper plant that comprises of subsystems namely chipping, feeding, pulping, washing, screening, bleaching, production of paper and collection, arranged in complex configuration is taken as a main system and the washing subsystem, an important functionary part of the paper plant, as a subject of discussion [5, 7]. The system consists of four main subsystems, defined as:

- **Filter (A)**. It consists of single unit which is used to drain black liquor from the cooked pulp.
- **Cleaners (B)**. In this subsystem three units of cleaners are arranged in parallel configuration. Each unit may be used to clean the pulp by centrifugal action. Failure of anyone will reduce the efficiency of the system as well as quality of paper.
- **Screeners (C)**. Herein two units of screeners are arranged in series. These are used to remove oversized, uncooked and odd shaped fibers from pulp through straining action. Failure of any one will cause the complete failure of the system.
- **Deckers (D)**. Two units of deckers are arranged in parallel configuration. The function of deckers is to reduce the blackness of pulp. Complete failure of decker occurs when both the components will fail.

The fault tree model of the washing system is shown in Fig. 1.

4 Result and Discussion

Under the information extraction phase, the data related to failure rates (λ_i^s) and repair times (τ_i^s) of the main components of the washing system is collected from the present/historical records of the paper plant. The collected data is integrated with expertise of maintenance personnel and is given in the Table 3.

Fig. 1 Fault tree of washing system

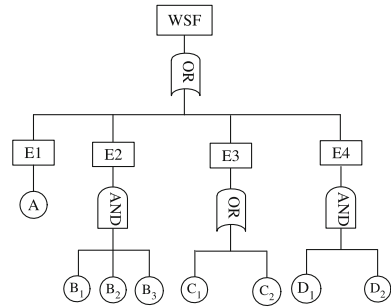


Table 3 Failure rate and repair time data for washing system

Component	Failure rate(λ_i) (failures/h)	Repair time(τ_i) (h)
Filter ($i = 1$)	1×10^{-3}	3
Cleaners ($i = 2, 3, 4$)	3×10^{-3}	2
Screeners ($i = 5, 6$)	5×10^{-3}	3
Deckers ($i = 7, 8$)	5×10^{-3}	3

From the fault tree of the system, the minimal cut sets are $\{ A \}$, $\{ B_1, B_2, B_3 \}$, $\{ C_i \}_{i=1,2}$ and $\{ D_1, D_2 \}$, obtained by using matrix method [3]. Now, by making use of the Table 1, the expressions for system failure rate (λ_s) and repair time (τ_s) take the following forms.

$$\lambda_s = \lambda_1 + \lambda_5 + \lambda_6 + \lambda_2\lambda_3\lambda_4(\tau_2\tau_3 + \tau_3\tau_4 + \tau_2\tau_4) + \lambda_7\lambda_8(\tau_7 + \tau_8)$$

$$\tau_s = \frac{(\lambda_1\tau_1 + \lambda_5\tau_5 + \lambda_6\tau_6 + \lambda_2\lambda_3\lambda_4\tau_2\tau_3\tau_4 + \lambda_7\lambda_8\tau_7\tau_8)}{\lambda_s}$$

Now using these expressions and Table 2, the system reliability indices expressions are obtained. After that, FLT, GABLT and NGABLT techniques have been applied to analyze the reliability of the system. The selected values of all the parameters for GA and ANN for applying GABLT and NGABLT techniques are given in Table 4. Following the basic steps of GABLT and NGABLT techniques, the fuzzy reliability indices for mission time $t = 10$ (hrs) with left and right spreads are computed and depicted graphically in Fig. 2 for $\pm 15\%$ spreads along with FLT technique results. When NGABLT technique has been applied, the error curves obtained during approximation of all the reliability indices by ANN are plotted and shown in Fig. 3. The crisp and defuzzified values for all the three techniques with $\pm 15, \pm 25$ and $\pm 60\%$ spreads are computed and tabulated in Table 5. For defuzzification center of gravity method has been applied [15]. From Table 5, it is evident that defuzzified values change with change of spread. For example the failure rate of the system increases by 0.09, 0.18 and 6.36% for FLT, GABLT and NGABLT respectively, when spread changes from ± 15 to $\pm 25\%$,

Table 4 GA and ANN parameters' values to apply GABLT and NGABLT techniques for washing system reliability analysis

Reliability indices	GABLT				NGABLT						
	Parameters for				Parameters for						
	GA				ANN						
	P_s	P_c	P_m	N_i	N_d	N_h	L_r	P_s	P_c	P_m	N_i
Failure rate	160	0.8	0.006	60	100	17	0.005	160	0.85	0.02	70
Repair time	160	0.8	0.005	80	110	25	0.008	160	0.85	0.02	80
MTBF	160	0.8	0.004	60	110	28	0.005	160	0.85	0.03	90
ENOF	160	0.8	0.006	60	120	28	0.002	160	0.85	0.02	90
Availability	160	0.8	0.005	70	100	27	0.007	160	0.85	0.02	80
Reliability	160	0.8	0.005	80	100	25	0.005	160	0.85	0.02	80

Notations:

P_s population size, P_c prob. of crossover, P_m prob. of mutation, N_i no. of iterations
 N_d no. of training data, N_h no. of hidden layers, L_r learning rate

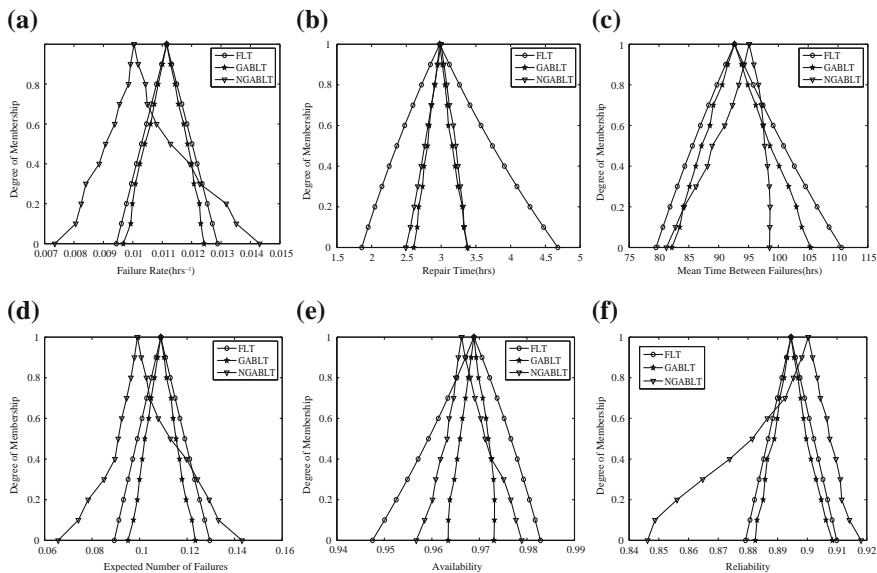


Fig. 2 Fuzzy reliability indices plots for washing system. **a** Failure rate, **b** repair time, **c** MTBF, **d** ENOF, **e** availability, **f** reliability

and it further increases by 0.54, 0.18 and 9.73 %, when spread changes from ± 25 to ± 60 %. From the results it is clear that the computed ranges of system reliability parameters considering GABLT results have compressed range of prediction in comparison of FLT technique results. On the other hand, computed ranges of system reliability parameters considering NGABLT results sometime have increased range of prediction (for failure rate, ENOF, reliability) and sometime

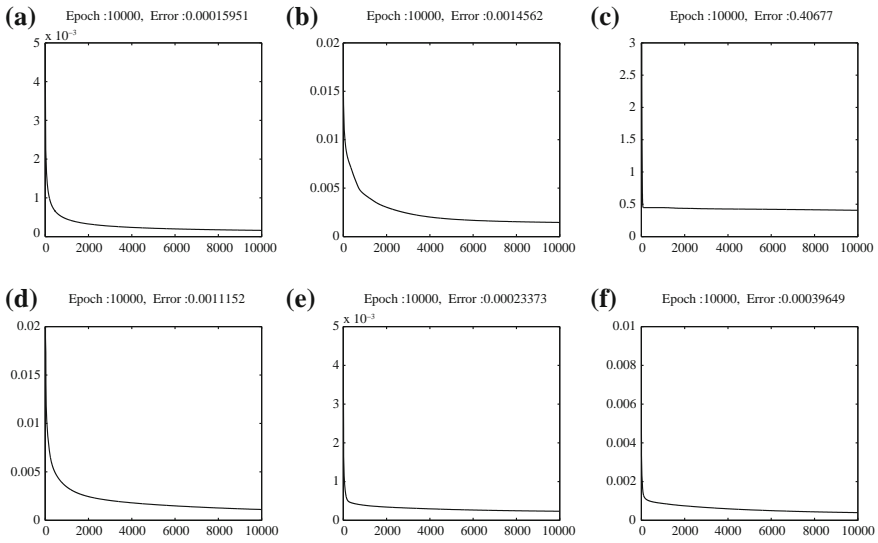


Fig. 3 Approximation error plots for washing system. **a** failure rate, **b** repair time, **c** MTBF, **d** ENOF, **e** availability, **f** reliability

Table 5 Crisp and defuzzified values of reliability indices for washing system

Reliability Indices	Crisp	Defuzzified values at (spread)		
		±15 %	±25 %	±60 %
Failure rate	0.01115	FLT: 0.01116	0.01117	0.01123
		GABLT: 0.01112	0.01114	0.01116
		NGABLT: 0.01053	0.01120	0.01229
Repair time	2.97975	3.12411	3.39742	6.48681
		2.98259	2.97592	2.95166
		2.96894	2.93378	2.80893
MTBF	92.6632	93.8539	96.0905	120.012
		93.3253	94.9451	112.433
		92.2845	92.5887	117.395
ENOF	0.10892	0.10918	0.10970	0.11761
		0.10917	0.10934	0.10956
		0.10342	0.09789	0.09553
Availability	0.96880	0.96701	0.96354	0.92599
		0.96867	0.96801	0.96757
		0.96769	0.96877	0.96901
Reliability	0.89448	0.89451	0.89454	0.89482
		0.89455	0.89472	0.89514
		0.88763	0.89035	0.89333

have reduced range of prediction (for repair time, MTBF, availability) in comparison of FLT results. It is observed that for washing system, NGABLT results do not perform consistently well while GABLT performs well. This is due to the errors involved in the approximation by ANN. Thus, it is inferred that if system analysts use GABLT results, then they may have less range of prediction which finally leads to more sound decisions.

5 Conclusion

In this chapter various reliability indices of a washing system have been computed in the form of fuzzy membership functions by using FLT, GABLT and NGABLT techniques. Depending upon the confidence level ' α ', the analyst can predict the behavior of the system. The defuzzified values of reliability indices for different level of uncertainties with their crisp values have been computed and tabulated. Based on the behavioral plots and the summary given in tabular form, the system manager may analyze the critical behavior of the system and plan for suitable maintenance. It is also observed from the analysis that GABLT performs consistently well in comparison of NGABLT and FLT techniques. If system analysts use GABLT results then they may predict the system behavior with more confidence. However, NGABLT technique provides the flexibility of extension of its present form in future for the systems' whose components' functional dependencies are imprecisely known. These hybridized techniques can be applied to a wide range of industrial systems for helping the reliability engineers to gain valuable information and also to evaluate and implement various maintenance strategies.

References

1. Komal, Sharma, S.P., Kumar, D.: RAM analysis of repairable industrial systems utilizing uncertain data. *Appl. Soft Comput.* **10**(4), 1208–1221 (2010)
2. Sharma, S.P., Kumar, D., Komal, : Stochastic behavior analysis of the feeding system in a paper mill using NGABLT technique. *Int. J. Qual. Reliab. Manage.* **27**(8), 953–971 (2010)
3. Knezevic, J., Odom, E.R.: Reliability modeling of repairable systems using Petri nets and Fuzzy Lambda-Tau Methodology. *Reliab. Eng. Syst. Saf.* **73**(1), 1–17 (2001)
4. Huang, H.Z., Zuo, M.J., Sun, Z.Q.: Bayesian reliability analysis for fuzzy lifetime data. *Fuzzy Sets Syst.* **157**(12), 1674–1686 (2006)
5. Sharma, R.K.: Analysis, design and optimization of QRM aspects in production systems. Indian Institute of Technology Roorkee, Roorkee, Uttarakhand, India (2006)
6. Rao, K.D., Kushwaha, H.S., Verma, A.K., Srividya, A.: Quantification of epistemic and aleatory uncertainties in level-1 probabilistic safety assessment studies. *Reliab. Eng. Syst. Saf.* **92**(7), 947–956 (2007)
7. Kumar, D.: Analysis and optimization of systems availability in sugar, paper and fertilizer Industries. University of Roorkee (Presently IIT Roorkee), Uttarakhand. India (1991)

8. Chen, S.M.: Fuzzy system reliability analysis using fuzzy number arithmetic operations. *Fuzzy Sets Syst.* **64**(1), 31–38 (1994)
9. Pedrycz, W.: Why triangular membership functions? *Fuzzy Sets Syst.* **64**(1), 21–30 (1994)
10. Tillman, F.A., Hwang, C.L., Kuo, W.: *Optimization of Systems Reliability*. Marcel Dekker, New York (1980)
11. Konak, A., Coit, D.W., Smith, A.: Multi-objective optimization using genetic algorithms: a tutorial. *Reliab. Eng. Syst. Saf.* **91**(9), 992–1007 (2006)
12. Goldberg, D.E.: *Genetic Algorithm in Search, Optimization and Machine Learning*. Addison-Wesley, Boston (1989)
13. Cybenko, G.: Approximation by superpositions of a sigmoidal function. *Reliab. Eng. Syst.* **2**(4), 303–314 (1989)
14. Kosko, B.: *Neural Networks and Fuzzy System: A Dynamical Systems Approach to Machine Intelligence*. Prentice-Hall, Englewood (1991)
15. Ross, T.J.: *Fuzzy Logic with Engineering Applications*, 2nd edn. Wiley, New York (2004)

Krishi-Bharati: An Interface for Indian Farmer

Soumalya Ghosh^{1*}, A. B. Garg^{2*}, Sayan Sarcar^{3^},
P.S.V.S Sridhar^{4*}, Ojasvi Maleyvar^{5*}, and Raveesh Kapoor^{6*}

^{*}University of Petroleum & Energy Studies, Dehradun, India

[^]Indian Institute of Technology Kharagpur, India

¹soumalyaghosh@gmail.com, ²abrarg@ddn.upes.ac.in, ³mailtosayan@gmail.com,

⁴psvssridhar@ddn.upes.ac.in, ⁵ojasvi.maleyvar@gmail.com, ⁶raveesh.aiasec@gmail.com

Abstract— Rapid growth in the field of ICT helps in basic aspects of mankind like- agriculture, education, healthcare etc. However, the moderate technical growth of ICT applications is confined to the community of a limited number of people, who live in digital pockets. The illiterate people like – farmer, shopkeeper etc. are unable to take the advantages of the ICT revolution. According to the UNESCO report, population of such people in the globe is 64% who are unable to use the technology either language or technical barrier. Moreover the percentage (76%) must be increased in the context of developing countries. The essential agriculture information is very useful to a farmer for taking effective decision thus we proposed to develop an iconic interface which is integrated with speech based interaction in Indian languages. The proposed interface is critically evaluated with the farmer from different states of India. The evaluation results proved the effectiveness of the proposed interface.

Keywords- Information and communication technology, human computer interaction, Internet, information retrieval, farming, Agriculture information system, iconic interface.

I. INTRODUCTION

The availability and accessibility of information are the crucial points in taking the optimal decision at right time. Nowadays, advancement of ICT make possible to retrieve almost any information from the global repository (internet). The information in internet is primarily maintained in English. So, a large number of people are deprived from the benefit of internet due to technical and English language illiteracy. This scenario is very bad in developing country like India where nearly 76 % are English illiterate¹. Moreover, a large percentage of the English literate people are also unable to find their exact need from the large database of internet due to lack of proficient knowledge in English. Indian farmers belong to such type of people who are not much sound in both technical as well as in English.

So, they are unable to access required information on the farming life cycle, seed selection, pesticides, market price etc. from the internet. As a consequence, they are not capable to take optimal decisions at different stages of farming life cycle, which make huge impact on the farmer's revenue. As a result suicide rate has been increased rapidly among the Indian farming community². According to the reports, those pathetic incidents are mainly happened due to the frustration that they are unable to pay their debts. These types of situations create huge impact on the agriculture sector. Consequently, the focus

of new generation is shifted from farming sector which will be threatening the near future in India. Our preliminary studies reveal that farmers require information at the right stage of the farming life cycle to take the right decisions [1]. However, farmers are unable to get this information from internet due to English language and technical illiteracy. Recently, some webpages like –Wikipedia, Indian Railway web page, etc. provide facility of internet access in many users' language other than English by supporting UTF-8 encoding³. However, it is observed that information is not so useful to the people who are having poor knowledge on internet and web browsing [2]. Moreover, this type of attempt is meaningless for the illiterate people. A large number of people from the Indian farmer community are unable to read/write even their own mother tongue. So, it is obvious that text based interface, instead of supporting farmer's own language, are not able to provide the required information.

The above mentioned scenario states that there is a requirement of alternative interaction technique(s). By considering this fact, Plauché et al. proposed a speech-driven agricultural query system for Tamil Nadu state of India [3]. However this work does not able to address the scenario of total India. Patel et al. designed an interactive voice application for small-scale farmers in Gujarat, India [4]. However, it does not provide a feature to search for specified content in the forum. There, user needs to answer the questions sequentially starting from the most recent question. User does not have the option to skip any question. Moreover, there is no guarantee of giving accurate answer, as the questions are answered by other users. Furthermore, this work is also confined to a particular area of India. In some recent efforts, expert system based text animation has been proposed for diagnosis of most common diseases occurring in Indian mango [5]. This work also uses picture based system alongwith the text query for easier understanding of the disease symptoms. Though, it is a good initiative for Indian farmer, but limited to a particular fruit. Another notable work was mobile based multimedia social networking platform – *GappaGoshti* for information and advice exchange, proposed by Lobo et al. [6]. Ramamritham et al. [7] design an online multilingual, multimedia based forum for common man of India. However, those forums and social networking platforms provide limited number of information as compared to the internet. Moreover, quality of information may not be up to the mark, so illiterate people are unable to get any information from there. To overcome the limitation of illiteracy, Samanta et al. [2] proposed and multimodal interface for the Indian common man. However, the iconic module of

¹ <http://theviewpaper.net/illiteracy-in-india>

² http://en.wikipedia.org/wiki/Farmers'_suicides_in_India

³ www.unicode.org

this work is not related to the agricultural domain. Other works [8, 9] also highlight the need of a systematic approach which is required to provide the precise information to farming community. Moreover, not only providing of the information to farmer, it is also essential to identify that how the farmers are motivated toward accessing the information [10].

All the aforementioned observations motivate us to conduct in depth research toward making an interface for Indian farmer community, which will be more useable, systematical, and needful for them irrespective of language and technical proficiency. Here, we propose an iconic interface integrated with a text to speech (TTS) engine to access the agricultural information from the internet's global repository for Indian farmer community. Further, we also integrate a local repository with the interface to access urgent information without connecting the internet.

The rest of the paper is organized as follows. The proposed approach is elaborated in Section III. Section IV provides the system implementation details. The user testing results are discussed in Section V. Finally, Section VI concludes the paper with the future directions of the research.

II. PROPOSED APPROACH

In this section, we discuss our proposed methodology of our developed interface for the Indian farmer community to access the agricultural information from the global internet repository and store them into local repository. The architecture of the interface is illustrated in Fig. 1. It may be noted that developing search engine is not a part of our work. Here, we integrate the existing search engine (Google search engine) with our proposed interface called Krishi-Bharati. The detailed description of each module of our developed Krishi-Bharati interface is given into the following section.

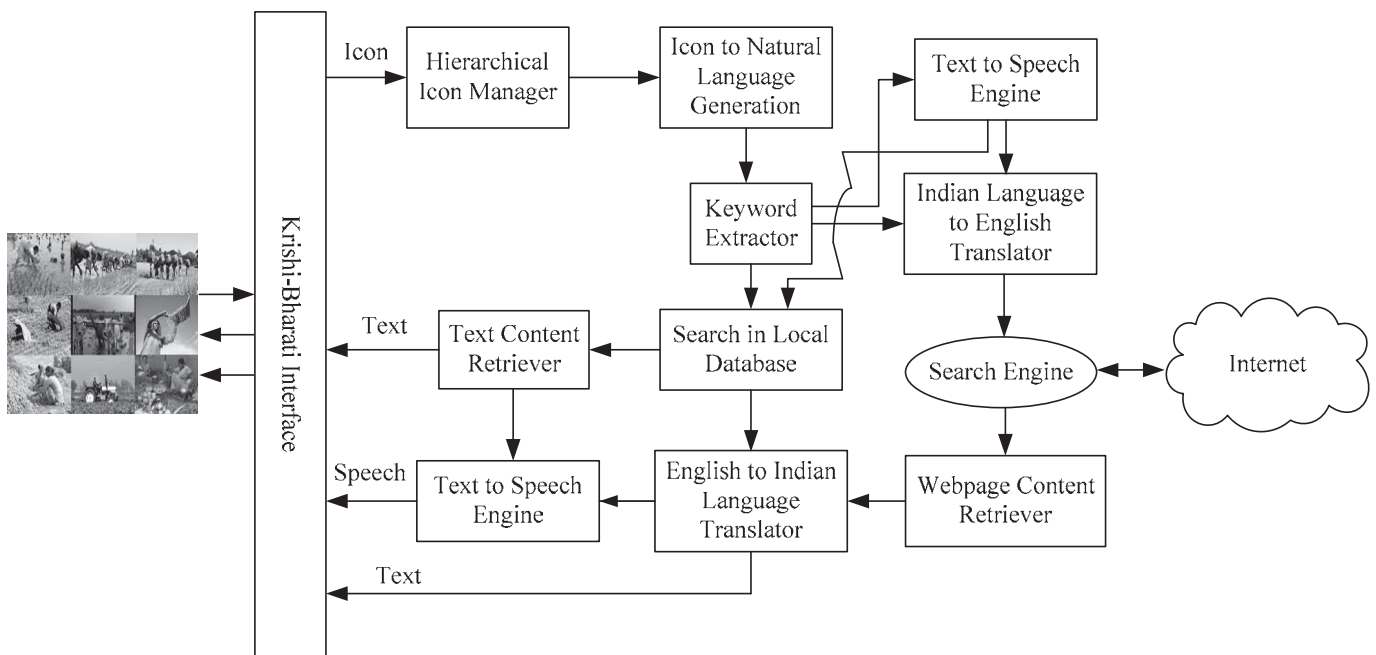


Fig. 1: Architecture of Krishi-Bharati Interface

In the Krishi-Bharati interface, user can only interact with the system through icons and results back with their intended agricultural information in Indian language text and spoken forms both. To access the intended agricultural information from internet and local repository, users have to form proper query. The query is generated by selecting the corresponding icon(s) displayed in the interface. All the icons are displayed in hierarchical fashion to reduce the conceded visual search time during icon search. After selecting the icon(s), the icon to natural language generation module convert the selected icon(s) to text in Indian language. Then, keyword extractor module extracts the proper Indian language query string (key word) from that text. However, illiterate users are unable to read the generated textual query. The interface has also integrates a text to speech system to provide the textual query in spoken form. User can be search into our local repository (data base) or internet's global repository with the query string.

In the case of local search, the returned Indian textual information are stored and are shown to the user by text content retriever module. However, illiterate users are unable to read that textual information. There also an alternative provision of speech base interaction for those language illiterate user. They can select text to speech module to listen to textual information in their own mother tongue. This module includes several tasks like addition of letter-to-sound and syllabification rules [11], selection of text corpus to be recorded [12] etc. to played the sound. On the other case of global search, the search query translates to English by the intervention of Indian language to English translator module. Then, the translated query goes to search engine for retrieve the webpages written in English. The retrieved information is stored into the webpage content retriever module. However, our English illiterate users are unable to collect their require information from the English pages. To address this limitation, Krishi-Bharati interface

translate pages in Indian language (Hindi) with the help of English to Indian language translator module. Here, the interface also has the similar text to speech synthesis provision for mother language illiterate user as discuss earlier.

III. KRISHI-BHARATI INTERFACE IMPLETATION

The above mentioned methodology was implemented in our Krishi -Bharati interface with C# in Visual Studio 2010. In Krishi-Bharati interface user searches their agriculture related query through icons and gets the intended information in both textual and spoken form. Here, we restrict our development to Hindi language by which all the resulting information are provided to the user. Hindi is the official language of India and the mother tongue for most of the people from northern, central and western part of India. The implementation detail of each module is given below.

In the Krishi-Bharati interface, users can only access their intended agricultural information from internet and local repository through icon based interaction. For this, user has to select or click the proper icon shown in the interface. All icons are arranged in a hierarchical order. In first level of the hierarchy six different icons are shown to represent the seeds, vegetable, oil, fruit, flower and other product like jute, tea etc. respectively. After clicking or selecting any icon from the first level, second level of the hierarchy is opened on the basis of the selected icon of first level. Then, first label is got deactivated. As an example, we can say if we select vegetable in first level, then different vegetables are only shown in second level. Then, similarly third level is opened by selecting any particular icon from second level. This level consists of several related icon to the previous selecting icons and some general purpose icons like back, forward, delete etc. Moreover, it is also to be noted that all the icons of second and third level are to be arranged according to the accessing frequency. The interface also provides a textual tooltip associate with each icon for easy understanding.



Fig. 2: Krishi-Bharati Interface



Fig. 3: Results return for local database search



Fig. 4: Translated webpage in Hindi

Then user's selected icons to corresponding Hindi language text are generated as shown in Fig. 2. After that, users' intended query string or keywords are extracted from that text. Moreover, here, the interface also provides a text to speech converter engine to listen the generated query string. Then the query string is fitted to the Google search engine or local repository according to the user's choice. In the case of local search the query string as it is the search send to the local database and corresponding results are shown to the user in Hindi as shown in Fig. 3. On the other case, the search query is translated to the corresponding English language by employing Google translation engine and it is being fed to the Google search engine⁴. This process will return the snippets in English. Then, the returning results need to be translated in Hindi. In this process, the Krishi-Bharati interface extracts tag and text portion of web pages by maintaining index table and then sends the text portion to English to Hindi translation engine for translating. Here, we also use Google translation service⁵ for translating English to Hindi. After getting back the Hindi translated text, original English text is replaced by those Hindi

⁴ <http://translate.google.com/#hi/en/>

⁵ <http://translate.google.com/#en/hi/>

text and painted to the web browser according to the index value. Next, relative web addresses will be changed to the absolute web address. Then, user will get the proper translated web page in Hindi acquiring their intended agricultural information as illustrate in Fig. 4.

However, this Hindi page is not helpful to language illiterate user. In our context, there is a large number of users are illiterate. So, our Krishi-Bharati interface integrated with a text to speech engine to give the output in spoken form. Here, we use Festival⁶ text to speech engine. The configuration has been changed to obtain the support for Hindi. Here, user has to select some portion of the returning webpage and then that portion will be read out in Hindi by clicking the listen icon of the interface. It should be provide special help for getting the information to the illiterate user.

IV. KRISHI-BHARATI INTERFACE EVALUATION

Every user-centric design should be evaluated by the actual users to identify the usability, accessibility, user satisfaction etc. related issues. It also the evidence of how much significantly the proposed design fulfill the need of the targeted users. Here, our targeted users are the Indian farmer community, who are mostly digitally and English language illiterate and not also properly read write in their own mother language (Hindi).

It is very difficult to evaluate any interface with the selected evaluator from all area of the Indian. In this evolutionary study, we restricted with users from different north Indian state like – Uttar Pradesh, Uttarakhand, Punjab, Haryana, and Himachal Pradesh. Though it is mentioned that, this type of user selection must cover with very much diversified agricultural products. As an example, the sates like Uttar Pradesh and Punjab are the excessively production area of Rice, Wheat, Sugarcane etc.⁷. In contradiction, Himachal Pradesh is famous for the apple⁸.

In our evolutionary study, we select 64 (35 male and 29 female) farmers from above mention states having diversified agricultural products. The age of the selected users varies from 22 to 58 years. They also have different educational, social and financial background. They have different level of experience on the usage of computing systems and internet. The computer proficiency can be classified in four levels: (a) at least 3 years of experience with a computer; knowing basic application software and different common services provided via internet (Level 1); (b) 1 to 3 years' experience and mainly familiar with application software like Microsoft Word, e-mail, and internet browsing (Level 2); (c) less than 1 year experience and very poor familiarity with computer-related tasks (Level 3); (d) never use computer (Level 4). The detail user characteristics of the selected user are shown in the Table 1.

The empirical study is conducted in two sessions namely, training and testing. In training session, initially, brief introduction is given to the users. Then detail functionalities

are demonstrated to them. Finally, the interface is given to the each user for familiarization.

After the completion of training session, testing session with the users is started. In this session, the Krishi-Bharati interface is given to the user for searching and acquiring their intended information related to agriculture. They also requested to use specific functionality like – search the price of paddy for current and previous year, pesticide requirement for potato, weather condition prerequisite for cultivating of apple etc. both from internet and local repository.

TABLE 1: USER DESCRIPTION

Age Group	Educational Background	Computer, Internet knowledge	State wise number of user				Total number of user
			UP	UK	HR	PB	
21-30	Graduate	Level 1	0	2	1	1	4
	Higher Secondary	Level 2	1	2	1	1	5
	Secondary	Level 3	1	2	2	1	6
	Primary	Level 4	3	1	1	2	7
31-40	Higher Secondary	Level 3	1	1	0	1	3
	Secondary	Level 3	0	1	0	2	3
	Primary	Level 4	2	0	1	1	4
	Illiterate	Level 4	3	2	2	1	8
41-50	Secondary	Level 4	0	0	1	1	2
	Primary	Level 4	1	1	1	1	4
	Illiterate	Level 4	3	1	2	1	7
≥51	Primary	Level 4	1	2	1	1	5
	Illiterate	Level 4	2	1	2	1	6

In this session, we find out that 77% of users are able to create proper query string (key word) and 72% of them are able to search the query in both internet and local repository. However, only 53% of them are able to find the proper information from the large information bank of internet. In contradiction, 67% are able to gather the required information from the local repository. This experimental results substantiated that underprivileged are not properly acquire the required information from internet even if their mother language textual or spoken form due to digital illiteracy.

We also evaluate the usability issues of our developed Krishi-Bharati interface with those users. After the testing session over, a feedback form is also given to each user. The feedback form contains the questionnaires related to usability of the system. The list of those questionnaires is shown in the Table 2. Further, users are requested to evaluate the system on a liker scale; strongly agree (SA), agree (A), neutral (N), disagree (D) and strongly disagree (SD). Here, strongly agree (SA) to strongly disagree (SD) are the sequences for superior to inferior in the entire question list expect error proneness. In case of error proneness, strongly disagree (SD) and strongly agree (SA) are the superior and inferior respectively. The user

⁶ <http://www.cstr.ed.ac.uk/projects/festival>

⁷ <http://civilsprep.in/major-crops-in-india-a-quick-review/>

⁸ <http://www.mapsofindia.com/indiaagriculture/fruits-map/apple-producing-states.html>

response is depicted in Fig. 5. It is an evidence of the wide applicability, usability, needfulness and satisfaction of the developed interface. It is also convey the significant impact of this interface.

TABLE II: INTERVIEW QUESTIONS

Serial No	Usability Questions
1	Query generation from the iconic interface
2	Searching agricultural queries from internet
3	Searching agricultural queries from local repository
4	Get the required information from internet
5	Get the required information from local repository
6	User satisfaction
7	Over all usability
8	Over all applicability
9	Error proneness

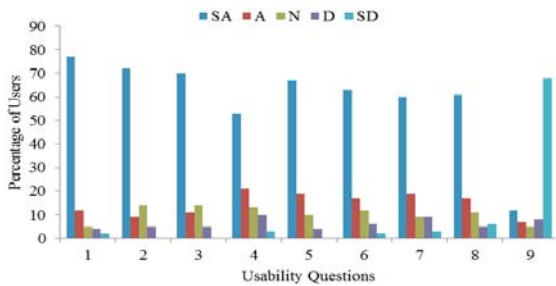


Fig 5. Results of users' feedback

V. CONCLUSION AND FUTURE WORK

An interface (Krishi-Bharati) to accessing the agricultural information from the global repository of internet and the local repository has been proposed in this paper. The proposed interface is able to overcome the digital and language confinement of the Indian farmers by employing the multiple modes of interaction techniques. The empirical evaluation through large diversified users reveals that the Krishi-Bharati interface adequately caters the need of the user. It also be concluded that the proposed interface is very much usable, applicable in the desired context. At the current stage the Krishi-Bharati interface is limited to access the agricultural information in the context of Indian languages. However, it can be extended toward the agricultural context of any country in the world, which proves that the approach is generic.

In future, we will extend the approach from large screen computing device to small screen mobile devices. Screen size and hardware issues need to be taken care properly. We also incorporate other different major Indian languages like-Bengali, Tamil, etc. with Krishi-Bharati interface.

REFERENCES

- [1] L. N. De Silva, J. S. Goonetillake, G. N. Wikramanayake, and A. Ginige, "Towards using ICT to enhance flow of information to aid farmer sustainability in Sri Lanka," in ACIS 2012: Location, location, location: Proceedings of the 23rd Australasian Conference on Information Systems, pp. 1-10. ACIS, 2012.
- [2] D. Samanta, S. Ghosh, S. Dey, S. Sarcar, M. K. Sharma, P. K. Saha, and S. Maiti, (2012, December). "Development of multimodal user interfaces to Internet for common people," in Intelligent Human Computer Interaction (IHCI), 2012 4th International Conference, pp. 1-8. IEEE, 2012.
- [3] P. Madelaine, and M. Prabaker, "Tamil market: a spoken dialog system for rural india," In CHI'06 extended abstracts on Human factors in computing systems, pp. 1619-1624. ACM, 2006.
- [4] N. Patel, D. Chittamuru, A. Jain, P. Dave, and T. S. Parikh, "Avaaj otalo: a field study of an interactive voice forum for small farmers in rural india," In Proceedings of the SIGCHI Conference on Human Factors in Computing Systems, pp. 733-742. ACM, 2010
- [5] R. Prasad, K. R. Ranjan, and A. K. Sinha, "AMRAPALIKA: An expert system for the diagnosis of pests, diseases, and disorders in Indian mango," Knowledge-Based Systems, 19(1), pp.9-21. Elsevier,2006.
- [6] Lobo, S., Doke, P., & Kimbahune, S. (2010, October). GappaGoshti™: a social networking platform for information dissemination in the rural world. In *Proceedings of the 6th Nordic Conference on Human-Computer Interaction: Extending Boundaries* (pp. 727-730). ACM.
- [7] Ramamritham, Krithi, Anil Bahuman, Ruchi Kumar, Aditya Chand, Subhasri Duttagupta, GV Raja Kumar, and Chaitra Rao. "aAQUA-A Multilingual, Multimedia Forum for the community." In *IEEE International Conference on Multimedia and Expo*, vol. 3. 2004.
- [8] PUNCHIHEWA, Devaka J., and Prasad Wimalaratne. "Towards an ICT Enabled Farming Community." *E-Governance in Practice, India* (2010): 201-207.
- [9] Parikh, T. S., Patel, N., & Schwartzman, Y. (2007, December). A survey of information systems reaching small producers in global agricultural value chains. In *Information and Communication Technologies and Development, 2007. ICTD 2007. International Conference on* (pp. 1-11). IEEE.
- [10] Ginige, T., & Richards, D. (2012). A model for enhancing empowerment in farmers using mobile based information system. In *ACIS 2012: Location, location, location: Proceedings of the 23rd Australasian Conference on Information Systems 2012* (pp. 1-10). ACIS.
- [11] S.P.Kishore and A. W. Black, "Unit Size in Unit Selection Speech Synthesis," in Proceedings of Eighth European Conference on Speech Communication and Technology, Geneva, Switzerland, 2003.
- [12] J. Matousek, J. Psutka, and J. Kruta, "Design of Speech Corpus for Text-to-Speech Synthesis," in Proceedings of Seventh European Conference on Speech Communication and Technology, Alborg, Denmark, 2001, pp. 2047-2050.

Land Slide Detection and Monitoring System using Wireless Sensor Networks (WSN)

G. N. L. Ravi Teja¹, V. K. R. Harish², Nayeem Muddin Khan D³, R. Bhargava Krishna⁴, Rajesh Singh⁵, S Chaudhary⁶
^{1,2,3,4} Robotics Engineering, University of Petroleum and Energy Studies, Dehradun, India

^{5,6} Electronics, Instrumentation and Control Engineering, University of Petroleum and Energy Studies, Dehradun, India

Abstract—Mass failures of slope, which includes movement in soil, rock, ice which cause a considerable damage to the natural habitat, environment, economy and other resources. Detection, monitoring and control are the three major issues regarding Real-Time applications. For a large scale detection of fault and monitoring the faults is one of the important applications that lead to advancement of many kind of technologies. In this paper A Land-Slide detection system is being developed at Bidholi (village), Dehradun, India, a region with high rainfall and versatile climatic behavior most of the year. Integrating Geo-physical sensors forming a heterogeneous wireless network helps in identifying the fault and this paper also includes development, deployment (analysis) and data retrieval of the sensors information using WSN.

Keywords: Wireless Sensor Network, Heterogeneous Networks, Landslide

I. INTRODUCTION

Wireless sensor networks have the capability of large scale sensor deployment and have the advantages of adaptability, easy maintenance, and low installation cost with scalability for different environmental scenarios [7], [14].

Disaster management of various environmental activities and detecting these conditions is one of the crucial parts that any technology should perform [1], [4], [11]. Real time environmental disaster detection and monitoring is one of the basic necessities of the world. Various technologies have been developed till now and wireless sensor networks are one of the technologies that can fulfill the requirement [15]. WSN has the capability of deploying in populated areas as well as data extraction and transmission is easy with low cost and low power consumption.

This paper describes a novel design and basic implementation of land-slide detection and monitoring system with various geo-physical sensors forming a heterogeneous network (MOTE) and transmitting the data to a ground station [9].

II. REVIEW WORK

WSN has its own area defined applications but then advancements in electronics industry paved improvement of WSN in various real-time and complex environment related applications. The Drought Forecast Alert System (DFAS) has been developed which uses mobile communication to alert public [9] and this system can also be deployed by using Wi-Fi, satellite communication and also by internet. This paper uses ZigBee protocol and a 2.4GHZ RF module as communication medium [6].

Besides this system research has shown that sensor

deployment is a basic requirement for any kind of fault detection system [7], monitoring can be achieved by using other techniques like remote sensing, GPS technology; automated terrestrial surveys and so on can also be used as an individual unit or in a combination to achieve the requirement.

In this paper, with the basic information gathered the deployment of heterogeneous network is being discussed. The ease of implementation, low power consumption, minimal maintenance cost paved for turning views to Wireless Sensor Network [8]. This paper includes about the electronic node designing using controller and its interface with various geo-physical sensors, software development with proteus (trial version) model.

III. LAND SLIDES

Gravity, soil moisture and climatic conditions determine the strength of the land. If due to any of these conditions the sand and rock of certain level deviates from its own state leading to slide [2]. Land sliding in general described as down sliding of rock, soil and organic material due to various parameters under the influence of gravity [4].

Various external parameters like environment issues and other problems also affect the strength of the land:

- A. *Earth quakes*: which produce shock and vibrations forms a significant factor in some hill areas.
- B. *Construction*: heavy industries and building constructions need big foundations which create internal vibrations.
- C. *Rainfall*: intense or heavy rainfall prone areas will always be in danger of land-slides especially hilly areas.
- D. *Under-Ground Constructions*: human activities including various transportation constructions like roadways and railways leading to steam erosions, heat wave actions.

These are some of the contributing factors leading to land-slides. Once the land-slide took place the material starts sliding from various mechanisms like falling, sliding and flowing [3], [8]. Land-slides vary with respect to the following properties:

- A. *Rate of Movement*: range of rate of movement varies from millimeters/year (slow creep) and meters/year (fast).
- B. *Type of Material*: bedrock, unconsolidated sediment and organic debris are the basic composition of the land-slide.
- C. *Nature of Movement*: sliding, slumping, falling and flowing.

In India land-slides mainly happens especially due to heavy rainfall which leads to considerable loss of life, communication damage, damage to agricultural and forest lands. The annual loss sometimes even crossed around \$400 million [18]. Most repeatedly at north-eastern region including Himalayan region and a section of Western Ghats including Vindhya mountain range has a significant problem of land-slide [21].

IV. SENSORS

This paper mainly intends to stress on land-slides due to heavy rainfall. Due to heavy rainfall, water infiltration due to rain on the slopes of the land causes instability leading to reduction in the factor of safety. Due to reduced factor of safety the following physical properties has a significant affect:

1. Water level height
2. Pressure variation
3. Reduced shear strength, which holds the soil or rock
4. Increase in soil weight leading to increase in soil's angle of repose.

If the rainfall is heavy for a certain period of time then hydraulic conductivity takes place at the slope and soil runoff. Based on the above property changes there occurs degradation of initial slope leading to transport of subsequent material and then the transported material is deposited by sliding [19].

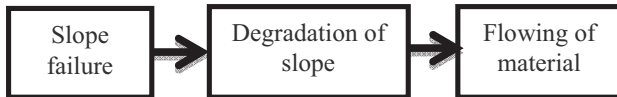


Fig 1: soil conductivity

Pore pressure and soil moisture are the two parameters that will increase due to high rainfall. In order to monitor them we require geo-physical sensors for detecting pressure using pore pressure sensor and moisture using dielectric moisture content transducer with a warning system. So this system includes pore pressure and moisture content sensor for monitoring in-site geophysical measurements.

Secondary conditions include slope failure, when this happens gradient of the slope change with vibrations so this monitoring is necessary and system should be effective to issue a warning immediately in severe failure or damage. To calibrate the slope movement and amount of slope gradient change should be measured which can be achieved using strain gauge, tilt sensor.

Along with this system another sensor for calibrating the vibrations are necessary with change in the seismic activity inside. Geo-phon is used as the source for analyzing the seismic activity and vibrations.

a) *Geophone*: a device which converts the ground displacement or movement into some voltage which may be recorded at a ground station for monitoring.



Fig 2: mechanical geophone

Under fault conditions if the measured voltage is more than normally measured then that responses are called 'seismic

response' and this can be collected for analyzing the structure of earth under various dependent conditions [17]. The geophone works with normal operating voltage of 30V and ground activities can be collected for every 30V change in voltage variation. But this is hard to design a NODE with this mechanical sensor forming a heterogeneous network for this condition we can use 'seismometer' on behalf of geophone which can fulfill the purpose. Thus this modification of geophone to seismometer converts the entire heterogeneous model into a 'smart NODE' which has even better advantage of direct interfacing with the controller based on requirement.

Deployment of this sensor is extended to maximum depth of 0.5 to 1.8 mts.

b) *Pore Pressure Sensor*: this sensor refers to the pressure of underground water during high rain conditions and even normal conditions held with in the soil.

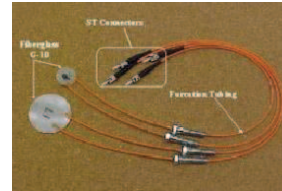


Fig 3: pressure sensor

This sensor mainly helps in to calculate the stress state of the ground with regarding to the soil mechanics.

c) *Dielectric Soil Moisture Sensor*: they determine the amount of moisture content by measuring the dielectric constant of the soil.

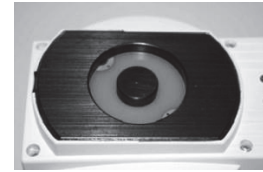


Fig 4: moisture sensor

The constant value for the dry soil is around 3 to 5, 80% for water and about one for air. Thus the changes in moisture content cause a substantial change in the moisture content value of the soil. Range of moisture content of 176 gms of water level of 1kg i.e., 28% to 46% for stability.

Deployment of this sensor is extended to maximum depth of 0.8 to 5.5 mts.

d) *Strain Gauge*: strain is the deformation due to applied force i.e., the frictional change due to physical pressure leads to deformation in length.

Deployment of this sensor is extended to maximum depth of 5.5 to 6.8 mts.



Fig 5: strain gauge

e) *Tilt Sensor*: can measure the tilting angle in two directional references. Accelerometer is the reference tilt sensor with ground variation.



Fig 6: tilt sensor

With the help of these sensors once the moisture, pressure, tilt is calibrated then requirement of soil deformation can be estimated.

Sensor	Output type	Signal pre-processing
Strain gauge piezometer	Dual wire analog	Level shifting amplification
Vibrating wire piezometer	RS-232 data logger	None
Di-electric moisture sensor	Single wire analog	None
Tiltmeter	Single wire analog	Voltage reduction, Amplification
Geophone	Dual wire analog	Level shifting, Amplification

Table 1: Interfacing Circuit Requirement

V. HARDWARE DESCRIPTION

To design the system of our requirement a NODE should be fabricated with a controller as a ‘master node’ for collecting the sensor data and transmitting the obtained data to the ‘receiving station’ with some intermediate nodes as middle layer transmitting medium, where the entire network leading to a WSN.

The detail descriptions of controller along with sensors were discussed here.

a) Controller: (ATMEGA16)

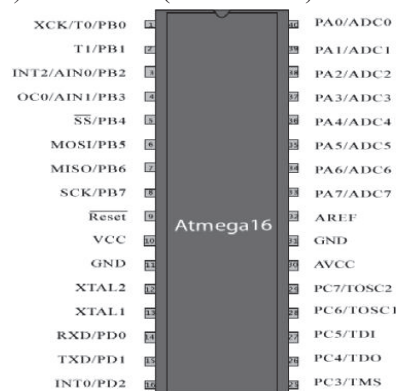


Fig 7: ATMEGA 16 controller

This advanced RISC architecture of ATMEGA16 has a throughput up to 16 MIPS with an on-chip 2 cycle multiplier and high endurance volatile memory which has an advantage of asynchronous data retrieval and transmission much faster and the pin configuration resembles the number of ADC, TIMER, USART, SPI and I2C configured pins which can be

sufficient for developing such heterogeneous NODE or by using MEMS sensors forming a ‘smart node’.

b) MAX232:

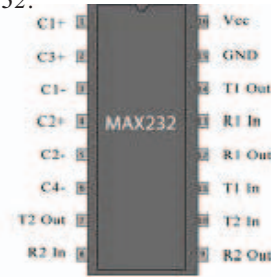


Fig 8: MAX-232

USART (Universal Synchronous Asynchronous Receiver Transmitter) is a communication protocol for transmitting the data between the and to control station. The internal RS-232 logic helps in creating the path by maintaining frequency and baud-rate.

c) 2.4 GHZ Receiver Transmitter Stations (ZIGBEE):

Wireless transmission can be achieved by a device which can facilitate the signal trans-receiving. This 2.4GHz frequency is un-pain frequency for general purpose as well as educational purpose. This can be further developed by integrating ETHERNET service along with zigbee for optimum data conversion and transmission. The size of the module is so small which can be easily portable for this application.

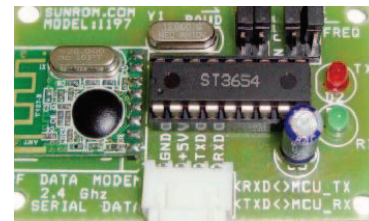


Fig 9: ZIGBEE module

WHY ZIGBEE: there were many wireless modules available in the market, but the low cost, high transmission range capability, ease of interfacing and low power consumption with regarding to NODE turns the views of the project to use the ZIGBEE module as a medium of communication.

d) Power Supply: Any NODE or any controller circuit requires power supply based on the requirement. For this NODE a battery can be used for fulfilling the requirement or an on-board power supply with a bridge rectifier circuit can be used for this purpose, which converts the AC supply to 12V DC supply and then 5V DC for running the controller, even for some sensors which require 5V as their operating voltage.

For this purpose an on-board power supply is being developed which supply electrical signals to run the circuit. This bridge rectifier converts the AC to DC. All the controller components and sensors use 5V, 500ma DC as the source for power supply. But some sensors like pore pressure and strain gauge transducer requires 12V requirement. So the bridge circuit developed in requires the fulfillment of both the power circuit at same time and a 9V-0-9V battery can be used as a source of power supply.

VI. NODE FABRICATION

Deployment of node is at bidholi/bidhauri, Dehradun. Node fabrication and data extractions are one issue, and then the problem is due to communication difference between the source and destination nodes. To achieve this, the node is being establishment at four different locations, each of 0.3 kms distant, which can easily transmit the monitored information without any packet loss while transmitting. Receiver node is established at University of Petroleum and Energy studies, which is 1.00 kms from the transmitter node.

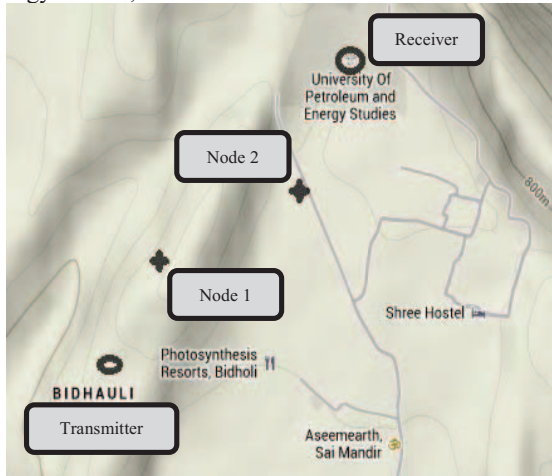
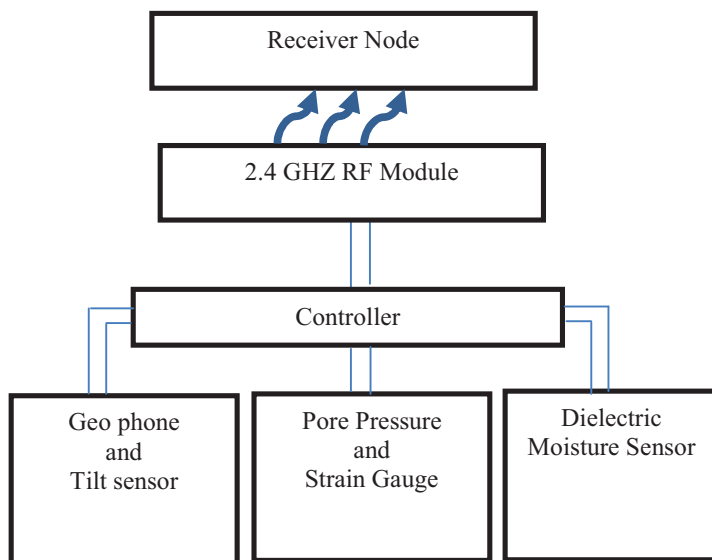


Fig 10: Node establishment location

Transmitter Node is the master node that will control all the sensor information that is being gathered through various sensors and transmits to the data to the Receiver Node across two intermediate nodes that helps in efficient transmitting of the gathered data without any missing information.

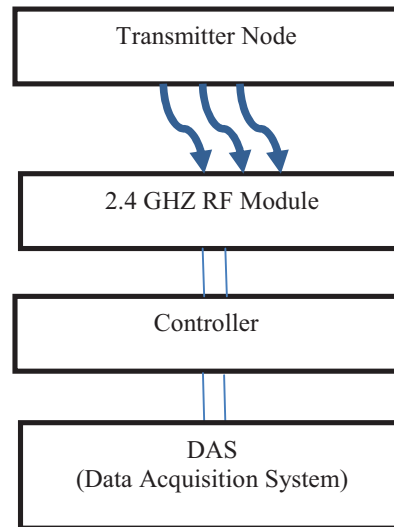
A. TRANSMITTER NODE:



Transmitter node consists of 3 controllers (1-ATMEGA16 and 2-Atmega8) which are connected by SPI mode where the 5 sensors were interfaced with 2 atmega8 (slaves) controllers and the atmega16 (master) will be gathering the information

from both the slave nodes and transmit the information using ZIGBEE and as well compare the obtained values with stored values, that helps in stability and time with respect to rate of change.

B. RECEIVER NODE:



The flow chart developed above only explains how the information is transmitted by the Transmitter Node to the Receiver Node and receiving end analysis. Intermediate nodes Node1 and Node2 comprises communication module (zigbee) and acts as Trans/Receiver Nodes.

C. VIRTUAL ANALYSIS:

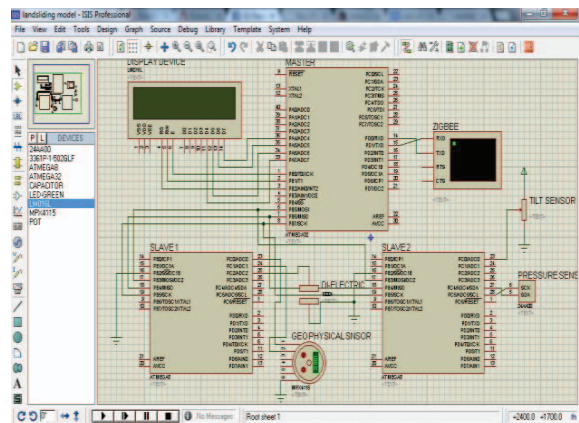


Fig 11: transmitter node

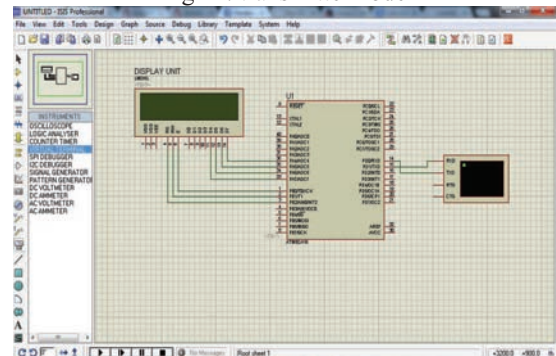
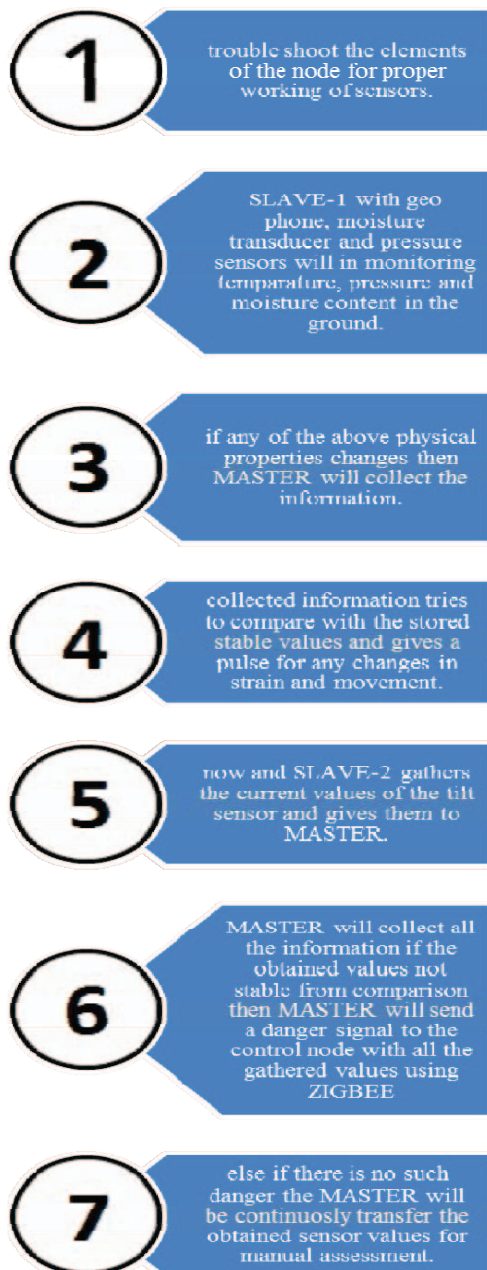


Fig 12: receiver node (control station node)

VII. ALGORITHM

Master controller will be interfaced with two other controllers that can communicate among them, which gathers the information. Moisture content, change in pressure w.r.t, strain induced will be continuously monitored, if any pressure varies due to change in moisture content then geophone gathers information about the vibrations that occurs internally and tilt sensor will check for any land movement and amount of deflection from the normal position. This data will be sent to the nearby node for further processing and to take precautionary steps. The algorithm below explains the monitoring.



VIII. RESULTS

Geophone calibration constants	No Damping ratio	With damping ratio
Vstep	0.998	2.961
Frequency f	0.6276 hz	1.1462 hz

Output of humidity sensor in serial monitor is

H:058 T:024

The above means Relative Humidity is 58% and Temperature is 24 degrees Celsius. Interpretation of above data is in 13 bytes is represented by

Byte	Hex	Char	Details
1	0A	\n	New line character
2	48	H	Fixed character H
3	3A	:	Fixed character
4	30	0	Humidity char hundreds
5	35	5	Humidity char Tens
6	38	8	Humidity char ones
7	20	"	space
8	54	T	Fixed Character T
9	3A	:	Fixed Character
10	30	0	Temperature char Hundreds
11	32	2	Temperature char Tens
12	34	4	Temperature char ones
13	0D	"	space

When there exist some vibrations in ground then the geophone calibrates the error between the damping and non-damping ratio then due to this seismic activity there might be a chance of sliding, so geophone will be continuously monitor along with the moisture sensor.

IX. CONCLUSION AND FUTURESCOPE

The deployed node has an advantage of obtaining optimum results with minimum cost and even more compatible for expanding with other communication devices for even more fast responses. The only problem arises with the serial communication between the controllers which might decrease the processing speed.

In general case Asia is the most affected continent due to land-slides and among Asian countries India one of the countries most affected with. About 25% of India's land mass (0.82 million square kilometers) is prone to land-slides. By use of Wireless Sensor Network any mechanical or geo-physical sensor can be interfaced easily for protection of our on livelihood as well as nation's wealth. This paper discussed a proto-model of NODE design for 'Land-Slide Monitoring' which of great importance especially in heavy rainfall and hilly areas. The WSN deployment leads to access many of the sensor information and by using Ethernet, Wi-Fi, Satellite or any other wireless protocol the danger intimation can be passed to the nearby villages and to the government officials.

The Data Acquisition System at the control station is equipped with all the necessary protection equipment for all necessary measures which can be easy for the officials to take necessary steps for disaster protection.

REFERENCES

- [1] K. Mishra, S.K. Shukla, S. Dutta, S.K. Chaulya, G.M. Prasad, Detection of Land-Slide using Wireless Sensor Network, Proceedings of International Conference organized by IEEE, 2011.
- [2] Thampi. P. K., Mathai. John, Sankar. G., Sidharthan. S., Landslides: Causes, Control and MitigationT, (based on the investigations carried out by the Centre for Earth Science Studies, Trivandrum).
- [3] P. D. Savvaidis, from stars to earth and culture, Existing Landslide Monitoring Systems and Techniques, The Aristotle University of Thessaloniki, In honor of the memory of Prof. Alexandros Tsoumias,, 2003.
- [4] Y.P. Sharda, Landslide Studies in India, Glimpse of Geoscience Research in India, The Indian report to IUGS, 2004-2008, Indian National Science Academy, Silver Jubilee Volume, 2009, pp 98-101.
- [5] Ramesh, M. V., Real-time Wireless Sensor Network for Landslide Detection, Proceedings of the Third International Conference on Sensor Technologies and Applications, SENSORCOMM 2009, IEEE, Greece, June 18-23, 2009.
- [6] Tien-wen seng, Ting-Ting wu, et.al., Reliable Data Broadcast for ZigBee Wireless Sensor Networks, Intelligent journal on smart sensing and intelligent systems, Vol 3, No. 3, September 2010.
- [7] Dr. Maneesha Vinodini Ramesh, Wireless Sensor Network for Disaster Monitoring, Amrita Center for Wireless Networks and Applications, Amrita Vishwa Vidhyapeetham (Amrita University), India.
- [8] Silvia Nittel, The Indo-US Science and Technology Forum, Workshop on Geo-spatial information for developing countries, jointly organized by IIT Bombay and University of Minnesota, December, 2009.
- [9] Alberto Rosi, Nicola Bicocchi, Gabriella Castelli Marco Mamei, Franco Zambonelli, Land-slide Monitoring with Sensor Networks: Experiences and Lessons learnt from a Real-World deployment, International Journal on Signal and Imaging systems Engineering, Italy.
- [10] LAN. Hengxing., ZHOU. Chenghu1., C. F. Lee., WANG .Sijing., WU. Faquan., Rainfall-induced landslide stability analysis in response to transient pore pressure - A case study of natural terrain landslide in Hong Kong.
- [11] National Disaster Management Guidelines: Management of Landslides and Snow Avalanches, National Disaster Management Authority, Government of India, June-2009.
- [12] Landslide Risk Treatment, Management of Landslides and Snow Avalanches, National Disaster Management Authority, Government of India, June-2009.
- [13] Wang, G., and K. Sassa., Pore-pressure generation and movement of rainfall-induced landslide: Effect of grain size and fine-particle content, Engineering Geology Vol 69, Pages 109-125, 2003.
- [14] Dr. Praveen Chaturvedi, Introduction to Wireless Sensor Networks, International Journal of Advanced Research in Computer Science and Software Engineering, ISSN NO: 2277 128X, Volume 2, Issue 10, October 2012.
- [15] He Yueshun, Zhang Wei, The Research on Wireless Sensor Network for Landside Monitoring, International Journal on Smart Sensing and Intelligent Systems, VOL-6, NO:3, ISSN: 1178-5608, June-2013.
- [16] DR. Vidar Kveldsvite, Norwegian GeoTechnical University, The Aknes rock slope: Early warning system and emergency preparedness, Second India Disaster Management Congress, 2009, NewDelhi.
- [17] Gordon B. Bowden, Calibration of Geophone Micro-seismic Sensors, Stanford Linear Accelerator Center, Stanford University, LCLS-TN-03-6, October, 2003.
- [18] Land-slides issue by NDTV: <http://www.ndtv.com/topic/landslides-in-uttarakhand>
- [19] National Instruments: <http://www.ni.com/white-paper/3642/en/>
- [20] Sensor Geophones: http://www.iongeo.com/content/documents/Resource%20Center/Brochures%20and%20Data%20Sheets/Brochures/BR_SEN_Geo_phones_091509.pdf
- [21] Volcano Hazard Programs: United States of America - <http://volcanoes.usgs.gov/activity/methods/deformation/tilt/>
- [22] http://www.decagon.com/products/soil_s/volumetric-water-content-sensors/
- [23] Wireless Serial Data RF Modem, 2.4GHZ, 30mts: <http://www.sunrom.com/214> <http://www.sunrom.com/214>

layer 3 services implementation in different routers

Ankur Dumka

Center of Information Technology
University of Petroleum and Energy Studies,
Dehradun, India
AnkurDumka2@gmail.com

Dr. Hardwari Lal Mandoria

College of technology
G.B.Pant University
Pantnagar, India
drmandoria@gmail.com

Abstract— Service implementation isto transmit customer data across service provider network & to transmit these services through MPLS or GRE tunnel so that each customer and services get separate path to travel . The way services gets implemented in L3 VPN is different in different routers. Here we had study the different way the services gets implemented in different routers.

Keywords-MPLS, VPN ,VRF , LER, LSR

I. INTRODUCTION

Historically, telecommunications service providers have deployed completely separate network to provide different type of services, such as time division multiplexing (TDM) technologies for real- time voice, Frame Relay and ATM for private network services with specific service levels and IP for best effort data services.

Factors that influence service providers to evolve to single network infrastructure that support delivery of wide range of telecommunication services are high cost of maintaining & operating discrete legacy network, service provider desire to continue to support high revenue legacy services like frame. relay& TDM, consumer demand for new services like wireless data & streaming videos, demand for high bandwidth services at decreasing prices.

Virtual private network (VPN) is a network in which a service provider shared infrastructure is used to provide private services to its customers. It is known as virtual private network as it donot require physical seperation hence logical and hence known as virtual & private in the sense that customer can maintain their own addressing & routing schemes fully independent of & transparent to other customer. A service is a logical globally unique entity that provides a uniform, end-to-end configuration, management & billing model for provisioning either internet or VPN connectivity between customer access points ; which can be either local or distributed.

There are different types of routers used for services specific functions in a network, they are as:

Service router which function as PE router in a service network. It is a scalable, full function IP/MPLS router that support full range of services types & customers.

Access routers support low speed internet access services & used for low bandwidth.

Core or provider routers support high speed interfaces & are primarily designed to provide the capacity for forwarding larger quantity of data. They are connected to other Provider Edge or Provider routers. Routing protocol run for purpose of internal routing in provider core in these routers.

Layer 3 VPN connect multiple sites in a routed domain over provider managed IP/MPLS network. Each layer 3 VPN consists of a set of customers sites connected to one or more PE routers. Each associated router maintain a separate IP forwarding table for each L3 VPN.

L3 VPN have advantages like sites are connected to private routed network administered by the service provider for that customer only, separate & independent IP address plan for L3 VPN, L3 VPN can operate over single local site or over multiple geographically dispersed site.

Services is to transmit customer data across service provider network & to transmit these services through MPLS or GRE tunnel. Separate tunnels are created for different services. When MPLS tunnels is used, customer data is encapsulated with two MPLS labels, an outer transport label & an inner service label. Label Switch Path (LSP) tunnel are used to transport traffic. Transport tunnel LSPs are identified by MPLS labels that are swapped at each intermediate router, also known as transit LSR. The service label or VC label is used to identify which service or customer owns the packet.

For GRE encapsulation tunnel IP header is used, where source IP address is the local PE router and the destination IP address is the far end PE router. Even though GRE is used for transport, an MPLS service label still exists so that far end PE can be demultiplex the service correctly. Thus, the outer IP header is used for forwarding the packet through service provider network and IP header is not swapped at each router as in MPLS tunnel. Signaling protocol use label distribution protocol(LDP) and/or Resource reservation protocol-Traffic engineering (RSVP-TE) to set up LSPs, which can be used for various service tunnel.

Service label are used to encapsulate and identify customer traffic belonging to a particular service. This label is applied to the customer traffic before the transport label is applied. T-LDP (targeted LDP) is protocol used for signaling transport label with few additional capabilities added. Multiprotocol-border gateway protocol (MP-BGP) protocol is used to exchange customer routes across L3 VPN. The BGP updates also include a label for these routes

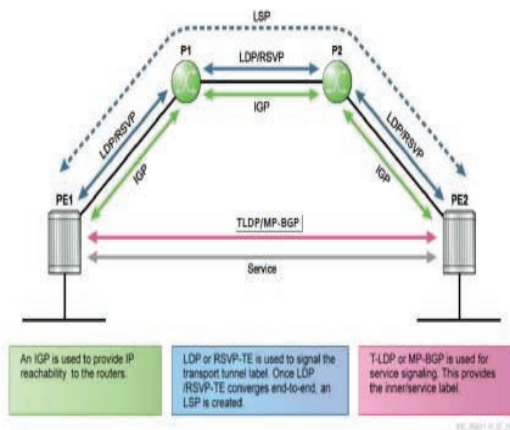


Fig. 1

Service implementation in different routers

Services implementation is different in different routers like REDACK routers , ZTE routers , ALCATEL router , CISCO router and JUNIPER router. Here the service implementation is studied in different routers.

In routers we create Layer 3 VPN for different service implementation , customer service description is created for Layer 3 VPN customer .Layer 3 VPN service instance is created using auto-bind LDP for the transport tunnel. Assigning a router ID, route-distinguisher and route target to the Layer 3 VPN. Customer interface is created in the layer 3VPN instance and assign a provider edge or customer edge port to interface. Different VLAN id can be used for different customer at customer edge router with port configuration. IP address is configured on service interface ,enable layer 3 VPN service instance.

Service implementation in redback router

It is done by making different context and assigning the interfaces under particular context carrying that particular service. One interface can carry more than one service so can be assign in more than one context.

```

service multiple-contexts
!
service inter-context routing
!
context local
!
ip address 10.0.4.177/32
logging console
!
context CN_CONTEXT vpn-rd 65000:1

!
interface RNC_IuCS_01
description RNC IUCS User Traffic
ip address 10.10.10.2/28
vrrp 21 backup
virtual-address 10.10.10.3
advertise-interval millisecond 300

```

```

priority 100
preempt hold-time 90
!

```

```

context CPC_OM vpn-rd 65000:06
!
noip domain-lookup
!
interface Mur
ip address 10.31.219.99/28
description RNC O&M Connectivity
vrrp 109 backup
virtual address 10.31.219.97
priority 100
advertise-interval millisecond 300
preempt hold-time 90
!

```

Service implementation in ZTE router

VRFAre created for different service implementation in following manner:

```

interface gei-0/2/0/7.1
ipvr forwarding Signal
ip address 10.10.10.1 255.255.255.240
!
interface gei-0/2/0/7.2
ipvr forwarding Media
ip address 10.10.10.2 255.255.255.240
!
interface loopback11
ipvr forwarding Signal
ip address 10.10.10.3 255.255.255.240
!
interface loopback12
ipvr forwarding Media
ip address 10.10.10.4 255.255.255.240
!
address-family ipv4 vrf Signal
redistribute connected
redistributeospf-ext 11
redistributeospf-int 11
$

address-family ipv4 vrf Media
redistribute connected
redistributeospf-int 12
redistributeospf-ext 12

```

Service implementation in CISCO routers

It is implemented by creating VRF for different customers having services in following manner :

```

ipvr cutomer1
rd 100:1
route-target both 1:100
int f0/0
ipvr forwarding customer

```

```
ip address 10.10.10.10 255.255.255.0
```

```
ipvrfd customer2
rd 100:1
route-target both 1:100
int f0/0
ipvrfd forwarding customer
ip address 10.10.10.11 255.255.255.0
```

service implementation in alcatel router

This implementation through creating VPRN creating different customer with different identity and run services in that services in following manner :

```
configure service
customer 10 create
description "customer1"
router id 10.10.10.10
route-distinguisher 100:1
vrf-target 100:1
auto-bind ldp
exit
```

```
configure service
customer 20 create
description "customer2"
router id 10.10.10.11
auto-bind ldp
exit
```

Service implementation in juniper router

It is implemented in following manner:

```
set interfaces ge-2/0/1 description "EoSDH connectivity with
Surat SR1"
set interfaces ge-2/0/1 per-unit-scheduler
set interfaces ge-2/0/1 vlan-tagging
set interfaces ge-2/0/1 unit 2555 description "EoSDH
connectivity with Surat SR1"
set interfaces ge-2/0/1 unit 2555 vlan-id 2555
set interfaces ge-2/0/1 unit 2555 family inet address
10.129.22.37/30
set interfaces ge-2/0/1 unit 2555 family mpls
```

```
set interfaces ge-3/1/3 description "EoSDH connectivity with
Vadodara SR1"
set interfaces ge-3/1/3 per-unit-scheduler
set interfaces ge-3/1/3 vlan-tagging
set interfaces ge-3/1/3 unit 2559 description "EoSDH
connectivity with Vadodara SR1"
set interfaces ge-3/1/3 unit 2559 vlan-id 2559
set interfaces ge-3/1/3 unit 2559 family inet address
10.129.22.69/30
set interfaces ge-3/1/3 unit 2559 family mpls
```

```
set protocols rsvp graceful-restart maximum-helper-restart-
time 300
set protocols rsvp graceful-restart maximum-helper-recovery-
time 400
set protocols rsvp refresh-time 60
set protocols rsvp interface ge-2/0/1
```

```
set protocols rsvp interface lo0.0
set protocols rsvp interface ge-3/1/3
set protocols rsvp interface lo0.0
```

```
set protocols mpls label-switched-path router1-router2 to
10.129.16.2
set protocols mpls label-switched-path router1-router2 ldp-
tunneling
set protocols mpls label-switched-path router1-router2 least-
fill
set protocols mpls label-switched-path router1-router2 fast-
reroute
set protocols mpls path router1-router2_Pri 10.10.10.45 strict
set protocols mpls path router1-router2_Sec
```

Conclusion

The service implementation is done for different services to be executed over same link with different routes tagged for different services. The ways the services implemented is different in different routers. The study of these implementation is studied over here. The practical implementation in different routers like cisco, alcatel, ZTE , Red back and juniper is done .

REFERENCES

- [1.] Lanjun and Lin bi ying, 2011 International Conference on Mechatronic Science, Electric Engineering and Computer, "Research for Service Deployment Based on MPLS L3 VPN Technology", August 19-22, 2011, Jilin, China page 1484-1488.
- [2.] R. Boutaba ,W. Szeto and Y.Iraqi, "Emerging Trends in Engineering and Technology, 2008. ICETET '08. First International Conference on Digital Object Identifier: 10.1109/ICETET.2008.58 Publication Year: 2008 , Page(s): 187 – 192
- [3.] Yoo-Hwa Kang, and Jong-Hyup Lee, "The Implementation of the Premium Services for MPLS IP VPNs" Advanced Communication Technology, 2005, ICACT 2005. The 7th International Conference on Volume: 2 Digital Object Identifier: 10.1109/ICACT.2005.246152 , Publication Year: 2005 , Page(s): 1107 - 1110
- [4.] Rahul Aggarwal, Juniper Networks, OAM Mechanisms in MPLS Layer 2 Transport Networks, IEEE communication magazine october 2004 , page 124-130.
- [5.] Young-Kyu Oh, Dong-Keun Kim, Hun-Je Yoen, Mi-sun Do and Jaiyong Lee, Scalable MPLS Multicast using Label Aggregation in Internet Broadcasting Systems, IEEE journal ,2003, pages 274-280.
- [6.] Norashidah Md Din, NorsheilaFisal, Dynamic Resource Allocation of IP Traffic for a DiffServ-MPLS Interface using Fuzzy Logic, IEEE journal ,2003, Page 339-343
- [7.] "www.cisco.com/en/US/docs/internetworking/technology/MPLS/VPN/handbook" from Cisco recognized site available.

Mass and Length Dependent Chaotic Behavior of a Double Pendulum

Mukul K. Gupta¹, Kamal Bansal², Arun K. Singh³

^{1,2}University of Petroleum and Energy Studies, Dehradun-248007, INDIA

³Visvasvaraya National Institute of Technology, Nagpur-440010, INDIA

¹ mukulvjti@gmail.com (Assistant Professor, Electrical Engineering, UPES Dehradun)

² kamalbansal@ddn.upes.ac.in (Professor, Electrical Engineering, UPES Dehradun)

³ aksinghb@gmail.com (Assistant Professor, Mechanical Engineering, VNIT Nagpur, corresponding author)

ABSTRACT: In this article, chaotic behavior of a double pendulum (DP) is studied numerically by varying its mass and length. The results are analyzed using time series plot, Poincare map and Lyapunov exponent plot. It is observed that the chaotic tendency of the DP increases with mass and length. However, both pendulums of the DP have varying effect on the Lyapunov exponent. The significance of the present study in the optimization and control of the dynamical systems based on the DP is also discussed.

Keywords: Chaos, Double Pendulum, Time series, Poincare Map, Lyapunov exponent

1. INTRODUCTION

A double pendulum (DP) is an interesting dynamical system since it shows chaotic motion (Baker and Gollub, 1990, Ohlhoff and Richter, 2006). Notably, experimental and numerical studies have been carried out of such a system considering the change in initial value of amplitude and angular velocity of the double pendulum (DP) (Baker and Gollub, 1990). It is observed that a DP shows periodic behaviour at low energy, transforms to quasi-periodicity at intermediate energy level and chaos at higher energy level finally again periodic motion as energy of the system increases further (Nunna, 2009). Despite significant study on the chaotic dynamics of the DP, there is no reported study in literature how the mass and length of a DP influences its chaotic behavior. Such a study is important from controlling and optimizing dynamical systems based on double pendulum for instance double arm robots (Behera and Kar, 2009). Chaos is a physical phenomenon in which a dynamical system shows random motion and the results depends on initial conditions (Baker and Gollub, 1990). Chaos is basically a manifestation of non-linearity in the dynamical system. However, all non-linear systems do not show chaotic behaviour. A condition for chaos is that the differential equations governing the dynamical system should contain non-linear terms. Moreover, it should be expressible in at least three or more phase variables (Baker and Gollub, 1990). Lyapunov exponent is generally used to characterize the chaos of a dynamical system. For instance, if the average value of Lyapunov exponent is negative then the system is non chaotic. However, if Lyapunov exponent positive, then it shows chaos. Linear stability analysis of the DP shows that its two natural frequencies depend on mass and length of

each pendulum in the system (Ohlhoff and Richter, 2006). Further it is to be noted that natural frequency of a pendulum also depends on the initial conditions of oscillation for instance amplitude.

Figure 1 presents the schematic sketch of double pendulum in a plane. Upper end of the top pendulum is pivoted to a fixed point while the lower end of the same is connect with the top end of the bottom pendulum. Mass and arm length of the both pendulum were changed in the numerical simulation in the present study. Moreover, mass of the each pendulum is concentrated at the end in the form of solid sphere and also arm of each pendulum is considered to be massless (Fig.1).

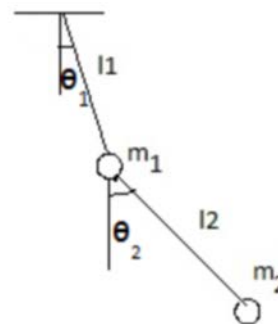


Figure 1: Schematic sketch of double pendulum under free oscillation.

Further $m_1, m_2, l_1, l_2, \theta_1$ and θ_2 are the mass, length and angular displacement of the top and bottom pendulum respectively.

2. MODELLING OF DOUBLE PENDULUM

A similar procedure is followed to derive the system of non-linear equation as reported in the reference (Nunna, 2009). Assuming the pivot point as the origin of the coordination system with the horizontal (x-axis) and the vertical (y-axis). The DP is assumed to be located in the fourth quadrant of the coordinate system. The coordinate position of top and bottom pendulum is given by

$$x_1 = l_1 \sin(\theta_1), y_1 = -l_1 \cos(\theta_1), x_2 = l_1 \sin(\theta_1) + l_2 \sin(\theta_2),$$

$$y_2 = -l_1 \cos(\theta_1) - l_2 \cos(\theta_2). \text{ And the corresponding angular velocity is given by the equations } \dot{x}_1 = l_1 \cos(\theta_1) \dot{\theta}_1$$

$$, \dot{y}_1 = l_1 \sin(\theta_1) \dot{\theta}_1, \dot{x}_2 = l_1 \cos(\theta_1) \dot{\theta}_1 + l_2 \cos(\theta_2) \dot{\theta}_2,$$

$$\dot{y}_2 = l_1 \sin(\theta_1) \dot{\theta}_1 + l_2 \sin(\theta_2) \dot{\theta}_2.$$

Kinetic energy of the double pendulum in Fig.1 is given by the following equation

$$K_2 = \frac{1}{2}(m_1 + m_2)l_1^2 \dot{\theta}_1^2 + \frac{1}{2}(m_2)l_2^2 \dot{\theta}_2^2 + m_2 l_1 l_2 \dot{\theta}_1 \dot{\theta}_2 \cos(\theta_1 - \theta_2) \quad (1)$$

And the potential energy is

$$V_2 = -(m_1 + m_2)gl_1 \cos \theta_1 - m_2 gl_2 \cos \theta_2 \quad (2)$$

The Lagrangian $L_2 = K_2 - V_2$ of two simply connected pendulums (Fig.1) is given by the following equation

$$L_2 = \frac{1}{2}(m_1 + m_2)l_1^2 \dot{\theta}_1^2 + \frac{1}{2}m_2 l_2^2 \dot{\theta}_2^2 + m_2 l_1 l_2 \dot{\theta}_1 \dot{\theta}_2 \cos(\theta_1 - \theta_2) + (m_1 + m_2)gl_1 \cos \theta_1 + m_2 gl_2 \cos \theta_2 \quad (3)$$

Further modifying the above equations:

$$(m_1 + m_2)l_1^2 \ddot{\theta}_1 + m_2 l_1 l_2 \ddot{\theta}_2 \cos(\theta_1 - \theta_2) + m_2 l_1 l_2 \dot{\theta}_2^2 \sin(\theta_1 - \theta_2) + (m_1 + m_2)gl_1 \sin \theta_1 = 0 \quad (4)$$

$$m_2 l_2^2 \ddot{\theta}_2 + m_2 l_1 l_2 \ddot{\theta}_1 \cos(\theta_1 - \theta_2) - m_2 l_1 l_2 \dot{\theta}_1^2 \sin(\theta_1 - \theta_2) + m_2 gl_2 \sin \theta_2 = 0 \quad (5)$$

Converting into non-dimensional form of above equations 4& 5.

$$\ddot{\theta}_1 + m_{2/12} l_{2/1} \ddot{\theta}_2 \cos(\theta_1 - \theta_2) + m_{2/12} l_{2/1} \dot{\theta}_2^2 \sin(\theta_1 - \theta_2) + gl_1^{-1} \sin(\theta_1) = 0 \quad (6)$$

$$\ddot{\theta}_2 + l_{1/2} \ddot{\theta}_1 \cos(\theta_1 - \theta_2) - l_{1/2} \dot{\theta}_1^2 \sin(\theta_1 - \theta_2) + gl_2^{-1} \sin(\theta_2) = 0 \quad (7)$$

Where $m_{2/12} = m_2 / (m_1 + m_2)$ and length of arm of the pendulum is $l_{2/1} = l_2 / l_1$ and $l_{1/2} = l_1 / l_2$. And the equation of momenta p_i of the DP is given by $p_i = \partial L_2 / \partial \dot{\theta}_i$ where $i = 1$ and 2

$$p_1 = (m_1 + m_2)l_1^2 \dot{\theta}_1 + m_2 l_1 l_2 \dot{\theta}_2 \cos(\theta_1 - \theta_2) \quad (8)$$

$$p_2 = m_2 l_2^2 \dot{\theta}_2 + m_2 l_1 l_2 \dot{\theta}_1 \cos(\theta_1 - \theta_2) \quad (9)$$

And the Hamiltonian $H_2 = K_2 + V_2$ of the DP is given by

$$H_2 = \frac{1}{2}(m_1 + m_2)l_1^2 \dot{\theta}_1^2 + \frac{1}{2}m_2 l_2^2 \dot{\theta}_2^2 + m_2 l_1 l_2 \dot{\theta}_1 \dot{\theta}_2 \cos(\theta_1 - \theta_2) - (m_1 + m_2)gl_1 \cos \theta_1 - m_2 gl_2 \cos \theta_2 \quad (10)$$

Above differential equations (6&7) were solved numerically in MATLAB using *ode45* by following the procedures similar to the given in the reference 1. All simulations were carried out for a fixed initial condition i.e., $(\theta_1, \theta_2, p_1, p_2) = (0.2, 0.2828, 0, 0)$. Time series of angular velocity of the two pendulum, Poincare map and the average value of Lyapunov exponent are plotted to understand the mass and length dependent chaotic behavior of the DP (wolf and Swift, 1985, Zaki and Noah 2002). Poincare map (section) i.e., $(\dot{\theta}_1, p_1)$ was generated for the top pendulum under the condition $\sin(\theta_2) = 0$ and $\dot{\theta}_2 > 0$ (Rosa Nunna, 2009). The results are discussed in next section.

3. RESULTS AND DISCUSSION

Fig.2 presents the plots concerning the time series (angular velocity), Poincare map and Lyapunov exponent for $m_1 = 1.0$ kg, $m_2 = 1.0$ kg, $l_1 = 1.0$ m and $l_2 = 1.0$ m and the Hamiltonian energy $E = -28.62$ J. It is obvious from the plot (a) in Fig.2 that angular velocity of both pendula is periodic and both are in phase. Moreover,

corresponding Poincare map is also regular as evident in plot (b) of the same Fig.2. Also the average Lyapunov exponent e is found to be $e = -0.1607$ which is negative. As mentioned earlier, dynamical system with negative exponent does not show the chaotic motion.

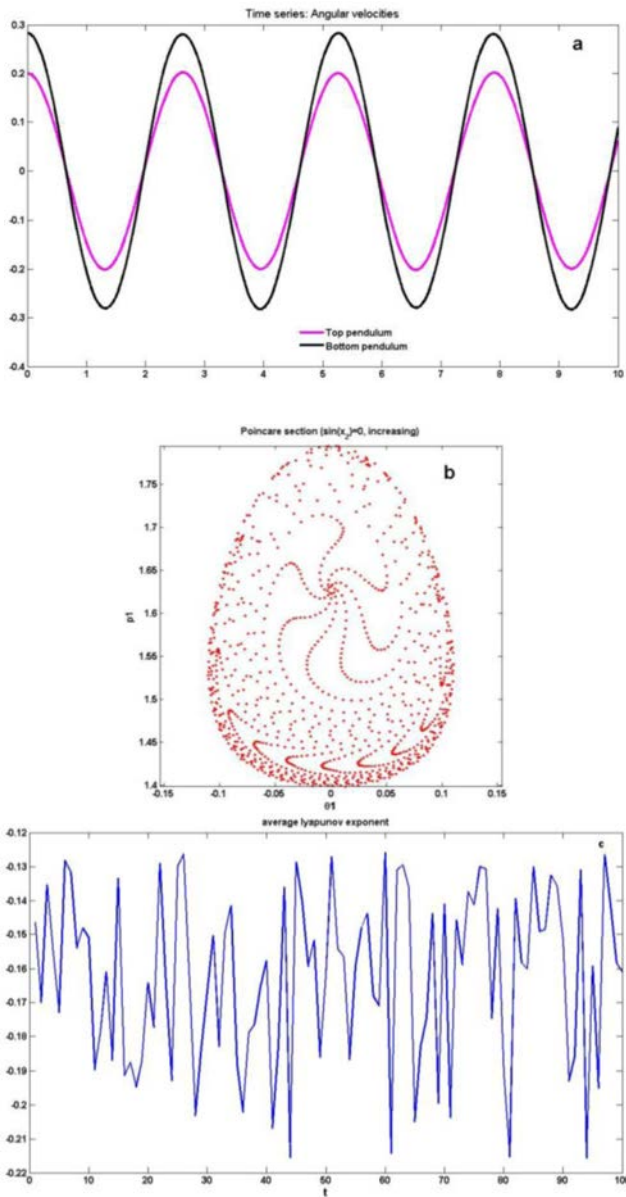


Fig.2 presents (a) Time series (b) Poincare map (c) Lyapunov exponent for $m_1 = 1, m_2 = 1, l_1 = 1$ and $l_2 = 1$, Hamiltonian $E = -28.62$.

It is now mass of the top pendulum is increased to $m_1 = 5$ while other parameters were considered the same as earlier. Now the energy corresponding to Hamiltonian increased to $E = -67.04$. Time series plot of angular velocity of the plot (a) of Fig.3 show that the motion is now quasi-periodic as there are two time period in the motion. And the corresponding Poincare map shows to be regular but with large area of null. The average Lyapunov

exponent $e = -0.1086$. This value of e is larger than in Fig.1. Thus it may be concluded that chaotic tendency of the DP increased with mass of the top pendulum.

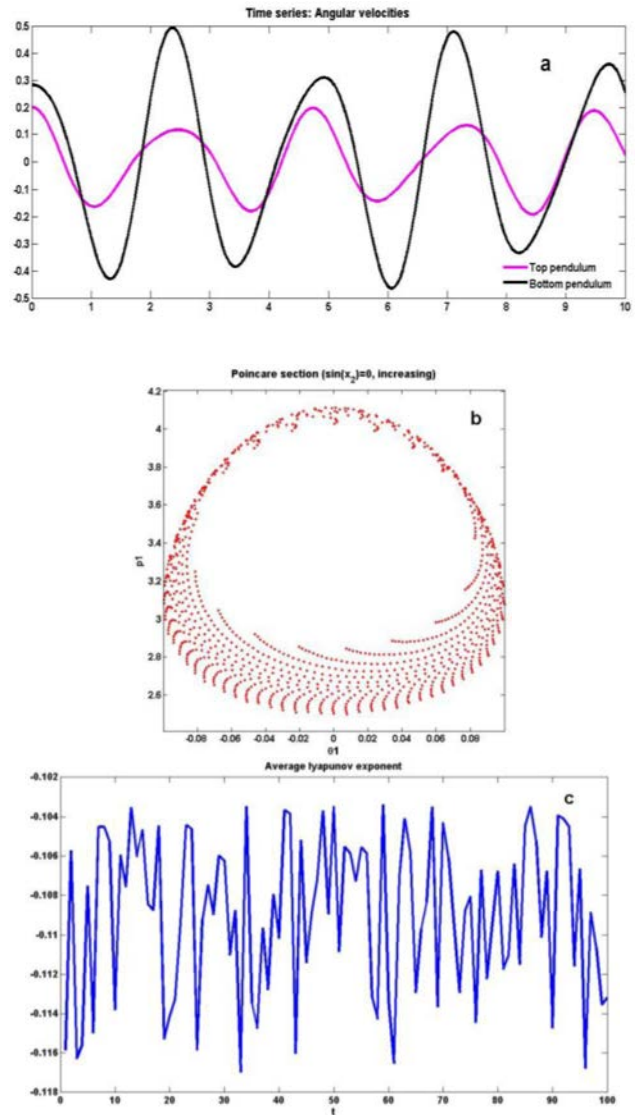


Fig.3 presents (a) Time series (b) Poincare map (c) Lyapunov exponent for $m_1 = 5, m_2 = 1, l_1 = 1$ and $l_2 = 1$, Hamiltonian $E = -67.04$.

Now in case of change in magnitude of the mass of the bottom pendulum i.e., $m_2 = 5$, the time series plot (a) in Fig.5 shows that the top pendulum is showing period oscillation while the bottom pendulum is random. The value of average Lyapunov exponent is $e = 0.0399$. As noted earlier that positive value of the average Lyapunov exponent results in chaotic oscillations. The chaotic behavior is also clear in plot (b) of Fig.4. It may be concluded that the bottom makes the DP more chaotic than the top pendulum.

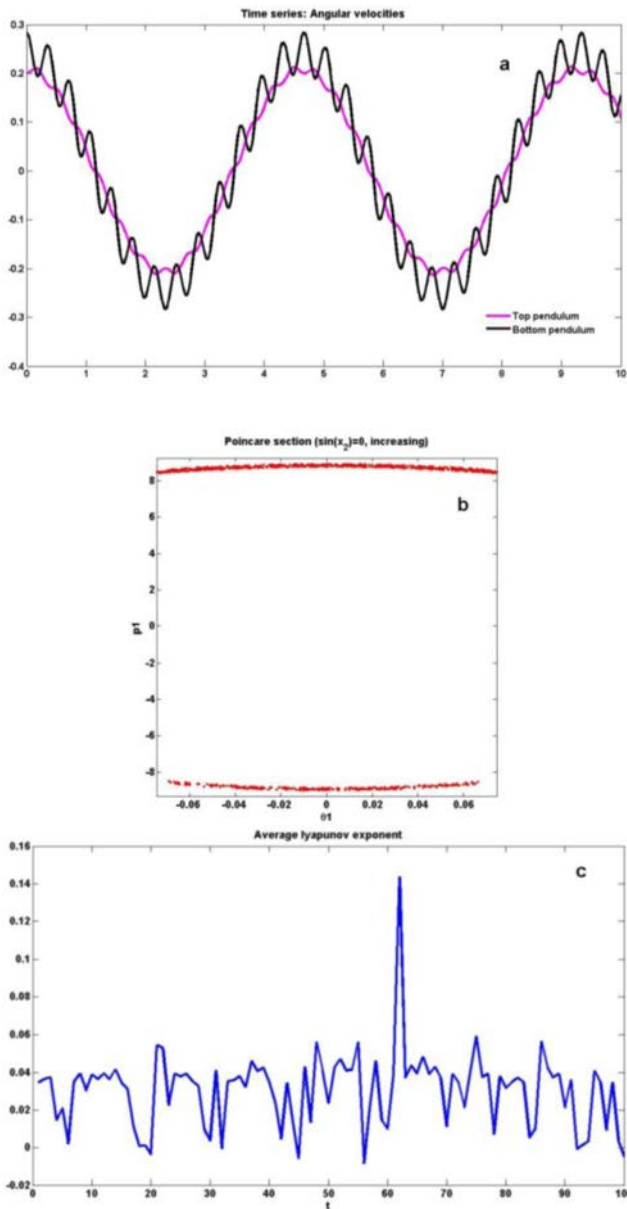


Fig.4 presents (a) Time series (b) Poincare map (c) Lyapunov exponent for $m_1 = 1, m_2 = 5, l_1 = 1$ and $l_2 = 1$ for Hamiltonian $E = -104.68$.

Motivated from the above study, it becomes interesting to know how arm length of pendula affects its chaotic dynamics. Length of the top pendulum was changed from $l_1 = 1$ to $l_1 = 3$. The result from the time series plot (a) in Fig.5 shows that the bottom pendulum is showing quasi-periodic oscillation while the top pendulum is still periodic. The value of average Lyapunov exponent is equal to -0.0991 . It is concluded that increasing arm length of the top pendulum results in quasiperiodic motion.

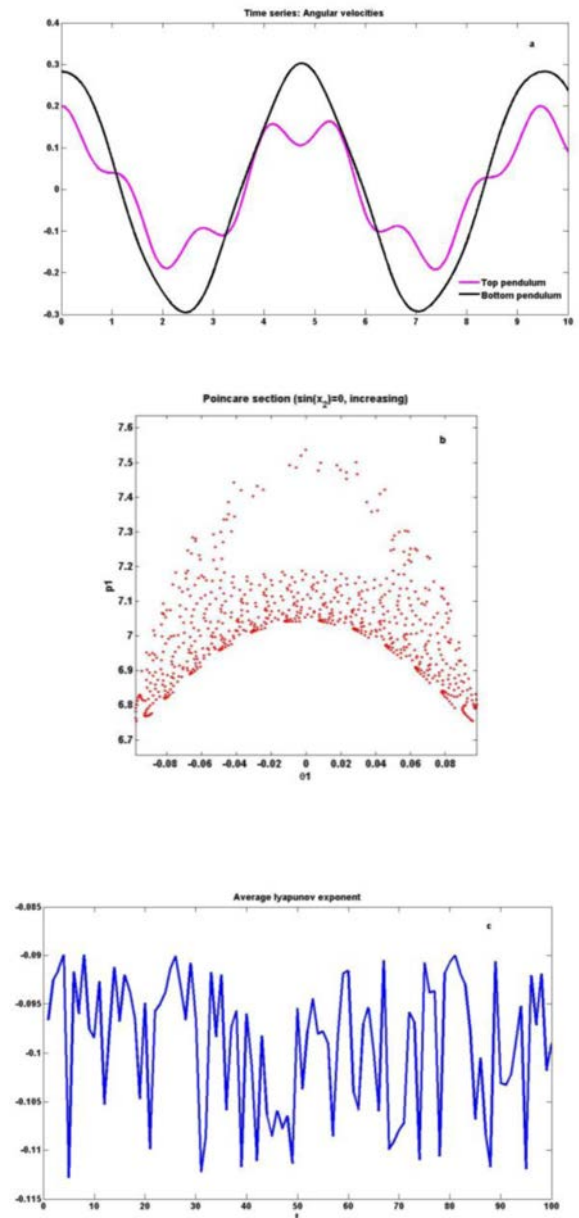


Fig.5 presents (a) Time series (b) Poincare map (c) Lyapunov exponent for $m_1 = 1, m_2 = 1, l_1 = 3$ and $l_2 = 1$, Hamiltonian $E = -67.04$.

Finally, arm length of the bottom pendulum was also changed in the simulation for $l_2 = 3$. The value of average Lyapunov exponent is $e = 0.0234$. The results in Fig.6 shows the DP is ultimately moving towards the chaos.

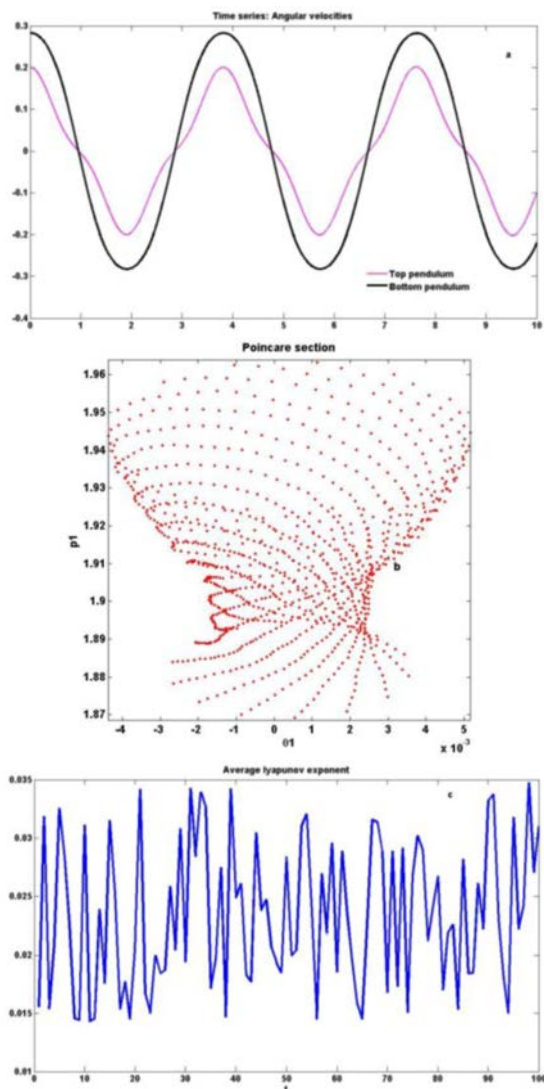


Fig.6 presents(a) Time series (b) Poincare map (c) Lyapunov exponent for $m_1 = 1, m_2 = 1, l_1 = 1$ and $l_2 = 3, E = -47.44 J$.

The summary of the above simulations is presented in the Table 1.

Table 1: Summary of the numerical simulations

Mass (Kg) and length (m) of each pendulum	Lyapunov exponent e and Hamiltonian energy E (Joule)	Chaotic/non-chaotic behavior
$m_1 = 1, m_2 = 1, l_1 = 1$ $l_2 = 1$	$e = -0.1607$ $E = -28.62 J$	Periodic
$m_1 = 5, m_2 = 1, l_1 = 1$ $l_2 = 1$	$e = -0.1086$ $E = -67.04 J$	Quasi-periodic

$m_1 = 1, m_2 = 5, l_1 = 1$ $l_2 = 1$	$e = 0.0399$ $E = -104.68 J$	Chaos
$m_1 = 1, m_2 = 1, l_1 = 3$ $l_2 = 1$	$e = -0.0991$ $E = -67.04 J$	Quasi-periodic
$m_1 = 1, m_2 = 1, l_1 = 1$ $l_2 = 3$	$e = 0.0234$ $E = -47.44 J$	Chaos

From the Table 1, it may be concluded that mass and length of the two pendulum have varying degree of effect on the average value of Lyapunov exponent. Thus there is an optimal combination of mass and arm length of the DP at which chaotic tendency of the system will be minimum. However further numerical and experimental studies are needed on this issue.

4. CONCLUSION

The chaotic behaviour of a double pendulum considering its mass and length is studied numerically. It is observed that chaotic tendency increases with mass and length. Moreover, top and bottom pendulum show varying effect on the chaos.

5. RFEERENCES

- A.Ohloff, P. H. Richter, Forces in the Double Pendulum, *ZAMM. Z. Angew. Math. Mech.*, 0, 1-22, 2006.
- L. Behera and I. Kar, *Intelligent Systems and Control*, Oxford university Press, 2009.
- G. Baker and J. Gollub, *Chaotic Dynamics*. Oxford University Press, Oxford, 1990.
- R. Nunna, Numerical Analysis of Dynamics of a Double Pendulum, 2009.
- http://www.math.dartmouth.edu/archive/m53f09/public_html/proj/Roja_writeup.pdf
- A.Wolf, J.Swift, H. Swinney and J.Vastano, Determining Lyapunov exponents from a time series, *Physica D*, 16, 285-317, 1985.
- K. Zaki, S. Noah, K. R. Rajagopal, and A. R. Srinivasa, Effect of Nonlinear Stiffness on the Motion of a Flexible Pendulum, *Nonlinear Dynamics* 27: 1-18, 2002.

Mass and Length Dependent Chaotic Behavior of a Double Pendulum

Mukul K. Gupta¹, Kamal Bansal², Arun K. Singh³

^{1,2}University of Petroleum and Energy Studies, Dehradun-248007, INDIA

³Visvasvaraya National Institute of Technology, Nagpur-440010, INDIA

¹ mukulvjti@gmail.com (Assistant Professor, Electrical Engineering, UPES Dehradun)

² kamalbansal@ddn.upes.ac.in (Professor, Electrical Engineering, UPES Dehradun)

³ aksinghb@gmail.com (Assistant Professor, Mechanical Engineering, VNIT Nagpur, corresponding author)

ABSTRACT: In this article, chaotic behavior of a double pendulum (DP) is studied numerically by varying its mass and length. The results are analyzed using time series plot, Poincare map and Lyapunov exponent plot. It is observed that the chaotic tendency of the DP increases with mass and length. However, both pendulums of the DP have varying effect on the Lyapunov exponent. The significance of the present study in the optimization and control of the dynamical systems based on the DP is also discussed.

Keywords: Chaos, Double Pendulum, Time series, Poincare Map, Lyapunov exponent

1. INTRODUCTION

A double pendulum (DP) is an interesting dynamical system since it shows chaotic motion (Baker and Gollub, 1990, Ohlhoff and Richter, 2006). Notably, experimental and numerical studies have been carried out of such a system considering the change in initial value of amplitude and angular velocity of the double pendulum (DP) (Baker and Gollub, 1990). It is observed that a DP shows periodic behaviour at low energy, transforms to quasi-periodicity at intermediate energy level and chaos at higher energy level finally again periodic motion as energy of the system increases further (Nunna, 2009). Despite significant study on the chaotic dynamics of the DP, there is no reported study in literature how the mass and length of a DP influences its chaotic behavior. Such a study is important from controlling and optimizing dynamical systems based on double pendulum for instance double arm robots (Behera and Kar, 2009). Chaos is a physical phenomenon in which a dynamical system shows random motion and the results depends on initial conditions (Baker and Gollub, 1990). Chaos is basically a manifestation of non-linearity in the dynamical system. However, all non-linear systems do not show chaotic behaviour. A condition for chaos is that the differential equations governing the dynamical system should contain non-linear terms. Moreover, it should be expressible in at least three or more phase variables (Baker and Gollub, 1990). Lyapunov exponent is generally used to characterize the chaos of a dynamical system. For instance, if the average value of Lyapunov exponent is negative then the system is non chaotic. However, if Lyapunov exponent positive, then it shows chaos. Linear stability analysis of the DP shows that its two natural frequencies depend on mass and length of

each pendulum in the system (Ohlhoff and Richter, 2006). Further it is to be noted that natural frequency of a pendulum also depends on the initial conditions of oscillation for instance amplitude.

Figure 1 presents the schematic sketch of double pendulum in a plane. Upper end of the top pendulum is pivoted to a fixed point while the lower end of the same is connect with the top end of the bottom pendulum. Mass and arm length of the both pendulum were changed in the numerical simulation in the present study. Moreover, mass of the each pendulum is concentrated at the end in the form of solid sphere and also arm of each pendulum is considered to be massless (Fig.1).

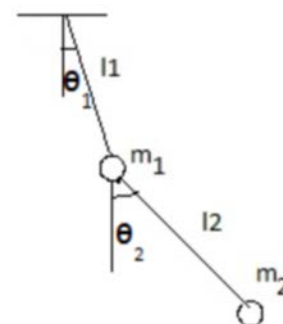


Figure 1: Schematic sketch of double pendulum under free oscillation.

Further $m_1, m_2, l_1, l_2, \theta_1$ and θ_2 are the mass, length and angular displacement of the top and bottom pendulum respectively.

2. MODELLING OF DOUBLE PENDULUM

A similar procedure is followed to derive the system of non-linear equation as reported in the reference (Nunna, 2009). Assuming the pivot point as the origin of the coordination system with the horizontal (x-axis) and the vertical (y-axis). The DP is assumed to be located in the fourth quadrant of the coordinate system. The coordinate position of top and bottom pendulum is given by

$$x_1 = l_1 \sin(\theta_1), y_1 = -l_1 \cos(\theta_1), x_2 = l_1 \sin(\theta_1) + l_2 \sin(\theta_2),$$

$$y_2 = -l_1 \cos(\theta_1) - l_2 \cos(\theta_2). \text{ And the corresponding angular velocity is given by the equations } \dot{x}_1 = l_1 \cos(\theta_1) \dot{\theta}_1$$

$$, \dot{y}_1 = l_1 \sin(\theta_1) \dot{\theta}_1, \dot{x}_2 = l_1 \cos(\theta_1) \dot{\theta}_1 + l_2 \cos(\theta_2) \dot{\theta}_2,$$

$$\dot{y}_2 = l_1 \sin(\theta_1) \dot{\theta}_1 + l_2 \sin(\theta_2) \dot{\theta}_2.$$

Kinetic energy of the double pendulum in Fig.1 is given by the following equation

$$K_2 = \frac{1}{2}(m_1 + m_2)l_1^2 \dot{\theta}_1^2 + \frac{1}{2}(m_2)l_2^2 \dot{\theta}_2^2 + m_2 l_1 l_2 \dot{\theta}_1 \dot{\theta}_2 \cos(\theta_1 - \theta_2) \quad (1)$$

And the potential energy is

$$V_2 = -(m_1 + m_2)gl_1 \cos \theta_1 - m_2 gl_2 \cos \theta_2 \quad (2)$$

The Lagrangian $L_2 = K_2 - V_2$ of two simply connected pendulums (Fig.1) is given by the following equation

$$L_2 = \frac{1}{2}(m_1 + m_2)l_1^2 \dot{\theta}_1^2 + \frac{1}{2}m_2 l_2^2 \dot{\theta}_2^2 + m_2 l_1 l_2 \dot{\theta}_1 \dot{\theta}_2 \cos(\theta_1 - \theta_2) + (m_1 + m_2)gl_1 \cos \theta_1 + m_2 gl_2 \cos \theta_2 \quad (3)$$

Further modifying the above equations:

$$(m_1 + m_2)l_1^2 \ddot{\theta}_1 + m_2 l_1 l_2 \ddot{\theta}_2 \cos(\theta_1 - \theta_2) + m_2 l_1 l_2 \dot{\theta}_2^2 \sin(\theta_1 - \theta_2) + (m_1 + m_2)gl_1 \sin \theta_1 = 0 \quad (4)$$

$$m_2 l_2^2 \ddot{\theta}_2 + m_2 l_1 l_2 \ddot{\theta}_1 \cos(\theta_1 - \theta_2) - m_2 l_1 l_2 \dot{\theta}_1^2 \sin(\theta_1 - \theta_2) + m_2 gl_2 \sin \theta_2 = 0 \quad (5)$$

Converting into non-dimensional form of above equations 4& 5.

$$\ddot{\theta}_1 + m_{2/12} l_{2/1} \ddot{\theta}_2 \cos(\theta_1 - \theta_2) + m_{2/12} l_{2/1} \dot{\theta}_2^2 \sin(\theta_1 - \theta_2) + gl_1^{-1} \sin(\theta_1) = 0 \quad (6)$$

$$\ddot{\theta}_2 + l_{1/2} \ddot{\theta}_1 \cos(\theta_1 - \theta_2) - l_{1/2} \dot{\theta}_1^2 \sin(\theta_1 - \theta_2) + gl_2^{-1} \sin(\theta_2) = 0 \quad (7)$$

Where $m_{2/12} = m_2 / (m_1 + m_2)$ and length of arm of the pendulum is $l_{2/1} = l_2 / l_1$ and $l_{1/2} = l_1 / l_2$. And the equation of momenta p_i of the DP is given by $p_i = \partial L_2 / \partial \dot{\theta}_i$ where $i = 1$ and 2

$$p_1 = (m_1 + m_2)l_1^2 \dot{\theta}_1 + m_2 l_1 l_2 \dot{\theta}_2 \cos(\theta_1 - \theta_2) \quad (8)$$

$$p_2 = m_2 l_2^2 \dot{\theta}_2 + m_2 l_1 l_2 \dot{\theta}_1 \cos(\theta_1 - \theta_2) \quad (9)$$

And the Hamiltonian $H_2 = K_2 + V_2$ of the DP is given by

$$H_2 = \frac{1}{2}(m_1 + m_2)l_1^2 \dot{\theta}_1^2 + \frac{1}{2}m_2 l_2^2 \dot{\theta}_2^2 + m_2 l_1 l_2 \dot{\theta}_1 \dot{\theta}_2 \cos(\theta_1 - \theta_2) - (m_1 + m_2)gl_1 \cos \theta_1 - m_2 gl_2 \cos \theta_2 \quad (10)$$

Above differential equations (6&7) were solved numerically in MATLAB using *ode45* by following the procedures similar to the given in the reference 1. All simulations were carried out for a fixed initial condition i.e., $(\theta_1, \theta_2, p_1, p_2) = (0.2, 0.2828, 0, 0)$. Time series of angular velocity of the two pendulum, Poincare map and the average value of Lyapunov exponent are plotted to understand the mass and length dependent chaotic behavior of the DP (wolf and Swift, 1985, Zaki and Noah 2002). Poincare map (section) i.e., $(\dot{\theta}_1, p_1)$ was generated for the top pendulum under the condition $\sin(\theta_2) = 0$ and $\dot{\theta}_2 > 0$ (Rosa Nunna, 2009). The results are discussed in next section.

3. RESULTS AND DISCUSSION

Fig.2 presents the plots concerning the time series (angular velocity), Poincare map and Lyapunov exponent for $m_1 = 1.0$ kg, $m_2 = 1.0$ kg, $l_1 = 1.0$ m and $l_2 = 1.0$ m and the Hamiltonian energy $E = -28.62$ J. It is obvious from the plot (a) in Fig.2 that angular velocity of both pendula is periodic and both are in phase. Moreover,

corresponding Poincare map is also regular as evident in plot (b) of the same Fig.2. Also the average Lyapunov exponent e is found to be $e = -0.1607$ which is negative. As mentioned earlier, dynamical system with negative exponent does not show the chaotic motion.

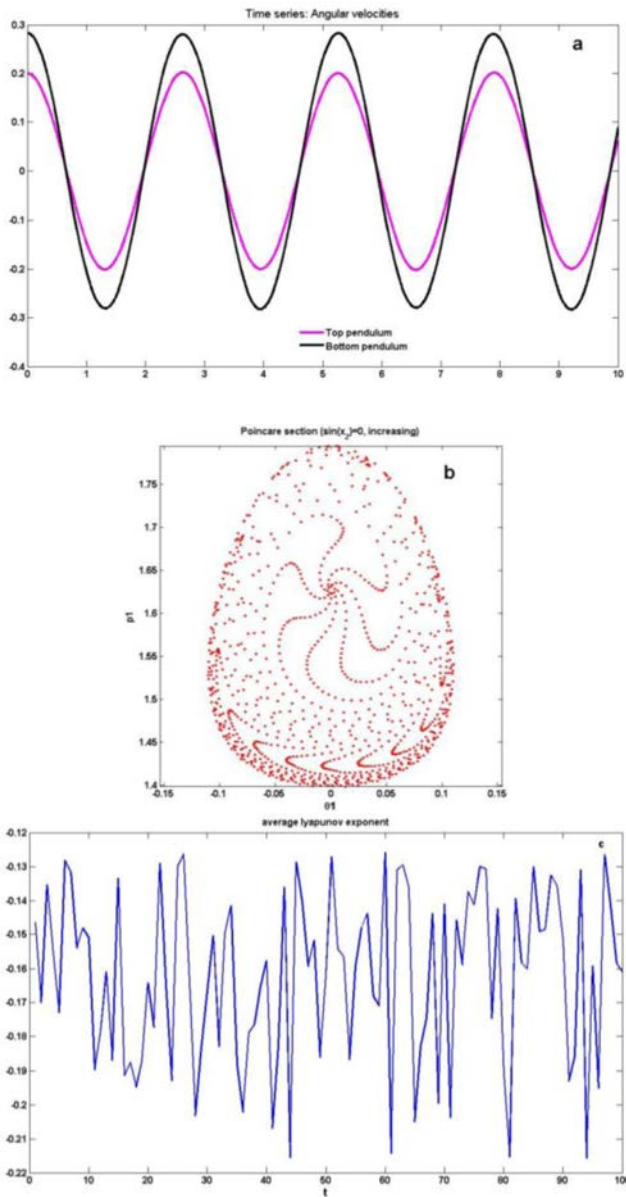


Fig.2 presents (a) Time series (b) Poincare map (c) Lyapunov exponent for $m_1 = 1, m_2 = 1, l_1 = 1$ and $l_2 = 1$, Hamiltonian $E = -28.62$.

It is now mass of the top pendulum is increased to $m_1 = 5$ while other parameters were considered the same as earlier. Now the energy corresponding to Hamiltonian increased to $E = -67.04$. Time series plot of angular velocity of the plot (a) of Fig.3 show that the motion is now quasi-periodic as there are two time period in the motion. And the corresponding Poincare map shows to be regular but with large area of null. The average Lyapunov

exponent $e = -0.1086$. This value of e is larger than in Fig.1. Thus it may be concluded that chaotic tendency of the DP increased with mass of the top pendulum.

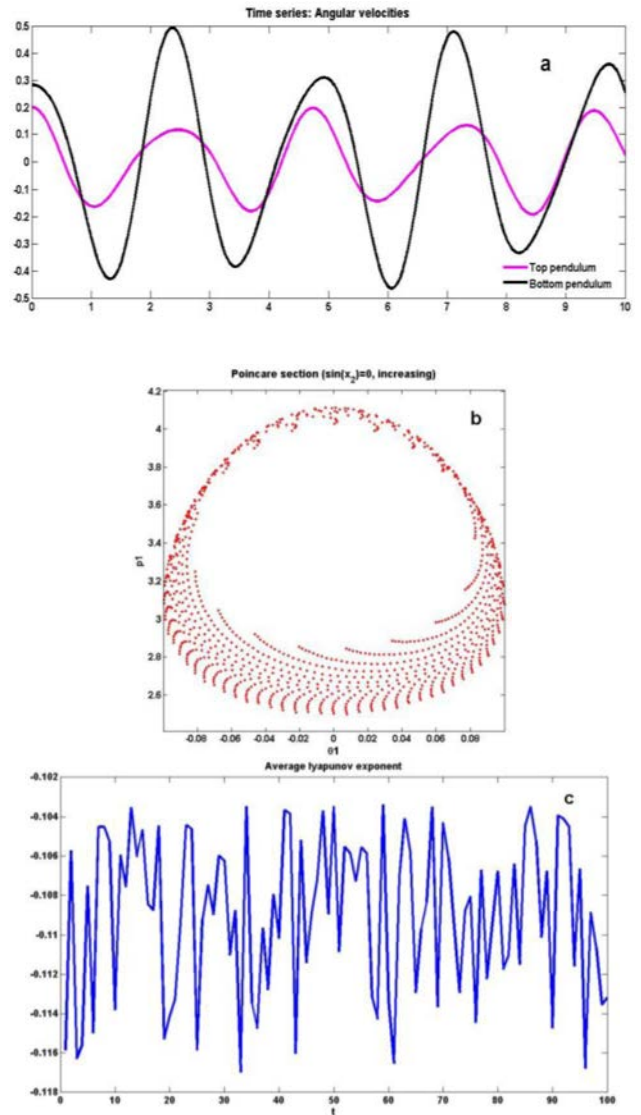


Fig.3 presents (a) Time series (b) Poincare map (c) Lyapunov exponent for $m_1 = 5, m_2 = 1, l_1 = 1$ and $l_2 = 1$, Hamiltonian $E = -67.04$.

Now in case of change in magnitude of the mass of the bottom pendulum i.e., $m_2 = 5$, the time series plot (a) in Fig.5 shows that the top pendulum is showing period oscillation while the bottom pendulum is random. The value of average Lyapunov exponent is $e = 0.0399$. As noted earlier that positive value of the average Lyapunov exponent results in chaotic oscillations. The chaotic behavior is also clear in plot (b) of Fig.4. It may be concluded that the bottom makes the DP more chaotic than the top pendulum.

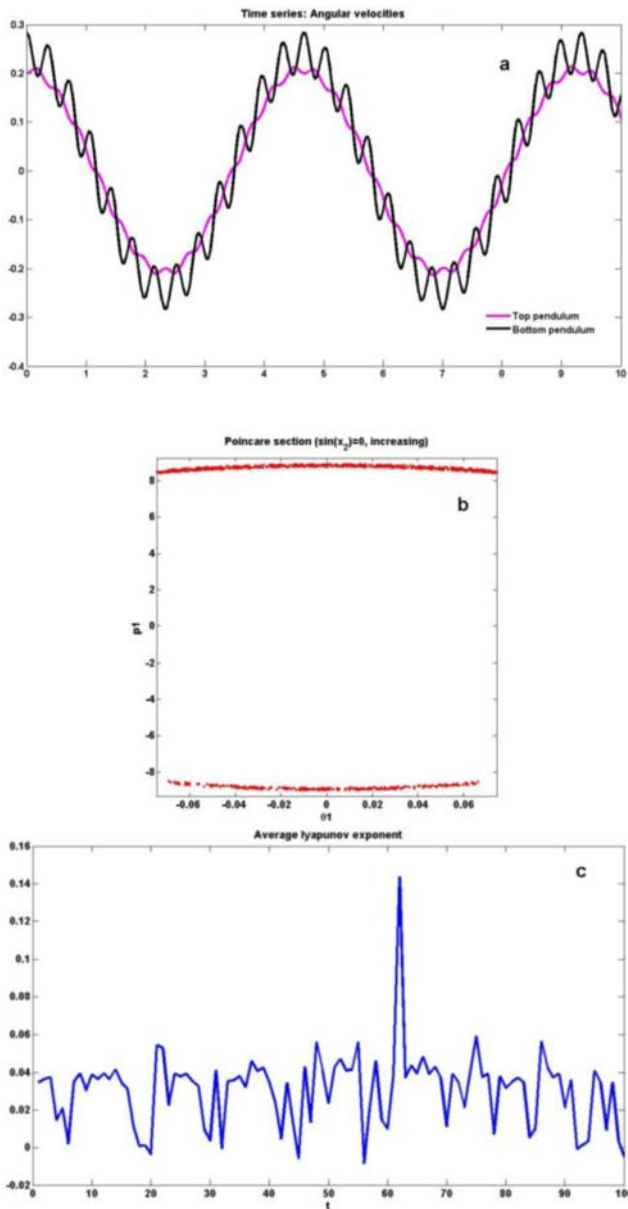


Fig.4 presents (a) Time series (b) Poincare map (c) Lyapunov exponent for $m_1 = 1, m_2 = 5, l_1 = 1$ and $l_2 = 1$ for Hamiltonian $E = -104.68$.

Motivated from the above study, it becomes interesting to know how arm length of pendula affects its chaotic dynamics. Length of the top pendulum was changed from $l_1 = 1$ to $l_1 = 3$. The result from the time series plot (a) in Fig.5 shows that the bottom pendulum is showing quasi-periodic oscillation while the top pendulum is still periodic. The value of average Lyapunov exponent is equal to -0.0991 . It is concluded that increasing arm length of the top pendulum results in quasiperiodic motion.

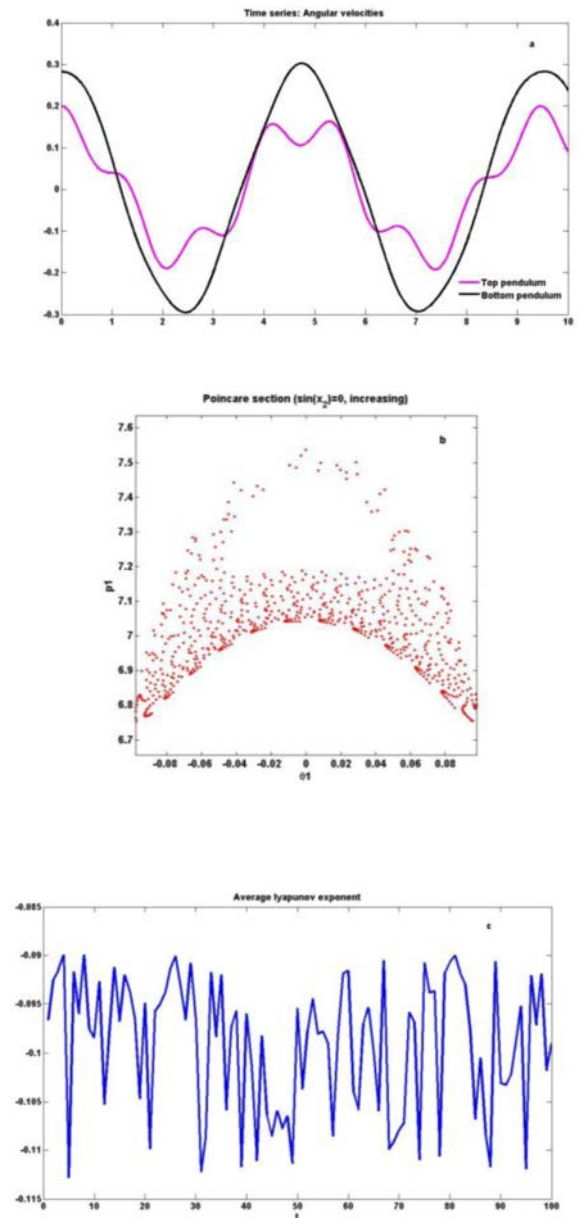


Fig.5 presents (a) Time series (b) Poincare map (c) Lyapunov exponent for $m_1 = 1, m_2 = 1, l_1 = 3$ and $l_2 = 1$, Hamiltonian $E = -67.04$.

Finally, arm length of the bottom pendulum was also changed in the simulation for $l_2 = 3$. The value of average Lyapunov exponent is $e = 0.0234$. The results in Fig.6 shows the DP is ultimately moving towards the chaos.

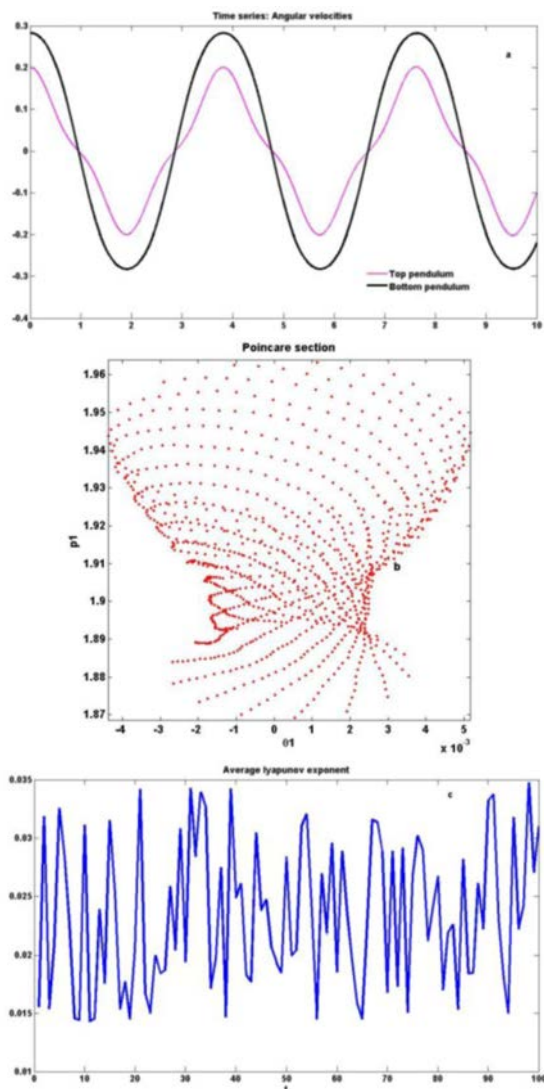


Fig.6 presents(a) Time series (b) Poincare map (c) Lyapunov exponent for $m_1 = 1, m_2 = 1, l_1 = 1$ and $l_2 = 3, E = -47.44 J$.

The summary of the above simulations is presented in the Table 1.

Table 1: Summary of the numerical simulations

Mass (Kg) and length (m) of each pendulum	Lyapunov exponent e and Hamiltonian energy E (Joule)	Chaotic/non-chaotic behavior
$m_1 = 1, m_2 = 1, l_1 = 1$ $l_2 = 1$	$e = -0.1607$ $E = -28.62 J$	Periodic
$m_1 = 5, m_2 = 1, l_1 = 1$ $l_2 = 1$	$e = -0.1086$ $E = -67.04 J$	Quasi-periodic

$m_1 = 1, m_2 = 5, l_1 = 1$ $l_2 = 1$	$e = 0.0399$ $E = -104.68 J$	Chaos
$m_1 = 1, m_2 = 1, l_1 = 3$ $l_2 = 1$	$e = -0.0991$ $E = -67.04 J$	Quasi-periodic
$m_1 = 1, m_2 = 1, l_1 = 1$ $l_2 = 3$	$e = 0.0234$ $E = -47.44 J$	Chaos

From the Table 1, it may be concluded that mass and length of the two pendulum have varying degree of effect on the average value of Lyapunov exponent. Thus there is an optimal combination of mass and arm length of the DP at which chaotic tendency of the system will be minimum. However further numerical and experimental studies are needed on this issue.

4. CONCLUSION

The chaotic behaviour of a double pendulum considering its mass and length is studied numerically. It is observed that chaotic tendency increases with mass and length. Moreover, top and bottom pendulum show varying effect on the chaos.

5. RFEERENCES

- A.Ohloff, P. H. Richter, Forces in the Double Pendulum, *ZAMM. Z. Angew. Math. Mech.*, 0, 1-22, 2006.
- L. Behera and I. Kar, *Intelligent Systems and Control*, Oxford university Press, 2009.
- G. Baker and J. Gollub, *Chaotic Dynamics*. Oxford University Press, Oxford, 1990.
- R. Nunna, Numerical Analysis of Dynamics of a Double Pendulum, 2009.
- http://www.math.dartmouth.edu/archive/m53f09/public_html/proj/Roja_writeup.pdf
- A.Wolf, J.Swift, H. Swinney and J.Vastano, Determining Lyapunov exponents from a time series, *Physica D*, 16, 285-317, 1985.
- K. Zaki, S. Noah, K. R. Rajagopal, and A. R. Srinivasa, Effect of Nonlinear Stiffness on the Motion of a Flexible Pendulum, *Nonlinear Dynamics* 27: 1-18, 2002.

Simulation of an Industrial FCC Riser Reactor using a Novel 10-Lump Kinetic Model and Some Parametric Sensitivity Studies

Prabha Kiran Dasila, Indranil R. Choudhury, Sanjeev Singh,
Santanam Rajagopal, Sawaran J Chopra, and Deoki N. Saraf

Ind. Eng. Chem. Res., **Just Accepted Manuscript** • DOI: 10.1021/ie5006433 • Publication Date (Web): 25 Aug 2014

Downloaded from <http://pubs.acs.org> on August 31, 2014

Just Accepted

“Just Accepted” manuscripts have been peer-reviewed and accepted for publication. They are posted online prior to technical editing, formatting for publication and author proofing. The American Chemical Society provides “Just Accepted” as a free service to the research community to expedite the dissemination of scientific material as soon as possible after acceptance. “Just Accepted” manuscripts appear in full in PDF format accompanied by an HTML abstract. “Just Accepted” manuscripts have been fully peer reviewed, but should not be considered the official version of record. They are accessible to all readers and citable by the Digital Object Identifier (DOI®). “Just Accepted” is an optional service offered to authors. Therefore, the “Just Accepted” Web site may not include all articles that will be published in the journal. After a manuscript is technically edited and formatted, it will be removed from the “Just Accepted” Web site and published as an ASAP article. Note that technical editing may introduce minor changes to the manuscript text and/or graphics which could affect content, and all legal disclaimers and ethical guidelines that apply to the journal pertain. ACS cannot be held responsible for errors or consequences arising from the use of information contained in these “Just Accepted” manuscripts.

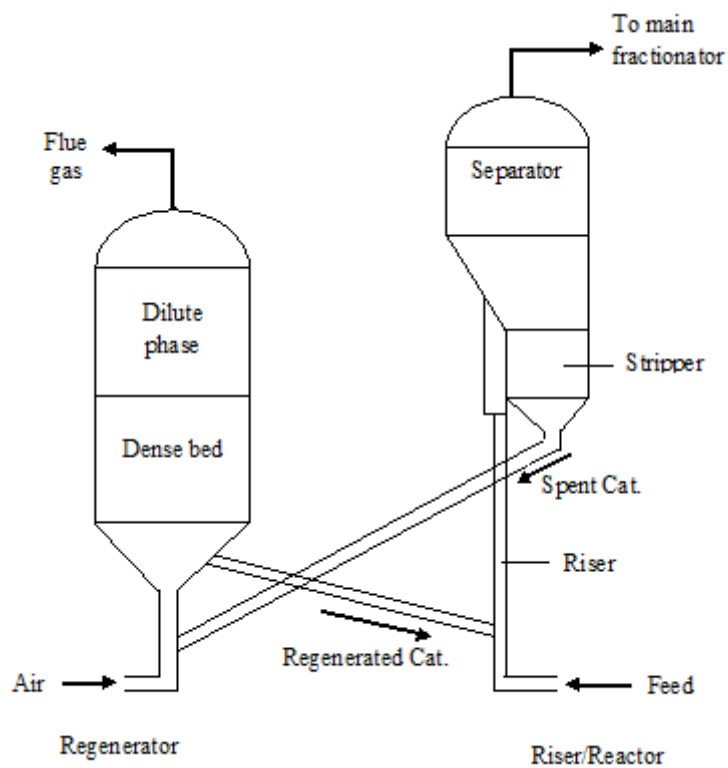
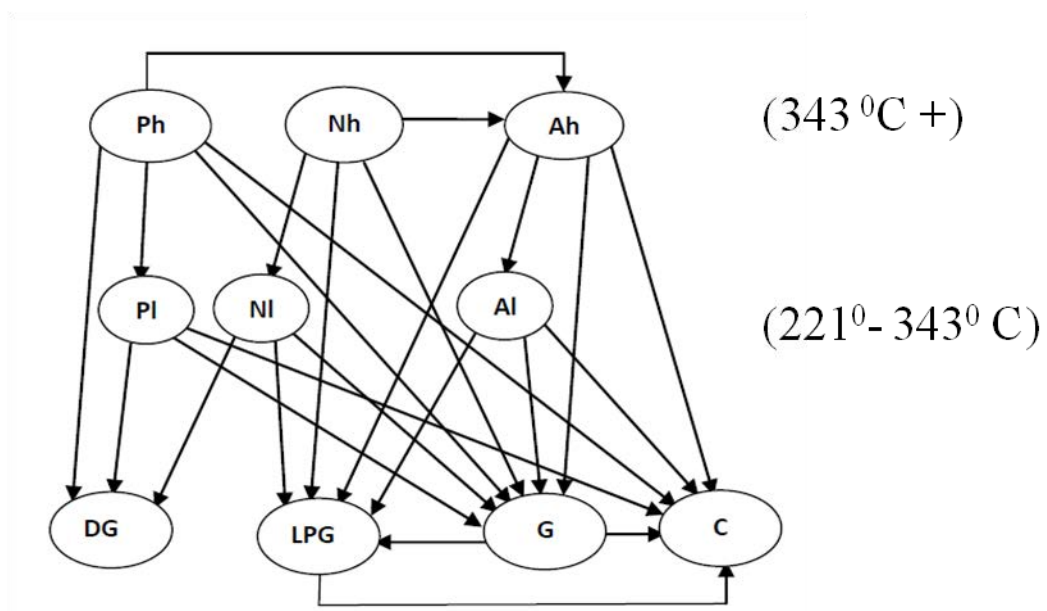


Figure 1



24
25
26
27
28
29
30
31
32
33
34
35
36
37
38
39
40
41
42
43
44
45
46
47
48
49
50
51
52
53
54
55
56
57
58
59
60

Figure 2

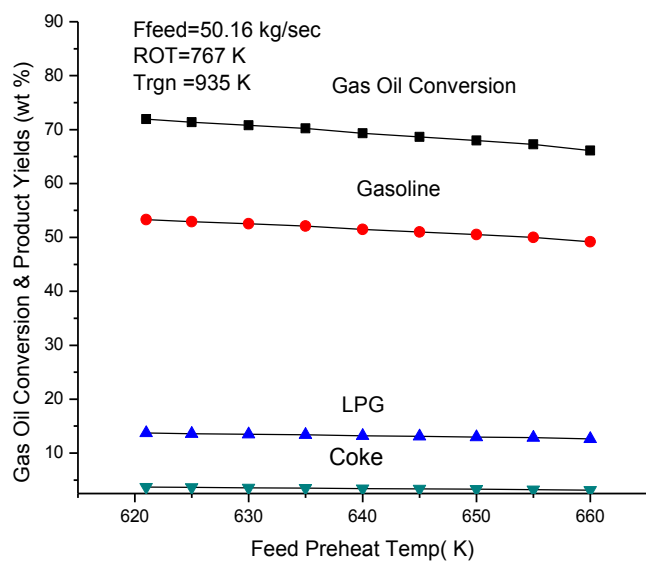
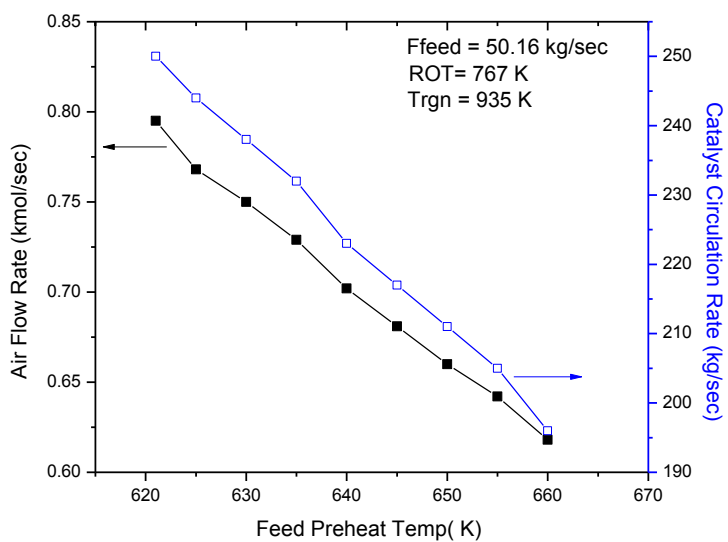
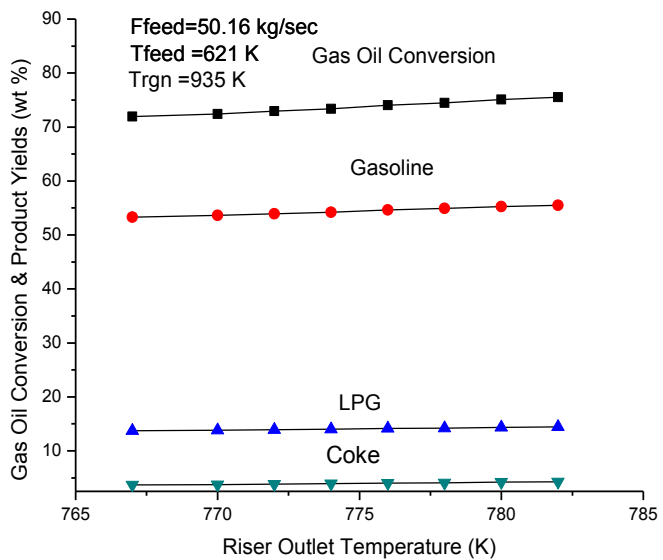
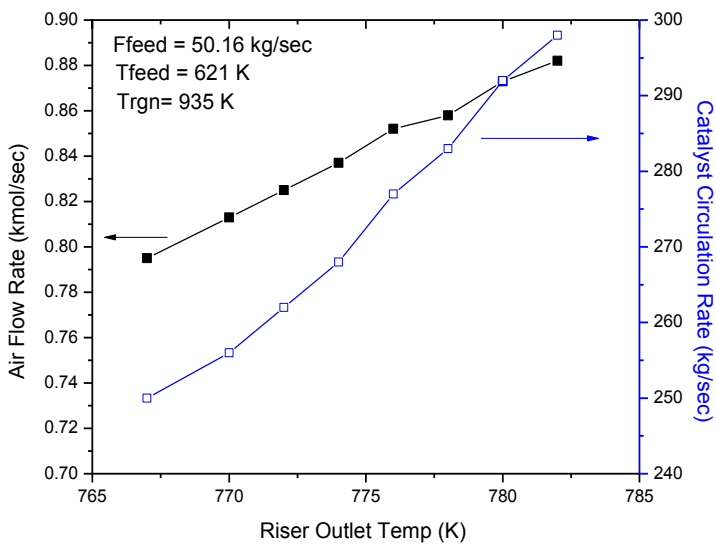


Figure 3

**Figure 4**

**Figure 5**

**Figure 6**

1
2
3
4
5
6
7
8
9
10
11
12
13
14
15
16
17
18
19
20
21
22
23
24
25
26
27
28
29
30
31
32
33
34
35
36
37
38
39
40
41
42
43
44
45
46
47
48
49
50
51
52
53

Simulation of an Industrial FCC Riser Reactor using a Novel 10- Lump Kinetic Model and Some Parametric Sensitivity Studies

Prabha K. Dasila,^{*, †, §} Indranil R. Choudhury,[§] Sanjeev Singh,[§] Santanam Rajagopal,[§]
Sawaran J. Chopra[†] and Deoki N. Saraf[†]

[†] University of Petroleum & Energy Studies, Dehradun- 248007, India

[§] Indian Oil Corporation Ltd, Research & Development Centre Faridabad-121007, India

*Corresponding Author. Tel.: +91-28840-12312. Fax: +91-28840-26329.

E-mail: dasila.prabha@gmail.com

Abstract

A FCC unit has been simulated by integrating FCC riser reactor and regenerator models. This simulation uses a new 10-lump riser reactor kinetic model developed in-house. The lumping scheme and reactions are based on more detailed description of the feed in terms of PNA (paraffins, naphthenes and aromatics) in both light and heavy fractions. An Artificial Neural Network (ANN) model, also developed in-house, relates routinely measured properties such as specific gravity, ASTM temperatures etc. to the detailed feed composition needed for the kinetic model development. The conversion and product yields obtained by integrating the model equations were found to be in close agreement with those measured in the plant in all the cases investigated. Simulation results using the present model, when compared with results from a conventional 5 lump model, clearly brought out the improvement in prediction because of detailed feed description calculated from ANN models. A parametric sensitivity study was undertaken in respect of operating conditions such as effects of feed preheat temperature, feed flow rate, and reactor outlet temperature (independent variables) on the performance of the FCC unit and the results have been discussed.

Keywords: FCC Unit, FCC Feed Compositions, Ten Lump Model, Parametric Sensitivity, Riser Reactor Model, Artificial Neural Networks, Plant Simulation.

1. Introduction

Fluid Catalytic Cracking (FCC) is an important secondary process, converting low-priced heavy feed stocks like heavy oil from either the refinery crude unit or vacuum unit and heavy fractions from other conversion units (cooker gas oil and hydrocracker fractionator bottoms etc.) into lighter, more valuable hydrocarbons such as liquefied petroleum gas (LPG) and gasoline thus increases the profitability of the entire refinery. Coke is formed as a byproduct during the process along with dry gas, both of which are undesirable. The conversion and yield pattern strongly depend on the feedstock quality, operating conditions of the riser reactor-regenerator sections and the type of catalyst.

The FCC process is very complex due to complicated hydrodynamics, heat transfer and mass transfer effects and complex cracking kinetics. These complex interactions coupled with economic importance of the unit have prompted many researchers to put their efforts on the modelling of FCC processes. Additionally, a small improvement in the operation or control of an FCC unit can result in impressive economic benefits. However, these can be achieved only if a satisfactory mathematical model is available which is analytical so that its optimization can lead to optimal operating conditions. Modeling is an iterative process and leads to deeper understanding of the physics involved, which can be used for designing better control of the process unit. Process optimization, can lead to improved productivity by maximizing throughput and choosing optimal operating conditions. Online optimization can help maximize long-term profits by reducing the cost and improving yields. Additionally, running a model simultaneously in parallel with the plant operation can help in monitoring the plant and its health.

There are several modeling approaches for FCCU available in the literature.¹⁻¹⁴ The kinetic lumping approach has been most widely used in which the large number of feed and the

1
2
3 products hydrocarbons are lumped into a few groups, called kinetic lumps, which are assumed to
4 take part in the reactions as single entities. A number of kinetic models have been developed by
5 various researchers using 2, 3, 4, 5, 6, 8, 10 or 12 lumps but because of the complexities involved, a
6 completely satisfactory model has eluded each one so far. The FCC kinetic modeling is based on a
7 specified number of lumps for feedstock and products rather than on individual molecules. These
8 lumps are considered either on the basis of boiling range of the feedstock and corresponding products
9 in the reaction system or based on type of hydrocarbon groups.¹⁰ Each type of hydrocarbons is
10 assumed as one lump and the products are considered by different lumps according to their boiling
11 range. In the often used, feed specific 5-lump model, the feed is represented by a single lump of
12 average carbon number and molecular weight and gasoline, LPG, dry gas and coke, present in
13 the product stream along with unconverted feed are the remaining lumps.⁵⁻⁹ The limitation of
14 models using single lump feed description is that the kinetics is valid only for the particular
15 vacuum gas oil (VGO) with which the model parameters were estimated and is generally not
16 applicable to other feeds especially if the composition is significantly different. The available ten
17 and twelve lump models are more accurate where the feed is described in terms of 6 or 8 kinetic
18 lumps consisting the heavy and light fractions of paraffins, naphthenes and aromatics¹⁰⁻¹⁵ but
19 these detailed kinetic models suffer from the requirement of detailed feed composition analysis
20 which is seldom possible in a field laboratory.

21
22
23
24
25
26
27
28
29
30
31
32
33
34
35
36
37
38
39
40
41
42
43
44
45
46 In the present work, a simulator embedding a 10 lump kinetic model of the riser reactor
47 developed our earlier work¹⁵, was integrated with regenerator model to simulate the FCC process.
48 The product yields were obtained by integrating the model equations along the length of the reactor.
49 The detailed feed composition in terms of heavier and lighter fractions of P, N and A required as
50 input to the kinetic model was obtained from a validated ANN model.¹⁶ The neural network model
51
52
53
54
55
56
57
58
59
60

1
2
3 used routinely measured feed properties in field laboratories such as specific gravity, ASTM
4
5 temperatures etc as input.
6
7

8 Parametric sensitivity studies can provide valuable information to the plant operator
9
10 where operator learns the effect of variations in the independent operating variables on the plant
11 performance. The effect of variation in three independent variables, feed flow rate, feed
12 temperature and reactor outlet temperature on conversion and product yields have been
13 investigated. Finally a comparison has been made between the performances of simulator with
14
15 10- lump and 5-lump kinetics.
16
17
18
19
20
21

22 **2. Description of FCC Process**

23

24 FCC units operate at high temperature and moderate pressure with finely divided
25 silica/alumina based catalyst. One of the important advantages of FCC is the ability of the
26 catalyst to flow easily when fluidized with reaction mixture in vapor phase. Due to this
27 fluidization of the catalyst, there is intimate interaction between the catalyst and hydrocarbons
28 leading to more cracking reactions.
29
30
31
32
33
34
35

36 The main components of FCCU are riser reactor and regenerator as shown in Figure 1. A
37 partially vaporized HGO/VGO charge meets a stream of regenerated hot catalyst at the base of
38 the riser. The liquid droplets of the feed receive heat from the hot catalyst particles and almost
39 instantaneously vaporize. As the vapors and catalyst particles move up the riser, the cracking
40 reactions take place. Carbon generated during cracking reactions gets deposited on the catalyst
41 surface and cracking activity progressively decreases. At the exit of the reactor, catalyst is
42 separated from the reaction mass, adsorbed hydrocarbons stripped off in a stripper with the help
43 of steam and the spent catalyst sent to regenerator. In the regenerator, the catalyst is continuously
44 regenerated by burning off the coke deposited during the cracking reaction. Other auxiliary units
45
46
47
48
49
50
51
52
53
54
55
56
57
58
59
60

1
2
3 such as feed preheat, air and flue gas systems are required for operation of the unit but have not
4
5 been included in the modeling exercise
6
7

8 **3. Modeling of Fluid Catalytic Cracking Unit**

9

10 In the present work, a ten lump kinetic model, developed in-house, was integrated with a
11 regenerator model for the simulation of the entire FCC unit. The steam stripper was assumed to
12 be ideal and hence its modeling was not included.
13
14
15

16 **3.1 Riser / Reactor Model**

17

18 A 10-lump kinetic description for riser reactor reported in our previous work¹⁵ has been
19 used for the present study. A total of 25 cracking reactions have been accounted for and the
20 reaction scheme is shown in Figure 2. The detailed lumping scheme uses 6 lumps to describe the
21 feed gas oil, namely; heavy paraffins, heavy naphthenes, heavy aromatics, light paraffins, light
22 naphthenes and light aromatics. This means we need the compositions in terms of these lumps
23 for every new feed used. To circumvent the problem of having to measure detailed composition
24 which is not very practical in field laboratories, an artificial neural network (ANN) - based model
25 was developed which provided the requisite composition as output, input being routinely
26 measured properties of VGO such as specific gravity, ASTM distillation temperatures,
27 Conradson carbon residue (CCR), total sulfur and total nitrogen.¹⁶ The detailed PNA analysis of
28 the several VGO samples for ANN model development were measured in the laboratory by using
29 high-resolution mass-spectrometric method.¹⁶
30
31
32
33
34
35
36
37
38
39
40
41
42
43
44
45
46
47

48 The complete set of model equations for the riser reactor and stripper are given in
49 Appendix A. The following assumptions from literature¹⁰⁻¹⁴ were made to develop the kinetic
50 model of the riser reactor: All cracking reactions are first order; reaction mass consists of only
51 two phases (solid and vapor phases); heat capacities and densities are constant throughout the
52
53
54
55
56
57
58
59
60

1
2
3 length of the reactor; catalyst deactivation is non-selective and related to coke on catalyst^{17,18}
4
5 only; the solid catalyst particles are in thermal equilibrium with the gaseous mixture at all times;
6
7 the flow is uniform, that is, there is no slip between solid catalyst and vapors; LPG and gasoline
8
9 do not crack to produce dry gas and dry gas produces no coke.
10
11

12 The aim of stripper is to remove residual hydrocarbons from catalyst surface after
13 cracking reactions. Being a minor unit, no effort was made to rigorously model this unit. The
14 spent catalyst temperature and flow rate were calculated from the model equations available in
15 Appendix A. A temperature drop of 10K was assumed across the stripper unit.^{5, 8}
16
17
18
19
20
21

22 **3.2 Regenerator Model**

23

24 An FCC regenerator usually consists of a large fluidized bed reactor with coke
25 combustion kinetics and complex hydrodynamics. The deposited coke on catalyst surface during
26 the cracking reactions in the riser is burned off in the regenerator in presence of air. These coke
27 combustion reactions taking place in the regenerator are strongly exothermic. There are usually
28 two regions in the regenerator: the dense phase and the dilute phase (freeboard). The dilute phase
29 is the region above the dense phase up to the cyclone inlet, and has a substantially lower catalyst
30 concentration. The dense bed has all the catalyst contained below the established bed level,
31 where, almost all reactions occur. The larger catalyst particles are separated from the gas in the
32 dilute phase and fall back to the bed. Any catalyst particles that do not separate in the dilute
33 phase enter into the regenerator cyclones. Catalyst entering the cyclones is separated by
34 centrifugal force with the larger particles being returned to the bed via the cyclone diplegs.
35 Catalyst fines too small to be separated by the cyclones are carried out of the regenerator with
36 the flue gas.
37
38
39
40
41
42
43
44
45
46
47
48
49
50
51
52
53
54
55
56
57
58
59
60

1
2
3 The regenerator has two main functions: it restores catalyst activity and supplies the
4 endothermic heat required to crack the feed in the riser. In the combustion reaction, the carbon
5 on spent catalyst can be converted to either CO or CO₂ and the hydrogen in the coke is
6 converted into steam. CO oxidation may take the form of either homogeneous oxidation in the
7 gas phase or heterogeneous oxidation in the presence of oxidation promoters.^{12, 19-23}

8
9
10
11
12
13
14
15 The entire mathematical model for the regenerator, developed by Arbel et al¹³ was
16 adopted for the carbon balance, flue gas composition and heat balance for the regenerator dense
17 and dilute beds except the model for calculating dense bed height.²¹ All these model equations
18 for regenerator are given in Appendix B.

24 3.3 Simulation of FCC Unit

25
26
27 A simulator has been developed where the coupled riser reactor and regenerator model
28 equations have been assembled along with solution procedures. These have been computer coded
29 using C programming language and available with the first author. The ordinary differential
30 equations and nonlinear algebraic equations for material and energy balance are solved by using
31 Runge Kutta fourth order integration scheme and Successive Substitution methods respectively.
32
33
34
35
36
37
38
39
40
41
42
43
44
45
46
47
48
49
50
51
52
53
54
55
56
57
58
59
60
Tables 1 to 3 provide data on feed composition, operating data, design data and thermodynamic
and other data, which were used for the present simulation studies. The values of kinetic
parameters for the regenerator simulation were used from literature.^{5, 13}

The solution of the model equations starts with initially guessed values of regenerated
catalyst temperature ($T_{\text{rgn}} = 900\text{K}$) and coke on regenerated catalyst ($C_{\text{rgc}} = 0.0025$), the product
yields are, then, calculated at the outlet of the reactor. Subsequently the temperature of spent
catalyst and coke on spent catalyst are calculated. The regenerator simulation followed by dense
bed calculations provide the new values of catalyst temperature (T_{cal}) and coke on regenerated

1
2
3 catalyst (C_{cal}) which are compared with the initial value of T_{rgn} and C_{rgc} . If T_{cal} and C_{cal} do not
4
5 match with assumed T_{rgn} and C_{rgc} then one needs to start the reactor calculation with newly
6
7 calculated values of T_{rgn} and C_{rgc} by using the successive substitution method. Finally all the
8
9 reactor and regenerator equations are solved with converged value of T_{rgn} and C_{rgc} . The
10
11 tolerance for the convergence of T_{rgn} and C_{rgc} used are $1\text{ }^{\circ}\text{C}$ and 10^{-4} kg of coke/kg of catalyst
12
13 respectively. The computational time required for simulation of FCC unit was 1.5 to 2 min with
14
15 the ~10000 iterations for successive substitution.
16
17
18

19 20 **3.4 Validation of FCC Model with Plant Data**

21
22 Several sets of test run data and one set of normal operating data were obtained from an
23
24 operating FCC plant in a refinery for validation of the developed simulator. A commercial
25
26 ASPEN FCC simulator²⁴ was also tuned for the plant data by adjusting non-default parameters
27
28 such as stripping efficiency (95%), fraction of non-vaporized feed to coke (0.04), fraction of
29
30 Concarbon to coke (0.48) and mass ratio of H₂ to metals coke (0.12) etc. The performance of the
31
32 model has been evaluated by comparing the model predicted values of conversion and yields
33
34 with the plant data as well as calculated values from ASPEN FCC simulator²⁴ at the riser outlet
35
36 for four different cases. The feeds for all the cases were mixtures of different heavy gas oils from
37
38 different crude mixes resulting in a wide variation in composition.
39
40
41
42

43 **Case I**

44
45
46 The ten lump model predicted yields were compared with the first set of refinery plant
47
48 data and the results were found to be in good agreement as shown in Table 4. Also included in
49
50 this table are results obtained from ASPEN FCC simulator for the same operating data. The
51
52 percent deviation between the plant and the present model as well as the plant and ASPEN FCC
53
54 were calculated. The deviation between the plant and the present model shows the heavy and
55
56
57
58
59
60

1
2
3 light fractions deviated about 5 percent whereas the other four products namely, Gasoline, LPG,
4
5 Dry Gas and Coke showed a maximum deviation of 7 percent. Similar deviations are seen for the
6
7 ASPEN FCC predictions except with smaller magnitude.
8
9

10 **Case II**

11
12 The model was again validated with second test run data from the same FCC unit but
13
14 with different feed composition and different operating conditions. Table 4 also shows similar
15
16 comparisons between the plant measured, ASPEN calculated and the present model calculated
17
18 values for case II. The comparison shows a good match between the present model and plant test
19
20 run with deviations less than 4.5 % except for the LPG yield (10.9 %). The performance of the
21
22 ASPEN FCC Simulator shows higher deviations from plant data deviating by as much as 16.7%.
23
24
25
26

27 **Case III**

28
29 A new set of daily operating data from the plant was used to simulate the model. The
30
31 results on yields and reactor outlet temperature from plant, ASPEN FCC model and the present
32
33 model are shown in Table 5. This case also shows a good match between the present model and
34
35 plant value for all the components except dry gas. Dry gas content being small (~1.6 %), its
36
37 measured value is likely to be uncertain to a larger extent because of measurement errors. It may
38
39 be noted that for this case, the ASPEN FCC model performance is quite inferior as compared to
40
41 the present model.
42
43
44
45

46 **Case IV**

47
48 The model was finally simulated with yet another set of plant data to facilitate wider
49
50 comparison between the model calculated values and the plant data and the results are also
51
52 shown in Table 5. The matches were found to be in the range of acceptable limits.
53
54
55
56
57
58
59
60

1
2
3 From above study with four different sets of real plant data obtained with different feed
4 compositions it can be seen that the present model represents the FCC riser reactor reasonably
5 well. The predictions from the present model are as good as those from ASPEN FCC simulator
6 and at times, even better.
7
8
9
10
11

12 **4. Five -Lump Kinetic Model**

13
14
15 The literature available five lump kinetic model^{5,7} was reconstructed by determining the new
16 rate constants. It uses only one lump to characterize the feed and hence does not require any ANN
17 prediction. An average molecular weight and an average molecular formula of the type, C_nH_m are
18 assigned to the feed lump which describes the feed. The data that were regressed to obtained
19 kinetic parameters for the 10 - lump model were reused to calculate kinetic parameters for the 5-
20 lump model to facilitate comparison between the two models. All the model equations for the
21 five lump kinetic model of FCC riser reactor were adopted from literature⁵ and also available in
22 Appendix A and recalculated kinetic parameters are given in Table 6. The kinetic parameters
23 were determined for all the 9 reaction involved in 5- lump kinetic scheme. The same
24 optimization technique, Genetic Algorithm²⁵ (GA) was used to calculate the kinetic parameters
25 as done in case of 10 lump model. The algorithm available in MATLAB Optimization Toolbox
26 was used in the present study.
27
28
29
30
31
32
33
34
35
36
37
38
39
40
41
42

43 **4.1 Comparison of Ten Lump FCC Kinetic Model with Five Lump Kinetic Model**

44
45 Finally, the results from 5 lump kinetic model were compared with those from 10 lump
46 model to establish the following: 1. single lump feed description leads to feed specific rate
47 constants not valid for other feeds. 2. more detailed feed description results in superior prediction
48 capability of the model for a variety of feeds.
49
50
51
52
53
54
55
56
57
58
59
60

1
2
3 Tables 7 shows comparison of model calculated values using both 10- lump and 5-lump
4 kinetics and plant measured experimental values. The five lump model was simulated with the
5 literature values^{6,7} of rate constants and also using tuned values of rate constants as given in Table 6.
6
7 While maximum deviation in unconverted gas oil was only 1.9 % for 10- lump model, it was as high
8 as one hundred percent for the 5 - lump model when literature value of kinetic parameters were used.
9
10 The calculated values of products also showed large deviations. These deviations were significantly
11 reduced for 5-lump model when tuned values of rate constants were used instead of literature values.
12
13 However, these deviations still considerable more than those obtained with 10-lump model. This
14 clearly brings out the strong dependence of rate constants on feed composition and hence inadequacy
15 of single lump description of FCC feed. The fact that predictions made with 10- lump kinetic
16 description were superior to those using 5-lump model even after tuning, vindicates the validity of
17 the detailed description of the feed used here.
18
19
20
21
22
23
24
25
26
27
28
29
30

31 **5. Parametric Sensitivity Study for Ten Lump Model With Respect to Operating** 32 **Conditions** 33 34 35

36 It will be interesting to use the above described FCC simulator to carry out some
37 optimization studies which could be off-line or on-line. A typical off-line optimization exercise
38 aims to find operating conditions which optimize an economic or technical objective function
39 subject to all the model equations and practical bounds on operating conditions as constraints.
40
41 Online optimization, on the other hand, is a supervisory level control function which may seek to
42 optimize profit over long time by updating regulatory controller set points from time to time.²⁶
43
44 All this requires economic and other data which most refineries do not like to share with
45 outsiders. However, plant personnel can use the present simulator for optimization of their FCC
46 units as long as they are processing heavy gas oil as feed. In absence of requisite economic data,
47
48
49
50
51
52
53
54
55
56
57
58
59
60

1
2
3 we have carried out parametric sensitivity studies with respect to operating conditions, which
4 may be looked upon as a substitute for off-line optimization since it provides the effect of change
5 in each operating condition on the performance of the FCC unit. The feed preheat temperature
6 (T_{feed}), feed flow rate (F_{feed}) and reactor outlet temperature (ROT) are the independent input
7 parameters which were found to influence the FCC operation most. These independent variables
8 were varied one at a time, keeping the other two constant at their base values and their effect on
9 steady regenerator temperature (T_{rgn}), air flow rate (F_{air}) into the regenerator for coke combustion
10 and catalyst circulation rate (CCR) through the riser reactor. Out of these three, two were
11 allowed to vary to keep two of the independent variables constant and the third dependent
12 variable, T_{rgn} or F_{air} was held constant. Catalyst circulation rate was always allowed to be
13 manipulated due to practical considerations. Another dependent variable which is important is
14 coke on regenerated catalyst (C_{rgc}) but one always wishes to keep it constant at a low value, since
15 increase in C_{rgc} adversely affects conversion.
16
17
18
19
20
21
22
23
24
25
26
27
28
29
30
31
32
33

34 **5.1 Effect of Variation in T_{feed} Keeping F_{feed} and ROT Constant at Base Value**

35
36 Two variants were investigated, keeping T_{rgn} constant at one time and F_{air} constant at
37 another time. At constant regenerator temperature, as feed preheat temperature is increased,
38 catalyst circulation rate must decrease to keep ROT constant. At constant feed rate, decrease in
39 CCR leads to decrease in conversion as well as product yields as shown in Figure 3. The slopes
40 in this figure are gentler and perhaps more accurate than those reported earlier⁸ obtained with
41 five lump model. Figure 4 shows variation in air flow rate and catalyst circulation rate as T_{feed}
42 increases. As seen in this figure, both F_{air} and CCR decrease continuously and almost linearly but
43 with different slopes. On the other hand, when F_{air} is held constant and T_{rgn} is varied then while
44 conversion and product yields have the same decreasing trend as seen in Figure 3 but unlike F_{air} ,
45
46
47
48
49
50
51
52
53
54
55
56
57
58
59
60

1
2
3 T_{rgn} increases and CCR decreases with increase in feed temperature. The plots for this case have
4
5
6 been omitted for brevity.

8 **5.2 Effect of Variation in ROT Keeping T_{feed} and F_{feed} Constant at Base Value**

9
10 As the reactor outlet temperature is increased, the gas oil conversion and product yields
11
12 increase at constant F_{feed} , T_{feed} and T_{rgn} (see Figure 5). This is due to increase in catalyst
13
14 circulation rate which leads to more cracking and hence higher yields. Both air flow rate and
15
16 catalyst circulation rate increase with increase in ROT at constant T_{rgn} as shown in Figure 6. At
17
18 higher conversion, coke on catalyst increases and to burn this extra coke, air flow rate has to
19
20 increase. Constant T_{rgn} keeps coke on regenerated catalyst, C_{rgc} , constant. When air flow rate, F_{air}
21
22 is held constant at its base value, regenerator temperature reduces because of less residence time
23
24 for coke combustion in the regenerator due to increase in CCR. Decrease in T_{rgn} may lead to
25
26 increase in C_{rgc} which is undesirable. However, the effect of increasing catalyst circulation rate is
27
28 more dominant than the increased value of coke on regenerated catalyst (C_{rgc}) when ROT is
29
30 increased leading to higher conversion and product yields similar to those seen in Figure 5.
31
32
33
34
35

36 **5.3 Effect of Variation in F_{feed} Keeping T_{feed} and ROT Constant at the Base Value**

37
38 Here again two cases were examined, in one case, T_{rgn} was held constant and in the other
39
40 case, F_{air} was fixed. When feed rate increases with the regenerator temperature, T_{rgn} held
41
42 constant, the gas oil conversion as well as product yields marginally decrease similar to that
43
44 shown in Figure 3. On the regenerator side the air flow rate increases with increased value of
45
46 feed rate to keep the T_{rgn} constant which keeps the C_{rgc} constant. The catalyst circulation rate also
47
48 increases but slowly. At constant air flow rate, the catalyst circulation rate must increase to keep
49
50 ROT constant. However, regenerator temperature decreases because of extra amount of carbon
51
52
53
54
55
56
57
58
59
60

1
2
3 coming in due to higher catalyst circulation with no extra air. This leads to less residence time
4
5 for burning all the coke in the regenerator.
6
7

8 **6. Conclusions**

9

10 An indigenously developed (and reported¹⁵ earlier) 10-lump kinetic model for the riser
11 reactor was integrated with a regenerator model for the simulation of the entire FCC unit. Several
12 sets of test run data and one set of normal operating data were obtained from an operating FCC
13 plant in a refinery for validation of the developed simulator. The ten lump model predictions for
14 all the cases investigated were in close agreement with plant measured values and deviations
15 were found to be similar to those with ASPEN FCC simulator.
16
17
18
19
20
21
22
23

24 A comparison was made for the present simulator performance with that using 5-lump
25 kinetics for riser reactor. Significantly larger deviations from measured values were obtained in
26 case of 5 lump model as compared to the present simulator, thus establishing the superiority of
27 model with more detailed description of the feed as compared to single lump representation used
28 in 5-lump model.
29
30
31
32
33
34
35

36 Parametric sensitivity study in respect of operating conditions such as effect of feed
37 preheat temperature, feed flow rate and reactor outlet temperature showed that the catalyst
38 circulation rate of riser reactor had stronger influence on gas oil conversion as compared to feed
39 preheat temperature for a fixed reactor outlet temperature. The sensitivity analysis is useful for
40 the refiners to understand the effects of individual parameters on the FCC performance and to
41 perform optimization study for better productivity of the unit. From the present sensitivity study,
42 it may be concluded that increasing ROT at fixed T_{rgn} or at fixed F_{air} should lead to improved
43 conversion whereas increase in F_{feed} or T_{feed} will deteriorate reactor performance. Although the
44 trends observed in this study are similar to those reported earlier⁸, we believe the present results
45
46
47
48
49
50
51
52
53
54
55
56
57
58
59
60

are quantitatively superior and more representative because of improved performance of the 10-lump model

Acknowledgment

The authors gratefully acknowledge Indian Oil Corporation Ltd (IOCL) and University of Petroleum & Energy Studies for allowing them to publish the present work. The first author acknowledges financial support from IOCL.

Appendix A. Riser Reactor Model Equations

A.1. Ten Lump Model

Material Balance:

The mass balance for the j^{th} lump over a differential element of riser height (dh) can be written as follows

$$\frac{dF_j}{dh} = A_{ris} H_{ris} (1 - \varepsilon) \rho_c \sum_{i=1}^{25} (\alpha_{kj})_i r_i \quad ; \quad i=1, \dots, 25 \text{ and } j, k=1, \dots, 10, j \neq k \quad (\text{A1})$$

where $(\alpha_{kj})_i = \frac{MW_k}{MW_j} = \text{for } k \rightarrow j \text{ in } i^{\text{th}} \text{ reaction.}$

$$h = \frac{Z}{H_{ris}} \quad (\text{A2})$$

$$\rho_v = \frac{P_{ris} MW_g}{RT} \quad \text{and} \quad \varepsilon = \frac{F_{feed}/\rho_v}{F_{feed}/\rho_v + F_{rgc}/\rho_c} \quad (\text{A3})$$

$$MW_g = \sum_{j=1}^{10} x_j MW_j \quad (\text{A4})$$

The rate equation for each i^{th} reaction is as follows:

$$r_i = k_{0i} \exp\left(-\frac{E_i}{RT}\right) C_j \phi \quad \text{for } i = 1, 2, 3, 4, 5 \text{ and } j = 1 \quad (\text{A5})$$

$$r_i = k_{0i} \exp\left(-\frac{E_i}{RT}\right) C_j \phi \quad \text{for } i = 6, 7, 8, 9 \text{ and } j = 2 \quad (\text{A6})$$

$$r_i = k_{0i} \exp\left(-\frac{E_i}{RT}\right) C_j \phi \quad \text{for } i = 10, 11, 12, 13 \text{ and } j = 3 \quad (\text{A7})$$

$$r_i = k_{0i} \exp\left(-\frac{E_i}{RT}\right) C_j \phi \quad \text{for } i = 14, 15, 16 \text{ and } j = 4 \quad (\text{A8})$$

$$r_i = k_{0i} \exp\left(-\frac{E_i}{RT}\right) C_j \phi \quad \text{for } i = 17, 18, 19 \text{ and } j = 5 \quad (\text{A9})$$

$$r_i = k_{0i} \exp\left(-\frac{E_i}{RT}\right) C_j \phi \quad \text{for } i = 20, 21, 22 \text{ and } j = 6 \quad (\text{A10})$$

$$r_i = k_{0i} \exp\left(-\frac{E_i}{RT}\right) C_j \phi \quad \text{for } i = 23, 24 \text{ and } j = 7 \quad (\text{A11})$$

$$r_i = k_{0i} \exp\left(-\frac{E_i}{RT}\right) C_j \phi \quad \text{for } i = 25 \text{ and } j = 8 \quad (\text{A12})$$

The catalyst activity (ϕ) was related to coke concentration on the catalyst^{17,18}(C_c):

$$\phi = (1 + 51 \cdot C_c)^{-2.78} \quad (\text{A13})$$

$$C_c = m\theta^n \quad (\text{A14})$$

The value of m was, tuned for the catalyst used from plant data in present study, whereas, value of the exponent¹⁹ of θ is 0.5.

Energy Balance:

$$\frac{dT}{dh} = \frac{A_{ris} H_{ris} \rho_c (1 - \varepsilon)}{F_{rgc} C_{pc} + F_{feed} C_{pfv}} \sum_{i=1}^{25} r_i (-\Delta H_i) \quad ; i = 1, \dots, 25 \quad (\text{A15})$$

$$T(h = 0) = \frac{F_{rgc} C_{pc} T_{rgn} + F_{feed} C_{pfl} T_{feed} - \Delta H_{evp} F_{feed} - Q_{loss,ris}}{F_{rgc} C_{pc} + F_{feed} C_{pfv}} \quad (\text{A16})$$

$Q_{loss,ris}$ in the riser has been taken to be 0.9 % of total heat. It can be estimated by trial and error method to match the ROT.

A.2. Five Lump Riser Reactor Model Equations

Mass Balance

$$\frac{dF_j}{dh} = A_{ris} H_{ris} (1 - \varepsilon) \rho_c \sum_{i=1}^9 (\alpha_{kj})_i r_i \quad (\text{A17})$$

Rate equations for each of the nine reactions is as follows:

$$r_i = k_{0i} \exp\left(-\frac{E_i}{RT}\right) C_j^2 \phi \quad \text{for } i = 1, 2, 3, 4 \text{ and } j = 1 \quad (\text{A18})$$

$$r_i = k_{0i} \exp\left(-\frac{E_i}{RT}\right) C_j \phi \quad \text{for } i = 5, 6, 7 \text{ and } j = 2 \quad (\text{A19})$$

$$r_i = k_{0i} \exp\left(-\frac{E_i}{RT}\right) C_j \phi \quad \text{for } i = 8, 9 \text{ and } j = 3 \quad (\text{A20})$$

Enthalpy Balance

$$\frac{dT}{dh} = \frac{A_{ris} H_{ris} \rho_c (1 - \varepsilon)}{F_{rgc} C_{pc} + F_{feed} C_{pfv}} \sum_{i=1}^9 r_i (-\Delta H_i) \quad (\text{A21})$$

$$T(h = 0) = \frac{F_{rgc} C_{pc} T_{rgn} + F_{feed} C_{pfl} T_{feed} - \Delta H_{evp} F_{feed} - Q_{loss,ris}}{F_{rgc} C_{pc} + F_{feed} C_{pfv}} \quad (\text{A22})$$

$$MW_g = \sum_{j=1}^5 X_j MW_j \quad (A23)$$

$$\rho_v = \frac{P_{ris} MW_g}{RT} \quad \text{and} \quad \varepsilon = \frac{F_{feed}/\rho_v}{F_{feed}/\rho_v + F_{rgc}/\rho_c} \quad (A24)$$

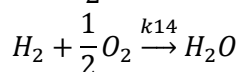
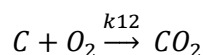
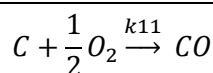
A.3. Stripper Modeling

$$T_{sc} = ROT - \Delta T_{sc} \quad (A25)$$

$$F_{sc} = F_{rgc}(1 + C_{sc}) \quad (A26)$$

Appendix B. Regenerator Model Equations

The main combustion reactions in the regenerator are as follows:



Rate equations for the combustion reactions in the regenerator

$$r_{11} = (1 - \varepsilon) \rho_c k_{11} \frac{C_{rgc}}{MW_c} P_{O_2} = (1 - \varepsilon) \rho_c k_{11} \frac{C_{rgc} f_{O_2}}{MW_c f_{tot}} P_{rgn} \quad (B1)$$

$$r_{12} = (1 - \varepsilon) \rho_c k_{12} \frac{C_{rgc}}{MW_c} P_{O_2} = (1 - \varepsilon) \rho_c k_{12} \frac{C_{rgc} f_{O_2}}{MW_c f_{tot}} P_{rgn} \quad (B2)$$

$$\begin{aligned} r_{13} &= k_{13} P_{O_2} P_{CO} = (X_{pt}(1 - \varepsilon) \rho_c k_{13c} + \varepsilon k_{13h}) P_{O_2} P_{CO} \\ &= (X_{pt}(1 - \varepsilon) \rho_c k_{13c} + \varepsilon k_{13h}) \frac{f_{O_2} f_{CO}}{f_{tot}} P_{rgn}^2 \end{aligned} \quad (B3)$$

$$\left(\frac{CO}{CO_2} \right)_{Surface} = \frac{k_{11}}{k_{12}} = \beta_c = \beta_{CO} \exp\left(\frac{-E_\beta}{RT}\right) \quad (B4)$$

$$k_c = k_{11} + k_{12} = k_{CO} \exp\left(\frac{-E_c}{RT}\right) \quad (B5)$$

$$k_{11} = \frac{\beta_c k_c}{\beta_c + 1} = \frac{\beta_c k_{c0} \exp\left(-\frac{E_c}{RT}\right)}{\beta_c + 1} \quad (\text{B6})$$

$$k_{12} = \frac{k_c}{\beta_c + 1} = \frac{k_{c0} \exp\left(-\frac{E_c}{RT}\right)}{\beta_c + 1} \quad (\text{B7})$$

$$k_{13c} = k_{13c0} \exp\left(-\frac{E_{13c}}{RT}\right) \quad (\text{B8})$$

$$k_{13h} = k_{13h0} \exp\left(-\frac{E_{13h}}{RT}\right) \quad (\text{B9})$$

B.1. Dense Bed Regenerator:

Material balance:

$$\frac{df_{O_2}}{dz} = -A_{rgn} \left(\frac{r_{11}}{2} + r_{12} + \frac{r_{13}}{2} \right) \quad (\text{B10})$$

$$\frac{df_{CO}}{dz} = -A_{rgn} (r_{13} - r_{11}) \quad (\text{B11})$$

$$\frac{df_{CO_2}}{dz} = A_{rgn} (r_{12} + r_{13}) \quad (\text{B12})$$

$$\frac{df_{N_2}}{dz} = 0 \quad (\text{B13})$$

Initial Conditions (at $z = 0$) for Dense Bed Modeling:

$$f_{h_2o} = F_{rgc} (C_{sc} - C_{rgc}) \frac{C_h}{MW_H} \quad (\text{B14})$$

$$f_{O_2} = 0.21 F_{air} - \frac{1}{2} f_{h_2o} \quad (\text{B15})$$

$$f_{CO} = f_{CO_2} = 0 \quad (\text{B16})$$

$$f_{N_2} = 0.79 F_{air} \quad (\text{B17})$$

$$f_{tot} = f_{O_2} + f_{CO} + f_{CO_2} + f_{h_2o} + f_{N_2} \quad (\text{B18})$$

Energy Balance :

$$\frac{dT_{rgn}}{dz} = 0 \quad (\text{B19})$$

Heat balance across the regenerator dense bed is given by the following equation:

$$Q_C + Q_H + Q_{air} + Q_{sc} + Q_{ent} = Q_{rgc} + Q_{sg} + Q_{loss} \quad (\text{B20})$$

$$\text{where } Q_c = f_{CO(Zbed)}H_{CO} + f_{CO_2(Zbed)}H_{CO_2} \quad (\text{B20.a})$$

$$Q_H = f_{H_2O}H_{H_2O} \quad (\text{B20.b})$$

$$Q_{air} = F_{air}C_{P_{air}}(T_{air} - T_{base}) \quad (\text{B20.c})$$

$$Q_{sc} = F_{sc}C_{P_{sc}}(T_{sc} - T_{base}) \quad (\text{B20.d})$$

$$Q_{rgc} = F_{rgc}C_{P_c}(T_{rgn} - T_{base}) \quad (\text{B20.e})$$

$$Q_{sg} = f_{CO_2(Zbed)}C_{P_{CO_2}} + f_{CO(Zbed)}C_{P_{CO}} + f_{O_2(Zbed)}C_{P_{O_2}} + f_{H_2O}C_{P_{H_2O}} + f_{N_2}C_{P_{N_2}}(T_{rgn} - T_{base}) \quad (\text{B20.f})$$

$$Q_{ent} = F_{ent}C_{P_c}(T_{dil(Zbed)} - T_{base}) = 0 \text{ (assumed)} \quad (\text{B20.g})$$

The final equation for the dense bed temperature is

$$T_{rgn} = T_{base} + \frac{f_{CO(Zbed)}H_{CO} + f_{CO_2}H_{CO_2} + f_{H_2O}H_{H_2O} + F_{air}C_{P_{air}}(T_{air} - T_{base}) + F_{sc}C_{P_c}(T_{sc} - T_{base}) + Q_{loss,rgn}}{F_{rgc}C_{P_c} + f_{CO_2(Zbed)}C_{P_{CO_2}} + f_{CO(Zbed)}C_{P_{CO}} + f_{O_2}C_{P_{O_2}} + f_{H_2O}C_{P_{H_2O}} + f_{N_2}C_{P_{N_2}}} \quad (\text{B21})$$

$$F_{sc}C_{sc}(1 - C_h) = F_{rgc}C_{rgc}(1 - C_h) + (f_{CO(Zbed)} + f_{CO_2(Zbed)})MW_c \quad (\text{B22})$$

$$C_{rgc} = \frac{[F_{sc}C_{sc}(1 - C_h) - (f_{CO(Zbed)} + f_{CO_2(Zbed)})MW_c]}{[F_{rgc}(1 - C_h)]} \quad (\text{B23})$$

a. Evaluation of Bed Characteristics ²²⁻²³:

$$\rho_g = \frac{P_{rgn}}{RT_{rgn}} \quad (\text{B24})$$

$$u = \frac{F_{air}}{\rho_g A_{rgn}} \quad (\text{B25})$$

$$\varepsilon_{den} = \frac{0.305u_1 + 1}{0.305u_1 + 2} \quad (\text{B26})$$

$$\rho_{c,dense} = \rho_c(1 - \varepsilon_{den}) \quad (\text{B27})$$

$$\rho_{c,dilute} = \text{Max}[0, (0.582u_1 - 0.878)] \quad \text{in (lb/ft}^3) \quad (\text{B28})$$

$$\varepsilon_{dil} = \frac{\rho_{dil}}{\rho_c} \quad (\text{B29})$$

$$F_{ent} = \rho_{c,dil}A_{rgn}u \quad (\text{B30})$$

b. Dense Bed Height: The regenerator dense bed height is calculated by the given correlation²²:

$$z_{\text{bed}} = 0.3048(\text{TDH}) \quad (\text{B31})$$

$$\text{where TDH} = \text{TDH}_{20} + (D - 20)$$

$$\log_{10}(\text{TDH}_{20}) = \log_{10}(20.5) + 0.07(u_1 - 3)$$

B.2. Dilute Bed Regenerator:

a. Material Balance

$$\frac{df_{\text{O}_2}}{dz} = -A_{\text{rgn}} \left(\frac{r_{11}}{2} + r_{12} + \frac{r_{13}}{2} \right) \quad (\text{B32})$$

$$\frac{df_{\text{CO}}}{dz} = -A_{\text{rgn}}(r_{13} - r_{11}) \quad (\text{B33})$$

$$\frac{df_{\text{CO}_2}}{dz} = A_{\text{rgn}}(r_{12} + r_{13}) \quad (\text{B34})$$

$$\frac{df_{\text{C}}}{dz} = -A_{\text{rgn}}(r_{11} + r_{12}) \quad (\text{B35})$$

b. Energy Balance:

$$\frac{dT_{\text{dil}}}{dz} = \frac{1}{C_{\text{P}_{\text{tot}}}} \left(H_{\text{CO}} \frac{df_{\text{CO}}}{dz} + H_{\text{CO}_2} \frac{df_{\text{CO}_2}}{dz} \right) = \frac{A_{\text{rgn}}}{C_{\text{P}_{\text{tot}}} f_{\text{tot}}} [H_{\text{CO}}(r_{11} - r_{12}) + H_{\text{CO}_2}(r_{11} - r_{12})] \quad (\text{B36})$$

$$\text{where } C_{\text{P}_{\text{tot}}} = \frac{C_{\text{P}_{\text{N}_2}} f_{\text{N}_2} + C_{\text{P}_{\text{O}_2}} f_{\text{O}_2} + C_{\text{P}_{\text{CO}}} f_{\text{CO}} + C_{\text{P}_{\text{CO}_2}} f_{\text{CO}_2} + C_{\text{P}_{\text{H}_2\text{O}}} f_{\text{H}_2\text{O}} + C_{\text{P}_{\text{c}}} F_{\text{ent}}}{f_{\text{tot}}}$$

Nomenclature

A_{rgn}	regenerator cross- section area, m^2
A_{ris}	riser cross- sectional area, m^2
C_{h}	weight fraction of hydrogen in coke, (kg of H_2)/ (kg of coke)
C_{c}	coke on catalyst, kg coke /kg catalyst
C_{i}	concentration of j^{th} component, kmol/m^3
C_{pc}	catalyst heat capacity, $\text{kJ}/(\text{kg.K})$
C_{pco}	mean heat capacity of CO, $\text{kJ}/(\text{kg.K})$
C_{pco_2}	mean heat capacity of CO_2 , $\text{kJ}/(\text{kg.K})$
C_{pfl}	liquid feed heat capacity, $\text{kJ}/(\text{kg.K})$
C_{pfv}	vapor feed heat capacity, $\text{kJ}/(\text{kg.K})$

1		
2		
3	C_{ph2o}	mean heat capacity of water, kJ/(kg.K)
4		
5	C_{pN2}	mean heat capacity of N_2 , kJ/(kg.K)
6		
7	C_{pO2}	mean heat capacity of O_2 , kJ/(kg.K)
8		
9	C_{rgc}	coke on regenerator catalyst, (kg coke)/kg-cat
10	C_{sc}	coke on spent catalyst, (kg coke)/kg-cat
11		
12	D	regenerator diameter, ft
13		
14	E_{β}	activation energy for CO/ CO_2 at the catalyst surface
15	E_j	activation energy of i^{th} cracking reaction in the riser
16		
17	E_c	activation energy of coke combustion
18		
19	E_{13c}	activation energy for homogeneous CO combustion
20	E_{13h}	activation energy for heterogeneous CO combustion
21		
22	f_c	molar flow rate of carbon in the regenerator, kmol/sec
23		
24	f_{co}	CO molar flow rate in the regenerator, kmol/sec
25		
26	f_{co2}	CO molar flow rate in the regenerator, kmol/sec
27		
28	f_{h2o}	H_2O molar flow rate in the regenerator, kmol/sec
29		
30	f_{N2}	N_2 molar flow rate in the regenerator, kmol/sec
31		
32	f_{O2}	O_2 molar flow rate in the regenerator, kmol/sec
33	f_{tot}	total gas molar flow rate in the regenerator, kmol/sec
34		
35	F_{air}	air flow rate to the regenerator, kmol/sec
36		
37	F_{ent}	entrained catalyst flow rate kg/sec
38	F_j	molar flow rate of j th lump, kmol/sec
39		
40	F_{rgc}	catalyst circulation rate (CCR), kg/sec
41		
42	F_{sc}	spent catalyst flow rate, kg/sec
43		
44	F_{feed}	oil feed flow rate, kg/sec
45		
46	h	dimensionless riser height
47	H_{ris}	riser height, m
48		
49	ΔH_{evp}	heat of vaporization of oil feed, kJ/kg
50	H_{co}	heat of Formation of oil feed, kJ/kmol
51		
52	H_{co2}	heat of formation of CO_2 , kJ/kmol
53		
54	H_{h2o}	heat of formation of H_2O , kJ/kmol
55		
56	ΔH_i	heat of cracking of i th lump, kJ/kmol
57	i	total no. of reactions in the reactor
58		
59		
60		

1		
2		
3		
4	j	total no. of kinetic lumps
5	k_i	rate constant of i^{th} reaction in the riser, $\text{m}^3/(\text{kg-cat. sec})$
6		
7	$k_{0,i}$	frequency factor for i^{th} reaction in the riser, $\text{m}^3/(\text{kg-cat. sec})$
8		
9	k_{11}	coke combustion rate coefficient for C to CO reaction
10	k_{12}	coke combustion rate coefficient for C to CO ₂ reaction
11		
12	k_c	Total coke combustion rate coefficient, $1/(\text{atm. sec})$
13		
14	k_{c0}	frequency factor for coke combustion, $1/(\text{atm. sec})$
15		
16	k_{13c}	frequency factor in heterogeneous CO combustion expression, (kmol of
17		
18	k_{13h}	frequency factor in homogeneous CO combustion expression, (kmol of
19	MW_j	molecular weight of j^{th} lump, kg/kmol
20		
21	MW_c	molecular weight of coke, kg/kmol
22		
23	MW_g	average molecular weight of gas oil feed, kg/kmol
24		
25	MW_H	molecular weight of hydrogen
26		
27	P_{ris}	riser pressure, atm
28		
29	P_{rgn}	regenerator pressure, atm
30		
31	P_{O_2}	average mean oxygen partial pressure, atm
32		
33	Q_{air}	heat flow rate with air, kJ/sec
34		
35	Q_C	heat released by the carbon combustion, kJ/sec
36		
37	Q_{ent}	heat input to the dense bed from entrained catalyst returning from
38		
39	Q_H	heat released by the hydrogen combustion, kJ/sec
40		
41	$Q_{\text{loss, ris}}$	heat losses from the riser base, kJ/sec
42		
43	Q_{rgc}	heat flow with regenerated catalyst, kJ/sec
44		
45	Q_{sc}	heat flow rate with spent catalyst, kJ/sec
46		
47	Q_{sg}	heat flow rate with gases from the regenerator dense bed, kJ/sec
48		
49	R	universal gas constant
50		
51	r_i	rate of the i^{th} reaction, kmol/ (kg-cat. sec)
52		
53	ROT	riser outlet temperature, K
54		
55	T	riser temperature at any axial height, K
56		
57	T_{air}	temperature of the air to the regenerator
58		
59	T_{base}	base temperature for heat balance calculations, K (assumed, 866.6 K)
60		
	T_{feed}	gas oil feed temperature, K

T_{dil}	regenerator dilute bed temperature, K
T_{rgn}	regenerator dense bed temperature/regenerated catalyst temperature, K
T_{sc}	temperature of spent catalyst, K
ΔT_{st}	stripper temperature drop ($\sim 10^0 C$)
u	velocity of gas in the riser or the regenerator, m/sec
u_1	superficial linear velocity, ft/sec
X_{pt}	relative catalytic CO combustion rate
x_j	mole fraction of j^{th} component
z	axial height from the entrance of the riser or regenerator, m
Z_{bed}	regenerator dense bed height, m
Z_{dil}	regenerator dilute phase height, m
Z_{rgn}	regenerator height, m

Greek Letters

$(\alpha_{kj})_i$	stoichiometric coefficient for lump $k \rightarrow j$ in i^{th} reaction
β_c	CO/CO ₂ ratio at the surface in the regenerator
β_{c0}	frequency factor in β_c expression
ε	riser or regenerator void fraction
ρ_c	catalyst density, kg/m ³
$\rho_{c,dense}$	catalyst density in the regenerator dense bed, kg/m ³
$\rho_{c,dilute}$	catalyst density in the dilute phase of the regenerator, kg/m ³
ρ_g	molar gas density in the regenerator, kmol/m ³
ρ_v	oil vapor density, kg/m ³
ϕ	catalyst activity
θ	catalyst residence time, sec

References

- (1) Weekman, V. W., Jr. A Model of Catalytic Cracking Conversion in Fixed, Moving, and Fluid Bed Reactors. *Ind. Eng. Chem. Process Des. Dev.* **1968**, 7, 90.
- (2) Weekman, V. W., Jr. Kinetics and Dynamics of Catalytic Cracking Selectivity in Fixed Bed Reactors. *Ind. Eng. Chem. Process Des. Dev.* **1969**, 8, 385.

- 1
2
3 (3) Lee, L.; Chen, Y.; Huang, T. Four-Lump Kinetic Model for Fluid Catalytic Cracking
4
5 Process. *Can. J. Chem. Eng.* **1989**, *67*, 615.
6
7
8 (4) Abul-Hamayel, M. A. Kinetic Modeling of High-Severity Fluidized Catalytic Cracking.
9
10 *Fuel*. **2003**, *82*, 1113.
11
12
13 (5) Dave, D. J.; Saraf, D.N. A Model Suitable for Rating and Optimization of Industrial FCC
14
15 Units. *Ind. Chem. Eng. Section A*. **2003**, *45*, 7.
16
17
18 (6) Ancheyta, J. J.; Lopez, I.F.; Aguilar, R.E. 5-Lump Kinetic Model for Gas Oil Catalytic
19
20 Cracking. *Appl. Catal. A*. **1999**, *177*, 227.
21
22
23 (7) Bollas, G. M.; Lappas, A. A.; Iatridis, D. K.; Vasalos, I. A. Five Lump Kinetic Model with
24
25 Selective Catalyst Deactivation for the Prediction of the Product Selectivity in the Fluid Catalytic
26
27 Cracking Process. *Catalysis Today*. **2007**, *127*, 31.
28
29
30 (8) Dasila, P.K.; Choudhury, I.; Saraf, D.N.; Chopra, S.; Dalai, A. Parametric Sensitivity
31
32 Studies in a Commercial FCC Unit. *Advances in Chemical Engineering and Science*. **2012**, *2*,
33
34 136.
35
36
37 (9) Kasat, R.B.; Kunzru, D.; Saraf, D.N.; Gupta, S.K. Multi-objective Optimization of
38
39 Industrial FCC Units using Elitist Non-Dominated Sorting Genetic Algorithm. *Ind. Eng. Chem.*
40
41 *Res.* **2002**, *41*, 4765.
42
43
44 (10) Jacob, S. M.; Gross, B.; Voltz, S.E.; Weekman, V.W., Jr. A Lumping and Reaction
45
46 Scheme for Catalytic Cracking. *AIChE J.* **1976**, *22*, 701.
47
48
49 (11) Gross, B.; Jacob, S. M.; Nace, D. M.; Voltz, S. E. Simulation of Catalytic Cracking
50
51 Process. U.S. Patent 3960707, 1976.
52
53
54 (12) Kumar, S.; Chadha A.; Gupta, R.; Sharma, R. CATCRACK: A Process Simulator for an
55
56 Integrated FCC-Regenerator System. *Ind. Eng. Chem. Res.* **1995**, *34*, 3737.
57
58
59
60

- 1
2
3
4
5
6
7
8
9
10
11
12
13
14
15
16
17
18
19
20
21
22
23
24
25
26
27
28
29
30
31
32
33
34
35
36
37
38
39
40
41
42
43
44
45
46
47
48
49
50
51
52
53
54
55
56
57
58
59
60
- (13) Arbel, A.; Huang, Z.; Rinard I.H.; Shinnar, R. Dynamic and Control of Fluidized Catalytic Crackers. I. Modeling of the Current Generation of FCC's. *Ind. Eng. Chem. Res.* **1995**, *34*, 1228.
- (14) Cerqueira, S. H.; Biscaia, E.C., Jr.; Sousa-Aguiar, E.F. Mathematical Modeling and Simulation of Catalytic Cracking of Gas Oil in a Fixed Bed: Coke Formation. *Appl. Catal. A.* **1997**, *164*, 35.
- (15) Dasila, P.K. Kinetic Modeling and Simulation of Fluid Catalytic Cracking Units. Ph.D Thesis, University of Petroleum and Energy Studies, Dehradun, India, April 2013.
- (16) Dasila, P.K.; Choudhury, I.R.; Saraf, D.N.; Kagdiyal, V.; Rajagopal, S.; Chopra, S.J. Estimation of FCC Feed Composition from Routinely Measured Lab Properties through ANN Model. *Fuel Process Technol.* **2014**, *125*, 155.
- (17) Yingxun, S. Deactivation by Coke in Residuum Catalytic Cracking. In *Catalysts Deactivation*; Bartholomew, C.H., Butt, J.B., Eds.; Elsevier: Amsterdam, 1991; Vol 68, pp 327.
- (18) Voorhies, A. Carbon Formation in Catalytic Cracking. *Ind. Eng. Chem.* **1945**, *37*, 318.
- (19) Avidan, A. A. Origin, Development, and Scope of FCC Catalysis. In *Fluid Catalytic Cracking: Science and Technology: Studies in Surface Science and Catalysis*; Magee, J. S., Mitchell, M. M., Jr., Eds.; Elsevier: Amsterdam, Netherlands, 1993; Vol 76, pp 1.
- (20) Avidan, A. A.; Shinnar, R. Development of Catalytic Cracking Technology. A Lesson in Chemical Reactor Design. *Ind. Eng. Chem. Res.* **1990**, *29*, 931.
- (21) Krishna, A. S.; Parkin, E. S. Modeling the Regenerator in Commercial Fluid Catalytic Cracking Units. *Chem. Eng. Prog.* **1985**, *81*, 57.
- (22) Ewell, R.B.; Gadmer, G. Design Cat Crackers by Computer. *Hydrocarbon process.* **1978**, *4*, 125.

1
2
3 (23) McFarlane, R.C.; Reineman, R.C.; Bartee, J.F.; Georgakis, C. Dynamic Simulation for
4 a Model IV Fluid Catalytic Cracking Unit. *Comput. Chem.Eng.* **1993**, *17*, 275.
5
6

7
8 (24) Aspen FCC User's Guide. Aspen Technology, Inc. Burlington, MA. USA, 2006,
9
10 <http://www.aspentech.com>.
11

12 (25) Balasubramanian, P.; Bettina, S. J.; Pushpavanam, S.; Balaraman. K. S. Kinetic Parameter
13 Estimation in Hydrocracking Using a Combination of Genetic Algorithm and Sequential
14 Quadratic Programming. *Ind. Eng. Chem. Res.* **2003**, *42*, 4723.
15
16
17

18 (26) Basak, K.; Abhilash, K. S.; Ganguly, S.; Saraf, D. N. Online Optimization of a Crude
19 Distillation Unit with Constraints on Product Properties. *Ind. Eng. Chem. Res.* **2002**, *41*, 1557
20
21
22
23
24
25
26
27
28
29
30
31
32
33
34
35
36
37
38
39
40
41
42
43
44
45
46
47
48
49
50
51
52
53
54
55
56
57
58
59
60

Figure Captions

Figure 1: Schematic diagram of the fluid catalytic cracking unit (FCCU).

Figure 2: Ten lump kinetic scheme

Figure 3: Effect of feed preheat temperature (T_{feed}) on gas oil conversion and product yields at fixed F_{feed} (50.16 kg/sec), fixed ROT (767 K) and fixed T_{rgn} (935 K)

Figure 4: Variation in air flow rate and catalyst circulation rate on increasing feed preheat temp (T_{feed}) at constant T_{rgn} (935K)

Figure 5: Effect of riser outlet temperature (ROT) on gas oil conversion and product yields at fixed F_{feed} (50.16 kg/sec), fixed T_{feed} (621 K) and constant T_{rgn} (935K)

Figure 6: Variation in air flow rate and catalyst circulation rate on increasing ROT at constant T_{rgn} (935K)

Table 1. Feed Composition and Properties Used in the Simulation

Parameters	Values			
	Case I	Case II	Case III	Case IV
Specific gravity @ 15 °C	0.8896	0.8896	0.8858	0.8949
<u>Distillation, ASTM D-1160, °C</u>				
0	288	268	253	282
5	370	357	358	352
10	386	383	384	372
30	425	417	416	408
50	450	438	445	437
70	483	464	466	475
90	530	505	509	517
95	542	517	519	536
100	546	525	526	555
CCR, wt%	0.15	0.22	0.21	0.38
Total sulfur, wt%	0.5	0.45	0.43	0.34
Basic nitrogen, ppm	307	299	281	-
Total nitrogen, ppm	900	717	672	-
<u>Feed composition from ANN model¹⁷</u>				
Paraffins ,wt%	17.7	11.8	12.7	17.2
Naphthenes ,wt%	33.3	36.6	34.0	21.4
Aromatics, wt%	49.0	51.6	53.3	61.5

Table 2. Plant Operating Data Used in Simulation

Operating parameters	Case I	Case II	Case III	Case IV
Feed rate, kg/s	49.3	50.2	46.7	47.2
Feed preheat temp, K	621.9	621.0	616.0	614.3
Reactor outlet temp, K	767.3	767.4	767.3	767.2
Cat circulation rate, kg/sec	225.0	250.8	237.8	211.8
Catalyst density, kg/m ³	817.0	831.0	850.0	800.0
Regenerator dense phase temp, K	938.0	935.0	935.0	945.0
Reactor pressure, kg/cm ²	2.3	2.3	2.2	2.3
Regenerator pressure, kg/cm ²	2.6	2.6	2.6	2.6
Air to regenerator temp, K	470	476	455	490
Air rate, kmol /sec	0.79	0.80	0.75	0.78
Hydrogen in coke , wt %	9.2	16.4	14.3	9.5

Table 3. Thermodynamic and Other Parameters Used in Simulation

Description	Test Run
C_{pc} , kj/(kg.K)	1.29 ^a
C_{pfl} , kj/(kg.K)	3.43 ^a
C_{pFv} , kj/(kg.K)	3.39 ^a
ΔH_{evp} , kj/kg	349 ^a
$C_{p,N2}$ (kj/kg K)	29.12
$C_{p,o2}$ (kj/kg K)	29.44
$C_{p,h2o}$ (kj/kg K)	41.01
$C_{p,co}$ (kj/kg K)	29.12
$C_{p,co2}$ (kj/kg K)	37.14
H_{co} (kJ/kmol)	110640
H_{co2} (kJ/kmol)	393520
H_{h2o} (kJ/kmol)	240590
X_{pt}	0.10
D_p (m)	$6.0 * 10^{-5}$
<u>Molecular weight of kinetic lumps kg/kmol</u>	
Ph, Nh, Ah	339
Pl, Nl, Al	240
G	114
LPG	54
DG	30
C	12
<u>Design data</u>	
Riser length, m	37
Riser diameter, m	0.7
Regenerator length, m	15
Regenerator diameter, m	5.6

^aData from Arbel et al., 1995.

Table 4. Comparison of Model Calculated Values with Plant Data (Case I & II)

	Case I			Case II		
	Measured Value	Calculated Values from Simulation		Measured Value	Calculated Values from Simulation	
		ASPEN FCC (% Dev)	Present Model (% Dev)		ASPEN FCC (% Dev)	Present Model (% Dev)
Riser outlet temp, K	767.3	767.4(0.0)	768.0(-0.1)	767.4	767.5(0.0)	770.9(-0.5)
Heavy paraffins (P _h), wt %		0.0	0.0		0.0	0.0
Heavy naphthenes (N _h), wt %		0.0	0.1		0.0	0.0
Heavy aromatics (A _h), wt %		14.1	13.6		10.8	12.8
Total heavy fraction (343 ⁺ °C), wt %	14.5	14.2(2.1)	13.7(5.3)	12.9	10.8(16.8)	12.8(1.2)
Light paraffins (P _l), wt %		2.7	2.3		1.3	1.3
Light naphthenes (N _l), wt %		3.3	2.6		1.5	2.2
Light aromatics (A _l), wt %		11.6	11.4		13.7	11.7
Total light fraction (221-343 °C), wt %	17.2	17.6(-2.6)	16.3(5.2)	15.6	16.4(-5.2)	15.2(2.6)
Gasoline (C5-221 °C), wt %	51.5	50.9(1.2)	52.1(-1.2)	54.3	54.8(-0.9)	53.3(1.8)
LPG, wt %	11.4	11.8(-3.4)	12.2(-6.8)	12.4	12.6(-1.8)	13.7(-10.9)
Dry gas, wt %	1.5	1.5(-0.3)	1.7(-7.4)	1.2	1.6(-35.1)	1.2(-3.3)
Coke, wt %	4.0	4.1(-1.6)	4.1(-3.2)	3.6	3.8(-6.6)	3.7(-4.4)

Table 5. Comparison of Model Calculated Values with Plant Data (Case III & IV)

	Case III			Case IV		
	Measured Value	Calculated Values from Simulation		Measured Value	Calculated Values from Simulation	
		ASPEN FCC (% Dev)	Present Model (% Dev)		ASPEN FCC (% Dev)	Present Model (% Dev)
Riser outlet temp, K	767.3	767.6(0.0)	769.7(-0.3)	767.2	767.4(0.0)	771(-0.6)
Heavy paraffins (P _h), wt %		0.0	0.0		0.0	0.0
Heavy naphthenes (N _h), wt %		0.0	0.0		0.0	0.1
Heavy aromatics (A _h), wt %		7.8	13.0		15.1	15.4
Total heavy fraction (343 ⁺ °C), wt %	12.1	7.8(35.8)	13.0(-7.4)	14.5	15.1(-4.4)	15.5(-7.3)
Light paraffins (P _l), wt %		0.4	1.4		1.1	2.4
Light naphthenes (N _l), wt %		0.6	2.1		1.4	1.9
Light aromatics (A _l), wt %		15.1	10.7		17.3	13.3
Total light fraction (221-343 °C), wt %	13.9	16.1(-15.5)	14.2(-2.2)	20.2	19.7(2.4)	17.7(12.7)
Gasoline (C5-221 °C), wt %	55.8	56.7(-1.6)	54.1(3.0)	48.6	48.9(-0.4)	50.8(-4.4)
LPG, wt %	12.9	14.2(-10.3)	13.6(-5.4)	11.1	11.3(-1.8)	10.8(2.8)
Dry gas, wt %	1.6	2.0(-21.9)	1.3(18.8)	1.4	1.5(- 4.8)	1.4(-2.7)
Coke, wt %	3.7	3.3(10.5)	3.8(-2.7)	4.1	3.5(14.7)	3.8(8.7)

Table 6. Calculated Kinetic Rate Constants for 5-Lump Model

Reaction Number (i)	Reactions	Rate Constants
1	Gas Oil → Gasoline	15.4508
2	Gas oil → LPG	3.1312
3	Gas Oil → DG	0.3722
4	Gas Oil → Coke	0.9331
5	Gasoline → LPG	0.0035
6	Gasoline → DG	0.0003
7	Gasoline → Coke	0.0016
8	LPG → DG	0.0012
9	LPG → Coke	0.0016

Table 7. Comparison of Ten Lump and Five Lump Model Calculated Values with Plant Data (Case II)

	Measured Value	Model Calculated Value		
		Ten Lump(% Dev)	Five Lump (% Dev)	
			Literature®	Tuned*
Riser outlet temp, K	767.4	770.9(-0.5)	778.4(-1.4)	769.5(-0.3)
Heavy paraffins (Ph)		0.0		
Heavy naphthenes (Nh)		0.0		
Heavy aromatics (Ah)		12.8		
Total heavy fraction (343+ °C)	12.9	12.8(1.2)		
Light paraffins (Pl)		1.3		
Light naphthenes (Nl)		2.2		
Light aromatics (Al)		11.7		
Total light fraction (221-343 ⁰ C)	15.6	15.2(2.6)		
Total unconverted gas oil (221 ⁺ °C)	28.5	28.0(1.9)	57.3(-100.6)	31.5(-9.4)
Gasoline (C5-221 °C)	54.3	53.3(1.8)	27.2(49.9)	51.5(5.6)
LPG	12.4	13.7(-10.8)	9.8(21.1)	11.8(4.7)
Dry Gas	1.2	1.2(-3.3)	2.7(-130.5)	1.5(-19.1)
Coke	3.6	3.7(-4.4)	3.1(14.0)	3.8(-5.2)

® Literature kinetic constants⁵ used for simulation

* Estimated rate constants (from Table 6) used for simulation

Stabilization of Triple Link Inverted Pendulum system based on LQR control Technique

Mukul K. Gupta
 Assistant Professor Electrical
 Engineering University of
 Petroleum and Energy Studies,
 Dehradun, INDIA
 mukulvjti@gmail.com,

Kamal Bansal
 Professor Electrical
 Engineering, University of
 Petroleum and Energy Studies,
 Dehradun, INDIA
 kamalbansal@ddn.upes.ac.in,

Arun Kumar Singh
 Assistant Professor, Mechanical
 Engineering, Visvasvaraya
 National Institute of Technology
 Nagpur, INDIA,
 aksinghb@gmail.com

Abstract- This paper first discusses the mathematical modeling of a dynamical system consists of triple link inverted pendulum (TLIP) on a moving cart using Lagrangian equation. This model is then used to design a controller based on the LQR method to maintain the TLIP vertically on the moving cart. The stability and controllability of the triple link inverted pendulum system are investigated and the choice of weights in LQR is also discussed. The system is simulated in MATLAB environment and the simulation results establish the satisfactory performance of the LQR controller in stabilizing the system.

Keywords- Triple link inverted Pendulum; Linear Quadratic Regulator; Lagrangian system.

I. INTRODUCTION

Inverted pendulums are inherently unstable and nonlinear systems thus present a challenging control problem [1]. As such, they provide an excellent test bench for the evaluation and comparison of different control strategies. The stabilization of single and double inverted pendulums has been the subject of numerous papers [1-4].

The study of a triple link system is, in contrast, a highly non-linear, multi-variable, higher order, unstable system. This can be used for the development of walking robots, flexible space structures, automatic aircraft landing system, biped locomotive machines since it can be considered a simplified model of the human standing on one leg[4-6]. In this paper, a TLIP mounted on a cart that can move horizontally is controllable and can be stabilized in the upward position with a single control input [3,7-8]. In this paper, a continuous time Linear Quadratic Regulator (LQR) is used for controlling the Triple link inverted pendulum in simulation.

The aim of the work is to improve the overall performance of the TLIP in the steady state. Some concepts such as stability and controllability are also discussed in this paper. The rest of this paper is organized as follows. Section 2 describes the mathematical model and equations of system. Section 3 is related to the design of the LQR controller. Simulation results are presented in section 4 followed by the conclusions in section 5.

II. MATHEMATICAL MODELING

The mathematical model of the TLIP is established by the Lagrange method [3] and its schematic representation is shown in Fig. 1. The pendulum's system consists of three steel links of various lengths mounted on a cart. The cart is driven on a rail track by a permanent magnet dc servo motor through a cable pulley assembly. The mathematical model for the pendulum is constructed using the Lagrange method [3-4] under the assumptions similar to those Furuta *et al.* (1980) [1, 5].

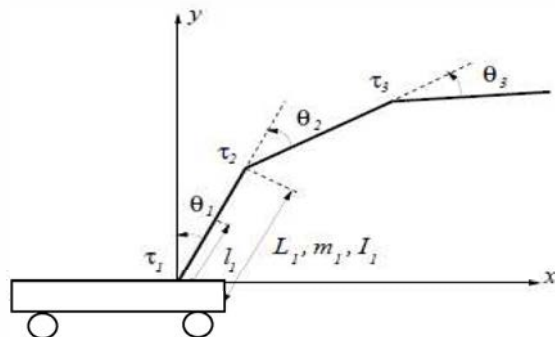


Fig. 1. Triple inverted pendulum system on cart

The TLIP in Fig.1 shows that M is Mass of the cart, m_i - Mass of the i th link, l_i - distance from the lower position sensor to the center of gravity of the i th link, L_i - Total length of the i th link, I_i - Mass moment of inertia of the i th link about its center of gravity, r - Cart's position from the middle of the rail track, θ_i - Angle of the i th link from the vertical position, C_c - Dynamic friction coefficient between the cart and the track, C_i - Dynamic friction coefficient for the i th link, μ_j - Coulomb friction coefficient for the j th link.

The kinetic, potential and friction dissipation energies are given as follows: the kinetic energy is

$$T = 0.5 \sum_{i=1}^3 I_i \dot{\theta}_i^2 + m_i \left\{ \left[\frac{d}{dt} \left(r + \sum_{k=i-2}^{i-1} L_k \sin(\theta_k) + l_i \sin(\theta_i) \right) \right]^2 + \left[\frac{d}{dt} \left(r + \sum_{k=i-2}^{i-1} L_k \cos(\theta_k) + l_i \cos(\theta_i) \right) \right]^2 \right\} + 0.5 M \dot{r}^2 \quad (1)$$

The potential energy is

$$V = \sum_{i=1}^3 m_i g (l_i \cos(\theta_i) + \sum_{k=i-2}^{i-1} L_k \cos(\theta_k)) \quad (2)$$

And the dissipation energy is

$$D = 0.5 \sum_{i=1}^3 C_1 (\dot{\theta}_i^2 - \dot{\theta}_{i-1}^2) + 0.5 C_c \dot{r}^2 \quad (3)$$

The system's nonlinear dynamics equations can then be given in the following form

$$F(q) \ddot{q} = -G(q, \dot{q}) \dot{q} - H(q) + L(q, u) \quad (4)$$

Where

$$F(q) = \begin{bmatrix} A_1 & A_2 \cos(\theta_1) & A_3 \cos(\theta_2) & A_4 \cos(\theta_3) \\ A_9 \cos(\theta_1) & A_{10} & A_{11} \cos(\theta_1 - \theta_2) & A_{12} \cos(\theta_1 - \theta_3) \\ A_{18} \cos(\theta_2) & A_{19} \cos(\theta_1 - \theta_2) & A_{20} & A_{21} \cos(\theta_2 - \theta_3) \\ A_{28} \cos(\theta_3) & A_{29} \cos(\theta_1 - \theta_3) & A_{30} \cos(\theta_2 - \theta_3) & A_{31} \end{bmatrix}$$

$$G(q, \dot{q}) = \begin{bmatrix} A_5 A_3 \sin(\theta_1) \dot{\theta}_1 & A_7 \sin(\theta_2) \dot{\theta}_2 & A_8 \sin(\theta_3) \dot{\theta}_3 \\ 0 & A_{13} & A_{14} \sin(\theta_1 - \theta_2) \dot{\theta}_2 + A_{15} & A_{16} \sin(\theta_1 - \theta_3) \dot{\theta}_3 \\ 0 & A_{22} \sin(\theta_1 - \theta_2) \dot{\theta}_1 + A_{23} & A_{24} & A_{25} \sin(\theta_2 - \theta_3) \dot{\theta}_3 + A_{26} \\ 0 & A_{33} \sin(\theta_1 - \theta_3) \dot{\theta}_1 & A_{35} \sin(\theta_2 - \theta_3) \dot{\theta}_2 + A_{36} & A_{32} \end{bmatrix}$$

$$q = \begin{bmatrix} r \\ \theta_1 \\ \theta_2 \\ \theta_3 \end{bmatrix}, \quad H(q) = \begin{bmatrix} 0 \\ A_{17} \sin(\theta_1) \\ A_{27} \sin(\theta_2) \\ A_{34} \sin(\theta_3) \end{bmatrix},$$

$$L(q, u) = \begin{bmatrix} K_s u - \text{sign}(r) \mu_r N_r \\ -\text{sign}(\theta_1) \mu_{\theta 1} N_{\theta 1} \\ -\text{sign}(\theta_2) \mu_{\theta 2} N_{\theta 2} \\ -\text{sign}(\theta_3) \mu_{\theta 3} N_{\theta 3} \end{bmatrix}$$

Where u is the control input and K_s is the overall systems input. The system parameters, as given in the appendix Matrix A, are determined either by the direct measurements or from the experimental data.

$$A = \begin{bmatrix} 0 & 0 & 0 & 0 & 1 & 0 & 0 & 0 \\ 0 & 0 & 0 & 0 & 0 & 1 & 0 & 0 \\ 0 & 0 & 0 & 0 & 0 & 0 & 1 & 0 \\ 0 & 0 & 0 & 0 & 0 & 0 & 0 & 1 \\ 0 & -7.6 & -0.156 & -0.0005 & -4.9 & 0.0005 & -0.0005 & 0 \\ 0 & 38.9 & -23.9 & -0.07 & 11.11 & -0.0046 & 0.0087 & -0.0037 \\ 0 & -37.03 & 82.75 & -2.01 & -10.55 & 0.0087 & -0.0234 & 0.0253 \\ 0 & -1.7 & -52.8 & 71.99 & -0.49 & -0.0037 & 0.0253 & -0.4 \end{bmatrix}$$

(5)

$$B = \begin{bmatrix} 0 \\ 0 \\ 0 \\ 0 \\ 0.903 \\ -2.02 \\ 1.91 \\ 0.09 \end{bmatrix}$$

(6)

The A_i is the systems constants given in the appendix.

III. LINEAR QUADRATIC REGULATOR

The plant is linear time invariant and the state space equation is

$$\dot{X} = AX + Bu \tag{7}$$

It can make the performance index J achieve the minimum value

$$J = \int_0^{\infty} (X^T Q X + u^T R u) dt \tag{8}$$

Where Q is a semi definite matrix, R is a positive definite matrix, Q and R are the weighting matrixes of state variable and input variables respectively [2] [8]. For the smallest performance index function. At first Hamilton function is constructed, derivation of this was obtained and makes it equal to zero, which can determined the optimal control rate:

$$u(t) = -Kx(t) = R^{-1} B^T P x(t) \tag{9}$$

Where P is the only positive definite symmetric solution which meets the Riccati equation

$$PA + A^T P - PBR^{-1} B^T P + Q = 0 \tag{10}$$

In the design of the controller, one of the key problems is to select weight matrix Q and R in the quadratic performance

indexes. For the Triple link inverted pendulum system, several different weighting matrices were tried and tested. The elements of the final Q matrix are larger than the elements of the R matrix. This selection translates into a controller that is more sensitive to the states of the system than the control input. The logic behind this choice is that since the main design criterion is stability, therefore the system states should dictate stability. The elements of the Q and R matrices of the LQR selected for the system under consideration are:

$$Q = \text{diag}([400 \ 6000 \ 700 \ 0 \ 0 \ 140 \ 0 \ 0.1]);$$

$$R = 1$$

Therefore the optimal feedback gain matrix is

$$K =$$

$$1.0e+003 *$$

$$[-0.0200 \ -0.3296 \ 0.8522 \ -3.5432 \ -0.0458 \ -0.1442 \ -0.0777 \ -0.4105]$$

The Eigen value of system Matrix A and closed loop system matrix A_c is given below in the following table 1.

TABLE I. EIGEN VALUES OF MATRIX A AND A_c

Sino	Eigen value A	Eigen value A_c
1	0	-25.7123
2	9.8691	-9.6201
3	8.1493	-8.8233
4	4.3265	-8.0303
5	-10.4277	-6.1828 + 1.0041i
6	-8.6358	-6.1828 - 1.0041i
7	-6.3749	-1.2164 + 0.9812i
8	-2.2345	-1.2164 - 0.9812i

From the Eigen value in Table 1, it is clear that for the system matrix A, it is unstable and after adding gain K and Matrix B, the new Eigen value of A_c are stable in nature.

IV. SIMULATION RESULTS

Based on the simulations, the plot in Figs.2a & 2b shows position and velocity of the cart respectively. It may be seen in Figs.2a & 2b that the cart stabilizes after going through initial transition. Similarly, Figs.3a&3b, Figs.4a &4b, and Figs. 5a&5b present the plots related with angular displacement and angular velocity of the bottom link, middle link and bottom link of the

TLIP. These plots also confirm that like cart, the links also stabilize with time. At the same time, it is obvious that settling time is very small. It is less than 4 seconds in almost all the cases which is a very good sign the efficacy of the LQR controller. In all simulations the systems was stable, conforming the LQR properties of the control system.

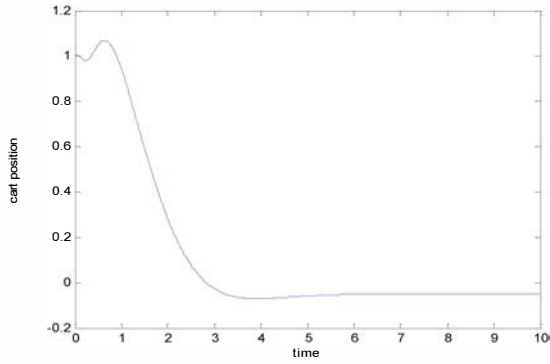


Fig. 2a. Cart Position

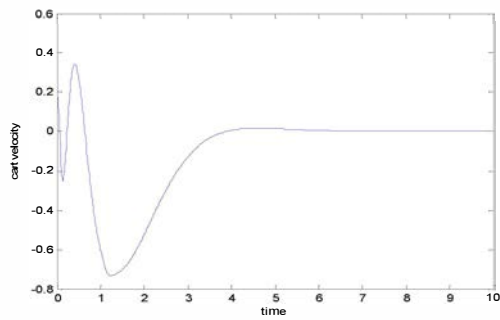


Fig. 2b. Cart Velocity.

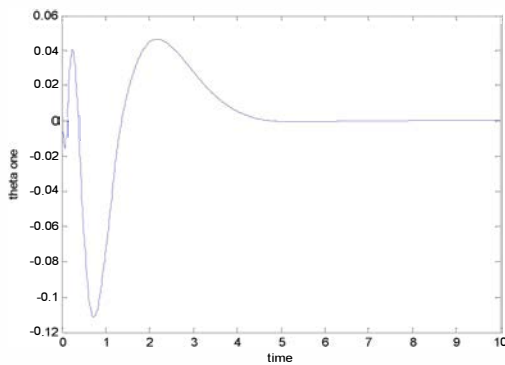


Fig. 3a. First link: Angular displacement

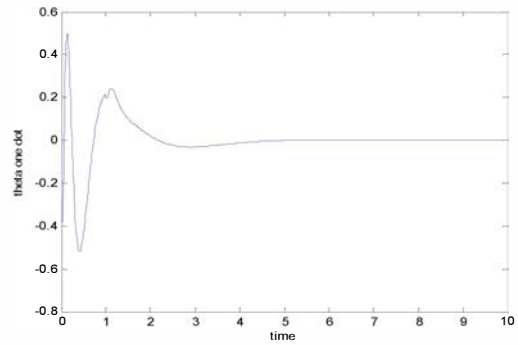


Fig. 3b. First link : Angular Velocity

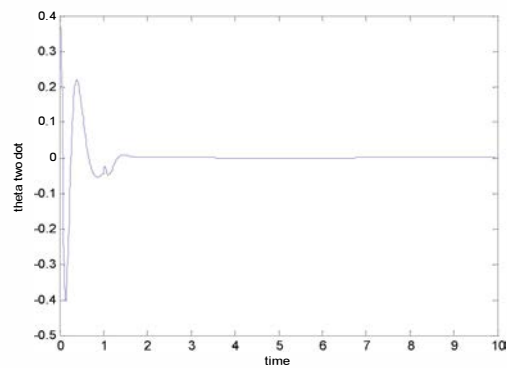


Fig. 4a. (Second link: Angular displacement)

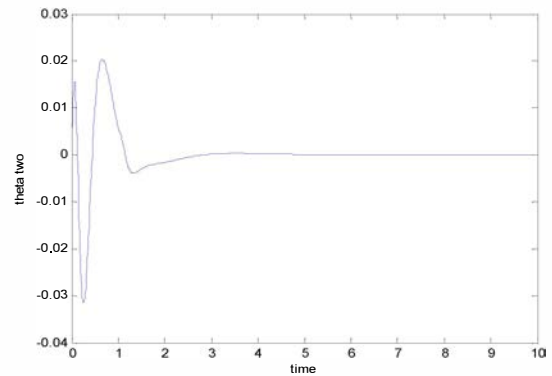


Fig. 4b. Second link: Angular velocity.

Appendix

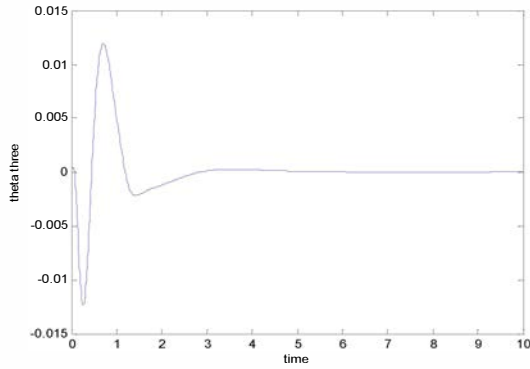


Fig. 5a. Third link: Angular displacement.

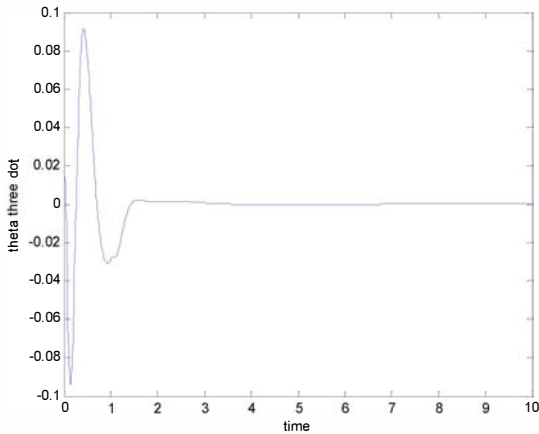


Fig. 5b. Third Link: Angular velocity.

V. CONCLUSION

This paper presents the use of the LQR controller to stabilize a TLIP on a moving cart. An optimal control system was designed to balance the same designed successfully. Simulation results clearly show the effectiveness of the proposed controller. Many other research problem are left for future work such as one can used intelligent control technique for the TLIP and other higher degree of freedom system.

Constants	Value	Constants	Value
A_1	$= M + m_1 + m_2 + m_3$	A_{19}	$= (m_2 l_2 + m_3 L_2) L_1$
A_2	$= m_1 l_1 + (m_2 + m_3) L_1$	A_{20}	$= I_2 + m_3 L_2^2 + m_2 l_2^2$
A_3	$= m_2 l_2 + m_3 L_2$	A_{21}	$= m_3 l_3 L_2$
A_4	$= m_3 l_3$	A_{22}	$= -(m_2 l_2 + m_3 L_2) L_1$
A_5	$= C_c$	A_{23}	$= -C_2$
A_6	$= -m_1 l_1 - (m_2 + m_3) L_1$	A_{24}	$= C_2 + C_3$
A_7	$= -(m_2 l_2 + m_3 L_2)$	A_{25}	$= m_3 l_3 L_2$
A_8	$= -m_3 l_3$	A_{26}	$= -C_3$
A_9	$= [m_1 l_1 + (m_2 + m_3) L_1]$	A_{27}	$= -g (m_2 l_2 + m_3 L_2)$
A_{10}	$= I_1 + m_2 l_1^2 + (m_2 + m_3) L_1^2$	A_{28}	$= m_3 l_3$
A_{11}	$= (m_2 l_2 + m_3 L_2) L_1$	A_{29}	$= m_3 l_3 L_1$
A_{12}	$= m_3 l_3 L_1$	A_{30}	$= m_3 l_3 L_2$
A_{13}	$= C_1 + C_2$	A_{31}	$= I_3 + m_3 l_3^2$
A_{14}	$= (m_2 l_2 + m_3 L_2) L_1$	A_{32}	$= C_3$
A_{15}	$= -C_2$	A_{33}	$= -m_3 l_3 L_1$
A_{16}	$= m_3 l_3 L_1$	A_{34}	$= -g m_3 l_3$
A_{17}	$= -g (m_1 l_1 + m_2 L_1 + m_3 L_1)$	A_{35}	$= -m_3 l_3 L_2$
A_{18}	$= m_2 l_2 + m_3 L_2$	A_{36}	$= -C_3$

REFERENCES

- [1] K.Furtura, T.Ochiai, and N.Ono, "Attitude Control of a triple inverted pendulum," International Journal of Control, vol.39, no.6, pp. 1351- 1365, 1984.
- [2] Desineni Subbaram Naidu, "Optimal Control Systems," Idaho State University, 2002, p. 129.
- [3] Eltohmy, K. G., and Kuo, C. Y., 1997, "Real-time stabilization of a triple link inverted pendulum using single control input." Proceedings of the Institution of Electrical Engineers, Pt D, **144**, 498- 504.
- [4] Elthomy K G and Kuo C.Y, 1999, "Nonlinear optimal control of a triple link inverted pendulum with single control input," INT. J. CONTROL, Taylor and Francis 1998, VOL. 69, NO. 2, 239-256
- [5] Lijuan Zhang, Yaqing Tu, "Research of Car Inverted Pendulum Model Based on Lagrange Equation," Proceedings of the 6th World Congress on Intelligent Control and Automation, IEEE Press, June 2006, pp. 820-824.
- [6] L. Y. Hu, G. P. Liu, X. P. Liu, et al., "Linear quadratic optimal algorithm for inverted pendulum system simulation and real-time control," Mechanical Design and Manufacturing, vol.47, no.1, pp.89-91, 2010.
- [7] I. fatoni and R Lozano," Non linear control for under actuated system," London Springer 2002
- [8] Medrano-Cerda, G. A., Eldukhri, E. E.,and Cetin, M., 1995, "Balancing and attitude control of double and triple inverted pendulums," Transactions of the Institute of Measurement and Control, **17**, 143- 154.
- [9] G. A. Medrano, "Cerda Robust stabilization of a triple inverted pendulum cart," International Journal of Control, Taylor and Francis, 08 Nov 2010, 849-866
- [10] Sponge, M. W., 1995, "the swing up control problem for the acrobat," IEEE Control Systems Magazine, **15**, 49-55.



The 6th International Conference on Applied Energy – ICAE2014

The Drivers of Oil Prices – A MI³ Algorithm approach

Neha Sehgal^a, Krishan K Pandey^{b,*}

^aJindal Global Business School, O. P. Jindal Global University, Sonapat, Haryana-131001, India

^bCollege of Management & Economic Studies, University of Petroleum & Energy Studies, Dehradun-248007, India

Abstract

The debate on significance of numerous political, economic and financial indicators driving crude oil prices is perpetual. There is no single indicator which can provide a complete picture of how prices can be determined. Nor a simple combination of input indicators can provide accurate and robust price forecast methods. In particular, feature selection plays a key role in designing a forecasting model for oil prices. However, all existing method of predicting oil prices have accounted for non-linearity, non-stationarity and time-varying structure of crude oil prices but seldom focus on selecting significant features with high predicting power. Besides, there is lack of competent feature selection techniques based on associations and dependency of indicators for designing the input vector of oil price forecast. For this purpose, a novel two-stage feature selection method “MI³Algorithm” is proposed for inferring non-linear dependence between oil prices and strategic indicators driving them by employing interaction information and mutual information as measure of redundancy(or synergy) and relevance. The study targets to figure out the importance and impacting mechanism of key indicators driving crude oil prices based on the proposed feature selection algorithm employing multi-layered perceptron neural network (MLP), general regression neural network (GRNN) and cascaded neural network (CNN) as forecasting engine for oil price prediction. The results confirmed the superiority of proposed algorithm compared to some other methods. Besides its high accuracy, the proposed algorithm provides non-redundant and most relevant features as compared to other methods employed in study.

© 2014 The Authors. Published by Elsevier Ltd. This is an open access article under the CC BY-NC-ND license (<http://creativecommons.org/licenses/by-nc-nd/3.0/>).

Peer-review under responsibility of the Organizing Committee of ICAE2014

Keywords: Feature Selection ;Mutual Information; Interaction Information; Neural Networks; Oil price forecasting

1. Introduction

The “price of oil” is a critical factor with substantial impact on world economics, be they are part of OPEC or Non-OPEC countries. According to BP , oil remains the world’s primary fuel, accounting to 33.1% of global energy consumptions. Oil prices have been steadily rising for several years and in July 2008 stand at a record high of above US\$140/bbl. Later, it declined due to global economic crisis at the end of 2008, which took long to recover by 2010 as US\$75/bbl. This rise or decline in oil prices

* Corresponding author. Tel.: +91-9458314387; +91-9760027312.
E-mail address: krishan.pandey@gmail.com.

stimulates for studying in detail the factors behind movements in the “price of oil”. There are large number of factors, which are complex, noisy, and uncertain influencing crude oil prices [1]. In order to build an effective model, careful attention should be paid on selecting informative and influential inputs which cause changes in prices [2]. However, until recently, the input variables of oil price forecast is selected on judgmental criteria or trial and error procedures [3]. Most of the studies were concentrated on non-linearity, non-stationarity and time varying properties of oil prices but seldom focus on designing a robust feature selection method for selecting significant inputs to improve forecasting accuracy. In this context, the study proposes a two stage non-linear feature selection method as discussed in next section.

2. MI3 Algorithm for feature selection

Inspired by the superiority of information-theoretic approaches, the study propose “MI3 Algorithm” composed of mutual information and interaction information for finding drivers of oil prices. The proposed algorithm consists of two stages. In the first stage, mutual information based irrelevance filter is used to select the most relevant features from the set of candidate inputs. In the second stage, interaction information based redundancy filter removes the redundant features from selected relevant candidates. The selected features are used as set of input variables to build MLP, GRNN and CNN forecasting models. The structure of the proposed MI3 Algorithm is shown in fig 1.

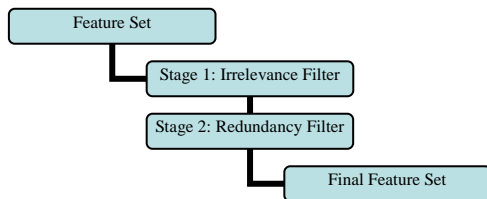


Fig 1 Structure of the proposed MI³ feature selection algorithm

3. Numerical Results

Globalization hypothesis of oil prices moving together holds independently of whether the market is crashing or booming. In this study, WTI crude oil spot price is chosen as target variable as it is considered benchmark oil in global terms. The factors driving oil prices are classified into eight classes: Supply, Demand, Reserves, Inventory, Future Market, Exchange Rate, Economy and Weather. The data is collected on monthly basis from EIA, World Bank and Bloomberg databases from January 1994 – December 2011. The data is pre-processed by scaling to (-1, 1) as input for MLP and it is standardized (by subtracting the median and dividing by the interquartile range) as input for GRNN. The proposed algorithm is used to identify the set of most relevant and non-redundant features. In stage 1, mutual information is computed. The candidate inputs with the relevance rank (normalized relevance value with respect to maximum MI) and feature number are shown in table 1.

Table 1 Selected input by Stage 1 irrelevance filter for WTI crude oil price market

Feature (Rank, No.)	NYMEX future prices (1, 18)	India Consumption (2, 6)	OPEC Reserves (3, 10)	China GDP (4, 22)	India GDP(5, 23)
Feature (Rank, No.)	OECD Reserves(6, 9)	U.S GDP (7,26)	Reserve-Production Ratio (8, 12)	U.S. Inflation (9,24)	U.S. Refinery Capacity (10, 17)

Feature (Rank, No.)	Strategic Petroleum Reserves (11, 13)	Non-OECD Consumption (12, 4)	China Consumption (13, 5)	OPEC Supply (14, 2)	Non-OPEC Production (15, 1)
Feature (Rank, No.)	EUR/ USD (16, 21)	China Reserves (17, 11)	U.S. import from Non-OPEC (18, 15)	OECD Stocks (19, 14)	JPY/ USD (20, 20)
Feature (Rank, No.)	OPEC Spare Capacity (21, 8)	GBP/ USD (22, 19)	U.S. import from OPEC (23, 16)	OECD Consumption (24, 3)	Primary Energy Consumption (25, 7)
Feature (Rank, No.)	U.S. Cooling degree days (26, 28)	U.S. Heating degree days (27, 27)	Geopolitical and Economic Events (28, 25)		

Further, the 3-variable interaction information is computed. The algorithm in stage 2 start with maximum relevance rank variable X_{18} . The interaction information is negative for a single set $\{Y, X_{18}, X_{25}\}$. The redundant variable is filtered by comparing mutual information $I\{Y, X_{18}\}$ and $I\{Y, X_{25}\}$. The results obtained in table 1 shows $I\{Y, X_{18}\} > I\{Y, X_{25}\}$, therefore, X_{25} is filtered out and the process continues for next subsequent ranked variables. The stage 2 of proposed algorithm has reduced the number of candidate input to 16 from 28 (approx. 50% of actual number) which are non-redundant and relevant in nature. In this experiment, the performance of two stage feature selection MI^3 algorithm is evaluated with known feature selection techniques as: Modified Relief + Mutual Information (MR + MI) [4], Modified Relief (MR) and Correlation feature selection (CFS). The proposed MI^3 algorithm with three forecasting engines is compared with 6 single-stage models (MR / CFS) and 3 two-stage models (MR + MI). The ultimate goal of this study is to select informative inputs to build effective forecasting model for crude oil price. The performance criteria to compare the effectiveness of the different models are root mean square error (RMSE), mean absolute error (MAE) and mean absolute percentage error (MAPE) and are shown in table 2 for 12 ensemble models. MI^3 algorithm with GRNN and MLP has performed superior to other competing ensemble methods (least RMSE, MAE & MAPE). CFS seems to be performed well with MLP but there are several limitations regarding relevance, redundancy and basic assumption of conditional independence associated with it. The proposed algorithm is superior in finding the set of non-redundant features compared to features selected through (MR+MI) algorithm as there exist two pairs of features selected for which interaction information is negative. The proposed algorithm is a fully automatic algorithm that doesn't require user to specify the number of features to be extracted or to specify any threshold. Most of the competing feature selection method fails to perform well as they assume that features are conditional independent within the classes. The proposed algorithm overcomes this limitation using the concept of interaction information. The explanatory power for oil price using sixteen selected features is 99.01%, indicating that the variable reduction is reasonable and will have no essential influence on subsequent analysis. The final features selected from proposed algorithm are shown in table 3. It shows enormous impact of emerging economies in driving crude oil prices. Our results have proved the importance of Non-OECD consumption through recent change in data post 2009. Further, Non-OPEC production which constitutes production from developed countries is also influential in deciding direction of crude oil prices. Results indicate that NYMEX future prices are not a sole indicator driving the directions of spot oil prices.

Table 2 Performance evaluation for WTI crude oil price forecasting

Model	RMSE	MAE	MAPE	Model	RMSE	MAE	MAPE
MI^3 + GRNN	0.32	0.25	0.92	MR+GRNN	2.38	1.55	3.99
MI^3 + MLP	0.60	0.46	1.68	MR+MLP	1.27	0.85	2.81
MI^3 + CNN	2.27	1.73	5.07	MR+CNN	4.11	2.81	8.65

MR+MI+ GRNN	1.51	0.96	2.38	CFS+GRNN	1.82	1.15	2.94
MR+MI+MLP	0.48	0.29	0.89	CFS+MLP	0.39	0.29	0.92
MR+MI+CNN	1.46	0.97	2.67	CFS+CNN	3.01	2.21	7.11

Table 3 Explanatory power of 16 selected factors based on MI³ algorithm

Feature	Non-OPEC Production	OPEC Supply	Non-OECD Consumption	China Consumption	India Consumption	OECD Reserves	OPEC Reserves	China Reserves
%	1.21	0.01	1.96	1.63	3.73	0.16	9.49	5.73
Feature	Reserve Production Ratio	Strategic Petroleum Reserve	U.S Refinery Capacity	NYEMX Future Price	China GDP	India GDP	U.S Inflation	U.S.GDP
%	15.09	2.96	4.27	15.89	10.67	5.32	11.22	10.67

4. Conclusions

In this paper, we presented a novel two stage MI³ algorithm for selecting informative inputs to build a forecasting model of crude oil forecasting. The algorithm is composed of informatics-theory approaches for studying the dependency and association of input variables for prediction problems. The results shows superiority of proposed algorithm in finding most relevant and non-redundant inputs compared to some known methods. The results highlighted MI³ + GRNN as best forecasting tool for crude oil prices. The proposed algorithm reduced the number of candidates to approximately half of actual number of inputs.

5. Reference

- [1]. De Souza e Silva, E. G., Legey, L. F., & de Souza e Silva, E. A. (2010, November). Forecasting oil price trends using wavelets and hidden Markov models. *Energy Economics*, 32(6), 1507-1519.
- [2]. Haidar, I., Kulkarni, S., & Pan, H. (2008). Forecasting Model for Crude Oil prices Based on Artificial Neural Networks. *International Conference on Intelligent Sensors, Sensor networks and Information Processing*, 103-108. IEEE.
- [3]. Jammazi, R. & Aloui, C. (2012). Crude oil price forecasting: Experimental evidence from wavelet decomposition and neural networks. *Energy Economics*, 34, 828-841
- [4] Amjady, N. & Daraeepour, A. (2009). Design of input vector for day-ahead price forecasting of electricity markets. *Experts Systems with Applications*, 36(10), 12281-12294.

Biography



Neha Sehgal is a Ph.D. candidate at College of Management & Economic Studies, University of Petroleum & Energy Studies. She is also the Research Associate at Jindal Global Business School, O. P. Jindal Global University. Her main research interests include data mining, energy economics and time series econometrics.



Krishan K. Pandey is Assistant Dean (Research) and Associate Professor at College of Management & Economic Studies, University of Petroleum & Energy Studies. His main research interests include statistical inference, statistical modeling for bio-fuels, LCA and EIA for energy crops and time series econometrics.